MATHEMATICAL MODELLING OF WIND EFFECTS ON CLOSED LAKES

by

ROBERT JOHN ARNOLD, B.Sc.(Hons) (Adelaide)

Thesis submitted for the degree of

Doctor of Philosophy at the

University of Adelaide,

Department of Applied Mathematics.

November, 1985

TABLE OF CONTENTS

SUMMARY

This thesis investigates general methods with which the circulation induced by a wind blowing over the surface of a closed basin may be calculated. Firstly, the linear, depth integrated equations describing such motions are used to model the motions induced by an oscillating wind blowing over a system of connected lakes each of constant depth. The techniques used to model this problem are the Collocation and Galerkin methods, which assume the basins are of rectangular shape, and a Boundary Integral Technique, which models basins of arbitrary contour. The performance of each of these methods is analysed.

By way of developing the above methods, the effect of the Coriolis force on the motion in rectangular lakes of various dimensions is also discussed. Results from the Boundary Integral Technique are also compared with analytic solutions available for simple geometries.

Various numerical methods of solving the depth integrated equations are also developed. Some of these methods can be used to calculate the effect of a wind blowing over a basin of arbitrary depth and contour. As part of this section of the thesis, finite difference approximations are developed which enable derivatives at a point near a curved boundary, along which a Neumann boundary condition applies, to be modelled with second order accuracy. Results from all the numerical models are compared with each other as well as with analytic solutions of problems with simple boundaries.

Finally, the depth variation of horizontal velocity in such flows is considered. Several analytic solutions, applicable to channel flow, are developed. These are compared with experimental observations. A turbulent energy closure scheme is also used to examine the vertical profile of velocity and comparisons are made between the results from this model and the analytic solutions as well as some experimental observations.

SIGNED STATEMENT

I hereby declare that this thesis contains no material which has been accepted for the award of any other degree or diploma in any University, and, to the best of my knowledge and belief, it contains no material previously published or written by any other person, except where due reference is made in the text of the thesis.

If this thesis is accepted for the award of the degree, then I give my consent that it be made available for photocopying and loan if applicable.

Robert John Arnold

ACKNOWLEDGEMENTS

I would like to thank my supervisor, Dr. B. J. Noye, for his encouragement and guidance in completing this thesis. Many thanks are also due to David Beard for his willingness to assist and advise on all matters relating to computing.

A portion of the work for this thesis was carried out from February 1978 to December 1979 during which time I was financed by a Commonwealth Postgraduate Research Award.

Finally, but most importantly, I must thank my wife, Julie, for her support and encouragement in finishing this thesis part time.

CHAPTER 1

THE EQUATIONS FOR GEOPHYSICAL FLOWS

§1.1 DERIVATION OF THE BASIC EQUATIONS

The equations which describe the motion of an incompressible fluid with constant molecular viscosity are the equations for mass conservation and momentum conservation, which in tensor notation, are:

$$\frac{\partial q_i}{\partial x_i} = 0 \qquad (1.1.1(a))$$

and

$$\rho \frac{Dq_i}{Dt} = -\frac{\partial p}{\partial x_i} + \rho F_i + \mu \nabla^2 q_i \qquad (1.1.1(b))$$

where

$\mathbf{x} = \mathbf{i}_1 x_1 + \mathbf{i}_2 x_2 + \mathbf{i}_3 x_3$ is the position vector,

t is time,

$\nabla^2 = \mathbf{i}_1 \frac{\partial^2}{\partial x_1^2} + \mathbf{i}_2 \frac{\partial^2}{\partial x_2^2} + \mathbf{i}_3 \frac{\partial^2}{\partial x_3^2}$,

$\mathbf{q} = \mathbf{q}(\mathbf{x}; t) = \mathbf{i}_1 q_1 + \mathbf{i}_2 q_2 + \mathbf{i}_3 q_3$ is the fluid velocity,

ρ is the constant fluid density,

$p = p(\mathbf{x}; t)$ is the fluid pressure,

$\frac{D}{Dt} = \frac{\partial}{\partial t} + q_1 \frac{\partial}{\partial x_1} + q_2 \frac{\partial}{\partial x_2} + q_3 \frac{\partial}{\partial x_3}$ is the material derivative,

$\mathbf{F} = \mathbf{F}(\mathbf{x}; t)$ are the body forces

$= \mathbf{i}_1 f q_2 - \mathbf{i}_2 f q_1 - \mathbf{i}_3 g$,

g is the acceleration due to gravity in the negative x_3 direction,

$f = 2\Omega \sin\phi$ is the Coriolis parameter,

Ω = angular speed of the earth's rotation,

$\phi = \phi(\mathbf{x})$ is the latitude and

μ is the molecular viscosity.

The above set of Navier-Stokes type equations contains information over a large range of scales. For oceanographic flows such as wind driven and tidal flows, these equations are usually averaged over a characteristic time interval, T. This results in the so-called Reynolds averaged equations. Writing

$$\mathbf{u} = \bar{\mathbf{q}}(\mathbf{x}; t) = \frac{1}{T}\int_{t-T/2}^{t+T/2} \mathbf{q}(\mathbf{x}; \tau)d\tau \qquad (1.1.2(a))$$

so that

$$\mathbf{q} = \mathbf{u} + \mathbf{u}' \qquad (1.1.2(b))$$

and similarly

$$p = P + p' \qquad (1.1.2(c))$$

where $\mathbf{u}'$ and p' define the instantaneous fluctuations of $\mathbf{q}$ and p about the time averaged means $\mathbf{u}$ and P, yields the following system of equations for the time averaged components $\mathbf{u}$ and P:

$$\frac{\partial u_i}{\partial x_i} = 0 \qquad (1.1.3(a))$$

$$\rho\frac{Du_i}{Dt} = -\frac{\partial P}{\partial x_i} + \rho F_i + \frac{\partial}{\partial x_j}(-\rho\overline{u_i' u_j'}) + \mu\nabla^2 u_i \qquad (1.1.3(b))$$

The terms $\frac{\partial}{\partial x_j}(-\rho\overline{u_i' u_j'})$ in the above equation represent additional stresses associated with all the velocity fluctuations at time scales less than the characteristic time interval, T.

For oceanographic tidal and wind driven flows the set of equations (1.1.3) may be further simplified. A scale analysis reveals that the magnitude of terms $\partial P/\partial x_3$ and ρg are much greater then the magnitude of the remaining terms in the equation for the conservation of vertical momentum (that is Equation (1.1.3(b)) with i=3). Thus, if the density ρ is constant over depth, the following equation is obtained

$$P(\mathbf{x};t) = P_a(x_1, x_2; t) + \rho g(\varsigma - x_3) \tag{1.1.4}$$

in which

$P_a(x_1, x_2; t)$ is the surface atmospheric pressure averaged over the time interval T and

$\varsigma = \varsigma(x_1, x_2; t)$ is the sea surface elevation with respect to $x_3 = 0$ also averaged over T.

Substituting Equation (1.1.4) into Equation (1.1.3(b)) and using Equation (1.1.3(a)) yields the final equations for momentum conservation, namely,

$$\frac{\partial u_i}{\partial t} + \frac{\partial}{\partial x_j}(u_i u_j) = -\frac{1}{\rho}\frac{\partial P_a}{\partial x_i} - g\frac{\partial \varsigma}{\partial x_i} + F_i + \frac{1}{\rho}\frac{\partial \tau_{ij}}{\partial x_{ij}} \qquad i = 1, 2 \tag{1.1.5}$$

where

$$\tau_{ij} = \mu\left(\frac{\partial u_i}{\partial x_j} + \frac{\partial u_j}{\partial x_i}\right) - \rho\overline{u_i' u_j'}.$$

Equations (1.1.5) and (1.1.3(a)) form the basic system of equations used to model most oceanographic and geophysical flows. However, this system of equations, as written above, cannot be solved due to the presence of the terms involving

τ_{ij}. The exact form for these stresses is not known but closure of the set of equations may be achieved in a number of ways, two of which are now briefly discussed.

§1.2 The Depth Integrated Equations

The simplest, way of solving Equations (1.1.3(a)) and (1.1.5) is to integrate the equations with respect to the depth direction. The resultant depth integrated model will provide information about the surface displacement as well as the depth averaged motion of the fluid.

The depth integrated horizontal velocity components U and V are defined by

$$U = \int_{-h}^{\zeta} u dz \qquad (1.2.1(a))$$

and

$$V = \int_{-h}^{\zeta} v dz. \qquad (1.2.1(b))$$

Integrating Equation (1.1.5) results in the following depth integrated Reynolds averaged equations for momentum conservation

$$\frac{\partial U}{\partial t} + \frac{\partial}{\partial x}\left(\frac{U^2}{\hbar}\right) + \frac{\partial}{\partial y}\left(\frac{UV}{\hbar}\right) - fV = -\frac{\hbar}{\rho}\frac{\partial P_a}{\partial x} - g\hbar\frac{\partial \zeta}{\partial x} + \frac{\tau_{sx} - \tau_{bx}}{\rho} \qquad (1.2.2(a))$$

$$\frac{\partial V}{\partial t} + \frac{\partial}{\partial x}\left(\frac{UV}{\hbar}\right) + \frac{\partial}{\partial y}\left(\frac{V^2}{\hbar}\right) + fU = -\frac{\hbar}{\rho}\frac{\partial P_a}{\partial y} - g\hbar\frac{\partial \zeta}{\partial y} + \frac{\tau_{sy} - \tau_{by}}{\rho} \qquad (1.2.2(b))$$

where

$$\hbar = \zeta + h \qquad (1.2.3)$$

is the total depth of the fluid. Inherent in the above two equations is the assumption that the horizontal and time variations of the stresses are negligible (see, for example, Noye and Flather (1985) and Kuipers and Vreugdenhil (1973)). By utilising the kinematic boundary conditions at the surface ($D\zeta/Dt = w_s$) and at the bottom ($Dh/Dt = -w_b$) and Liebnitz's rule, the mass conservation equation becomes

$$\frac{\partial \zeta}{\partial t} + \frac{\partial U}{\partial x} + \frac{\partial V}{\partial y} = 0. \tag{1.2.4}$$

The system of equations described by Equations (1.2.2) and (1.2.4) form the usual set of equations used in a depth integrated model of wind and/or tidal driven flows. This system of equations is solved using the following boundary conditions.

At a solid boundary, that is, a land-water interface, the velocity component normal to the boundary is required to be zero. At open boundaries where the modelled region joins another region of water a choice of several boundary conditions can be applied. The simplest condition is to specify the surface elevation or the normal component of velocity as a function of position along the boundary and time. There are other ways of specifying the open boundary condition discussed in Baltzer and Lai (1968), Reid and Bodine (1968), Wurtele et. al. (1971), Reid et. al. (1977), Flather (1979) and Noye and Flather (1985).

The closure of the problem has been brought about by the specification of the stress terms. The assumptions concerning the depth integrated stress terms are that the horizontal gradients of stress are negligible and that the remaining

two terms, $\boldsymbol{\tau}_s$ and $\boldsymbol{\tau}_b$ are known. The usual method of determining $\boldsymbol{\tau}_s$ and $\boldsymbol{\tau}_b$ is to utilise the quadratic drag laws which are of the form (see, for example, Nihoul (1977))

$$\boldsymbol{\tau}_s = \rho_a C_s \mathbf{W}|\mathbf{W}| \qquad (1.2.5(a))$$

$$\boldsymbol{\tau}_b = \frac{\rho C_b}{\hbar^2}\mathbf{U}|\mathbf{U}| - m\boldsymbol{\tau}_s \qquad (1.2.5(b))$$

where

ρ_a is the density of the atmosphere,

C_s is the non-dimensional surface drag coefficient,

C_b is the non-dimensional bottom drag coefficient,

$\mathbf{W}$ is the wind velocity at some reference height above the fluid surface and

$\mathbf{U}$ is the depth integrated velocity vector, $\mathbf{U} = (U,V)$.

The term $m\boldsymbol{\tau}_s$ in Equation (1.2.5(b)) is included to account for the relative additional contribution that the bottom stress makes to the surface stress. For laminar, wind induced flow in a lake of uniform depth, Hellstrom (1941) and Keulegan (1951) have deduced $m = 0.5$. Francis (1953) showed that in realistic turbulent flows m is generally less than 0.1. If this term is not included an anomaly in using Equation (1.2.5(b)) results. In a situation where there is no net flow when $\mathbf{U} = 0$ as occurs in the equilibrium wind set-up in a closed basin, Equation (1.2.5(b)) without the last term included would predict that the bottom stress would be zero. However, clearly there would be stress exerted on the bottom by return currents near the bottom. It is for this reason that the $m\boldsymbol{\tau}_s$ term is included.

Actual values for C_s and C_b must be experimentally determined. For a summary of the many empirical formulations suggested for the surface drag coefficient see, for example, Wilson (1960) or Welander (1961). In particular, the formula of Wu (1982), namely,

$$C_s = (0.8 + 0.065W_{10})\text{x}10^{-3} \tag{1.2.6}$$

where W_{10} is the wind speed measured at a height of 10m above the surface is recommended. This formula appears to be applicable for all wind speeds.

Obtaining a value for C_b is much more difficult. Often in numerical models using depth integrated equations, a value for C_b is obtained by calibrating the model with observed results. Bowden et. al. (1959) suggested C_b=2.5x10^{-3} whilst Bowden and Fairbairn (1952) deduced 1.8x10^{-3}. In a model of tidal flow in an estuary, Johns (1978) found that the value of C_b varied greatly during a tidal cycle; from 1.24x10^{-3} to 1.39x10^{-1}. This variation in values of C_b was also experimentally observed by Sternberg (1968) who found $8.7\text{x}10^{-4} < C_b < 1.11\text{x}10^{-2}$. These ranges of values for C_b suggest that Equation (1.2.5(b)) will never completely represent the bottom stress, τ_b, over an entire cycle in an oscillating flow. There are other formulations for C_b based on empirical relationships. One such formula allows C_b to depend on the total depth. This is known as the Chezy formula for bottom friction and is given by

$$C_b = \frac{gn^2\hbar^{-1/3}}{(1.003)^2} \tag{1.2.7}$$

where n is Manning's roughness coefficient which varies according to the roughness of the sea floor.

The next four chapters of this work deal with the depth integrated equations. The equations actually used are Equations (1.2.4) and the linearized form of Equation (1.2.2). The bottom stress will also be linearized by assuming $r = C_b|\mathbf{U}|/\hbar^2$ is always a constant.

§1.3 The Three Dimensional Equations

As has been shown there are several problems involved in the application of depth integrated models. One other disadvantage is that they supply no information about the nature of the flow in the vertical direction. The second method of closing Equations (1.1.3(a)) and (1.1.5) results in a three dimensional model capable of providing a complete description of the wind forced or tidal motion in an arbitrary shaped basin. Such models are becoming increasingly important, especially in the field of environmental control and off-shore engineering.

This closure scheme involves modelling the terms $-\rho\overline{u_i'u_j'}$. The oldest proposal for modelling these terms is the Boussinesq eddy viscosity concept which presumes an analogy between the molecular motion, which leads to Stokes' viscosity law in laminar flow, and the turbulent flow. In general, this concept may be expressed as

$$-\overline{u_i'u_j'} = N\left(\frac{\partial u_i}{\partial x_j} + \frac{\partial u_j}{\partial x_i}\right) - \frac{2}{3}k\delta_{ij} \tag{1.3.1}$$

where

$N = N(\mathbf{x}; t)$ is the turbulent eddy viscosity and

$k = k(\mathbf{x}; t)$ is the turbulent kinetic energy, given by

$$k = u_i'^2/2. \tag{1.3.2}$$

The term involving the Kronecker delta, δ_{ij}, in the above equation is sometimes not seen in discussions of this sort. However, it is necessary in order to make the expressions for the Reynolds stresses applicable for the normal stresses when $i = j$. Consider Equation (1.3.1) with the last term on the right hand side omitted. In this case, the sum of the normal stresses would be $u_i'^2 = -2N\partial u_i/\partial x_i$ which is identically zero using Equation (1.1.3(a)). However, by definition, the sum of the normal stresses should equal $2k$ which is always a positive constant. Hence, the δ_{ij} term is included in Equation (1.3.1) to ensure the requirement of Equation (1.3.2) is fulfilled. The addition of this extra term in Equation (1.3.1) does not complicate the governing equations, however. Like the pressure, P, k is a scalar quantity and when Equation (1.3.1) is substituted into Equation (1.1.3(b)), for example, the second part of (1.3.1) can be absorbed by the pressure gradient term. That is, in effect the pressure P is replaced by $P + 2k/3$ but for simplicity this quantity is designated by P.

The equations resulting from substituting Equation (1.3.1) into Equation (1.1.5) may be greatly simplified for most flows. In general, the cross product terms $-\rho\overline{u_i'u_j'}$, $i \neq j$ are greater in magnitude then the normal stress $-\rho\overline{u_i'^2}$ (see, for example, Duncan et. al. (1978)). For most flows, the Reynolds stresses are much greater in magnitude than the molecular stresses. Also, for geophysical flows, horizontal variations in the velocity components are much smaller than the

vertical direction. Hence, using these assumptions the resultant three dimensional equations involving the eddy viscosity are:

$$\frac{\partial \zeta}{\partial t} + \frac{\partial U}{\partial x} + \frac{\partial V}{\partial y} = 0, \qquad (1.3.3(a))$$

$$\frac{\partial \hbar u}{\partial t} + \frac{\partial}{\partial x}\hbar u^2 + \frac{\partial}{\partial y}\hbar uv + \hbar\frac{\partial}{\partial \eta}u\omega - \hbar f v = -\hbar g\frac{\partial \zeta}{\partial x} - \frac{\hbar}{\rho}\frac{\partial P_a}{\partial x} + \frac{1}{\hbar}\frac{\partial}{\partial \eta}N\frac{\partial u}{\partial \eta}, \qquad (1.3.3(b))$$

$$\frac{\partial \hbar v}{\partial t} + \frac{\partial}{\partial x}\hbar vu + \frac{\partial}{\partial y}\hbar v^2 + \hbar\frac{\partial}{\partial \eta}v\omega + \hbar f u = -\hbar g\frac{\partial \zeta}{\partial y} - \frac{\hbar}{\rho}\frac{\partial P_a}{\partial y} + \frac{1}{\hbar}\frac{\partial}{\partial \eta}N\frac{\partial v}{\partial \eta} \qquad (1.3.3(c))$$

and

$$\omega = \frac{1}{\hbar}\left[\eta\frac{\partial}{\partial x}U - \frac{\partial}{\partial x}\hbar U(\eta) + \eta\frac{\partial}{\partial y}V - \frac{\partial}{\partial y}\hbar V(\eta)\right], \qquad (1.3.3(d))$$

in which,

$\eta = \frac{z+h}{\zeta+h}$ is a transformed depth,

ω is the transformed vertical velocity component and

$U(\eta) = \int_0^\eta u d\eta'$ and $V(\eta) = \int_0^\eta v d\eta'$.

The boundary conditions which are used in conjunction with the above set of equations are:

(1) at a solid boundary, the velocity normal to the boundary is zero,

(2) a no-slip condition applies at the sea bed that is

$$u = v = \omega = 0 \text{ at } \eta = 0. \qquad (1.3.4)$$

Sometimes a slip velocity condition is used at the bottom. This is, however, only an approximation.

(3) at the sea surface the following holds:

$$\tau_{sx} = \frac{\rho N}{\hbar}\frac{\partial u}{\partial \eta} \qquad \text{at } \eta = 1, \qquad (1.3.5(a))$$

$$\tau_{sy} = \frac{\rho N}{\hbar}\frac{\partial v}{\partial \eta} \qquad \text{at } \eta = 1, \qquad (1.3.5(b))$$

where $\boldsymbol{\tau}_s$ may be related to the wind stress by (1.2.5(a)).

(4) at open boundaries the height of the surface elevation is usually specified, although there are several other alternatives as mentioned in the previous section dealing with the depth integrated equations.

A fully three dimensional description of the fluid flow field is available from Equations (1.3.3) provided a suitable formulation for N is available. Not only does this set of equations provide a more complete description, but it also has less dependence on empirical laws then the depth integrated model. Nihoul (1977) suggests that investigations into a complete three dimensional model are necessary if only to check the validity of Equation (1.2.5(b)). Various formulations for N which have been deduced from laboratory experiments and field observations will be discussed in Chapter 6. Also in this chapter will be discussed the various forms of N which have been used in numerical models. Finally, methods which allow N to be calculated as part of the solution procedure will be discussed.

CHAPTER 2

CORIOLIS FORCE AND THE CONNECTED LAKE PROBLEM

§2.1 INTRODUCTION

In Walsh (1974), numerical and analytic models were developed to predict the effect of a wind blowing over a system of two lakes connected by a narrow channel and these models were applied to the Murray Mouth lake system in South Australia. However, Walsh's analytic model was only reasonably satisfactory; an improved model is presented in this work.

Three different methods will be used to solve this problem: the Collocation and Galerkin techniques (both examples of the method of Weighted Residuals) and a boundary integral approach. The latter approach will be developed in Chapter 3 ; the two other methods will be described in Section 4 of this Chapter. Comparisons between all three methods will be made in Chapter 4.

A statement of the connected lake problem will be presented in Section 2 but firstly the effects, if any, of the Coriolis force will be examined. Walsh (1974) considers a rotating circular basin and concludes from the resulting analytic solution that the effect of the Coriolis force can be ignored. In order to check this conclusion an analytic solution for a rotating rectangular basin is now developed.

§2.2 Rotating Rectangular Basin

Consider a closed rotating rectangular basin of constant depth H, length L and breadth B as shown in Figure 2.1. An $x-y$ Cartesian coordinate system is positioned near the bottom left hand corner of the basin. Movement of the surface of the basin is excited by a variable wind stress, $\boldsymbol{\tau}_s$.

It will be assumed that the components of the surface wind stress can be expressed in the form

$$\tau_{sx}(x,y,t) = \tau_{0x}(x,y)e^{\iota\sigma t} \qquad (2.2.1(a))$$

$$\tau_{sy}(x,y,t) = \tau_{0y}(x,y)e^{\iota\sigma t}, \qquad (2.2.1(b))$$

where

τ_{sx}, τ_{sy} are respectively the x and y components of the surface wind stress $\boldsymbol{\tau}_s$,

σ is the circular frequency of the wind stress,

τ_{0x}, τ_{0y} are the amplitudes of the x and y components of wind stress,

$\iota = \sqrt{-1}$ and

t is time (in secs).

Letting the response of the surface, ζ, be

$$\zeta(x,y,t) = Z(x,y,\sigma)e^{\iota\sigma t} \qquad (2.2.2)$$

then Z satisfies the Helmholtz Equation (see Walsh (1974))

$$(\nabla^2 + k^2)Z = \frac{K}{c^2\beta}(\beta D + fC) \qquad (2.2.3)$$

where

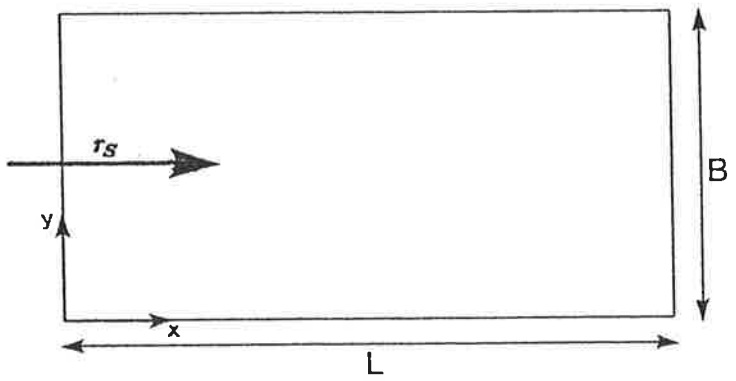

FIGURE 2.1: *A closed rectangular basin over which a surface wind stress, τ_s, is blowing in the x direction.*

$$\nabla^2 = \frac{\partial^2}{\partial x^2} + \frac{\partial^2}{\partial y^2}, \qquad (2.2.4(a))$$

$$k^2 = \frac{-\iota\sigma\beta}{c^2}\left(1 + \frac{f^2}{\beta^2}\right), \qquad (2.2.4(b))$$

$$D = \frac{\partial \tau_{0x}}{\partial x} + \frac{\partial \tau_{0y}}{\partial y}, \qquad (2.2.4(c))$$

$$C = \frac{\partial \tau_{0y}}{\partial x} - \frac{\partial \tau_{0x}}{\partial y}, \qquad (2.2.4(d))$$

$$K = (1+m)/\rho, \qquad (2.2.4(e))$$

and

$$\beta = \iota\sigma + 2\alpha, \qquad (2.2.4(f))$$

in which

f is the Coriolis parameter,

m is a constant value and takes a value of about 0.05 for turbulent flow,

$2\alpha = r/H$ where r is a friction parameter,

ρ is the density of the water (assumed constant) and

$c = \sqrt{gH}$ is the free gravity wave celerity.

If the x and y components of the depth integrated velocity of the lake are denoted by U and V respectively, then the following forms for these components are assumed:

$$U(x,y,t) = P(x,y,\sigma)e^{\iota\sigma t}, \qquad (2.2.5(a))$$

$$V(x,y,t) = Q(x,y,\sigma)e^{\iota\sigma t}. \qquad (2.2.5(b))$$

Walsh (1974) has shown that P and Q may be determined once Z is known using the following relations

$$P = \frac{1}{f^2+\beta^2}\left[K\left(\beta\tau_{0x} + f\tau_{0y}\right) - c^2\left(\beta\frac{\partial Z}{\partial x} + f\frac{\partial Z}{\partial y}\right)\right], \qquad (2.2.6(a))$$

$$Q = \frac{1}{f^2+\beta^2}\left[K\left(\beta\tau_{0y} - f\tau_{0x}\right) - c^2\left(\beta\frac{\partial Z}{\partial y} - f\frac{\partial Z}{\partial x}\right)\right]. \qquad (2.2.6(b))$$

The above equations are easily derived from Equations (1.2.2) and (1.2.4) by linearizing these equations and assuming a linear bottom friction law.

Equation (2.2.3) is subject to the boundary condition that there is no flow across the boundary of the lake. Hence, the following conditions hold:

$$P = 0 \qquad \text{at } x = 0, L;\ y \in [0, B], \qquad (2.2.7(a))$$

$$Q = 0 \qquad \text{at } y = 0, B;\ x \in [0, L]. \qquad (2.2.7(b))$$

The above boundary conditions may also be expressed in terms of Z using Equations (2.2.6(a),(b)), yielding

$$\beta\frac{\partial Z}{\partial x} + f\frac{\partial Z}{\partial y} = \frac{K}{c^2}\left(\beta\tau_{0x} + f\tau_{0y}\right) \qquad x = 0, L;\ y \in [0, B], \quad (2.2.8(a))$$

$$\beta\frac{\partial Z}{\partial y} - f\frac{\partial Z}{\partial x} = \frac{K}{c^2}\left(\beta\tau_{0y} - f\tau_{0x}\right) \qquad y = 0, B;\ x \in [0, L]. \quad (2.2.8(b))$$

Hence, the problem is reduced to one of solving Equation (2.2.3) subject to the boundary conditions (2.2.8(a),(b)). If the wind stress is assumed to be homogeneous and unidirectional and the Coriolis force is neglected, then simple analytic solutions may be obtained for Z (and thus P and Q). Such solutions are presented in Walsh (1974). For a similar wind stress and a rotating basin ($f \neq 0$), then a solution to the equations may be obtained using the method of Collocation as will be shown below.

The amplitude of the stress described above is denoted by

$$\tau_{0x}(x,y) = \tau_0, \qquad (2.2.9(a))$$

$$\tau_{0y}(x,y) = 0, \qquad (2.2.9(b))$$

which corresponds to a homogeneous, unidirectional wind stress aligned in the x direction. For such a wind stress, the right hand side of Equation (2.2.3) becomes zero and the boundary conditions given by Equations (2.2.8(a),(b)) are simplified so that the system which is to be solved becomes

$$\left(\nabla^2 + k^2\right) Z = 0, \qquad (2.2.10(a))$$

subject to

$$\beta\frac{\partial Z}{\partial x} + f\frac{\partial Z}{\partial y} = \frac{K\beta\tau_0}{c^2} \qquad x = 0, L;\ y \in [0, B], \qquad (2.2.10(b))$$

$$\beta\frac{\partial Z}{\partial y} - f\frac{\partial Z}{\partial x} = -\frac{Kf\tau_0}{c^2} \qquad y = 0, B;\ x \in [0, L]. \qquad (2.2.10(c))$$

The solution to the above system of equations may be obtained in the following manner. The function Z is written

$$Z(x,y,\sigma) = Z_0(x,y,\sigma) + Z_1(x,y,\sigma) \qquad (2.2.11)$$

where Z_0 is a particular solution of Equation (2.2.10(a)) which satisfies the boundary conditions at $y = 0, B$ described by Equation (2.2.10(c)) but not necessarily those at $x = 0, L$. Consequently, Z_1 also satisfies Equation (2.2.10(a)) as well as homogeneous boundary conditions at $y = 0, B$; that is, Z_1 satisfies Equation (2.2.10(c)) where the right hand side of this equation is set identically to zero.

An expression for Z_0 may be obtained by assuming that this function depends only on y. Therefore, Z_0 satisfies the equation

$$\frac{d^2 Z_0}{dy^2} + k^2 Z_0 = 0 \qquad (2.2.12(a))$$

subject to

$$\frac{dZ_0}{dy} = -\frac{Kf\tau_0}{\beta c^2} \qquad \text{at } y = 0, B \qquad (2.2.12(b))$$

which has the solution

$$Z_0 = \frac{Kf\tau_0}{\beta k c^2} \left\{ \frac{(1 - \cos kB)}{\sin kB} \cos ky - \sin ky \right\}. \qquad (2.2.13)$$

Because Z_1 satisfies homogeneous boundary conditions, the elevation Z_1 represents free motion in the infinite channel $0 < y < B$. Hence, Z_1 may be considered to be a linear superposition of two Kelvin waves and a double infinity of Poincaré waves. These two sets of solutions may be derived in the following manner.

The function Z_1 satisfies the system

$$\left(\nabla^2 + k^2\right) Z_1 = 0, \qquad (2.2.14(a))$$

subject to

$$\beta \frac{\partial Z_1}{\partial y} = f \frac{\partial Z_1}{\partial x} \qquad y = 0, B; \; x \in [0, L]. \qquad (2.2.14(b))$$

The y component of depth integrated velocity associated with this free motion is denoted by $Q_1(x, y, \sigma)$, an expression for which is obtainable from Equation (2.2.6(b)) where τ_{0x} and τ_{0y} have been set to zero.

Firstly a solution for Z_1 will be found for which Q_1 is zero throughout the lake. From Equation (2.2.6(b)), it is clear that such a condition on Q_1 implies

$$\beta\frac{\partial Z_1}{\partial y} = f\frac{\partial Z_1}{\partial x} \qquad y = 0, B;\ x \in [0, L]. \tag{2.2.15}$$

A function which satisfies the above expression will also satisfy the boundary condition (2.2.14(b)). The solution to Equation (2.2.15) may be obtained by the method of separation of variables. This expression is then substituted into Equation (2.2.14(a)) thus yielding one set of solutions for Z_1, namely

$$Z_1 = Z_a = A_0 e^{\iota\gamma_0 x - \theta_0 y} + B_0 e^{-\iota\gamma_0 x + \theta_0 y} \tag{2.2.16}$$

where A_0 and B_0 are unknown constants and

$$\iota\gamma_0 = \left(\frac{\iota\sigma\beta}{c^2}\right)^{\frac{1}{2}}, \tag{2.2.17(a)}$$

$$\theta_0 = -\frac{f\iota\gamma_0}{\beta}. \tag{2.2.17(b)}$$

Solutions of this type, with the factor $e^{\iota\sigma t}$ adjoined, are called Kelvin waves.

Another type of solution, Z_b, to Equation (2.2.14) may be obtained by applying the standard separation of variables technique to Equation (2.2.14(a)) in conjunction with Equation (2.2.14(b)). This yields the following solution for Z_1:

$$\begin{aligned} Z_1 = Z_b = \sum_{n=1}^{\infty}\Big\{ & A_n e^{\gamma_n x}\left[\cos\theta_n y + \phi_n \sin\theta_n y\right] \\ & + B_n e^{-\gamma_n x}\left[\cos\theta_n y - \phi_n \sin\theta_n y\right]\Big\}, \end{aligned} \tag{2.2.18}$$

where, for $n = 1, 2, \ldots$, A_n and B_n are unknown constant coefficients and

$$\phi_n = \frac{f\gamma_n}{\beta\theta_n}, \tag{2.2.20(a)}$$

$$\gamma_n^2 = \theta_n^2 - k^2 \tag{2.2.20(b)}$$

and

$$\theta_n = \frac{n\pi}{B}. \qquad (2.2.20(c))$$

Waves of the type described by Z_b, with the factor $e^{\iota\sigma t}$ adjoined, are called Poincaré waves.

The two solutions Z_a and Z_b constitute a complete set of solutions to the system of equations (2.2.14). Hence, a solution to Equation (2.2.10(a)) subject to Equation 2.2.10(c)) is

$$Z = Z_0 + Z_a + Z_b,$$

that is,

$$\begin{aligned} Z(x,y,\sigma) = {} & \frac{Kf\tau_0}{\beta kc^2}\left\{\frac{(1-\cos kB)}{\sin kB}\cos ky - \sin ky\right\} \\ & + A_0 e^{\iota\gamma_0 x - \theta_0 y} + B_0 e^{-\iota\gamma_0 x + \theta_0 y} \\ & + \sum_{n=1}^{\infty}\left\{e^{\gamma_n x}A_n\left[\cos\theta_n y + \phi_n \sin\theta_n y\right]\right. \\ & \qquad \left. + e^{-\gamma_n x}B_n\left[\cos\theta_n y - \phi_n \sin\theta_n y\right]\right\}. \qquad (2.2.20) \end{aligned}$$

The above form for Z may be substituted into Equations (2.2.6(a),(b)) to yield the following expressions for P and Q:

$$\begin{aligned} P(x,y,\sigma) = {} & \frac{1}{f^2+\beta^2}\left\{K\beta\tau_0\left[1 + \frac{f^2}{\beta^2}\left\{\frac{(1-\cos kB)}{\sin kB}\sin ky + \cos ky\right\}\right]\right. \\ & + \frac{c^4\gamma_0 k^2}{\sigma}\left[A_0 e^{\iota\gamma x - \theta_0 y} - B_0 e^{-\iota\gamma x + \theta_0 y}\right] \\ & + fc^2k^2\sum_{n=1}^{\infty}\left\{\frac{e^{\gamma_n x}A_n}{\theta_n}\left[\frac{\theta_n\gamma_n c^2}{f\iota\sigma}\cos\theta_n y + \sin\theta_n y\right]\right. \\ & \left.\left. + \frac{e^{-\gamma_n x}B_n}{\theta_n}\left[\frac{-\theta_n\gamma_n c^2}{\iota\sigma}\cos\theta_n y + \sin\theta_n y\right]\right\}\right\} \qquad (2.2.21(a)) \end{aligned}$$

and

$$Q(x,y,\sigma) = \frac{1}{f^2+\beta^2}\left\{Kf\tau_0\left[-1+\frac{(1-\cos kB)}{\sin kB}\sin ky+\cos ky\right]\right.$$
$$\left.+c^2\sum_{n=1}^{\infty}\left(e^{\gamma_n x}A_n+e^{-\gamma_n x}B_n\right)\left(f^2\gamma_n^2+\beta^2\theta_n^2\right)\frac{\sin\theta_n y}{\beta\theta_n}\right\}. \quad (2.2.21(b))$$

Using the Collocation technique together with boundary condition (2.2.10(b)) enables values to be found for the unknowns A_n and B_n for n=0,1,2,.... in the following manner. If the infinite series in Equation (2.2.20) are truncated to N terms then there will be a total of $2N+2$ unknowns contained in the expression for Z. This truncated form of Z is forced to satisfy the boundary condition (2.2.10(b)) by substituting $x = 0$ and $x = L$ into the expression for Z and in both cases also letting y take the values $y = Bi/(N+2)$ for $i = 1,\ldots,N+1$. This process results in $2N+2$ equations from which values for the unknown coefficients may be obtained.

After substituting Equation (2.2.20) into (2.2.10(b)), the Galerkin technique could also be applied. Instead of letting y take on particular values as indicated above, the equation resulting from the above-mentioned substitution is first multiplied by weighting functions, $\omega_m(y)$, for $m = 0,1,\ldots,N$ and then integrated from $y = 0$ to $y = B$. Suitable weighting functions for the above Z are

$$\omega_0 = e^{\theta_0 y} \quad (2.2.22(a))$$

$$\omega_m = \sin\theta_m y + \phi_m\cos\theta_m y \qquad m = 1,\ldots,\mathrm{N}. \quad (2.2.22(b))$$

This procedure was not carried out here however because satisfactory convergence was achieved using the Collocation technique. Also, the equations resulting from

the application of the Galerkin technique are algebraically complicated. Equations resulting from the use of both methods will be given in later sections in which the connected lake problem is treated.

To ascertain if the Coriolis parameter is significant, the above solution will be compared with a solution of Equation (2.2.10) in which f is set to zero. Ignoring the parameter f results in an essentially one dimensional system in which the y coordinate may be neglected. The solution for the amplitude, Z, of this simplified system is (see Walsh (1974))

$$Z = \frac{K\tau_0 \sin\left[k\left(x - L/2\right)\right]}{kc^2 \cos\left(kL/2\right)}. \tag{2.2.23}$$

From Walsh and Noye (1973), the largest of the two lakes situated near the Murray mouth in South Australia, Lake Alexandrina, may be approximated by a rectangular lake of dimensions $L = 24\ km.$, $B = 8\ km.$ and depth , $H = 3\ m.$ A wind stress given by Equation (2.2.9) is assumed to be blowing over the lake where the x axis is parallel to the largest side of the lake (see Figure 2.1). A value of $\tau_0 = 0.1 Nm^{-2}$ is used and a value of $f = -8.5\text{x}10^{-5} sec^{-1}$ is applicable. The larger of the two lakes is considered in this study because it will be most likely to be affected by the Coriolis force. The gain and phase lag of the elevation and velocity components will be examined. The gain, G, and phase ,ϕ, of the surface elevation, ζ, are given by

$$G = \left\{\left[\Re\left(Z\right)\right]^2 + \left[\Im\left(Z\right)\right]^2\right\}^{\frac{1}{2}}, \tag{2.2.24(a)}$$

$$\phi = -\arctan[\Im(Z)/\Re(Z)] \tag{2.2.24(b)}$$

in which $\Re$ and $\Im$ denote the real and imaginary parts respectively of the function Z. The gain and phase lag of the depth integrated velocity components are similarly given.

In Figure 2.2, the results for the gain and phase lag of the elevation from the basin with $f = 0$ (Equation (2.2.23)) are compared with results obtained for the case where $f \neq 0$ (Equation (2.2.20)). The results for the gain of the elevation have been normalised with respect to the equilibrium solution, $Z_{eq} = K\tau_0(x - L/2)/c^2$, available from (2.2.23) with $\sigma = 0$. Various values of the friction parameter, α, are considered. In all cases, the results are taken from values occurring at the point $x = 3L/4$, $y = B/2$. It is immmediately obvious that the Coriolis effect is very small. As can be seen from the graphs, almost identical results are obtained for the gain and phase lag for both the cases $f = 0$ and $f \neq 0$. At any given x position, the value of the gain and phase lag of the amplitude do not vary significantly at various positions across the lake. The most noticeable differences occur when the friction parameter , α, is zero. These differences, which are too small to show on the graphs in Figure 2.2, are presented in Table 2.1. Note that when α is non-zero the gain takes the same value across the lake and the phase lag changes only slightly (by at most 2%). Also note that the values obtained for $f = 0$ and $f \neq 0$ agree closely for all cases of α. The worst agreement for both the gain and phase lag occurs when $\alpha = 0$. However, the friction parameter in a real lake is never zero. The presence of a resonance peak indicates that severe flooding of a lake would occur at certain frequencies if the friction parameter was zero. Indeed, even for very small values of friction, it can be seen from the figure that

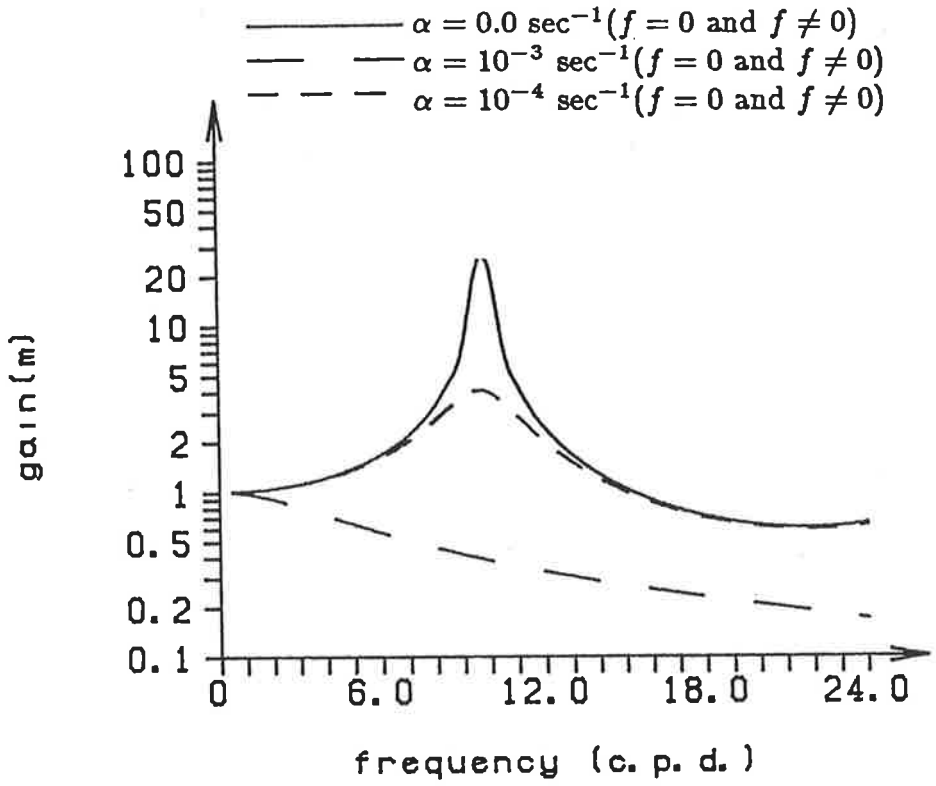

FIGURE 2.2(a): *The gain (m) of displacement,ς, for the two cases $f \neq 0$ and $f = 0$ for a rectangular basin of length 24 km., breadth 8 km. and depth 3 m.*

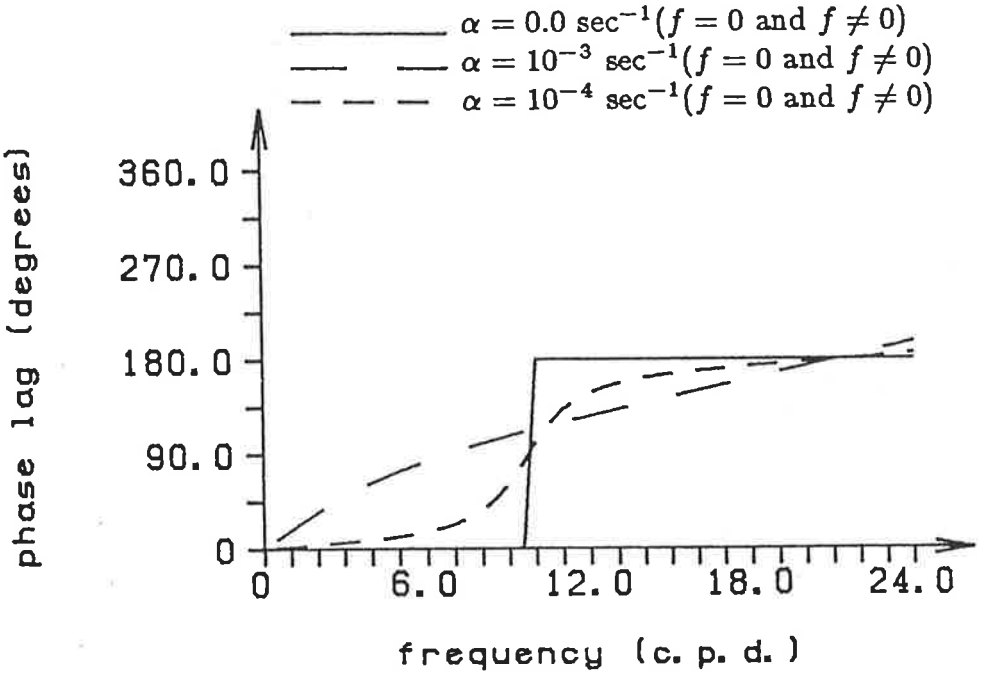

FIGURE 2.2(b): *As in Figure 2.2(a) except for the phase lag.*

GAIN						
	$\alpha = 0$		$\alpha = 10^{-3}$		$\alpha = 10^{-4}$	
y	f=0	f≠0	f=0	f≠0	f=0	f≠0
B/4	1.0120	1.0108	0.9711	0.9711	1.0116	1.0114
B/2	1.0120	1.0104	0.9711	0.9711	1.0116	1.0114
3B/4	1.0120	1.0108	0.9711	0.9711	1.0116	1.0114

PHASE LAG						
	$\alpha = 0$		$\alpha = 10^{-3}$		$\alpha = 10^{-4}$	
y	f=0	f≠0	f=0	f≠0	f=0	f≠0
B/4	0.0000	0.0035	0.3217	0.3252	0.0330	0.0368
B/2	0.0000	0.0000	0.3217	0.3218	0.0330	0.0335
3B/4	0.0000	0.0035	0.3217	0.3183	0.0330	0.0299

TABLE 2.1: *Values of the gain and phase lag obtained at $x = 3L/4$ and for a frequency of $\sigma = 1$ c.p.d. and for various values of y and α and for $f = 0$ (Equation 2.2.23) and $f \neq 0$ (Equation 2.2.20). The values for the gain (in metres) have been normalized by dividing by the gain obtained from Equation (2.2.20) with $\alpha = 0$. The phase lag is in radians.*

the gain in displacement rises rapidly at frequencies near the resonance point. This means that even when the friction is non-zero, the behaviour of the lake changes radically at particular frequencies. At such frequencies the displacement is significantly greater than might be expected and severe flooding of the lake would be likely. The agreement between the results obtained for $f = 0$ and $f \neq 0$ are close enough to be able to conclude that the Coriolis effect is negligible. The invariance of the elevation across the lake for $f \neq 0$ was highlighted when the real time surface response (obtainable from Equation (2.2.23) with $e^{\iota\sigma t}$ adjoined) was examined. In no instance did the change in surface height affect the fourth

significant figure, that is, the variation was always less then 1 mm.

In Figure 2.3 the results for the gain and phase lag of the x-component of velocity are presented for the case $f = 0$ and $f \neq 0$. Once again, there is very little difference in the phase lags for either value of f and for any of the values of α. There is also no significant difference between the values obtained for the gain for either $f = 0$ and $f \neq 0$ and for non-zero values of the friction parameter. However, when $\alpha = 0$ (no friction) an interesting shift of the position of the resonance peak occurred. When $f = 0$ and $\alpha = 0$, a single discontinuity occurs in the graph of the velocity gain (and also the amplitude gain) at about 9.76 c.p.d. (cycles per day). However, when $f \neq 0$, this resonance peak is split into a pair of resonance peaks centred about $\sigma = 9.76$ c.p.d. This phenomenon was also observed by Walsh (1974) in his study of rotating circular lakes. Once again, because the friction in a real lake is never zero, it seems from the above Figure that the Coriolis parameter does not greatly affect the U component of transport. Just as for the elevation, the value of the response, P, did not vary greatly across the breadth of the lake. It is also interesting to note that when $\alpha \neq 0$, the value of the gain obtained for the V component of depth integrated velocity was insignificant when compared with U. The gain of V was always at least two orders of magnitude smaller then that of U for $\alpha \neq 0$. However, in the frictionless case, V attained values of the same order as U. Some results are presented in Table 2.2. For the special case of $f \neq 0$, the gain of both U and V for two different values of the dimensionless friction parameter, α, is presented graphically in Figure 2.4. From both the Table and the Figure it is clear that for $\alpha \neq 0$, the gain of V is negligible when compared

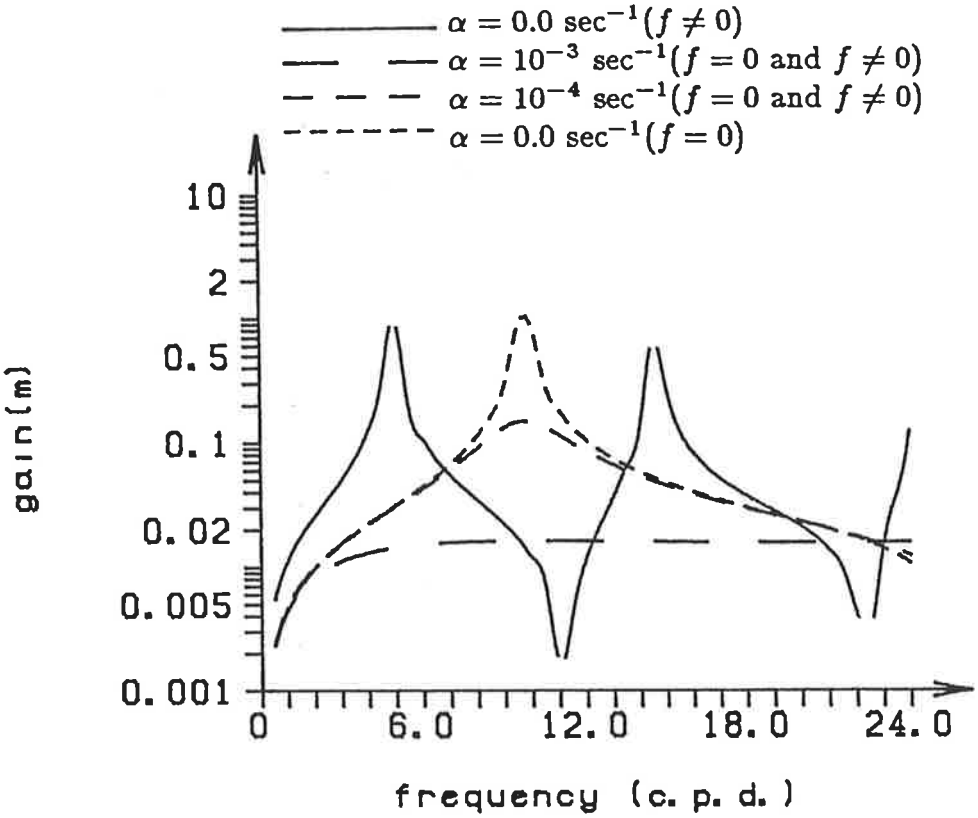

FIGURE 2.3(a): *The gain (m) of velocity, U, for the two cases $f \neq 0$ and $f = 0$ for a rectangular basin of length 24 km., breadth 8 km. and depth 3 m.*

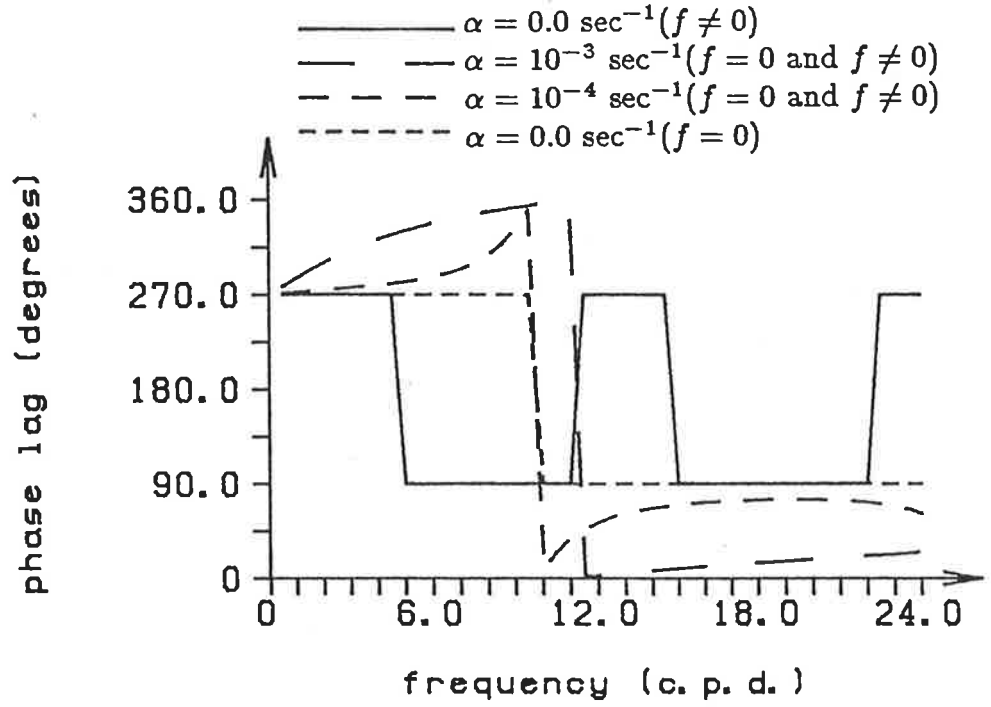

FIGURE 2.3(b): *As in Figure 2.3(a) except for the phase lag.*

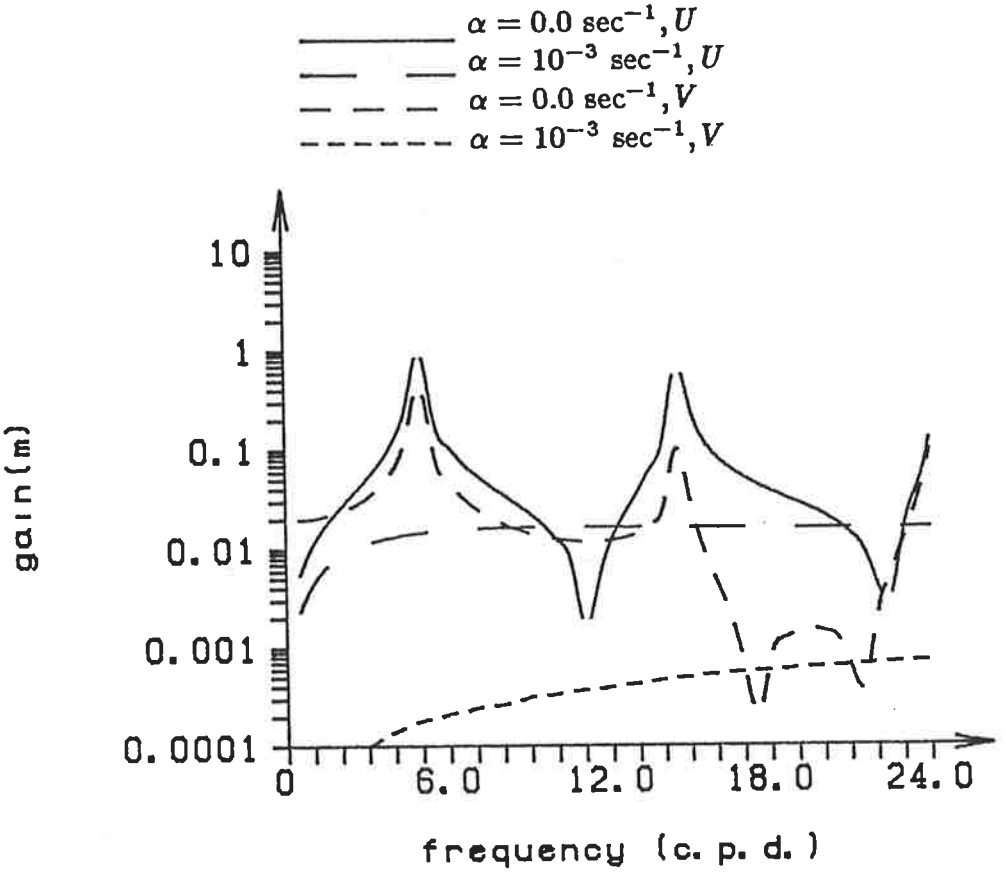

FIGURE 2.4: *The gain (m) of the two horizontal components of velocity, U and V for the case $f \neq 0$ for a rectangular basin of length 24 km., breadth 8 km. and depth 3 m.*

with the gain of U. From the solution for Q (Equation (2.2.6(b)) it is clear that when $f = 0$ and the wind stress is given by Equation (2.2.9) then the gain of V will always be zero for all values of α. However, when $f \neq 0$ the value of Q is non-zero and for the special case $\alpha = 0$, Q attains values comparable to P. Hence, from this point of view, if α is chosen to be zero, then certainly the Coriolis force cannot be neglected.

	P		Q	
	$f = 0$	$f \neq 0$	$f = 0$	$f \neq 0$
$\alpha = 0$	0.0047	0.0113	0.0000	0.0199
$\alpha = 10^{-3}$	0.0045	0.0045	0.0000	0.0000
$\alpha = 10^{-4}$	0.0047	0.0049	0.0000	0.0000

TABLE 2.2: *Comparison of the gains of P and Q obtained at $x = 3L/4$ and for $\sigma = 1$ c.p.d. for various values of α and f.*

For the small, shallow rectangular lake described above, the only significant differences between results obtained with $f = 0$ and $f \neq 0$ occurred when α was set to zero. This is never the case in a real lake and so it was concluded that for such lakes the Coriolis force may be neglected. Before ending this section it is of interest to investigate the responses of the above rectangular lake as some of the parameters are changed. For example, the physical dimensions of the basin will be altered and the resultant responses will be presented. In the following work, the effect of various values of the friction parameter, r, will be considered with respect to basins of various dimensions.

Figures 2.5(a) and (b) display the results for the phase lag and the gain of ζ obtained for a basin of the same horizontal dimensions as previously discussed (that is, 24 *km.* x 8 *km.*) but with a much greater depth (20 *m.* instead of 3 *m.*). Clearly, for a basin of this nature the results obtained are very insensitive to the value of the friction parameter. Virtually identical results are obtained in both figures with only a slight difference occurring for large values of the frequency. The results for the gain and phase lag of U, presented in Figure 2.6(a) and (b), also show that for $r \neq 0$, the results are insensitive to the value of r. However, when $r = 0$, there is considerable difference between the solutions obtained for $f = 0$ and $f \neq 0$. This is due to the presence of a resonance peak at about 12.5 c.p.d. which occurs in the solutions for $f \neq 0$. In fact, for all of the basins which were considered, major differences in the phase lag and gain of both ζ and U were obtained in the solutions using $f = 0$ and $f \neq 0$ with $r = 0$ in both cases. For this reason only results obtained with $r = 10^{-3}\ msec^{-1}$ are presented in the next four figures. As long as $r \neq 0$, similar results to those shown in the next figures are obtained since, for the depths considered, the results are insensitive to r.

In Figures 2.7 and 2.8 results for the gain and phase lag of ζ and U are presented for a basin of much larger horizontal dimensions then were previously considered. The depth was kept constant at 20 m. but the horizontal dimensions were increased to 240 km. x 240 km. It is immediately clear that for a larger basin such as the one described the results obtained using $f = 0$ are sometimes considerably different than those obtained using $f \neq 0$. From Figure 2.7(a) and (b), it is seen that for larger values of frequency the two solutions are virtually

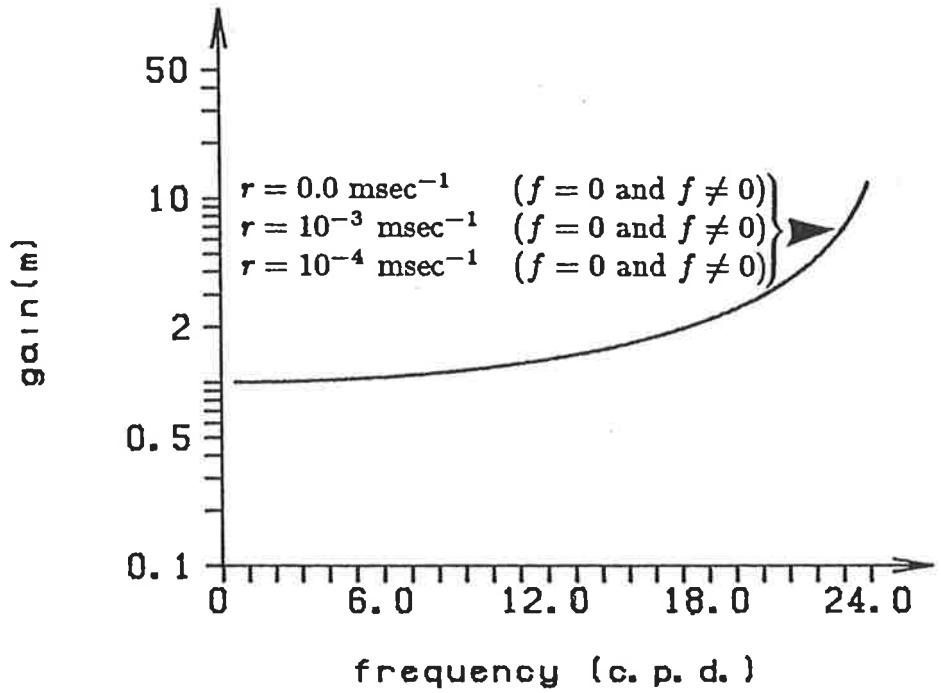

FIGURE 2.5(a): *The gain (m) of the displacement, ζ for the two cases $f \neq 0$ and $f = 0$ for a rectangular basin of length 24 km., breadth 8 km. and depth 20 m.*

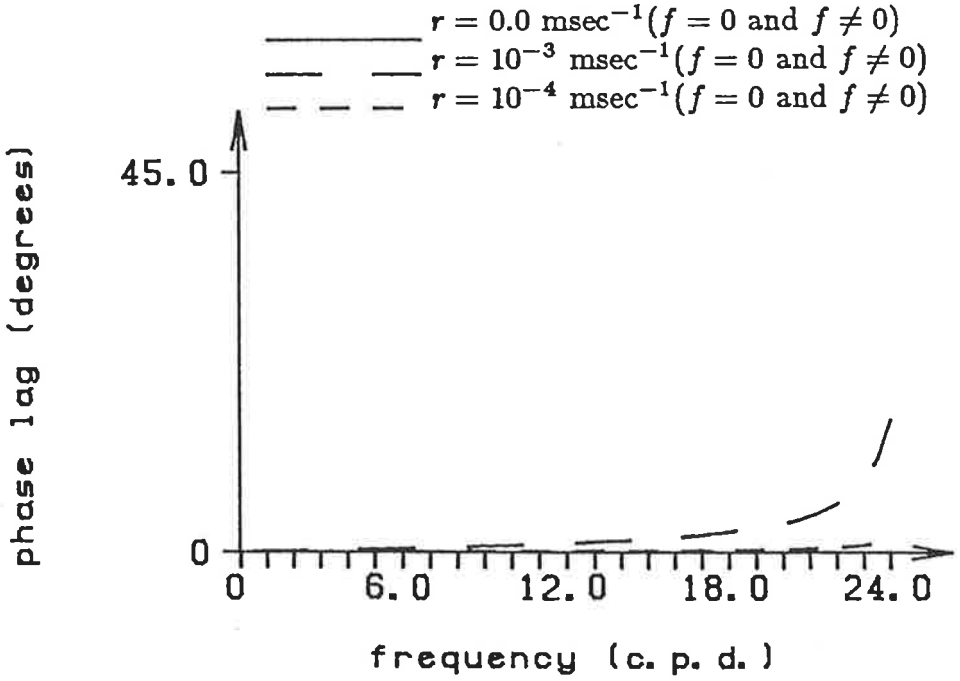

FIGURE 2.5(b): *As in Figure 2.5(a) but for the phase lag.*

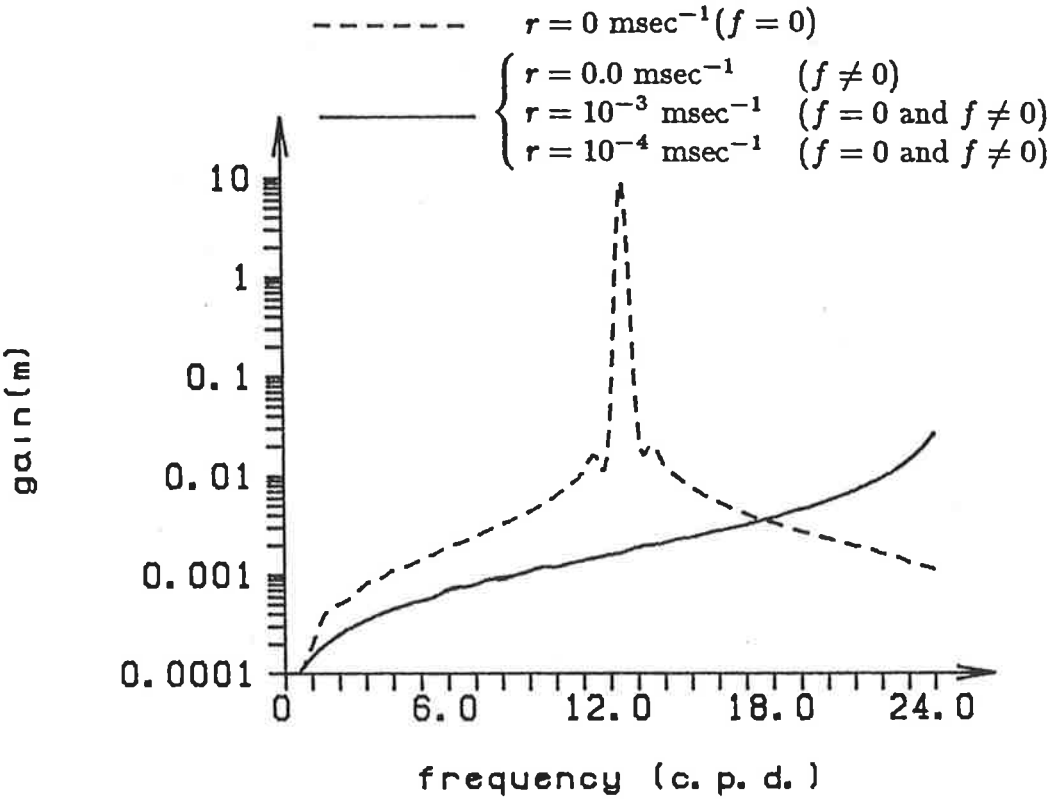

FIGURE 2.6(a): *The gain (m) of the velocity, U, for the two cases $f \neq 0$ and $f = 0$ for a rectangular basin of length 24 km., breadth 8 km. and depth 20 m.*

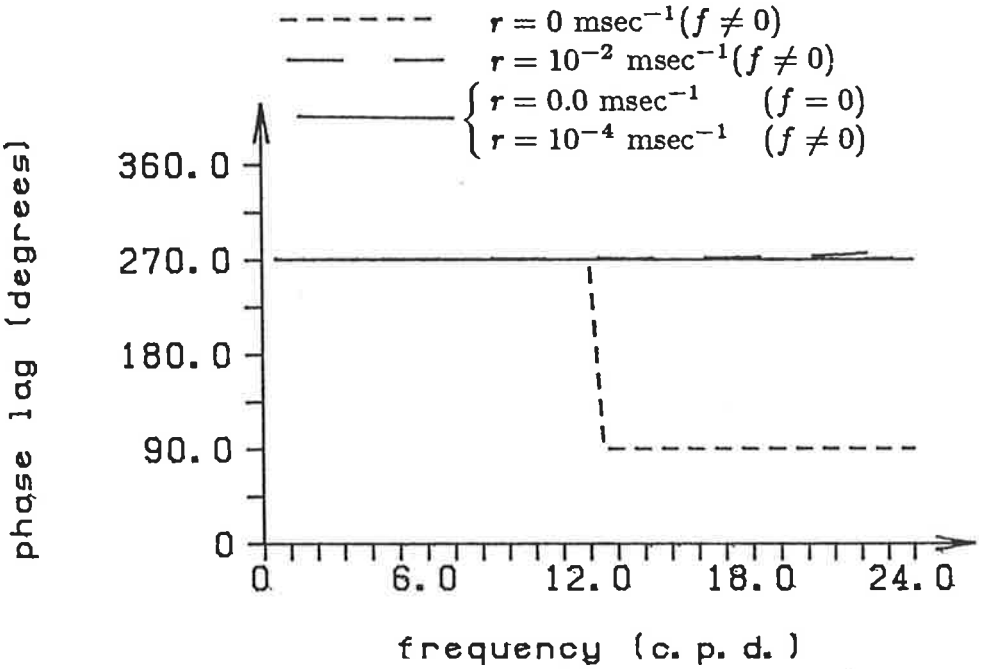

FIGURE 2.6(b): *As in Figure 2.6(a) but for the phase lag.*

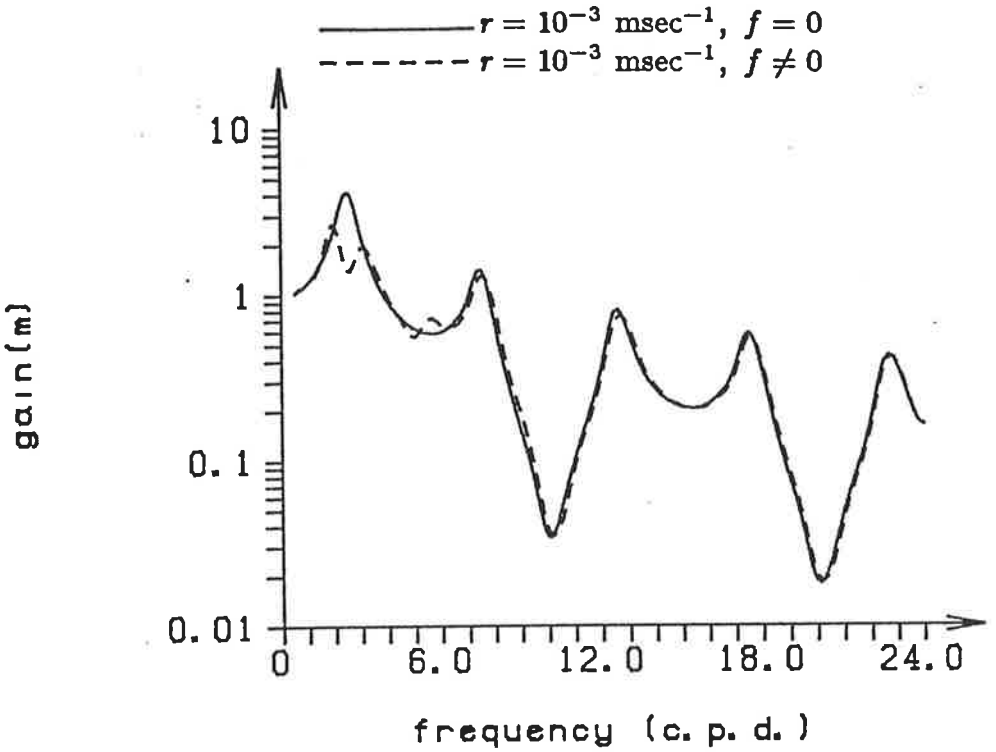

FIGURE 2.7(a): *The gain (m) of the displacement, ς, for the two cases $f \neq 0$ and $f = 0$ for a rectangular basin of length 240 km., breadth 240 km. and depth 20 m.*

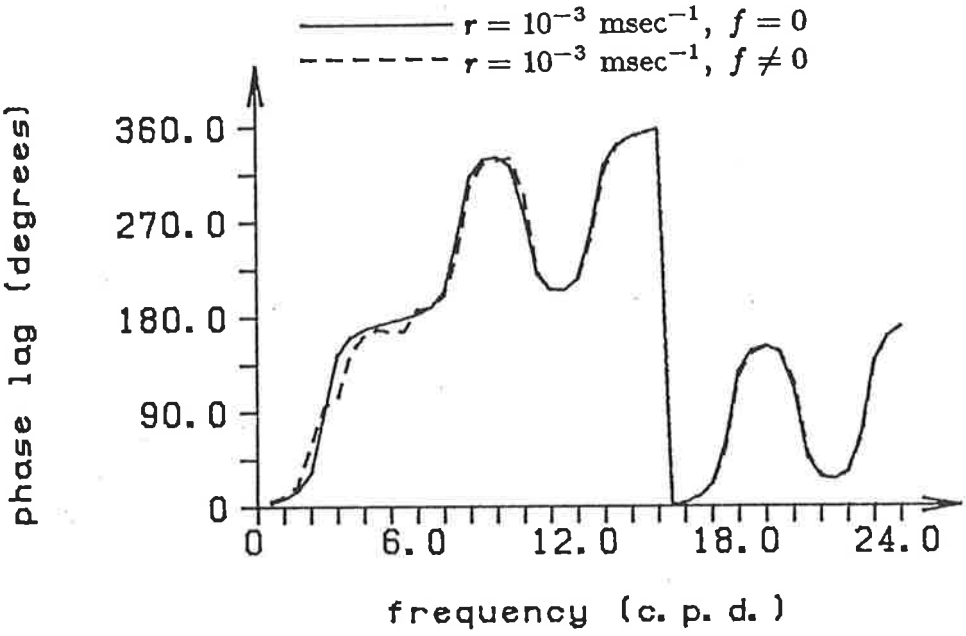

FIGURE 2.7(b): *As in Figure 2.7(a) but for the phase lag.*

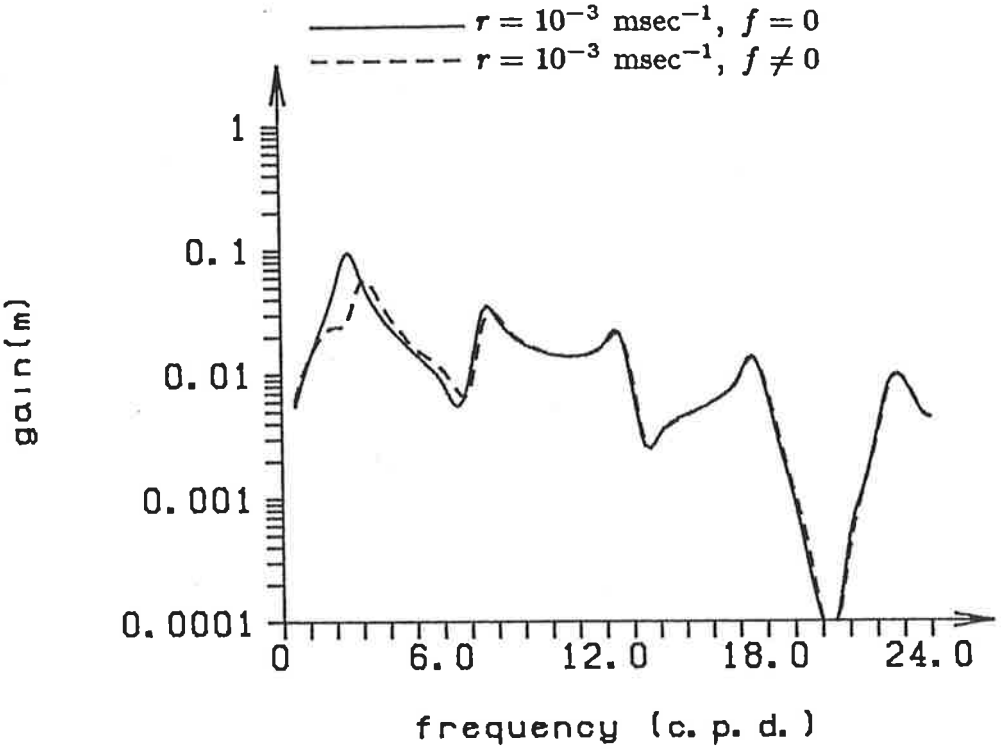

FIGURE 2.8(a): *The gain (m) of the velocity, U, for the two cases $f \neq 0$ and $f = 0$ for a rectangular basin of length 240 km., breadth 240 km. and depth 20 m.*

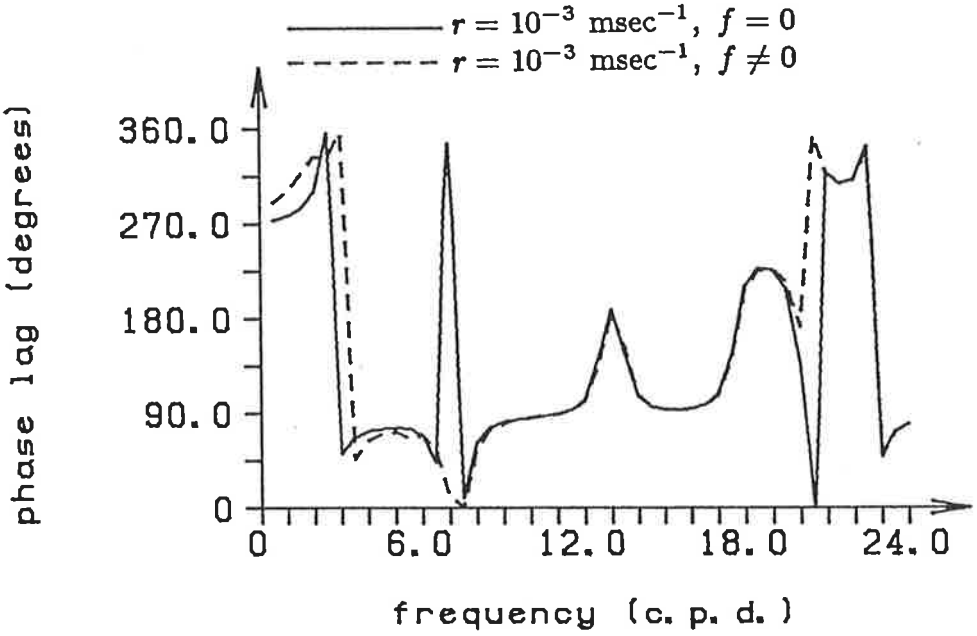

FIGURE 2.8(b): *As in Figure 2.8(a) but for the phase lag.*

identical. However, at the lower end of the frequency spectrum, the results sometimes vary quite considerably. For example, when the frequency is 3 c.p.d. the gain of ζ obtained when $f = 0$ differs by about 2.0 m from that obtained with $f \neq 0$. There is a difference of about 30° on the phase lag at the same frequency. Similar results are displayed in Figure 2.9 which was obtained for a basin of identical horizontal dimensions but with a depth of 50m. Figures 2.8 and 2.10 display the gain and phase lags for U for the two basins. Once again, at the upper end of the frequency spectrum, the two solutions for the gain of U are similar. Large differences occur in the gain at the lower end with the differences being greater for the deeper basin. At the lower of the frequency spectrum, the phase lag of U obtained for the two cases of f can differ quite markedly. From Figure 2.10(b) it is clear that for the deeper basin this difference can be as high as about 45°. In most other points on the frequency spectrum, the solutions agree quite well except near resonance points. The resonance splitting mentioned earlier which occurs at these points results in large differences occurring in the solutions for the phase lag of U.

Results for a basin of similar horizontal dimensions but with a depth of 3 m were also examined. For both ζ and U, the phase lag and gain obtained for $f = 0$ and $f \neq 0$ were identical.

The above discussion illustrates the behaviour of the gain and phase lag of both ζ and U. Clearly for shallow basins of any horizontal dimensions, solutions obtained for ζ and U do not significantly depend on f when the friction parameter

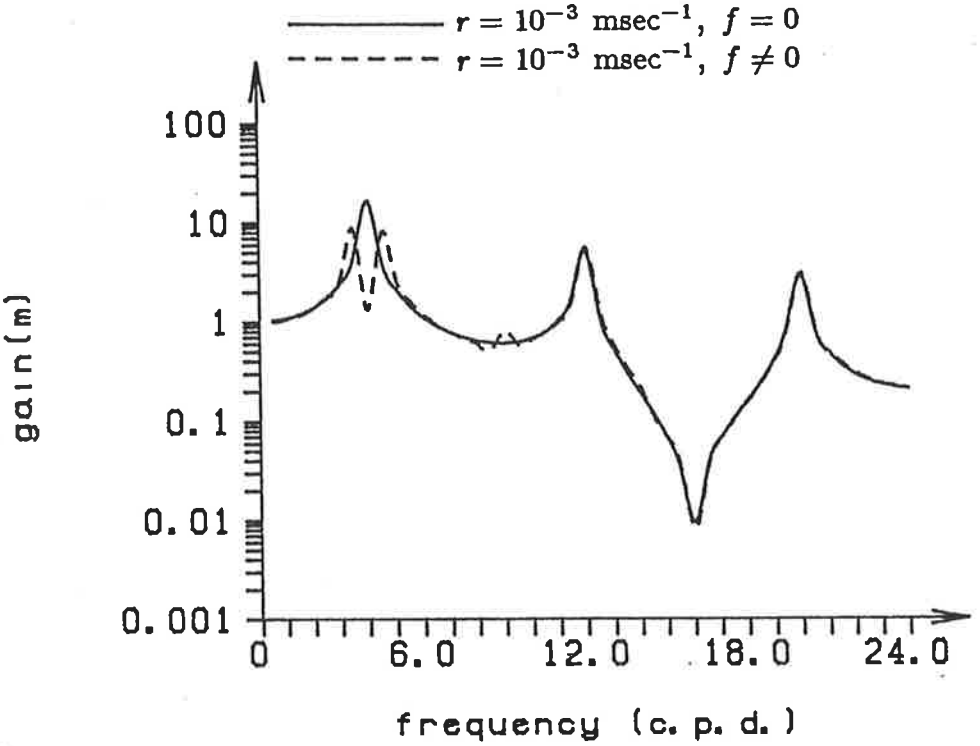

FIGURE 2.9(a): *The gain (m) of the displacement, ς, for the two cases $f \neq 0$ and $f = 0$ for a rectangular basin of length 240 km., breadth 240 km. and depth 50 m.*

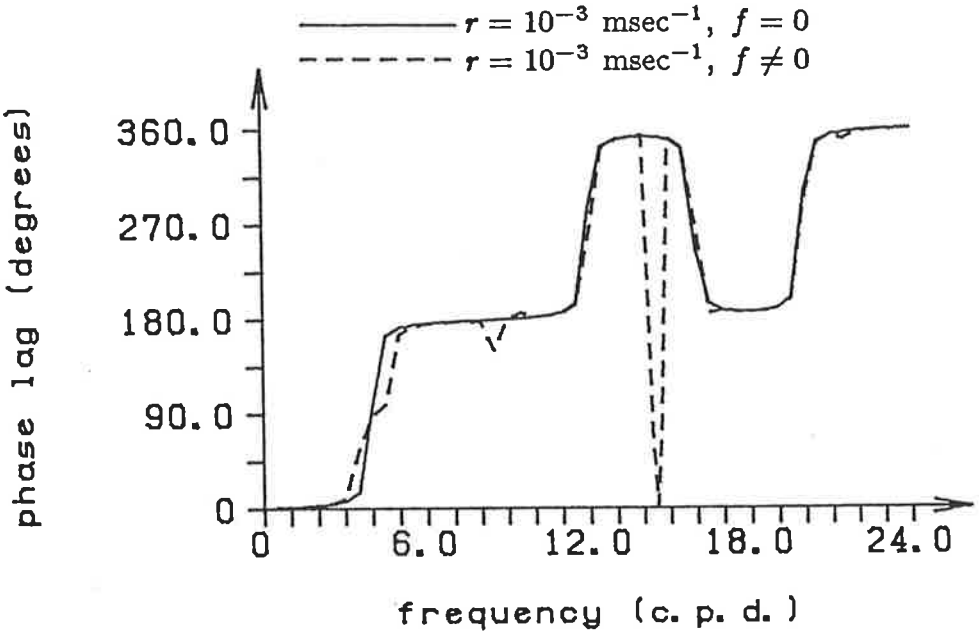

FIGURE 2.9(b): *As in Figure 2.9(a) but for the phase lag.*

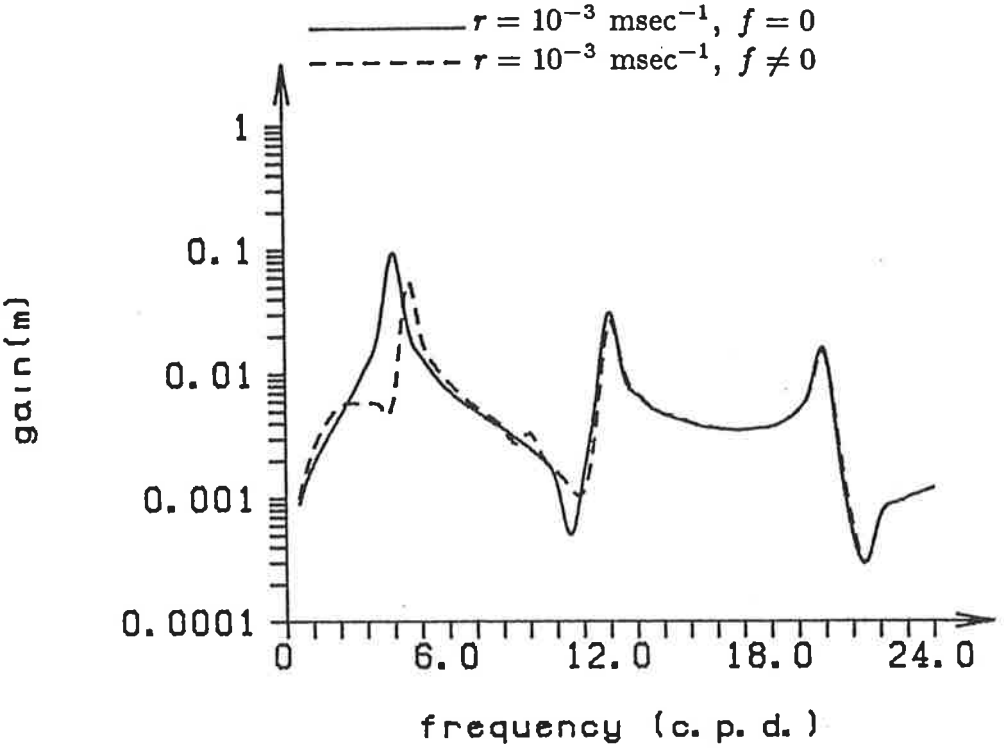

FIGURE 2.10(a): *The gain (m) of the velocity, U, for the two cases $f \neq 0$ and $f = 0$ for a rectangular basin of length 240 km., breadth 240 km. and depth 50 m.*

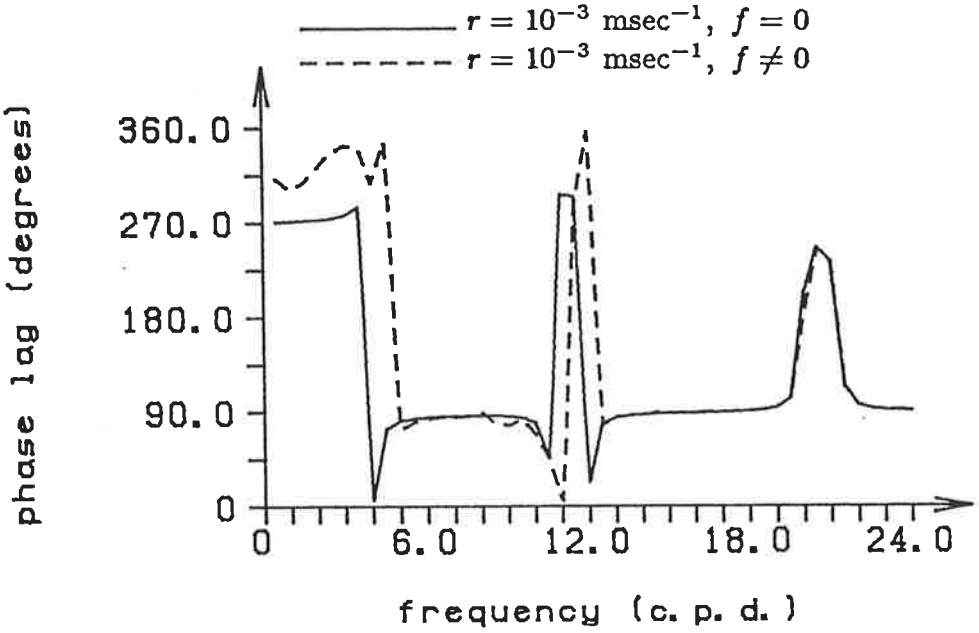

FIGURE 2.10(b): *As in Figure 2.10(a) but for the phase lag.*

is non-zero. The solutions are, however, very dependent on the value of the friction parameter. For deeper basins, however, the results are not as dependent on the friction parameter but different results are obtained depending on whether $f = 0$ or $f \neq 0$. This dependence on depth is expected, since for shallow basins the parameter $\alpha = r/2H$ will be larger than f and so friction effects dominate the flow. However, for deeper water, the parameter α will become comparable to or even less than the magnitude of f and so the flow is affected by both the friction and Coriolis forces, or, if f is larger in magnitude, then the flow is dominated by the Coriolis force. Presented above are situations in which f can and cannot be ignored. Also, figures are displayed which show the way in which the Coriolis force affects the gain and phase lag as the basin gets deeper.

§2.3 The Connected Lake Problem

Consider two rectangular lakes connected by a channel as shown in Figure 2.11. Each of the separate lakes is of constant depth. A solution is sought to the amplitude, ζ, of the oscillating set-up caused when a wind stress described by Equations (2.2.1) and (2.2.9) blows over the surface of the system. Solutions to the transport components are then obtained using Equation (2.2.6).

The basins are labelled 1, 2 or 3 as indicated in Figure 2.11. A similar notation to that used in the previous section is used except that subscripts 1, 2 or 3 indicate to which region a particular variable pertains. For example Z_1 will describe the elevation response function in Region 1, H_2 will be the depth of Region 2 and k_3

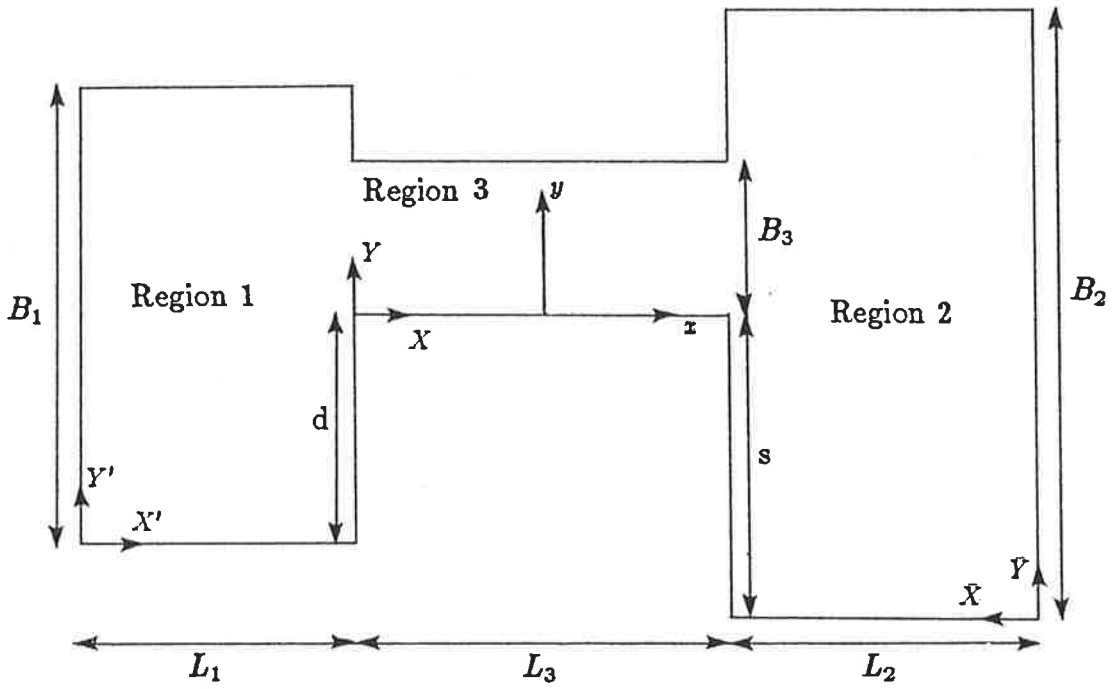

FIGURE 2.11: *The connected lake system showing the coordinate systems* $X - Y$, X'-Y' *and* $\bar{X} - \bar{Y}$, *related to Regions 1, 2 and 3 and the final coordinate system,* $x - y$.

will be the variable described by Equation (2.2.4(b)) using values of the depth and friction appropriate for Region 3.

The method determines expressions for Z_i for i=1,2,3 for each region separately. The solution for each region is obtained relative to separate coordinate systems as shown in Figure 2.11. Once these solutions have been obtained the various expressions are transformed so that they are all in terms of the same coordinate system, namely the $x-y$ system shown in Figure 2.11.

The system of equations which must be solved in order to obtain the amplitude of the surface response of the system is:

$$(\nabla^2 + k_i^2)Z_i = 0 \qquad i = 1,2,3 \tag{2.3.1(a)}$$

subject to the conditions

$$P_1 = 0 \qquad x = -L_3/2 - L_1;\ y \in [-d, B_1 - d], \tag{2.3.1(b)}$$

$$P_1 = \begin{cases} 0 & y \in [-d, 0] \\ P_3 & y \in [0, B_3]; \qquad x = -L_3/2 \\ 0 & y \in [B_3, B_1 - d] \end{cases} \tag{2.3.1(c)}$$

$$Q_1 = 0 \qquad y = B_1 - d;\ x \in [-L_3/2 - L_1, -L_3/2], \tag{2.3.1(d)}$$

$$Q_1 = 0 \qquad y = -d;\ x \in [-L_3/2 - L_1, -L_3/2], \tag{2.3.1(e)}$$

$$Q_3 = 0 \qquad y = B_3;\ x \in [-L_3/2, L_3/2], \tag{2.3.1(f)}$$

$$Q_3 = 0 \qquad y = 0;\ x \in [-L_3/2, L_3/2], \tag{2.3.1(g)}$$

$$Q_2 = 0 \qquad y = B_2 - s;\ x \in [L_3/2, L_3/2 + L_2], \tag{2.3.1(h)}$$

$$Q_2 = 0 \qquad y = -s;\ x \in [L_3/2, L_3/2 + L_2], \tag{2.3.1(i)}$$

$$P_2 = \begin{cases} 0 & y \in [-s, 0] \\ P_3 & y \in [0, B_3]; \qquad x = L_3/2 \\ 0 & y \in [B_3, B_2 - s] \end{cases} \tag{2.3.1(j)}$$

$$P_2 = 0 \qquad x = L_3/2 + L_2;\ y \in [-s, B_2 - s], \tag{2.3.1(k)}$$

$$Z_1 = Z_3 \qquad x = -L_3/2;\ y \in [0, B_3] \tag{2.3.1(l)}$$

and

$$Z_2 = Z_3 \qquad x = L_3/2;\ y \in [0, B_3]. \tag{2.3.1(m)}$$

The conditions above state that the normal component of the depth integrated velocity is zero at any closed boundary and at the open boundaries connecting two regions at $x = -L_3/2$ and $L_3/2$ there is continuity of volume flux and surface amplitude.

Considering the results in the previous section, solutions which ignore the effect of the Coriolis term will be obtained. In the following section the Collocation and Galerkin techniques will be used to provide such solutions whilst in the next chapter it will be shown how to use an integral equation approach to obtain a solution.

§2.4 The Collocation and Galerkin Techniques.

Firstly a solution to the response function, Z_1 which occurs in Region 1 will be obtained. The function Z_1 must satisfy

$$(\nabla^2 + k_1^2)Z_1 = 0 \tag{2.4.1}$$

where k_1 is obtained from Equation (2.2.4(b)) which, with $f = 0$ yields

$$k_j^2 = (\sigma^2 - 2\alpha_j \iota\sigma)/c_j^2 \qquad j = 1, 2, 3 \tag{2.4.2}$$

where $c_j^2 = gh_j$ and α_j denotes the friction parameter appropriate for Region j. Equation (2.4.1) will be solved subject to the conditions (2.3.1(b), (d) and (e)) which, in terms of the X, Y coordinate system shown in Figure 2.11, and with the aid of Equation (2.2.6) may be written as

$$\frac{\partial Z_1}{\partial X} = \frac{K\tau_0}{c_1^2} \qquad X = 0;\ Y \in [0, B_1] \tag{2.4.3(a)}$$

$$\frac{\partial Z_1}{\partial Y} = 0 \qquad Y = 0, B_1;\ X \in [0, L_1]. \tag{2.4.3(b)}$$

The system of Equations (2.4.1) and (2.4.3) may be solved by first simplifying using the expression

$$Z_1 = Z_1^* + \frac{K\tau_0 \sin[k_1(X - L_1/2)]}{c_1^2 k_1 \cos[k_1 L_1/2]}. \tag{2.4.4}$$

Substituting (2.4.4) into Equations (2.4.1) and (2.4.3) yields

$$(\nabla^2 + k_1^2) Z_1^* = 0 \tag{2.4.5(a)}$$

such that

$$\frac{\partial Z_1^*}{\partial X} = 0 \qquad X = 0;\ Y \in [0, B_1] \tag{2.4.5(b)}$$

and

$$\frac{\partial Z_1^*}{\partial Y} = 0 \qquad Y = 0, B_1;\ X \in [0, L_1]. \tag{2.4.5(c)}$$

The general solution to Equation (2.4.5(a)) is obtained using separation of variables. The values of three of the four arbitrary constants resulting from this method may be found using the boundary conditions (2.4.5(b) and (c)). In this manner the following solution to Z_1 is obtained:

$$Z_1 = \frac{K\tau_0 \sin[k_1(X - L_1/2)]}{c_1^2 k_1 \cos[k_1 L_1/2]} + \sum_{n=0}^{\infty} D_n \cosh(\gamma_{1n} X) \cos(\theta_{1n} Y), \tag{2.4.6}$$

where, for $n = 0, 1, 2, \ldots$

$$\gamma_{1n} = \sqrt{\theta_{1n}^2 - k_1^2}, \qquad (2.4.7(a))$$

$$\theta_{1n} = \frac{n\pi}{B_1} \qquad (2.4.7(b))$$

and D_n is an arbitrary constant.

By symmetry, the solution for the elevation in Region 2 with respect to the $\bar{X}$, $\bar{Y}$ coordinate system is

$$Z_2 = \frac{-K\tau_0 \sin[k_2(\bar{X} - L_2/2)]}{c_2^2 k_2 \cos[k_2 L_2/2]} + \sum_{n=0}^{\infty} C_n \cosh(\gamma_{2n}\bar{X}) \cos(\theta_{2n}\bar{Y}), \qquad (2.4.8)$$

where, for $n = 0, 1, 2, \ldots$

$$\gamma_{2n} = \sqrt{\theta_{2n}^2 - k_2^2}, \qquad (2.4.9(a))$$

$$\theta_{2n} = \frac{n\pi}{B_2} \qquad (2.4.9(b))$$

and C_n is an arbitrary constant. This solution satisfies the conditions given by Equations (2.3.1(h),(i) and (k)).

The solution for the elevation in Region 3 is

$$\begin{aligned} Z_3 = & \frac{K\tau_0 \sin[k_3(X' - L_3/2)]}{c_3^2 k_3 \cos[k_3 L_3/2]} \\ & + \sum_{n=0}^{\infty} (A_n \cosh(\gamma_{3n}X') + B_n \sinh(\gamma_{3n}X')) \cos(\theta_{3n}Y') \end{aligned} \qquad (2.4.10)$$

in which A_n and B_n are constant coefficients and, for $n = 0, 1, 2, \ldots$,

$$\gamma_{3n} = \sqrt{\theta_{3n}^2 - k_3^2}, \qquad (2.4.11(a))$$

and

$$\theta_{3n} = \frac{n\pi}{B_3}. \qquad (2.4.11(b))$$

This solution was obtained using separation of variables and satisfies boundary conditions (2.3.1(f) and (g)).

Using the coordinate transformations

$$X = x + L_1 + L_3/2, \qquad (2.4.12(a))$$

$$Y = y + d, \qquad (2.4.12(b))$$

$$\bar{X} = L_3/2 + L_2 - x, \qquad (2.4.12(c))$$

$$\bar{Y} = y + s, \qquad (2.4.12(d))$$

$$X' = x + L_3/2 \qquad (2.4.12(e))$$

and

$$Y' = y, \qquad (2.4.12(f))$$

Equations (2.4.6, 2.4.8 and 2.4.10) may be written in terms of the $x-y$ coordinate system as follows:

$$Z_1 = \frac{K\tau_0 \sin[k_1(x + L_1/2 + L_3/2)]}{c_1^2 k_1 \cos[k_1 L_1/2]} + \sum_{n=0}^{\infty} D_n \cosh[\gamma_{1n}(x + L_1 + L_3/2)] \cos[\theta_{1n}(y + d)], \qquad (2.4.13(a))$$

$$Z_2 = -\frac{K\tau_0 \sin[k_2(L_3/2 + L_2/2 - x)]}{c_2^2 k_2 \cos[k_2 L_2/2]} + \sum_{n=0}^{\infty} C_n \cosh[\gamma_{2n}(L_3/2 + L_2 - x)] \cos[\theta_{2n}(y + s)] \qquad (2.4.13(b))$$

and

$$Z_3 = \frac{K\tau_0 \sin[k_3 x]}{c_3^2 k_3 \cos[k_3 L_3/2]} + \sum_{n=0}^{\infty}\Big(A_n \cosh[\gamma_{3n}(x + L_3/2)] + B_n \sinh[\gamma_{3n}(x + L_3/2)]\Big)\cos(\theta_{3n} y). \qquad (2.4.13(c))$$

Using Equation (2.2.6) with $f = 0$ enables expressions for the depth integrated velocity components in each region to be obtained. The following equations result:

$$P_1 = \frac{K\tau_0}{\beta_1}\left\{1 - \frac{\cos[k_1(x + L_1/2 + L_3/2)]}{\cos[k_1 L_1/2]}\right\} - \frac{c_1^2}{\beta_1}\sum_{n=0}^{\infty} D_n \gamma_{1n} \sinh[\gamma_{1n}(x + L_1 + L_3/2)]\cos[\theta_{1n}(y + d)], \qquad (2.4.14(a))$$

$$Q_1 = \frac{c_1^2}{\beta_1}\sum_{n=0}^{\infty} D_n \theta_{1n} \cosh[\gamma_{1n}(x + L_1 + L_3/2)]\sin[\theta_{1n}(y + d)], \qquad (2.4.14(b))$$

$$P_2 = \frac{K\tau_0}{\beta_2}\left\{1 - \frac{\cos[k_2(L_3/2 + L_2/2 - x)]}{\cos[k_2 L_2/2]}\right\} + \frac{c_2^2}{\beta_2}\sum_{n=0}^{\infty} C_n \gamma_{2n} \sinh[\gamma_{2n}(L_3/2 + L_2 - x)]\cos[\theta_{2n}(y + s)], \qquad (2.4.15(a))$$

$$Q_2 = \frac{c_2^2}{\beta_2}\sum_{n=0}^{\infty} C_n \theta_{2n} \cosh[\gamma_{2n}(L_3/2 + L_2 - x)]\sin[\theta_{2n}(y + s)], \qquad (2.4.15(b))$$

$$P_3 = \frac{K\tau_0}{\beta_3}\left\{1 - \frac{\cos[k_3 x]}{\cos[k_3 L_3/2]}\right\} - \frac{c_3^2}{\beta_3}\sum_{n=0}^{\infty}\Big(A_n \gamma_{3n} \sinh[\gamma_{3n}(x + L_3/2)] + B_n \gamma_{3n} \cosh[\gamma_{3n}(x + L_3/2)]\Big)\cos(\theta_{3n} y) \qquad (2.4.16(a))$$

and

$$Q_3 = \frac{c_3^2}{\beta_3}\sum_{n=0}^{\infty}\Big(A_n \cosh[\gamma_{3n}(x + L_3/2)] + B_n \sinh[\gamma_{3n}(x + L_3/2)]\Big)\theta_{3n} \sin(\theta_{3n} y). \qquad (2.4.16(b))$$

Not all of the conditions listed in Equation (2.3.1) are satisfied by the above

expressions for the elevation and transport, which still involve as yet unknown complex coefficients. The conditions which remain to be satisfied are:

(1) continuity of elevation at $x = -L_3/2;\ y \in [0, B_3]$, that is,

$$Z_1 = Z_3 \qquad \text{at } x = -L_3/2;\ y \in [0, B_3], \tag{2.4.17(a)}$$

(2) continuity of elevation at $x = L_3/2;\ y \in [0, B_3]$, that is,

$$Z_2 = Z_3 \qquad \text{at } x = L_3/2;\ y \in [0, B_3], \tag{2.4.17(b)}$$

(3) continuity of transport at $x = -L_3/2;\ y \in [0, B_3]$, that is,

$$P_1 = \begin{cases} 0 & y \in [-d, 0] \\ P_3 & y \in [0, B_3]; \\ 0 & y \in [B_3, B_1 - d] \end{cases} \qquad x = -L_3/2 \tag{2.4.17(c)}$$

(4) continuity of transport at $x = L_3/2;\ y \in [0, B_3]$, that is,

$$P_2 = \begin{cases} 0 & y \in [-s, 0] \\ P_3 & y \in [0, B_3]; \\ 0 & y \in [B_3, B_1 - s] \end{cases} \qquad x = L_3/2 \tag{2.4.17(d)}$$

An approximation technique must be used to enable the above conditions to be satisfied and the unknown coefficients which appear in Equation (2.4.13) to be determined. The Collocation and Galerkin methods will be used here. Each of the series expressions for the elevations or velocties is truncated after N terms. Applying the four conditions above yields a system $4N$ simultaneous linear equations in the $4N$ unknown coefficients A_n, B_n, C_n, and D_n, for $n = 0, \ldots, N-1$. The four conditions are now treated in turn.

(1) The condition $Z_1 = Z_3$ at $x = -L_3/2$; $y \in [0, B_3]$.

Using Equations (2.4.13(a) and (c)) with the series terms truncated as mentioned above and substituting the value of $x = -L_3/2$ for x yields

$$\frac{K\tau_0}{c_1^2 k_1}\tan(k_1 L_1/2) + D_0\cosh(\gamma_{10}L_1) + \sum_{n=1}^{N-1} D_n \cosh(\gamma_{1n}L_1)\cos[\theta_{1n}(y+d)]$$
$$= -\frac{K\tau_0}{c_3^2 k_3}\tan(k_3 L_3/2) + A_0 + \sum_{n=1}^{N-1} A_n \cos(\theta_{3n}y) \tag{2.4.18}$$

for $y \in [0, B_3]$.

The Collocation technique consists of substituting suitable values for y into Equation (2.4.17) thus giving an equation in the unknowns A_n and D_n for $n = 0, \ldots, N-1$. A total of N values of y would be used to ensure that the correct number of equations needed to obtain a solution for the unknowns is obtained.

The Galerkin technique operates further on Equation (2.4.18). The above equation is multiplied by the weighting functions $\omega_m(y) = \cos(\theta_{3m}y)$ for $m = 0, \ldots, N-1$ and then integrated with respect to y from $y = 0$ to B_3. This procedure yields the equations

$$\frac{B_3 A_m}{2} = \sum_{\substack{n=1 \\ n\neq J}}^{N-1} D_n \frac{\theta_{1n}}{\theta_{1n}^2 - \theta_{3m}^2}\cosh(\gamma_{1n}L_1)\{(-1)^m \sin[\theta_{1n}(B_3+d)] - \sin(\theta_{1n}d)\}$$
$$+ D_J \frac{\cosh(\gamma_{1J}L_1)}{2\theta_{1J}}\{\theta_{1J}B_3\cos(\theta_{1J}d) + \cos[\theta_{1J}(B_3+d)]\sin(2\theta_{1J}B_3)\} \tag{2.4.19(a)}$$

where

$$m = 1, \ldots, N-1$$

and J is such that

$$\frac{J}{B_1} = \frac{m}{B_3}$$

The condition described above involving J is required in case $\theta_{1n} = \theta_{3m}$ in which case the summation term above becomes undefined. A similar equation to Equation (2.4.19(a)) is obtained for $m = 0$ and is

$$\left\{\frac{K\tau_0}{c_1^2 k_1}\tan(k_1 L_1/2) + D_0\cos(k_1 L_1)\right\} B_3$$
$$+ \sum_{n=1}^{N-1} D_n \frac{\cosh(\gamma_{1n} L_1)}{\theta_{1n}} \{\sin[\theta_{1n}(B_3 + d)] - \sin(\theta_{1n} d)\} \qquad (2.4.19(b))$$
$$= \left\{-\frac{K\tau_0}{c_3^2 k_3}\tan(k_3 L_3/2) + A_0\right\} B_3.$$

(2) The condition $Z_2 = Z_3$ at $x = L_3/2;\ y \in [0, B_3]$.

In a similar manner to the process used above, Equations (2.4.13(b) and (c)) are used to give

$$-\frac{K\tau_0}{c_2^2 k_2}\tan(k_2 L_2/2) + C_0\cosh(\gamma_{20} L_2) + \sum_{n=1}^{N-1} C_n \cosh(\gamma_{2n} L_2)\cos[\theta_{2n}(y + s)]$$
$$= \frac{K\tau_0}{c_3^2 k_3}\tan(k_3 L_3/2) + A_0\cosh(\gamma_{30} L_3) + B_0\sinh(\gamma_{30} L_3)$$
$$+ \sum_{n=1}^{N-1} \{A_n\cosh(\gamma_{3n} L_3) + B_n\sinh(\gamma_{3n} L_3)\}\cos(\theta_{3n} y), \qquad (2.4.20)$$

which holds for all $y \in [0, B_3]$. As before, the above equation is the one used in conjunction with N y points in the Collocation method. Application of the weighting functions $\cos(\theta_{3m} y)$ for $m = 0, \ldots, N-1$ yields

$$\frac{B_3}{2}\{A_m\cosh(\gamma_{3m} L_3) + B_m\sinh(\gamma_{3m} L_3)\}$$
$$= \sum_{\substack{n=1 \\ n \neq J}}^{N-1} C_n \frac{\theta_{2n}}{\theta_{2n}^2 - \theta_{3m}^2}\cosh(\gamma_{2n} L_2)\{(-1)^m \sin[\theta_{2n}(B_3 + s)] - \sin(\theta_{2n} s)\}$$
$$+ C_J \frac{\cosh(\gamma_{2J} L_2)}{2\theta_{2J}}\{\theta_{2J} B_3\cos(\theta_{2J} s) + \cos[\theta_{2J}(B_3 + s)]\sin(2\theta_{2J} B_3)\} \qquad (2.4.21(a))$$

where

$$m = 1, \ldots, N-1,$$

$$\frac{J}{B_2} = \frac{m}{B_3}$$

and also

$$\begin{aligned}
&\left\{ -\frac{K\tau_0}{c_2^2 k_2} \tan(k_2 L_2/2) + C_0 \cos(k_2 L_2) \right\} B_3 \\
&+ \sum_{n=1}^{N-1} C_n \frac{\cosh(\gamma_{2n} L_2)}{\theta_{2n}} \{\sin[\theta_{2n}(B_3 + s)] - \sin(\theta_{2n} s)\} \qquad (2.4.21(b)) \\
&= \left\{ \frac{K\tau_0}{c_3^2 k_3} \tan(k_3 L_3/2) + A_0 \cos(k_3 L_3) + \iota B_0 \sin(k_3 L_3) \right\} B_3.
\end{aligned}$$

(3) The condition $P_1 = \begin{cases} 0 & y \in [-d, 0] \\ P_3 & y \in [0, B_3]; \\ 0 & y \in [B_3, B_1 - d] \end{cases} \qquad x = -L_3/2.$

Utilising Equations (2.4.14(a)) and (2.4.16(a)) yields

$$\begin{aligned}
&\frac{c_1^2}{\beta_1} \left\{ -D_0 k_1 \sin(k_1 L_1) + \sum_{n=1}^{N-1} D_n \gamma_{1n} \sinh(\gamma_{1n} L_1) \cos[\theta_{1n}(y + d)] \right\} \\
&= \begin{cases} 0 & y \in [-d, 0] \\ \frac{c_3^2}{\beta_3} \left\{ B_0 k_3 \iota + \sum_{n=1}^{N-1} B_n \gamma_{3n} \cos(\theta_{3n} y) \right\} & y \in [0, B_3] \\ 0 & y \in [B_3, B_1 - d] \end{cases} \qquad (2.4.22)
\end{aligned}$$

Multiplying the above equation by the weighting functions $\cos[\theta_{1m}(y + d)]$ and then integrating with respect to y from $y = -d$ to $y = B_1 - d$ gives the two equations used in the Galerkin technique, namely,

$$\begin{aligned}
&\frac{c_1^2 B_1}{2\beta_1} \gamma_{1m} \sinh(\gamma_{1m} L_1) D_m = \\
&\frac{c_3^2}{\beta_3} \left\{ \sum_{\substack{n=1 \\ n \neq J}}^{N-1} B_n \frac{\gamma_{3n} \theta_{1m}}{\theta_{1m}^2 - \theta_{3n}^2} [(-1)^m \sin[\theta_{1m}(B_3 + d)] - \sin(\theta_{1m} d)] \right. \qquad (2.4.23(a)) \\
&\left. + B_J \frac{\gamma_{3J}}{2\theta_{1J}} [\theta_{1J} B_3 \cos(\theta_{1J} d) + \cos[\theta_{1J}(B_3 + d)] \sin(2\theta_{1J} B_3)] \right\}
\end{aligned}$$

in which

$$m = 1, \ldots, N-1,$$

and J such that

$$\frac{J}{B_1} = \frac{m}{B_3},$$

and also the equation

$$-\frac{c_1^2 k_1 B_1}{\beta_1} \sin(k_1 L_1) D_0 = \frac{\iota c_3^2 B_3 k_3}{\beta_3} B_0. \qquad (2.4.23(b))$$

(4) The condition $P_2 = \begin{cases} 0 & y \in [-s, 0] \\ P_3 & y \in [0, B_3]; \\ 0 & y \in [B_3, B_1 - s] \end{cases} \quad x = L_3/2.$

Combining this condition with Equations (2.4.15(a)) and (2.4.16(a)) yields

$$\frac{c_2^2}{\beta_2} \left\{ -C_0 k_2 \sin(k_2 L_2) + \sum_{n=1}^{N-1} C_n \gamma_{2n} \sinh(\gamma_{2n} L_2) \cos[\theta_{2n}(y+s)] \right\}$$

$$= \begin{cases} 0 & y \in [-s, 0] \\ \frac{-c_3^2}{\beta_3} \Big\{ -A_0 k_3 \sin(k_3 L_3) + B_0 k_3 \iota \cos(k_3 L_3) & \\ + \sum_{n=1}^{N-1} \gamma_{3n} \left[A_n \sinh(\gamma_{3n} L_3) + B_n \cosh(\gamma_{3n} L_3) \right] \cos(\theta_{3n} y) \Big\} & y \in [0, B_3] \\ 0 & y \in [B_3, B_2 - s] \end{cases} \qquad (2.4.24)$$

Using the weighting functions $\cos[\theta_{2m}(y+s)]$ and integrating with respect to y from $y = -s$ to $y = B_2 - s$ yields

$$\frac{c_2^2 B_2}{2\beta_2} \gamma_{2m} \sinh(\gamma_{2m} L_2) C_m =$$

$$-\frac{c_3^2}{\beta_3} \Bigg\{ \sum_{\substack{n=1 \\ n \neq J}}^{N-1} \gamma_{3n} \left[A_n \sinh(\gamma_{3n} L_3) + B_n \cosh(\gamma_{3n} L_3) \right] \cdot$$

$$\frac{\theta_{2m}}{\theta_{2m}^2 - \theta_{3n}^2} \left[(-1)^m \sin[\theta_{2m}(B_3 + s)] - \sin(\theta_{2m} s) \right] \qquad (2.4.25(a))$$

$$+ \frac{\gamma_{3J}}{2\theta_{2J}} \left[A_J \sinh(\gamma_{3J} L_3) + B_J \cosh(\gamma_{3J} L_3) \right] \cdot$$

$$\left[\theta_{2J} B_3 \cos(\theta_{2J} s) + \cos[\theta_{2J}(B_3 + s)] \right] \sin(2\theta_{2J} B_3) \Bigg\}$$

for

$$m = 1, \ldots, N-1,$$

$$\frac{J}{B_2} = \frac{m}{B_3}$$

and also

$$\frac{c_2^2 k_2 B_2}{\beta_2} \sin(k_2 L_2) C_0 = \frac{c_3^2 B_3 k_3}{\beta_3} \left[-A_0 \sin(k_3 L_3) + \iota B_0 \cos(k_3 L_3) \right]. \quad (2.4.25(b))$$

The $4N$ unknowns may now be determined using either Equations (2.4.19, 2.4.21, 2.4.23 and 2.4.25) or Equations (2.4.18, 2.4.20, 2.4.22, and 2.4.24) together with a complex matrix inversion routine. Results are presented in Chapter 4 where comparisons are made with the boundary integral equation method which will be described in the next chapter.

CHAPTER 3

BOUNDARY INTEGRAL SOLUTION

§3.1 DERIVATION OF THE SOLUTION

A generalized theory for determining the time varying wind effects on a lake of arbitrary contour, $\partial\Gamma$, and constant depth, H, will now be developed. The effect of the earth's rotation will be neglected. The following results are a considerable improvement on solutions used before (for example, see Walsh (1974)) in which basins were approximated by rectangles or circles.

As has been shown in the previous chapter, when a wind stress defined by

$$\tau_{sx} = \tau_0 e^{i\sigma t}, \qquad (3.1.1(a))$$

$$\tau_{sy} = 0 \qquad (3.1.1(b))$$

acts over the surface of a non-rotating constant depth basin, then the amplitude, Z, of the surface displacement satisfies the Helmholtz equation given by

$$(\nabla^2 + k^2)Z = 0 \qquad (3.1.2)$$

where k^2 is given by Equation (2.2.4(b)) with $f = 0$. For an arbitrary shaped basin, the boundary condition for the above equation is given as (see Walsh (1974))

$$\left.\frac{\partial Z}{\partial n}\right|_{\partial\Gamma} = \left.\frac{K\tau_{0n}}{c^2}\right|_{\partial\Gamma} \qquad (3.1.3)$$

where n denotes the outward normal direction and τ_{0n} signifies the amplitude of wind stress in that direction.

The use of integral equations to solve systems of equations like Equation (3.1.2) and (3.1.3) has been largely ignored by workers in fields examining wind forced or tidal flows. However, because of the linearity of Equation (3.1.2), the above problem can be readily reduced to a boundary integral equation.

Helmholtz's Equation frequently occurs in the fields of electromagnetism and acoustics. Some of the first workers to publish results pertaining to this equation were Banaugh and Goldsmith (1963) who looked at the diffraction of acoustic waves caused by surfaces of arbitary shape. Hwang and Tuck (1970) and Lee (1971) have also investigated the oscillations of harbours of constant depth and arbitrary shape by studying this equation.

The development of the solution to Equation (3.1.2) subject to Equation (3.1.3) is now briefly described. Detailed descriptions of the method of solution can be found in Banaugh and Goldsmith (1963) and Lee (1969 and 1971).

Using Green's Theorem, a solution to Equation (3.1.2), known as Weber's solution, is (see Banaugh and Goldsmith (1963))

$$Z(\mathbf{x_i}) = -\frac{\iota}{4}\int_{\partial\Gamma}\left(Z\frac{\partial}{\partial n}H_0^{(1)}(kr) - H_0^{(1)}(kr)\frac{\partial Z}{\partial n}\right)dS \qquad (3.1.4)$$

where $\mathbf{x_i} = (x, y)$ defines some point inside the domain bounded by $\partial\Gamma$, r is the distance between this interior point and any point on the boundary, dS is a small

incremental distance along the boundary and $H_0^{(1)}(kr)$ is the Hankel function of the first kind and zero order. Equation (3.1.4) thus represents an expression for the amplitude, Z, at any point inside the region of interest in terms of an integral around the boundary. In fact, the term on the right hand side of Equation (3.1.4) represents a distribution of sources and sinks and doublets around the boundary.

All of the terms contained in the integrand in Equation (3.1.4) are known except for the value of Z along the boundary, $\partial\Gamma$. An expression for Z along the boundary is obtained also using Equation (3.1.4). An interior point, $\mathbf{x_i}$, is allowed to approach the boundary at a point, $\mathbf{x_0}$. The path of integration along $\partial\Gamma$ is then deformed around $\mathbf{x_0}$ using a small circle of radius ϵ and centre $\mathbf{x_0}$. For such a contour, Equation (3.1.4) may now be used by letting $\epsilon \rightarrow 0$ in conjunction with integration in the Cauchy sense to provide an expression for $Z(\mathbf{x_0})$. Such a procedure is described in Lee (1969) and results in the following expression

$$Z(\mathbf{x_0}) = -\frac{\iota}{2}\int_{\partial\Gamma}\left(Z(\mathbf{x_0'})\frac{\partial}{\partial n}H_0^{(1)}(kr) - H_0^{(1)}(kr)\frac{\partial}{\partial n}Z(\mathbf{x_0'})\right)dS(\mathbf{x_0'}) \qquad (3.1.5)$$

where $\mathbf{x_0}$ and $\mathbf{x_0'}$ are points on $\partial\Gamma$ and r is the distance between the particular point $\mathbf{x_0}$ on the boundary and all points $\mathbf{x_0'}$ which also lie on the boundary. The above formula holds if the boundary is sectionally smooth. If the point $\mathbf{x_0}$ is a corner point then a slightly modified formula is used (see, for example, Lee (1969)).

Equation (3.1.5) represents an integral equation which, in general, must be solved numerically. The boundary, $\partial\Gamma$, is divided into N segments of length $(\Delta S)_j$ for $j = 1, \ldots, N$. These segments need not be of uniform length. If the midpoint

of $(\Delta S)_j$ is $\mathbf{x_j} = (x_j, y_j)$ then Equation (3.1.5) may be approximated by

$$Z(\mathbf{x_0}) = -\frac{\iota}{2}\sum_{j=1}^{N}\left\{Z(\mathbf{x_j})\frac{\partial}{\partial n}H_0^{(1)}(kr_{0j}) - H_0^{(1)}(kr_{0j})\frac{\partial}{\partial n}Z(\mathbf{x_j})\right\}(\Delta S)_j \qquad (3.1.6)$$

where

$$r_{0j} = |\mathbf{x_0} - \mathbf{x_j}| = r_{j0}.$$

The above equation is more conveniently written in the matrix form

$$\left(-\frac{\iota}{2}H_n - I\right)\mathbf{Z_b} = -\frac{\iota}{2}H\mathbf{Z_n} \qquad (3.1.7)$$

where

$$(\mathbf{Z_b})_j = Z(\mathbf{x_j}) \qquad j = 1, \ldots, N$$

is a vector of the unknown values of Z at the point $\mathbf{x_j}$ on the boundary,

$$(H_n)_{ij} = \frac{\partial}{\partial n}H_0^{(1)}(kr_{ij})(\Delta S)_j \qquad i, j = 1, \ldots, N$$

is an N x N matrix containing the normal derivatives of the Hankel function and $r_{ij} = |\mathbf{x_i} - \mathbf{x_j}|$ where $\mathbf{x_i}$ and $\mathbf{x_j}$ are both points on the boundary,

$$(\mathbf{Z_n})_j = \frac{\partial}{\partial n}Z(\mathbf{x_j}) \qquad j = 1, \ldots, N$$

is a vector containing the normal derivative of Z at points along the boundary (this information is available from Equation (3.1.3)),

$$(H)_{ij} = H_0^{(1)}(kr_{ij})(\Delta S)_j \qquad i, j = 1, \ldots, N$$

is an N x N matrix similar to H_n and

$$(I)_{ij} = \delta_{ij} \qquad i, j = 1, \ldots, N$$

is the N x N identity matrix where δ_{ij} is 1 if $i = j$ but is zero otherwise.

By using a matrix inversion routine, Equation (3.1.7) may be used to solve for Z along the boundary. A similar approximation to that shown in Equation (3.1.6) is used for Equation (3.1.4) and in this manner a complete solution for Z is obtained at any point inside the arbitrary contour $\partial\Gamma$. The solution for Z at an interior point, $\mathbf{x_i} = (x, y)$, is, therefore,

$$Z(\mathbf{x_i}) = -\frac{\iota}{4}\sum_{j=1}^{N}\left\{Z(\mathbf{x_0})\frac{\partial}{\partial n}H_0^{(1)}(kr_{ij}) - H_0^{(1)}(kr_{ij})\frac{\partial}{\partial n}Z(\mathbf{x_0})\right\}(\Delta S(\mathbf{x_0}))_j \quad (3.1.8)$$

where

$$r_{ij} = |\mathbf{x} - \mathbf{x_0}|.$$

The elements which appear in the matrices defined above are all easily calculated except for those expressions involving Hankel functions. Difficulties with using these functions have been overcome, however, by workers such as Banaugh and Goldsmith(1963) and Lee(1979) and their formulations will be used in this work.

Similar expressions to Equation(3.1.4) are available for the depth integrated velocity components, P and Q. Substituting Equation (3.1.4) into Equation (2.2.6(a) and (b)) with $f = 0$ yields

$$P(\mathbf{x_i}) = \frac{K\tau_0}{\beta} + \frac{\iota c^2}{4\beta}\int_{\partial\Gamma}\left\{Z(\mathbf{x_0})\frac{\partial}{\partial n}\left[\frac{-kH^{(1)}(kr_{ij})(x - x_0)}{r_{ij}}\right]\right.$$
$$\left. + \frac{kH^{(1)}(kr_{ij})(x - x_0)}{r_{ij}}\frac{\partial}{\partial n}Z(\mathbf{x_0})\right\}dS(\mathbf{x_0}) \qquad (3.1.9(a))$$

and

$$Q(\mathbf{x}_i) = \frac{\iota c^2}{4\beta} \int_{\partial\Gamma} \left\{ Z(\mathbf{x}_0) \frac{\partial}{\partial n} \left[\frac{-kH^{(1)}(kr_{ij})(y - y_0)}{r_{ij}} \right] \right.$$
$$\left. + \frac{kH^{(1)}(kr_{ij})(y - y_0)}{r_{ij}} \frac{\partial}{\partial n} Z(\mathbf{x}_0) \right\} dS(\mathbf{x}_0). \qquad (3.1.9(b))$$

Each of the above formulae may be discretised in a manner similar to that used to form Equation (3.1.8).

§3.2 Comparison With Analytic Solutions

The performance of the model described in the previous section will be examined by comparing the results produced by Equation (3.1.8) with those produced from analytic solutions for special shapes such as rectangles and circles. As mentioned in Chapter 2, the response function, Z, of the surface oscillation which occurs in a rectangular lake when a wind stress described by Equation (3.1.1) blows over its surface, is

$$Z = \frac{K\tau_0 \sin[k(x - L/2)]}{kc^2 \cos[kL/2]} \qquad (3.2.1)$$

where L is the length of the basin in the x direction. For similar conditions, the displacement which occurs in a circular basin of radius a at the location r, θ is (from Walsh (1974))

$$Z = \frac{K\tau_0 J_1(kr)\cos\theta}{kc^2[J_0(ka) - J_1(ka)/ka]} \qquad (3.2.2)$$

where J_0 and J_1 denote the Bessel fuctions of zero and first order respectively.

The results obtained from Equation (3.2.1) and (3.2.2) will be compared with those obtained using Equation (3.1.8). A rectangular basin of dimensions $L = 24$

km, $B = 8$ km and depth $H = 3$ m and a circular basin of radius 7.5 km and depth 2.0 m are modelled. These two basins may be used as a crude approximation to Lakes Alexandrina and Albert at the Murray Mouth respectively (see Walsh (1974)). In both cases, various values of the circular frequency, σ, and the friction parameter, α, were used.

Firstly, the convergence of the approximation given by Equation (3.1.8) was examined. Values of $\alpha = 10^{-4} sec^{-1}$ and $\sigma = 2\pi/(24\text{x}3600) sec^{-1}$ were used. This value of σ corresponds to a freqency of one cycle per day (c.p.d.). A comparison of the gain and phase lag of the surface displacement, ζ, for a rectangular lake obtained using Equations (3.2.1) and (3.1.8) with different values of N is displayed in Table 3.1. A similar analysis was carried out for the circular lake and the results obtained are shown in Table 3.2. For the rectangular lake, the results obtained using Equation (3.1.8) are in close agreement with the analytic results. The integral equation method gives answers for both the gain and phase lag which become closer to the analytic solution as N increases. For the circular lake, the results obtained for the gain and phase lag using Equations (3.1.8) and (3.2.2) agree equally as well as for the rectangular lake. The errors in the answers obtained using the integral equation method applied to both the circular and rectangular lakes are considered to be well within acceptable bounds.

Further comparisons between Equation (3.1.8) and the analytic solutions (3.2.1) and (3.2.2) were carried out. The differences between the solutions for the gain and phase lag of the displacement obtained for various σ values (σ=1,

GAIN								
$N =$	36		48		72		144	
Location	∇	%	∇	%	∇	%	∇	%
L/4	0.0007	3.02	0.0005	2.36	0.0004	1.80	0.0002	1.15
L/2	0.0000		0.0000		0.0000		0.0000	
3L/4	0.0007	3.02	0.0005	2.36	0.0004	1.80	0.0002	1.15

PHASE LAG								
$N =$	36		48		72		144	
Location	∇	%	∇	%	∇	%	∇	%
L/4	0.0003	0.01	0.0003	0.00	0.0002	0.00	0.0001	0.00
L/2	0.0687	4.13	0.0888	5.34	0.0549	3.30	0.0002	0.01
3L/4	0.0003	0.88	0.0002	0.65	0.0001	0.42	0.0001	0.20

TABLE 3.1: *A comparison of the values for the gain and phase lag obtained using Equation (3.1.8) for various values of N and the analytic solution, Equation (3.2.1) at various locations in the rectangular lake (all positions taken at $y = B/2$). The parameter ∇ is defined as the absolute difference between the analytic and integral approximation and the other column contains the relative percentage errors. When the analytic solution is zero, no relative error is calculated.*

GAIN								
$N =$	36		48		72		144	
Location	∇	%	∇	%	∇	%	∇	%
$a/4,\ \theta = 0$	0.0000	0.00	0.0000	0.00	0.0000	0.00	0.0000	0.00
$a/2,\ \theta = 0$	0.0001	0.29	0.0001	0.28	0.0001	0.23	0.0000	0.13
$a/4,\ \theta = \pi/2$	0.0000		0.0000		0.0000		0.0000	
$a/4,\ \theta = \pi/2$	0.0000		0.0000		0.0000		0.0000	

PHASE LAG								
$N =$	36		48		72		144	
Location	∇	%	∇	%	∇	%	∇	%
$a/4,\ \theta = 0$	0.0001	0.50	0.0001	0.54	0.0001	0.47	0.0001	0.29
$a/2,\ \theta = 0$	0.0001	0.52	0.0001	0.57	0.0001	0.51	0.0001	0.31
$a/4,\ \theta = \pi/2$	0.0397	1.26	0.0363	1.15	0.0294	0.93	0.0180	0.57
$a/4,\ \theta = \pi/2$	0.0217	0.69	0.0217	0.68	0.0156	0.49	0.0093	0.29

TABLE 3.2: *As in Table 3.1 except for the circular lake which has the analytic solution described by Equation (3.2.2).*

2, 4, or 16 c.p.d.) and for various friction values ($\alpha = 0, 10^{-3}$ or 10^{-4} sec^{-1}) for both basins are presented in Tables 3.3 and 3.4. In all cases the value of the summation variable used in the integral approximation was kept constant at $N = 72$. The results used for comparison were obtained at $x = 3L/4$ and $y = B/2$ in the rectangular basin and at $r = a/2$ and $\theta = 0$ in the circular basin. Once again, the analysis shows that Equation (3.1.8) has performed satisfactorily. In general, the larger errors occur in calculating the phase lag although in all instances the absolute error, ∇, is still small.

§3.3 Connected Lakes

In this section, the theory developed earlier in this chapter is used to model the connected lake problem presented in Section 3 of Chapter 2. A method similar to that described in Section 2.4 is used. Equation (3.1.4) is applied to each region. This does not present any problems except at the interface between two regions since along these interfaces the value of the normal derivative of Z is not known.

Because integral equations have been used, the general connected lake problem presented in Figure 3.1 can be solved. Notation similar to that used in Chapter 2 where a subscripted variable denoted the value of that variable in the appropriate region will again be employed here.

As before, the value that Z takes along the boundary of each region must be determined first. From Equation (3.1.7) we have

$$\mathbf{Z_{bi}} = M_i \mathbf{Z_{ni}}, \qquad i = 1, 2, 3 \tag{3.3.1}$$

GAIN						
$\alpha =$	0		10^{-3}		10^{-4}	
$\sigma(c.p.d.)$	∇	%	∇	%	∇	%
1	0.0002	0.92	0.0000	0.00	0.0005	2.30
2	0.0004	1.77	0.0001	0.52	0.0004	1.78
4	0.0005	1.90	0.0002	1.31	0.0004	1.53
16	0.0000	0.00	0.0000	0.00	0.0001	0.55

PHASE LAG						
$\alpha =$	0		10^{-3}		10^{-4}	
$\sigma(c.p.d.)$	∇	%	∇	%	∇	%
1	0.0006		0.0047	1.46	0.0000	0.00
2	0.0027		0.0096	1.55	0.0023	3.39
4	0.0043		0.0121	1.10	0.0102	6.66
16	0.0026		0.0231	0.88	0.0001	0.00

TABLE 3.3: *Analysis of the rectangular lake for various σ and α values caried out at $x = 3L/4$ and $y = B/2$. A value of $N = 72$ is used in Equation (3.1.8). When the analytic result is zero, no analysis of the percentage error is carried out.*

GAIN						
$\alpha =$	0		10^{-3}		10^{-4}	
$\sigma(c.p.d.)$	∇	%	∇	%	∇	%
1	0.0000	0.00	0.0000	0.00	0.0001	0.50
2	0.0000	0.00	0.0000	0.00	0.0000	0.00
4	0.0000	0.00	0.0000	0.00	0.0001	0.46
16	0.0020	1.19	0.0000	0.00	0.0004	0.37

PHASE LAG						
$\alpha =$	0		10^{-3}		10^{-4}	
$\sigma(c.p.d.)$	∇	%	∇	%	∇	%
1	0.0000		0.0003	2.09	0.0000	0.00
2	0.0002		0.0014	0.49	0.0001	0.34
4	0.0008		0.0034	0.60	0.0009	1.47
16	0.0097	0.31	0.0103	0.51	0.0136	0.61

TABLE 3.4: *As in Table 3.3 except for the circular basin with results calculated at* $r = a/2$ *and* $\theta = 0$.

where M_i is known and is given by

$$M_i = -\frac{\iota}{2}\left(-\frac{\iota}{2}H_{ni} - I_i\right)^{-1} H_i \qquad i = 1,2,3.$$

The above equation yields the values of Z along the boundary. However, it assumes knowledge of the normal derivative of Z along all the boundary. Along the closed boundaries, represented by $\partial\Gamma_i$, $i = 1,2,3$ in Figure 3.1, the components of $\mathbf{Z_{ni}}$ are given simply by the boundary condition (3.1.3). The normal derivative of Z at the open boundaries is obtained by matching the wave heights and the stream values at each interface. That is, the following conditions are enforced:

$$\left.\begin{aligned} Z_1 &= Z_3 \\ P_1 &= P_3 \end{aligned}\right\} \text{along } \Gamma_{c1} \qquad (3.3.2(a))$$

and

$$\left.\begin{aligned} Z_2 &= Z_3 \\ P_2 &= P_3 \end{aligned}\right\} \text{along } \Gamma_{c2}. \qquad (3.3.2(b))$$

The boundary defining Region 1 is assumed to be discretised into N_1 segments. Of these, p are assumed to be located along the boundary between Regions 1 and 3 represented by the curve Γ_{c1}. Similarly, there are q segments across the interface between Regions 2 and 3 and $N_2 - q$ points along the remainder of the boundary of Region 2. Region 3 is divided up into N_3 segments as shown in Figure 3.2. The midpoints of each segment at which actual values of Z, H, $\partial H/\partial n$, etc. are calculated are labelled counter-clockwise as shown in Figure 3.2.

With the notation used in Figure 3.2, the condition of continuity of surface elevation may be written

$$(\mathbf{Z_{b1}})_j = (\mathbf{Z_{b3}})_{q+r_1+p+1-j} \qquad \text{for } j = 1,\ldots,p \qquad (3.3.3(a))$$

$$(\mathbf{Z_{b2}})_j = (\mathbf{Z_{b3}})_{q-j+1} \qquad \text{for } j = 1,\ldots,q. \qquad (3.3.3(b))$$

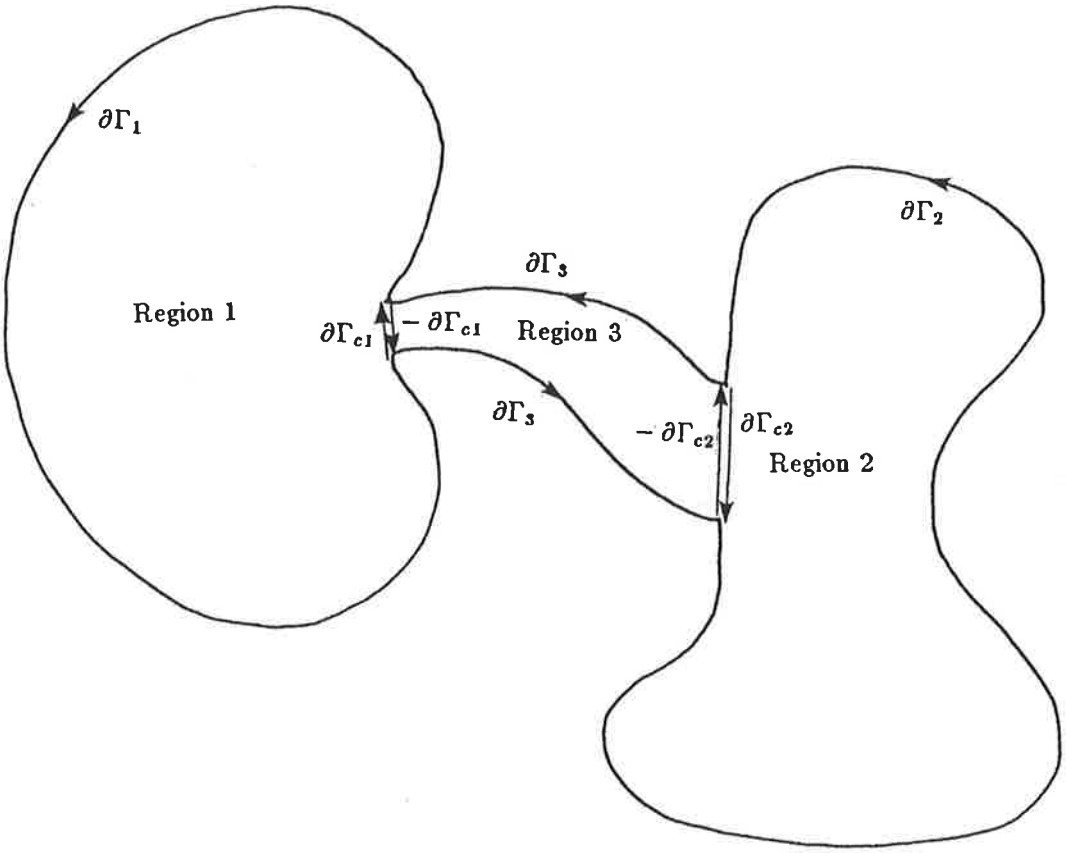

FIGURE 3.1: *The connected lake system to be solved by the integration method. Note the boundary of Region 1 consists of curves $\partial\Gamma_1 + \partial\Gamma_{c1}$, Region 2 consists of $\partial\Gamma_2 + \partial\Gamma_{c2}$ whilst Region 3 is bounded by $-\partial\Gamma_{c2} - \partial\Gamma_{c1} + \partial\Gamma_3$.*

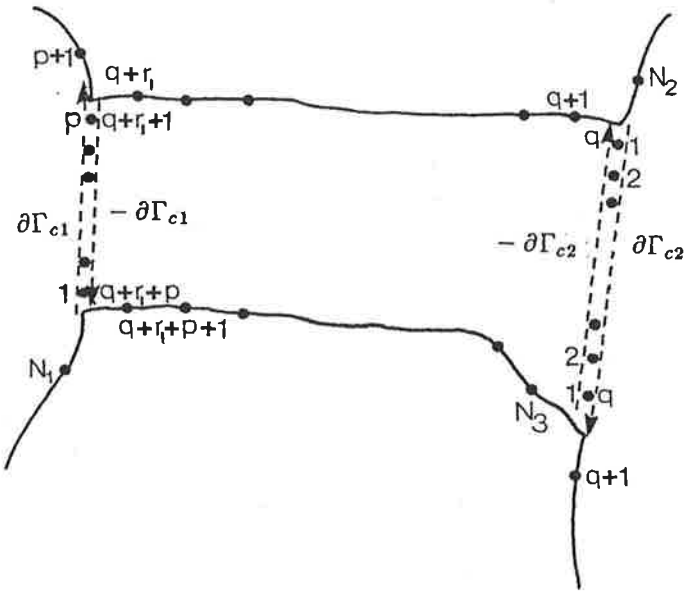

FIGURE 3.2: *Labelling of the integration points along the connecting channel.*

Using Equations (2.2.6) with $f = 0$ and remembering that the direction n is always directed outwards from the boundary, then the remaining two conditions presented in Equation (3.3.2) may be written

$$(\mathbf{Z_{n1}})_j = \frac{K\tau_0}{c_1^2} - \frac{k_1^2}{k_3^2}\left[\frac{K\tau_0}{c_3^2} + (\mathbf{Z_{n3}})_{q+r_1+p-j+1}\right] \quad j = 1,\ldots,p, \quad (3.3.4(a))$$

$$(\mathbf{Z_{n2}})_j = -\frac{K\tau_0}{c_2^2} - \frac{k_2^2}{k_3^2}\left[-\frac{K\tau_0}{c_3^2} + (\mathbf{Z_{n3}})_{q-j+1}\right] \quad j = 1,\ldots,q. \quad (3.3.4(b))$$

With the aid of Equation (3.3.1), the two equations presented above are substituted into the (p+q) equations given in Equation (3.3.3). Hence, the (p+q) unknown values of the normal derivative of $\mathbf{Z_{n3}}$ may be obtained. Once all of the values of $\mathbf{Z_{n3}}$ are obtained then Equation (3.3.4) is utilised to yield values of the normal derivative of Z_1 at the left hand interface and also the q values of the normal derivative of Z_2 at the right hand interface.

Now that the elements of the vectors $(\mathbf{Z_{ni}})$ for $i = 1,2,3$ have been determined, then Equation (3.3.1) is used to provide the values of Z at the boundary of each region. Once these values are known then the value of Z at any interior point of any of the regions may be obtained using Equation (3.1.8).

Results from the above approach for connected lakes are presented in Chapter 4 and comparisons are made with the previously described methods of Chapter 2. Further comparisons will be made between the boundary integral method and a number of numerical methods in Chapter 5.

CHAPTER 4

THE CONNECTED LAKE PROBLEM

§4.1 THE CONNECTED LAKE SYSTEM

In the preceding chapters several alternative techniques have been described which may be used to model a system of connected lakes as shown in Figure 2.11. Such a system of lakes may be used to model the Lake Albert-Alexandrina system which is located at the mouth of the River Murray in the south-east of South Australia. For the purposes of this study then, the following parameters are chosen to describe the dimensions of each lake (see Figure 2.11 for the definition of each symbol)

$$H_1 = 3.0\ m, \qquad H_2 = 2.0\ m, \qquad H_3 = 2.5\ m,$$

$$L_1 = 14.0\ km, \qquad L_2 = 8.0\ km, \qquad L_3 = 8.0\ km,$$

$$B_1 = 24.0\ km, \qquad B_2 = 12.0\ km, \qquad B_3 = 2.0\ km,$$

$$d = 17.0\ km, \qquad s = 10.0\ km.$$

In all of the following studies, a wind with an amplitude of $\tau_0 = 0.1\ Nm^{-2}$ is used. The value of the friction coefficient, r, which is used in Regions 1 and 2 is $5\text{x}10^{-4}\ msec^{-1}$ and from Walsh (1974) a value of $r = 10^{-3}\ msec^{-1}$ is used in the channel (denoted Region 3 in Figure 2.11). Walsh suggests using a much higher value for the friction in the channel to account for the very weedy nature of this region. A value of $\sigma = 1$ c.p.d. is used in the following work.

§4.2 Convergence Of The Galerkin Technique

Using the above parameter values, the convergence of the Galerkin method is tested by checking that the residuals in each of the four conditions listed in Equation (2.4.17) become smaller as the value of N is increased.

The errors in the condition $Z_1 = Z_3$ at $x = -L_3/2$ and for $0 \leq y \leq B_3$ are presented in Table 4.1. The parameter ∇ in this table is defined by the absolute difference between the gain or the phase lag of the two solutions Z_1 and Z_3. In relation to the gain, the percentage error is calculated according to the ratio of ∇ to the gain in Z_1 whilst for the phase lag, the ratio of ∇ to the phase lag in Z_1 is used. The cyclic nature of the phase lag is taken into account when calculating the absolute difference used in calculating ∇ for the tables relating to the phase lag.

As can been seen from this table, the condition on the amplitudes at $x = -L_3/2$ as indicated in Equation (2.4.17(a)) is satisfied. Further, the method converges rapidly. Values obtained for $N = 2$ and $N = 4$ were almost identical although there is a slight improvement in the result for the phase lag when $N = 4$.

Similar tests were carried out on the last three conditions displayed in Equation (2.4.17). In all cases rapid convergence was achieved, producing results almost identical to Table 4.1. For this reason, the results are not tabulated. The results obtained with the Galerkin method illustrate the advantages of this method; only small values of N need to be used to obtain very good results.

GAIN				
$N =$	2		4	
y	∇	%	∇	%
B/4	0.0002	1.14	0.0002	1.14
B/2	0.0002	1.14	0.0002	1.14
3B/4	0.0002	1.14	0.0002	1.14

PHASE LAG				
$N =$	2		4	
y	∇	%	∇	%
B/4	0.1100	1.71	0.1000	1.62
B/2	0.1100	1.71	0.1000	1.62
3B/4	0.1100	1.71	0.1000	1.62

TABLE 4.1: *The error in the displacement condition* $Z_1 = Z_3$ *at* $x = -L_3/2$ *for* $0 \leq y \leq B_3$ *using the Galerkin technique for different values of* N.

§4.3 Convergence Of The Collocation Technique

The convergence of the Collocation technique is now assessed also by examining the residuals in each of the four conditions listed in Equation (2.4.17). In Table 4.2, the error in the condition indicated by Equation (2.4.17(a)) is examined. The parameter ∇ has an identical meaning as in Section 4.2 and the percentage error is calculated using the same procedure as described previously.

Clearly, the Collocation method does not converge as quickly as the Galerkin technique. Similar accuracy may be achieved using the Galerkin technique with $N = 2$ as may be obtained with the Collocation method and $N = 6$. Once again, similar tables to Table 4.2 are produced when the other matching conditions are examined and so they are not presented here. It must be stated, however, that although similar accuracy to that shown in Table 4.2 was achieved with the velocity conditions given by Equations (2.4.17(c) and (d)) for $N = 6$, very poor answers were obtained for smaller values of N. Indeed, for $N = 3$ the relative error was often of the order of 100%.

§4.4 The Boundary Integral Method

The integral equation solution developed in Section 3 of Chapter 3 is applied to the connected lake system described earlier in this Chapter. However, firstly results obtained when all the basins are of the same depth and the friction parameters are of the same value is analysed. Values of $H_1 = H_2 = H_3 = 3.0\ m$ and

GAIN				
$N =$	3		6	
y	∇	%	∇	%
B/4	0.0028	11.20	0.0000	0.00
B/2	0.0027	10.80	0.0000	0.00
3B/4	0.0028	11.20	0.0000	0.00

PHASE LAG				
$N =$	3		6	
y	∇	%	∇	%
B/4	0.0001	12.15	0.0000	0.92
B/2	0.0072	87.12	0.0000	0.92
3B/4	0.0001	12.15	0.0000	0.92

TABLE 4.2 *The error in the displacement condition* $Z_1 = Z_3$ *at* $x = -L_3/2$ *for* $0 \leq y \leq B_3$ *using the Collocation technique for different values of* N.

$r = 6\text{x}10^{-4}\ msec^{-1}$ throughout are used. Such a system as this may also be solved using the scheme developed in Section 1 of Chapter 3 (that is, Equation(3.1.8)). The contour of integration in this case is simply the total boundary of all three regions as shown in Figure 2.11. The results obtained from both methods are compared and in this way a useful check on the program developed to solve the connected system can be made.

Firstly, for the method of Section 3.3, the matching conditions on velocity flux and displacement at the junctions between each region are examined when the depths of each basin are assumed to be equal. The four conditions which are described in Equation (3.3.2) are found to be obeyed exactly. In Table 4.3 the error in the gain and the phase lag for the condition $Z_1 = Z_3$ is examined. Clearly, to the accuracy shown in the table, there is no error in modelling this condition using the techniques outlined in Section 3.3. The remaining three conditions were also found to be modelled exactly, producing identical results to those shown in Table 4.3.

A comparison of results obtained using the method presented in Section 3 of Chapter 3 and Equation (3.1.8) is undertaken in Table 4.4. The difference in results for the phase lag and gain of the displacement at various locations in the lake system is shown in this table. The parameter, ∇, is simply the absolute value of this difference whilst the relative percentage error is determined by the ratio of ∇ with the result produced by the boundary integral method of Section 3.3.

Overall, results obtained agree quite well. The largest difference in solutions

	GAIN		PHASE LAG	
y	∇	%	∇	%
B/4	0.0000	0.00	0.0000	0.00
B/2	0.0000	0.00	0.0000	0.00
3B/4	0.0000	0.00	0.0000	0.00

TABLE 4.3: *The error in the displacement condition* $Z_1 = Z_3$ *at* $x = -L_3/2$ *for* $0 \leq y \leq B_3$ *using the integral formulation of Section 3.3.*

			GAIN		PHASE LAG	
region	x (km)	y (km)	∇	%	∇	%
1	-11	1	0.0005	4.17	0.7578	9.47
1/3	-4	1	0.0003	6.47	0.5159	9.73
3	-1	1	0.0009	3.88	0.4307	7.92
3	1	1	0.0007	2.39	0.4152	7.15
3/2	4	1	0.0004	1.15	0.0329	0.52
2	8	1	0.0008	1.50	0.2370	3.93
2	8	-5	0.0008	1.53	0.2381	3.95

TABLE 4.4: *The difference bewteen the gain and phase lag of displacement using the method of Section 3.3 for equal depths in each region and Equation (3.1.8).*

occurs in region 1. It is unclear why this is so but certainly the absolute error is always less than 1 mm.

Three techniques, namely the Collocation, Galerkin and boundary integral method, have been presented as means of solution to the connected lake problem. If the basins are of the same depth, then a simplified boundary integral formulation may be used. A comparison between all three methods used when the basins are of unequal depths is made in Table 4.5 in which values of the gain and phase lag of the amplitude are presented. A value of $N = 2$ was used in the Galerkin method whilst $N = 6$ was used in the Collocation technique.

In Table 4.5, some large differences occur in the phase lag. This apparently large difference is due to the cyclic nature of the phase lag. From Table 4.5, it is clear that the Galerkin techniques and the boundary integral method yield very similar results. The Collocation technique does not provide results which are in as close agreement as these. The largest difference between the Galerkin and integral equation methods occurs at the junction between Regions 1 and 3. Here, the error in the gain is 0.0011 m which is a relative difference of 6.96%. At the same location the difference in the phase lag is 0.1005 radians or 1.66%. The percentage differences presented here are all relative to the solution obtained using the boundary integral method. The next largest difference in gain is only 0.009m or 1.72%. The difference in the phase lag at this point is 0.0768 radians or 0.12%.

Clearly, the solution to the connected lake problem may be successfully obtained using either the Galerkin or boundary integral techniques. Both methods

			GAIN		
region	x (*km*)	y (*km*)	Galerkin	Integral	Collocation
1	-11	1	0.0103	0.0103	0.0000
1/3	-4	1	0.0147	0.0158	0.0250
3	-1	1	0.0212	0.0217	0.0314
3	1	1	0.0254	0.0255	0.0357
3/2	4	1	0.0319	0.0313	0.0421
2	8	1	0.0533	0.0524	0.0636
2	8	-5	0.0533	0.0523	0.0636

			PHASE LAG		
region	x (*km*)	y (*km*)	Galerkin	Integral	Collocation
1	-11	1	3.1975	3.5313	3.1370
1/3	-4	1	6.1440	6.0435	0.0011
3	-1	1	6.2405	6.1414	0.0011
3	1	1	6.2773	6.1826	6.2820
3/2	4	1	6.1441	6.2246	6.2794
2	8	1	0.0511	6.2575	6.2819
2	8	-5	0.0511	6.2610	6.2803

TABLE 4.5: *A comparison of the gain and phase lag of displacement obtained at various locations using the Galerkin, Collocation and Boundary Integral methods.*

are relatively simple in concept although the Galerkin technique is probably the easier to program on a computer. A major drawback of the Galerkin technique is that it can be applied only to simple shapes. If the basins have a complicated boundary then the boundary integral technique should be used. However, because this method involves the inversion of several large complex matrices, it takes much longer to run on the computer. The matrices involved are not banded and do not lend themselves to special techniques for inversion.

CHAPTER 5

NUMERICAL MODELS

§5.1 TWO NUMERICAL MODELS

Developed in this chapter are two numerical models both of which use finite difference techniques to solve wind forced problems. The first model is described by the following set of equations which are available from Equation (2.2.6) with $f = 0$, that is,

$$P = \frac{1}{\beta}\left(K\tau_{0x} - c^2\frac{\partial Z}{\partial x}\right), \qquad (5.1.1(a))$$

$$Q = \frac{1}{\beta}\left(K\tau_{0y} - c^2\frac{\partial Z}{\partial y}\right). \qquad (5.1.1(b))$$

The functions, P and Q, are related to Z by the conservation of mass equation

$$\frac{\partial P}{\partial x} + \frac{\partial Q}{\partial y} = -\iota\sigma Z. \qquad (5.1.1(c))$$

A finite difference solution to Equations (5.1.1) is obtained and thus the solutions for ζ, U and V for a basin with varying depth and acted upon by a general non-homogeneous wind stress can be obtained. The model could also be used to solve for the more general case when $f \neq 0$. All solutions so far discussed have been for constant depth basins subject to a wind stress invariant with horizontal position. This model, which will be developed in the next section, can be used to solve for wind effects in arbitrary shaped basins. The performance of this numerical model will be tested against analytic solutions of rectangular and circular basins of

constant depth (see Equations (3.2.1) and (3.2.2)). The finite difference equations used in this model are all second order accurate. However, the model approximates a curved boundary by a series of steps each parallel to or perpendicular to the finite difference grid lines. This results in the approximations made for derivatives near a curved boundary being less than second order accurate. The effects of approximating a curved boundary in this manner will be determined by comparing the results obtained for a circular basin with an analytic solution.

The effects of a varying depth will be examined by applying this model to Lake Albert in South Australia. Also, by assuming this lake to be of constant depth, the effects of approximating the boundary by a series of steps will be further examined by comparing the results from the finite difference method with the solution obtained using the boundary integral method described in the Chapter 3.

It will be shown that major differences in the solutions are obtained by approximating the boundary in the manner described. This result prompted the development of a finite difference model which could be used for constant depth basins of arbitrary shape but which also could model a curved boundary without loss of accuracy in the finite difference approximations near the bondary.

Hence, the second finite difference model deals with the numerical solution of the equations used in Chapter 3, namely,

$$(\nabla^2 + k^2)Z = 0 \qquad (5.1.2(a))$$

subject to

$$\left.\frac{\partial Z}{\partial n}\right|_{\partial\Gamma} = \frac{K\tau_0}{c^2}. \qquad (5.1.2(b))$$

where, as before, $\partial\Gamma$ describes the boundary of the basin and n is the outward normal direction. Conventional second order differences are used to solve this system of equations for all interior points away from the influence of the boundary. Appropriate second order differences which are available from Appendix A are used at grid points next to the boundary.

The performance of this model is again tested against the analytic solution for a circular basin and compared with results from the first numerical model as well as the integral equation solution. The results using this second model are shown to be superior to those obtained by the former numerical model suggesting that this model should be used whenever a constant depth assumption may be made.

In the next section, a general methodology and notation for solving finite difference equations is described. This information is explained with reference to the finite difference equations approximating Equation (5.1.1). However, the method and notation can be readily applied to the finite difference approximation to Equation (5.1.2). In Sections 5.3 and 5.4 results are presented for the finite difference solution of Equation (5.1.1). In section 5.5, results obtained using finite difference approximations to Equation (5.1.2) are given.

§5.2 A Finite Difference Model For Equation (5.1.1)

A staggered grid as shown in Figure 5.1 is used. Constant grid spacings are used with generally different values in each direction. An element of this grid

system consists of three points labelled X, $\rightarrow$ and $\uparrow$. The distance between an X-point and an $\rightarrow$-point is Δx, while an X-point and an $\uparrow$-point are separated by a distance of Δy. Corresponding points in adjacent elements in the x direction are separated by a distance $2\Delta x$ and corresponding points in adjacent elements in the y direction are separated by $2\Delta y$. At the $\rightarrow$-points values of the depth integrated velocity, U, are calculated. Values of Q, which is related to the other component of depth integrated velocity, V, are calculated at $\uparrow$-points. All other variables are calculated at X-points. In the following, the notation P_i is used to represent the approximation for $P(x, y)$ at the $\rightarrow$-point in the i^{th} element.

When writing a computer program to solve Equation (5.1.1) the above mentioned grid scheme is laid over a map of the particular body of water being investigated and each of the grid elements numbered appropriately. For example, consider the body of water shown in Figure 5.2. This may be modelled as shown. The heavy line indicates the approximation to the boundary which will be used in the numerical model. However, this simplistic approach, although it has been used many times in depth integrated hydrodynamic models, is not very satisfactory. For example, it wastes much computer space because storage space must be allocated to many land elements which are of no interest. One of the biggest problems with this approach is the amount of book-keeping involved in writing a program. Not only must elements representing land be distinguished from those representing water but the various types of water elements must be distinguished. For example, movement of water in those elements surrounded by water will be

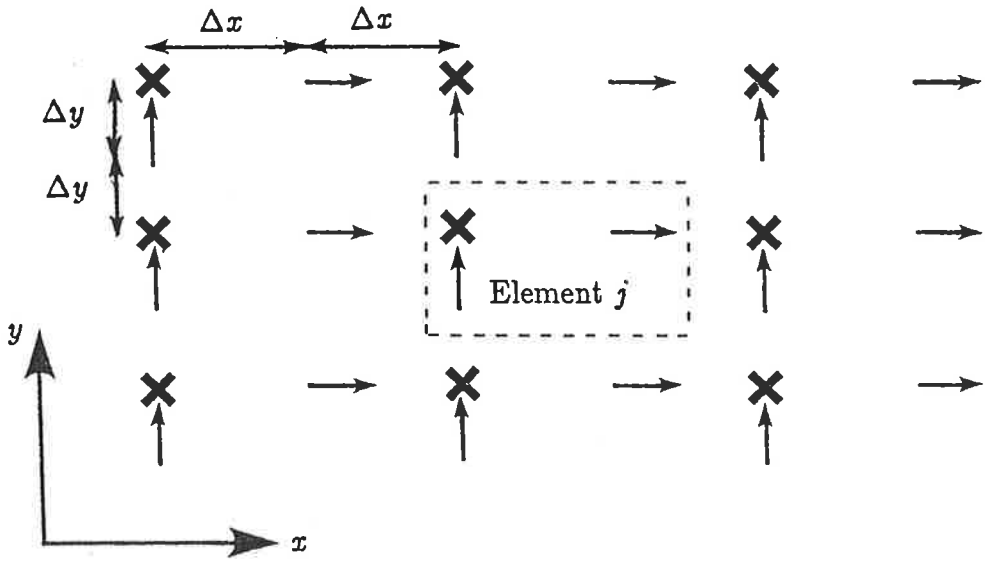

FIGURE 5.1: *Plan view of the staggered grid.*

8	16	24	32	40	48	56	64	72
7	15	23	31	39	47	55	63	71
6	14	22	30	38	46	54	62	70
5	13	21	29	37	45	53	61	69
4	12	20	28	36	44	52	60	68
3	11	19	27	35	43	51	59	67
2	10	18	26	34	42	50	58	66
1	9	17	25	33	41	49	57	65

FIGURE 5.2: *A simplistic grid scheme.*

described by different equations from those used in elements with boundaries running through them. The finite difference equations applicable in each element will therefore be different. Each type of boundary element must be distinguished. For example, the element labelled 10 in Figure 5.2 is surrounded by land on three sides whilst the element numbered 12 is surrounded on two sides by land. Hence, the way in which some of the terms in the equations are numerically modelled will be different in each element. It is thus difficult to write a "general" program which is applicable for any shape of basin using this approach.

Some improvements can be made, however. For example, in any numerical approximation using finite difference techniques, one only needs information from the elements immediately adjoining each particular element. Hence, a method of labelling as shown in Figure 5.3 is introduced. The two elements above and below the j^{th} element are indicated by $j+1$ and $j-1$ respectively. The $j2$ label indicates the element immediately to the right of the j^{th} element with $j2 \pm 1$ indicating elements above and below this element. The $j1$ label indicates the element immediately to the left of the j^{th} element with $j1 \pm 1$ being interpreted in the obvious way. Thus, with reference to Figure 5.2, if the element being considered is labelled 36 then $j1$ is 28, $j2$ is 44 and so on. This labelling scheme not only simplifies the notation used in writing down the finite difference equations but also facilitates the writing of a more economical computer program.

Another feature which reduces the amount of book-keeping which must be carried out in the program to keep account of the type of element being considered

j1+1	j+1	j2+1
j1	j	j2
j1-1	j-1	j2-1

FIGURE 5.3: *The general method of referencing elements with respect to the central element, j.*

4	16	128
2		64
1	8	32

FIGURE 5.4: *The value of the weights for each of the surrounding eight elements.*

and the shape of the body of water which is being modelled was developed by Stevens and Noye (1984) and is now briefly described. Associated with each active element, that is, an element that lies within the boundaries of the region of water being considered, is a special identification number. There are eight elements surrounding any particular active element and each of them is given a weight of $2^j, j = 0, \ldots, 7$ (see Figure 5.4). In determining the identification number for an active element, the weight of each surrounding element which is non-active (that is, one representing land only) is added together to form a single identification for each element. An element is non-active if there is land at the X-point of the particular grid. For example, the identication number of the element labelled 58 in Figure 5.2 is 232. The weights given to each of the surrounding elements are chosen to be powers of two because any resultant identification number can be decomposed into a sum of powers of two in only one way. Hence, the identification number uniquely determines the types of elements surrounding a particular element.

Using the above techniques, a general program may be written. The locations of active and non-active elements are input into a computer program. From such information, the identification numbers of each element are determined together with the labels of the eight elements which immediately surround each particular element. When individual terms of the finite difference scheme are being programmed, appropriate code is written for particular identification numbers. For example, the code for the finite difference approximation for P is the same for all elements except those with an identification number of 64 in which case P is simply set to zero. Such a computer program is thus applicable to and easily utilised for any arbitrary shaped basin. The scheme can also be used for non-linear and time dependent three dimensional wind driven or tidal flows.

Using the techniques and notation described above, together with centred finite difference approximations, enables Equations (5.1.1) to be discretised in the following manner:

$$\frac{K\tau_{0x} - \beta_j^P P_j}{g(h_{j2} + h_j)/2} = (Z_{j2} - Z_j)/2\Delta x + O\left\{(\Delta x)^2\right\} \qquad (5.2.1(a))$$

$$\frac{K\tau_{0y} - \beta_j^Q Q_j}{g(h_j + h_{j-1})/2} = (Z_j - Z_{j-1})/2\Delta y + O\left\{(\Delta y)^2\right\} \qquad (5.2.1(b))$$

$$-\iota\sigma Z_j = (P_j - P_{j1})/2\Delta x + (Q_{j+1} - Q_j)/2\Delta y + O\left\{(\Delta x)^2, (\Delta y)^2\right\} \qquad (5.2.1(c))$$

where β_j^P and β_j^Q are the β terms calculated at an $\rightarrow$-point and $\uparrow$-point respectively. That is,

$$\beta_j^P = \iota\sigma + 2r/(h_{j2} + h_j) \qquad (5.2.2(a))$$

$$\beta_j^Q = \iota\sigma + 2r/(h_j + h_{j-1}) \qquad (5.2.2(b))$$

for some value of the friction parameter, r. These equations are rearranged to give, in explicit form, the following equations for the evaluation of P_j, Q_j and Z_j at all active grid points:

$$Z_j = Z_{j1} + \frac{4(K\tau_{0x} - \beta_j^P P_{j1})\Delta x}{g(h_j + h_{j1})}, \qquad (5.2.3(a))$$

$$Q_j = \frac{1}{\beta_j^Q}\left[K\tau_{0y} - \frac{g(h_{j-1} + h_j)(Z_j - Z_{j-1})}{4\Delta y}\right], \qquad (5.2.3(b))$$

$$P_j = P_{j1} - 2\Delta x\left[\iota\sigma Z_j + \frac{(Q_{j+1} - Q_j)}{2\Delta y}\right]. \qquad (5.2.3(c))$$

These expressions are obtained by rearranging Equations (5.2.1(a), (b) and (c)) respectively. They are solved in the following order: if necessary, Z_2 is calculated first, then Q_2 and then P_1; Z_3 is calculated next, then Q_3 and P_2 and so on. When calculated in this manner the equations are explicit. Values for Q_1 and Z_1 need not be calculated since Q_1 will always be zero (see Figure 5.5) and, as will be discussed shortly, Z_1 is always assigned a value.

The solution of Equation (5.2.3) is found using an implicit marching method (Noye (1984)), referred to as the EVP method by Roache (1974). This method was chosen because it is readily adaptable to irregular boundary geometries and varied combinations of boundary conditions. Also, a formal error analysis exists for the method (see Noye (1984)) and it can be shown that the largest error which results from the application of the this method will occur along the boundary at which end values are calculated. This fact will make it easier to test the performance of the method.

Consider Figure 5.5 which describes how the body of water considered in Figure 5.2 is labelled. Elements which are non-active (land elements) are labelled

zero. The elements at the western end of the grid ,namely those labelled 1, 2, 3, 4, 6 and 10 are assigned values for the amplitude Z. The explicit equations (5.2.3) together with the boundary conditions $Q = 0$ along any east-west boundary and $P = 0$ along any north-south boundary, may now be used to produce a set of values for the velocity P along the eastern boundary (that is, at elements 22, 33, 34, 35, 36 and 37). These values of course should be zero. The correct starting values are determined by finding the end values produced by specific starting values.

Because Equations (5.2.1) are linear, the end values, contained in vector $\mathbf{e}$, are related to the starting values contained in $\mathbf{s}$ by the relation

$$\mathbf{e} = \psi\mathbf{s} + \boldsymbol{\phi} \tag{5.2.4}$$

where ψ is an N x N square complex matrix and $\boldsymbol{\phi}$ is the vector produced by the starting values $\mathbf{s} = \mathbf{0}$. The number of starting values (which must equal the number of end values) is assumed to be N. If starting values defined by $\mathbf{s}_i = \delta_{ij}$ for $i, j = 1, \ldots, N$ are used then the i^{th} column of ψ, denoted by $\boldsymbol{\psi}_i$, is obtained from

$$\boldsymbol{\psi}_i = \mathbf{e}_i - \boldsymbol{\phi} \tag{5.2.5}$$

where $\mathbf{e}_i$ is the vector of end values obtained using $\mathbf{s}_i$. Once ψ and $\boldsymbol{\phi}$ have been determined in this manner, the correct starting values, $\mathbf{s}^*$, are obtained from

$$\mathbf{s}^* = \psi^{-1}(\mathbf{e}^* - \boldsymbol{\phi}) \tag{5.2.6}$$

where $\mathbf{e}^*$ is the desired end vector. Of course, for this problem $\mathbf{e}^* = \mathbf{0}$ and so

$$\mathbf{s}^* = -\psi^{-1}\boldsymbol{\phi} \tag{5.2.7}$$

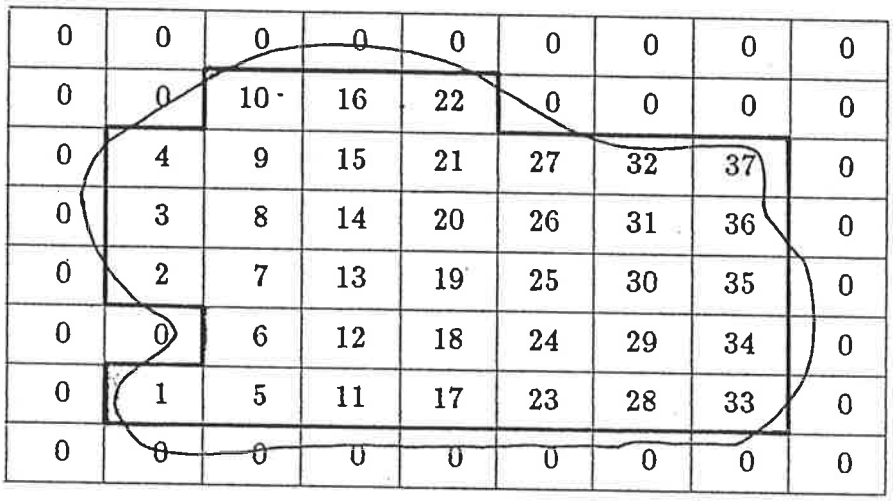

FIGURE 5.5: *The new grid labelling scheme for the body considered in Figure 5.2.*

Once the correct starting values have been obtained a final sweep through the grid produces the values for Z, P and Q throughout the region.

§5.3 Comparison With Analytic Solutions

The performance of the numerical method described in the previous section was tested against results obtained from analytic solutions for the elevation occurring in rectangular and circular lakes of constant depth (Equations (3.2.1) and (3.2.2)). Results are presented in Tables 5.1 and 5.2. In the former case, results are presented for the rectangular lake for $\sigma = 1$ c.p.d., $\alpha = 10^{-4}\ sec^{-1}$ and at points $x = L/2$, $y = B/2$ and $x = 3L/4$, $y = B/2$. The dimensions of the basin are those which have already been used. Similar parameters are used in the comparison for the circular basin presented in Table 5.2 but in this case results are presented at positions $r = a/4$, $\theta = 0$ and $r = a/4$, $\theta = \pi/2$. The dimensions of the circular basin are also those which have been previously described. In both cases values are presented for various values of Δx and Δy. The relative percentage error is defined by the ratio of the difference between the numerical and the analytic solutions, defined by ∇, with the result obtained using the analytic solution.

From Tables 5.1 and 5.2, it is clear that the numerical method will adequately predict the gain in displacement occurring in both types of basins. In general, the results obtained for the rectangular basin are better than those obtained for the circular basin. This reflects the errors introduced by approximating the boundary of a circle in a step-wise fashion. The rectangular boundary can, of course, be

		GAIN		PHASE LAG	
		∇	%	∇	%
$\Delta x = \Delta y = 500m$	$x = L/2$	0.0018		0.0553	3.33
	$x = 3L/4$	0.0000	0.00	0.0000	0.00
$\Delta x = \Delta y = 1000m$	$x = L/2$	0.0036		0.0553	3.33
	$x = 3L/4$	0.0000	0.00	0.0000	0.00
$\Delta x = \Delta y = 2000m$	$x = L/2$	0.0072		0.1063	6.39
	$x = 3L/4$	0.0000	0.00	0.0003	0.91

TABLE 5.1: *The gain and phase of the displacement for the rectangular lake predicted using the numerical model for various grid sizes and compared with the analytic solution.*

		GAIN		PHASE LAG	
		∇	%	∇	%
$\Delta x = \Delta y = 500m$	$r = a/4, \theta = 0$	0.0000	0.00	0.0041	26.86
	$r = a/4, \theta = \pi/2$	0.0000	0.00	0.0029	0.09
$\Delta x = \Delta y = 1000m$	$r = a/4, \theta = 0$	0.0006	6.26	0.0045	29.23
	$r = a/4, \theta = \pi/2$	0.0000	0.00	0.0236	0.75

TABLE 5.2: *As in Table 5.1 except for the circular lake.*

modelled exactly. In the circular case, the performance of the model appears to behave badly along the line $\theta = 0$. However, along this line the phase lag is very small (of the order of 0.01 radians) and so even though the absolute error is sufficiently small (of the order of 0.001 radians) the resulting relative percentage errors are significant. Along the line $\theta = \pi/2$ where the phase lag is of the order of π, the absolute errors are certainly not a lot smaller than before but the relative percentage errors are considerably smaller because of the significant order of the phase lag along this line.

§5.4 A Model For Lake Albert

The numerical model and associated grid scheme is used to analyse the amplitude of the response of Lake Albert to a surface wind stress. The contour of the lake is shown in Figure 5.6 together with the grid scheme which is used. The grid spacing is $\Delta x = \Delta y = 500\ m$. In Figure 5.6, each of the squares contains an element of the numerical scheme as has been previously described. Each square is therefore 1 km x 1 km in size. An array of 14 elements in the x direction and 15 elements in the y direction was needed. Only those elements which lie within the heavy step-wise varying curve which approximates the boundary are active. There are 150 such active elements for which calculations for Z, P and Q will be made. The total number of elements is 14 x 15 = 210.

To further illustrate the ease with which the numerical method described in the earlier section of this chapter may be applied, it is useful to look at the input

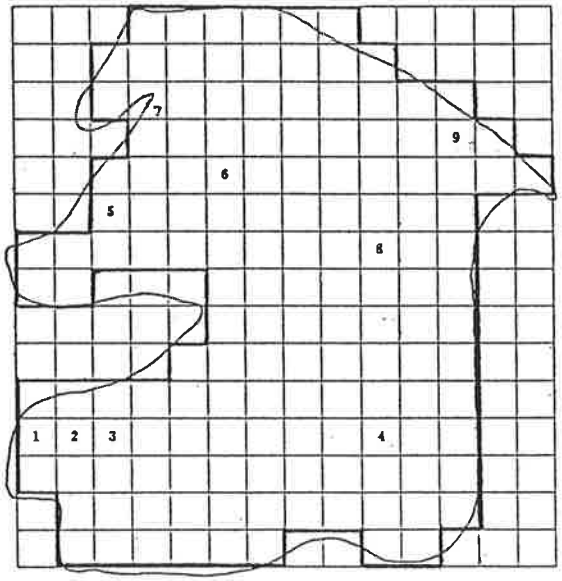

FIGURE 5.6: *A model for Lake Albert. Each square (1 km. x 1 km.) represents an element of the numerical scheme. The heavy step-wise varying curve is the approximation to the actual boundary used by the numerical model. The numbers in the squares designate locations at which some analysis will be carried out.*

```
0 0 0 1 1 1 1 1 1 0 0 0 0 0
0 0 1 1 1 1 1 1 1 1 1 0 0 0 0
0 0 1 1 1 1 1 1 1 1 1 1 1 0 0
0 0 0 1 1 1 1 1 1 1 1 1 1 1 0
0 0 1 1 1 1 1 1 1 1 1 1 1 1 1
0 0 1 1 1 1 1 1 1 1 1 1 1 0 0
1 1 1 1 1 1 1 1 1 1 1 1 1 0 0
1 1 0 0 1 1 1 1 1 1 1 1 1 0 0
0 0 0 0 1 1 1 1 1 1 1 1 1 0 0
0 0 0 0 1 1 1 1 1 1 1 1 1 0 0
1 1 1 1 1 1 1 1 1 1 1 1 1 0 0
1 1 1 1 1 1 1 1 1 1 1 1 1 0 0
1 1 1 1 1 1 1 1 1 1 1 1 1 0 0
0 1 1 1 1 1 1 1 1 1 1 1 1 0 0
0 1 1 1 1 1 1 0 0 1 1 0 0 0
```

FIGURE 5.7: *The array describing the location of active elements (denoted by 1) and the land elements (denoted by zero).*

which was required by the program to model this particular lake. The number number of grid elements in the x and y directions was the first input. In this case values of 14 and 15 respectively were required. The overall dimensions of the grid were next input; the required values for this problem are 14 km in the x direction and 15 km in the y direction. The location in the grid of the active elements is also required by the program. This is achieved by inputting a series of 0's and 1's where 1 represents an active element (water) and 0 represents an inactive element (land). This part of the input file is shown in Figure 5.7. Finally, the depth of the lake at each active element is input to the program. Simply by changing the above data the program can be used for any lake.

Values used for the other parameters required by the problem were $\sigma = 1$ c.p.d., $\alpha = 10^{-4}\ sec^{-1}$ and $\tau_0 = 0.1\ Nm^{-2}$.

The numerical method was first used to analyse the effects of assuming a constant depth bathymetry. Lake Albert has an average depth of 2.0 m and the actual profile varies from about 1.5 m to 2.9 m. The deepest region of the lake occurs near the element labelled 8 in Figure 5.6. A comparison of the values obtained at the nine elements indicated in Figure 5.6 for a constant depth and variable bathymetry is made Table 5.3. The relative percentage error is defined by the ratio of the difference between the two results, denoted by ∇, with the result obtained using the actual bathymetry.

Clearly, using a constant depth bottom does not cause excessive absolute errors. The absolute difference between the two results for the gain is never more

	GAIN		PHASE LAG	
Location	∇	%	∇	%
1	0.0013	5.68	0.0013	0.04
2	0.0000	0.00	0.0011	0.03
3	0.0017	9.94	0.0017	0.05
4	0.0016	9.30	0.0017	9.88
5	0.0036	25.17	0.0000	0.00
6	0.0041	13.27	0.0001	0.00
7	0.0043	21.08	0.0002	0.00
8	0.0031	19.74	0.0033	38.37
9	0.0011	2.11	0.0019	0.03

TABLE 5.3: *Comparison of results obtained for gain and phase lag of displacement using a constant depth bottom and the actual bathymetry.*

	GAIN		PHASE LAG	
Location	∇	%	∇	%
1	0.0060	20.36	0.0173	0.67
2	0.0034	14.01	0.0210	0.67
3	0.0007	3.67	0.0235	0.75
4	0.0002	0.96	0.0020	0.41
5	0.0061	56.54	0.0339	1.08
6	0.0012	4.48	0.1868	5.95
7	0.0009	5.81	0.0454	0.72
8	0.0060	3.19	0.0020	0.41
9	0.0181	33.96	0.0019	0.03

TABLE 5.4: *Comparison of results obtained for gain and phase lag of displacement using the numerical model with a constant depth bottom and the boundary integral approach.*

than about 4 *mm*. whilst even better agreement is achieved for the phase lag. In terms of the percentage error some of the results differ quite markedly. It was found that at the locations where these differences occurred, the depth differed significantly from 2 *m*. For example, at locations 5 and 8, where the depth is 1.5 *m* and 2.8 *m* respectively, large percentage differences were observed.

An analysis is now be performed on the difference between solutions obtained using the numerical method with a constant depth bottom and the integral equation approach described in Chapter 3. As has been shown by comparison with analytic solutions for simple geometries, both of these methods adequately model the gain and phase lag of the response. Any difference in the solutions obtained should be entirely due to the different ways in which the boundary of the lake is being approximated. Seventy two unevenly spaced segments were used in the integral equation model to approximate the boundary of the lake.

A comparison of the results obtained from the two methods is made in Table 5.4. From here it can be seen that the absolute differences between the two models can be more significant than those which were achieved by assuming a constant depth. For instance, at one location the absolute error has reached a value of a centimetre. Clearly, significant errors can result in having to approximate a boundary in a step-wise fashion as is necessary in the finite difference model presented here.

Consider the elements labelled 1, 2, 3, and 4 in Figure 5.6. The *X*-point at which *Z* is calculated is 500 *m* from the boundary used in the finite difference model. However, this same point is about 800 *m* away from the boundary used in

the integral equation solution. This difference is reflected in the percentage error for the gain at Location 1 as shown in Table 5.4. The further one moves away from the boundary (that is, at Locations 2, 3 and 4) the less significant is the resulting percentage error. At Location 2 the error decreases to about 14%, at 3 it is about 4% and at Location 4 the error has dwindled to about 1%. This trend reflects the decreasing significance of the error introduced by the approximation made for the boundary as one moves away from it. The other locations with high percentage errors all occur near boundaries where the approximate shape used in the numerical method differed significantly from the boundary used in the integral equation method.

§5.5 A Finite Difference Solution For Equation (5.1.2)

In this section, a new finite difference solution to Equation (5.1.2) is constructed. The approximations used are second order accurate everywhere, including those points near the boundary. However, the boundary curve, Γ, is not approximated by a series of steps as in most conventional finite difference models but retains its shape.

Results from this model are compared with those obtained with a conventional model of Equation (5.1.2) in which the boundary is approximated by a series of steps. Although this is the treatment of the boundary that has been used in solving Equation (5.1.1) in Sections 5.3 and 5.4, in order to get an exact comparison between the model developed in this section and conventional models

which alter the boundary, a conventional model is also described which models Equation (5.1.2).

Exactly the same notation and computer methods are used as are described in the earlier sections. For solving Equation (5.1.2) a staggered grid is not needed since only one variable, Z, is being considered. In this model a grid element consists of a cell containing only one point, namely a Z point. A grid element is located at the intersection of grid lines so that the point Z_i in the finite difference scheme refers to the point in the top right hand corner of a grid element labelled i. Each Z point is separated by a distance Δx in the horizontal and Δy in the vertical. This differs with the previous finite difference model in which the points at which Z is calculated were separated by a distance of $2\Delta x$ in the horizontal and $2\Delta y$ in the vertical. All points lying inside the boundary are active points. All such points for which one or more of the surrounding points $j+1$, $j-1$, $j1$ and $j2$ are land elements are called boundary points. The region described in Figure 5.2 will now be labelled as shown in Figure 5.8. The computer program described in Section 5.2 readily determines whether any grid element lies near the boundary or is an internal point.

Assuming $\Delta x = \Delta y$ then a suitable second order approximation for the Helmholtz Equation is

$$Z_{j1} + Z_{j2} + Z_{j+1} + Z_{j-1} + (\Delta x^2 k^2 - 4)Z_j = 0. \qquad (5.5.1)$$

This formula may be used for all interior grid points, that is, those for which no neighbouring grid point in the direction of either coordinate axis lies outside the

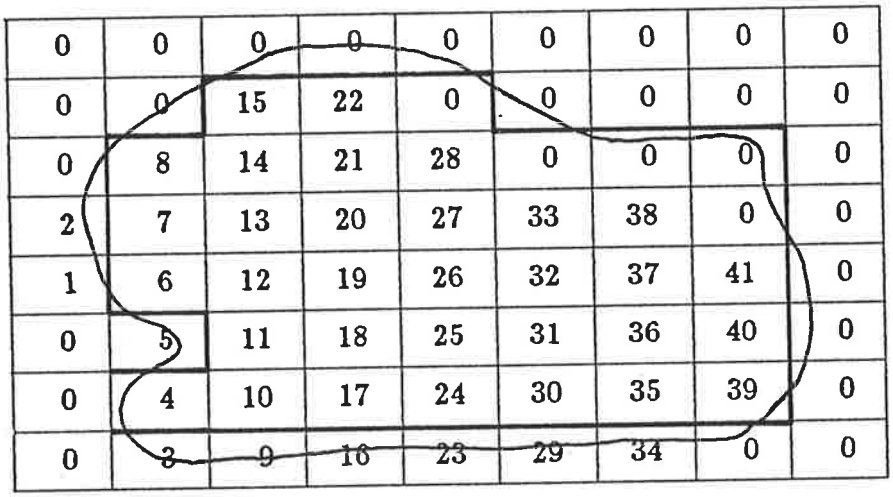

FIGURE 5.8: *The new grid labelling for the region shown in Figure 5.2*

boundary. Interior points at which the above formula is valid are easily detected by the computer program since these are points, j, for which the locations at $j+1$, $j-1$, $j1$ and $j2$ are all water elements.

Alternative formulae must be used at boundary points, j, for which one or more of the surrounding points $j+1$, $j-1$, $j1$ and $j2$ are land elements. Formulae for the finite difference approximations to the derivatives $\partial^2 Z/\partial x^2$ and $\partial^2 Z/\partial y^2$ at such points are given in Appendix A.

For Type 1 boundary points where two of the four neighbouring grid points lie outside of the boundary, the second order accurate approximation used to model Helmholtz's Equation is of the form

$$(s_{XX1} + s_{YY1})Z_T + (s_{XX2} + s_{YY2})Z_Q + (s_{XX3} + s_{YY3} + k^2\Delta x^2 s_{XX4})Z_j = -(s_{XX5} + s_{YY5})\Delta x \tag{5.5.2}$$

This formula assumes that the vertical and horizontal grid spacings are the same, that is, $\Delta x = \Delta y$. The coefficients s_{XX1}, s_{XX2} etc. are given in Equations (A9(b)-(e)) and Equation (A6(e)) of Appendix A. The coefficients s_{YY1}, s_{YY2} etc. are given by Equations (A11(b)-(e)) and Equation (A6(e)). Type 1 boundary elements for which the expression (5.5.2) is valid can occur in any of four possible orientations, labelled 11, 12, 13 and 14 in Appendix A. The coefficients s_{XX1}, s_{YY1} etc. are modified as determined by the orientation of the boundary elements. The values of the points T and Q which appear in Equation (5.5.2) also are determined by whether the boundary element is of orientation 11, 12, 13 or 14.

Consider the element labelled 15 in Figure 5.8. The program readily detects that the neighbouring elements $j2$ and $j-1$ (in this case elements 22 and 14 respectively) are water elements. Similarly it detects that the points $j1$ and $j+1$ are land elements. Thus, grid element 15 is determined to be a boundary point. In fact it is a Type 1 boundary point since two of the neighbouring grid points are land elements. Further, because of the nature of the four neighbouring grid points the program can determine that element 15 has the orientation 12. Therefore, the appropriate approximation to Helmholtz's Equation at grid element 15 is given by Equation (5.5.2) in which the coefficients are given by (A6(e)), (A9(b)-(e)) and (A11(b)-e)). The modifications which have to be made to these expressions for the coefficients because of the particular orientation of this boundary point are given by (A15 and A17). In a similar way, the finite difference approximations to the derivatives at all boundary points is obtained.

For Type 2 boundary elements, j, in which only one neighbouring grid point lies outside of the boundary, the following approximation may be used:

$$(q_{XX1}+q_{XX5})Z_T + q_{XX2}Z_Q + (q_{XX3}+q_{XX5})Z_R + (q_{XX4}-2q_{XX5}+k^2\Delta x^2 q_{XX5})Z_j = -q_{XX6}\Delta x. \tag{5.5.3}$$

where the coefficients q_{XX1}, q_{XX2} etc. are given by Equations (A24(b)-(f)) and (A23(f)). Once again, boundary elements of this type can occur in four possible orientations. The modifications which need to be made to q_{XX1}, q_{XX2} etc. because of these different orientations are given in Appendix A as are the positions of the points T, Q and R for each orientation.

The above equations (5.5.1, 5.5.2 and 5.5.3) are solved implicitly to give the solution for Z at each grid point.

The difference in the solutions from the two numerical models so far developed may not be due entirely to the way in which the boundary has been modelled. The first model is based on Equation (5.1.1) using the scheme presented in Section 5.2, whilst the second finite difference approach uses Equation (5.1.2) and an implicit solution to the approximations. For this reason, two more numerical solutions are developed for Equation (5.1.2) which firstly alter the boundary so that it lies along grid lines and secondly use second order approximations to the derivatives at the boundary. Hence, any difference between these last two numerical models and the one presented so far in this section must be due to the way in which the boundary is being modelled since all the models are second order and solved implicitly.

The first of these more conventional models is one in which the grid points are considered to lie along the boundary. Consider the point P lying along the straight boundary as shown in Figure 5.9. The grid points are separated by a distance Δx in both coordinate directions. An approximation for Helmholtz's Equation at P is

$$Z_T + Z_Q + Z_R + Z_S + (k^2\Delta x^2 - 4)Z_P = 0 \qquad (5.5.4)$$

which is simply the second order approximation for an interior point given in Equation (5.5.1). The problem with using Equation (5.5.4) is that the point T lies outside of the region. To find an expression for Z_T, a second order approximation is made to the boundary condition (5.1.2(b)). At P, the boundary condition implies

$$\frac{\partial Z}{\partial x} = -\frac{K\tau_0}{c^2}. \qquad (5.5.5)$$

Applying the second order approximation for the left hand side of the above equation yields

$$Z_T = Z_R + 2\Delta x \frac{K\tau_0}{c^2} \tag{5.5.6}$$

which may be substituted into Equation (5.5.4) to give the required expression for the approximation to the Helmholtz Equation, namely,

$$Z_Q + Z_S + 2Z_R + (k^2\Delta x^2 - 4)Z_P = -\frac{2\Delta x K\tau_0}{c^2}. \tag{5.5.7}$$

A boundary point, j, as defined earlier will be in this model a point such as P in Figure 5.9 which lies on a boundary. As discussed earlier in this section and in Appendix A, this point can be orientated in any of four ways which are once again denoted 11, 12, 13 and 14. These orientations are shown in Figure 5.10. In a similar fashion to the previous model a general formula can be given for all boundary points. This formula is then adjusted according to the particular orientation. From Equation (5.5.7) we have, for a boundary point, j,

$$Z_Q + Z_S + 2Z_R + (k^2\Delta x^2 - 4)Z_j = -2\Delta x A, \tag{5.5.8}$$

where:

(1) for orientation 11

$$Q = j + 1, \tag{5.5.9(a)}$$

$$S = j - 1, \tag{5.5.9(b)}$$

$$R = j2 \tag{5.5.9(c)}$$

and

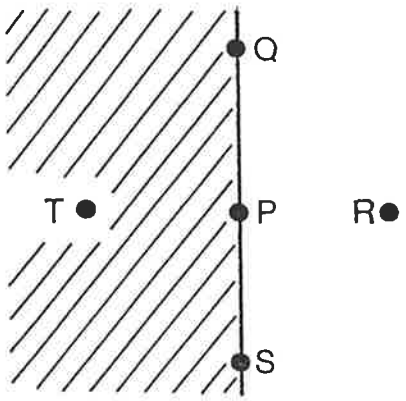

FIGURE 5.9: *A grid point, P, lying on a straight boundary with the four neighbouring grid points labelled Q, R, S and T. The shaded region lies outside of the closed basin.*

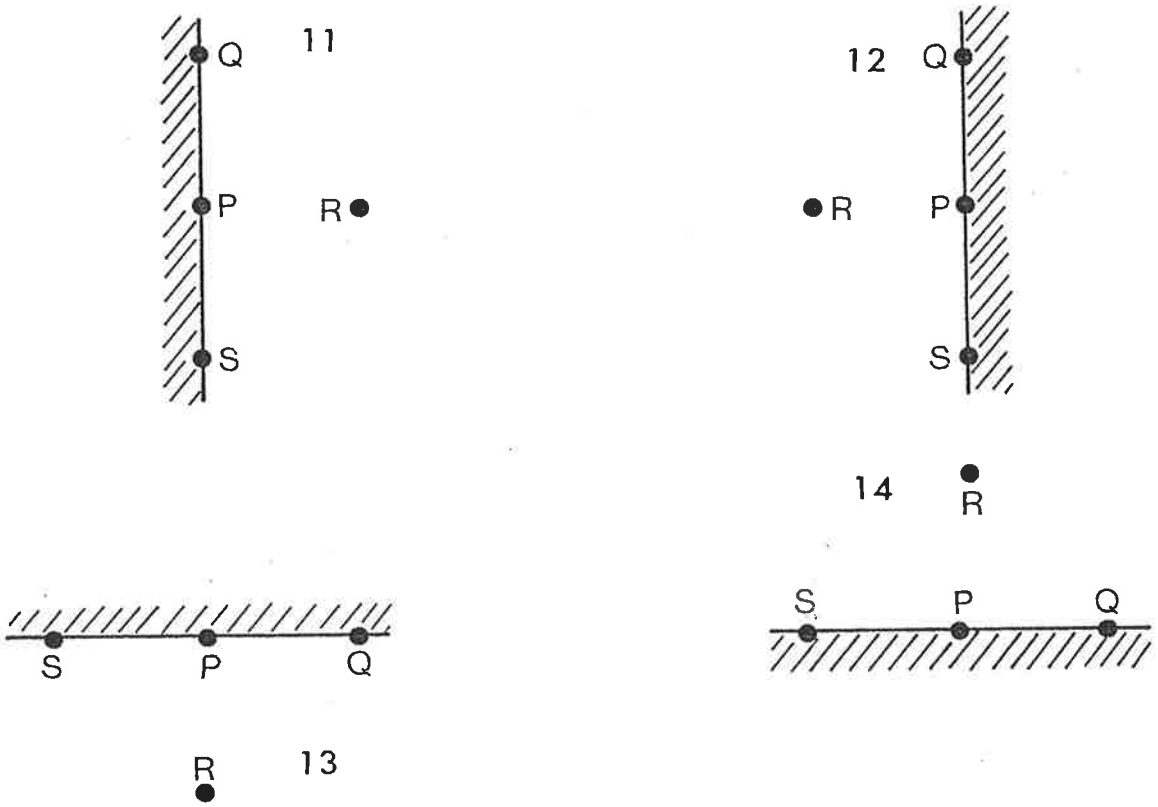

FIGURE 5.10: *The four possible orientations, labelled 11, 12, 13 and 14, of a boundary point such as P.*

$$A = -\frac{K\tau_0}{c^2}. \qquad (5.5.9(d))$$

(2) for orientation 12

$$Q = j + 1, \qquad (5.5.10(a))$$

$$S = j - 1, \qquad (5.5.10(b))$$

$$R = j1 \qquad (5.5.10(c)$$

and

$$A = \frac{K\tau_0}{c^2}. \qquad (5.5.10(d))$$

(3) for orientation 13

$$Q = j2 \qquad (5.5.11(a))$$

$$S = j1, \qquad (5.5.11(b))$$

$$R = j - 1 \qquad (5.5.11(c)$$

and

$$A = 0. \qquad (5.5.11(d))$$

(4) for orientation 14

$$Q = j2, \qquad (5.5.12(a))$$

$$S = j1, \qquad (5.5.12(b))$$

$$R = j + 1 \qquad (5.5.12(c)$$

and

$$A = 0. \qquad (5.5.12(d))$$

The boundary point, j, may also be a boundary point which lies on a corner as shown in Figure 5.11. Once again, there are four possible orientations for such a point, each denoted 21, 22, 23 and 24, and these are illustrated in Figure 5.11. A general formula for Helmholtz's Equation for such a boundary point is

$$2Z_S + 2Z_R + (k^2\Delta x^2 - 4)Z_j = -2\Delta x A, \qquad (5.5.13)$$

where:

(1) for orientation 21

$$R = j2, \qquad (5.5.14(a))$$

$$S = j - 1 \qquad (5.5.14(b))$$

and

$$A = -\frac{K\tau_0}{c^2}. \qquad (5.5.14(c))$$

(2) for orientation 22

$$R = j1, \qquad (5.5.15(a))$$

$$S = j - 1 \qquad (5.5.15(b))$$

and

$$A = \frac{K\tau_0}{c^2}. \qquad (5.5.15(c))$$

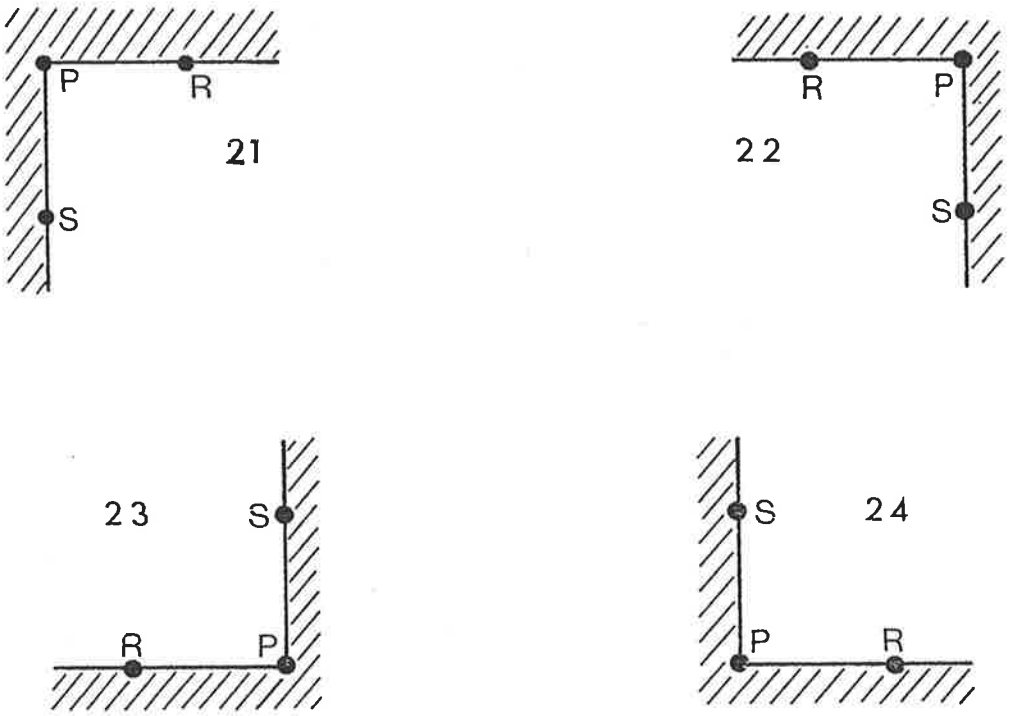

FIGURE 5.11: *The four possible orientations, labelled 21, 22, 23 and 24 of a corner boundary point such as P.*

(3) for orientation 23

$$R = j1, \qquad (5.5.16(a))$$

$$S = j + 1 \qquad (5.5.16(b))$$

and

$$A = \frac{K\tau_0}{c^2}. \qquad (5.5.16(c))$$

(4) for orientation 24

$$R = j2, \qquad (5.5.17(a))$$

$$S = j + 1 \qquad (5.5.16(b))$$

and

$$A = -\frac{K\tau_0}{c^2}. \qquad (5.5.16(c))$$

In this model, all points lying inside the boundary are interior points and the approximation at these points is given by Equation (5.5.1). The three sets of equations (5.5.1, 5.5.8 and 5.5.13) form the complete set of finite difference equations which may be used to model Helmholtz's Equation for the given normal derivative boundary condition. This set also forms the first of the conventional models which will be discussed. The model will be applied to a circle and the finite difference grid is positioned so that the grid points lie on the straight lines approximating the circle.

The second conventional model which will be described is very similar to the one described above. In this model, however, the grid lines of the finite difference

scheme are positioned so that the straight lines approximating the curved boundary lie midway between two parallel grid lines (see figure 5.12). In this model a boundary point is any point which lies immmediately adjacent to the boundary and is inside the boundary.

For all interior points, Equation (5.5.1) holds. All the remaining points may be placed into two groups as above. Also, just as above, there are four possible orientations for each group of boundary points. These orientations are exactly the same as those presented in Figures 5.10 and 5.11 except for the relocation of the boundary so that the points P, Q, R and S all lie exactly $\Delta x/2$ inside the solid boundary. For a point j such as shown in Figure 5.10 (with the boundary adjusted as indicated) the following approximation holds:

$$Z_Q + Z_R + Z_S + (k^2\Delta x^2 - 3)Z_j = -A\Delta x \tag{5.5.18}$$

where, for each of the orientations 11, 12, 13 and 14 the parameters Q, R, S and A are given respectively by Equations (5.5.9, 5.5.10, 5.5.11 and 5.5.12). For all the corner boundary points such as shown in Figure 5.11 (with the boundary adjusted) the following approximation holds:

$$Z_R + Z_S + (k^2\Delta x^2 - 2)Z_j = -\Delta x A \tag{5.5.19}$$

where, for each of the orientations 21, 22, 23 and 24, the parameters R, S and A are given respectively by Equations (5.5.14, 5.5.15, 5.5.16 and 5.5.17). The above two equations (5.5.18 and 5.5.19) are derived using the fact that the spatial derivatives at the boundary are approximated by formulae such as

$$\frac{\partial Z}{\partial x} = (Z_P - Z_T)/\Delta x. \tag{5.5.20}$$

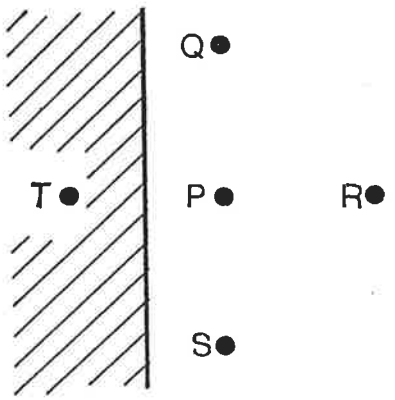

FIGURE 5.12: *The position of the boundary in relation to the grid points in the second conventional model.*

This second model represented by Equations (5.5.1, 5.5.18 and 5.5.19) will also be used to solve Equation (5.1.2) with a circular basin. The finite difference grid is positioned so that the staight lines approximating the curved boundary lie midway between adjacent lines of the grid. Differences between these two conventional models will be described in the next section.

§5.6 Comparisons Between The Finite Difference Models

Firstly, the performance of the numerical models described in the previous section was tested against results obtained from the analytic solution for the displacement occurring in a circular basin. All the parameters used in the comparison are the same as those used in producing Table 5.2. In this Section, however, a comparison is made using only a grid spacing of $\Delta x = \Delta y$ =2000 m. Note that this spacing corresponds to a spacing of $\Delta x = \Delta y$ = 1000 m. in the staggered grid model. The analytic solution is available from Equation (3.2.2).

A comparison between the first numerical method developed in the previous section and the analytic solution is made in Table 5.5. Clearly, this finite difference model performs well. The largest relative percentage error of 2.6% was found to occur along the line $\theta = 0$. This result is far better than that achieved with the previous numerical solution discussed (see Table 5.2). A comparison is made in Table 5.6 between the three models models so far tabulated (that is, the integral equation method, the numerical solution of Section 5.3 and the first model of Section 5.5). This table, therefore, summarises results presented in Tables 3.2,

		GAIN		PHASE LAG	
		∇	%	∇	%
$\Delta x = \Delta y = 2000\ m$	$r = a/4, \theta = 0$	0.0000	0.00	0.0004	2.60
	$r = a/4, \theta = \pi/2$	0.0000	0.00	0.0000	0.02

TABLE 5.5: *Comparison of the first numerical model for Helmholtz's Equation presented in Section 5.5 against the analytic solution for a circle.*

	GAIN		PHASE LAG	
	∇	%	∇	%
Integral Equation Solution; Table 3.2	0.0000	0.00	0.0001	0.50
First Numerical Solution; Table 5.2	0.0006	6.26	0.0045	29.23
Second Numerical Solution; Table 5.5	0.0000	0.00	0.0004	2.60

TABLE 5.6: *Comparison of the three methods used so far for the wind forced problem with a circular basin. The results are presented at $\theta = 0$ and $r = a/4$. The results for the Integral Solution are obtained with $N = 36$.*

5.2 and 5.5. Clearly, the two methods which most closely approximate the real boundary are to be recommended. Of these two, the integral equation approach appears to be better. However, it is difficult to make a direct comparison between these two methods because of the difficulty in relating the grid spacing, Δx, to the summation number, N. For the given values of Δx and N used in Table 5.6, the integral equation method needed substantially more CPU time to solve the problem then did the finite difference solution and so from this point of view, the finite difference approach could be preferred.

A further comparison was made between the finite difference model which does not alter the curved boundary and the boundary integral solution. A useful comparison of the two methods can be made by requiring the two solutions to use a similar amount of computer CPU time when the programs are run. For a value of $\Delta x = 1000m$ in the finite difference model, a value of $N = 115$ resulted in the boundary integral solution using about the same CPU time.

Table 5.7 compares the two methods with the analytic solution. The largest errors which occurred when using the finite difference method were found to lie along the line $\theta = 0$ and for this reason the comparisons in Table 5.7 are made along this line at $r = a/4$. The results shown in this table suggest that under the criterion of equivalent CPU times the finite difference solution appears to be better. This is an encouraging result. A major reason for using boundary integral techniques is often because the boundary of the region of interest can be modelled more correctly. However, as has been shown, if special finite difference formulae are used which are capable of modelling the boundary accurately, then results which are at least as good as those obtained with the boundary integral approach may be achieved.

In Table 5.8 the differences between the finite difference solution first developed in the previous section and the two conventional models are displayed. A grid spacing of $\Delta x = 2000\ m$ is used. Once again, the largest error in results was found to lie along the line $\theta = 0$ and results from the various models are given for the point $\theta = 0$ at a distance of $a/4$ from the origin. From Table 5.8, it is clear

	GAIN		PHASE LAG	
	∇	%	∇	%
Boundary Integral Solution	0.00002	0.16	0.00005	0.35
Second Finite Difference Solution	0.00001	0.01	0.00005	0.34

TABLE 5.7: *Comparison of the curved boundary finite difference solution presented in Section 5.5 with the Boundary Integral solution with* $\Delta x = 1000\ m$ *and* $N = 115$.

	GAIN		PHASE LAG	
	∇	%	∇	%
First Conventional Solution	0.0000	0.00	0.0015	9.70
Second Conventional Solution	0.0000	0.00	0.0010	6.50
Curved Boundary Solution; Table 5.5	0.0000	0.00	0.0004	2.60

TABLE 5.8: *Comparison of the three numerical models presented in Section 5.5 and used to solve Helmholtz's Equation.*

that the first model discussed in the previous Section which uses second order differences to approximate the curved boundary provides superior results. Of the two conventional models, both of which are second order, the one in which the boundary bisects two adjacent grid lines provides the best results.

Comparing Table 5.6, 5.7 and 5.8 it is apparent that in solving wind forced problems for which either Equation (5.1.1) or Equation (5.1.2) may be used, better overall results were obtained using Equation (5.1.2) than with the method presented for Equation (5.1.1). Using methods which enable the boundary points to be modelled with the same accuracy as the interior points gives far better re-

sults than a conventional treatment in which the boundary is approximated by a set of straight line segments.

CHAPTER 6

EDDY VISCOSITY - A REVIEW

All of the work discussed so far has dealt only with depth integrated models. These models provide no information about the nature of the vertical profile of the horizontal velocity components. In order to achieve this information, equations similar in form to (1.3.3) must be used. However, as was stated in Chapter 1, in order to use these equations the eddy viscosity, N, must be specified. This chapter examines the various formulations for N which have been deduced from laboratory and field experiments and also those forms of N which have been used in numerical models. Finally, methods which allow the eddy viscosity to be calculated as part of the solution procedure are discussed. The following work is directed mainly at wind driven flows but, because of their similarity with and because they are often considered in conjunction with wind driven flows, tidal flows will also be mentioned.

§6.1 EXPERIMENTAL OBSERVATIONS

Because of the relationship between the eddy viscosity and the gradient of velocity, it is useful to first discuss observations of currents which have been made in tidal or wind driven oscillating flows. In particular, since the vertical gradient of the horizontal velocity components is dominant in the types of flows considered here, the vertical profile of the horizontal components is of prime importance.

In the following work, the variable u is used to represent the horizontal velocity components. Analogous results hold for v. Similarly, for other vector components; equations will be given only for the x-component, with analogous results holding for the other components. Also, in the following discussion the transformed depth, η, defined in Chapter 1, will be used.

In the bottom boundary layer of such geophysical flows (that is as $\eta \to 0$), the Reynolds stresses may be assumed to be constant (see, for example, Bowden et. al. (1959), Engelund (1973), Swift et. al. (1979) or Duncan et. al. (1978)). This leads to the universal law of the wall which states that

$$u \sim \log \eta \qquad \text{as } \eta \to \text{wall}, \tag{6.1.1}$$

that is, the vertical profile of velocity is logarithmic near a solid boundary. From Equation (1.3.1) this law implies that

$$N \sim \eta \qquad \text{as } \eta \to \text{wall}. \tag{6.1.2}$$

That is, in the boundary layer near a wall it is expected that N increases linearly with height above the wall from some small value usually taken to be zero or the kinematic viscosity, ν, of the water. If a wind stress is acting upon the surface of the water, then it would be expected that the above relationships between N and u and depth would also hold near the surface.

Whether the fluid in tidal and wind driven flows does in fact behave in this manner, has been examined by many workers since early this century. As early

as 1925, Powell (1925), examined the tidal flow in the Sound of Jura which has a depth of about 50 m. He concluded, however, that the velocity of tidal current decreased with the square of depth. Van Veen (1938), from his observations of the tidal current in a channel, proposed

$$u = u_s \eta^{\beta} \tag{6.1.3}$$

where u_s is the surface velocity and β is some constant. The best fit of Equation (6.1.3) to the data was achieved with $\beta^{-1} = 5.2$. This is very near to a logarithmic variation of u with η for small η.

Bowden et. al. (1959) observed the tidal current in homogeneous water of depth of 22 m. in the Irish Sea. They concluded that a reasonable approximation to the velocity profile was given by a model in which the profile was logarithmic to a height αh above the sea floor (where h is the depth of water and α is a constant) and the profile was parabolic above this height. From their observations they concluded that $\alpha = 0.14$.

Dyer (1970) measured the vertical profile of horizontal currents in a channel for a complete tidal cycle in the West Solent near Southampton. In most observations, the bottom 2.3 m of water (in a total depth of about 18 m) could well be represented by a linear relationship between velocity and the logarithm of height.

During investigations in six tidal channels at depths of 8 m to 42 m. in Puget Sound and the Strait of Juan de Fuca area, Sternberg (1968) found logarithmic

profiles near the bottom occurred for 85% of the time, although for individual channels the proportion ranged from 62% to 100%.

Further investigations of the vertical profile of velocity are to be found in Grace (1929), Harvey and Vincent (1977), Wolf (1979), Heathershaw (1979) and Soulsby and Dyer (1981).

The existence of a logarithmic velocity profile near solid boundaries is thus well established. The mathematical analysis predicting its existence (the law of the wall) was established considering steady flows. Presumably, this logarithmic profile is observed in tidal flows because the time scale of the oscillating flow near the wall is small compared with the tidal period, enabling a quasi-steady state to develop.

It was stated above that just as the bottom shear stress causes a logarithmic velocity profile near the bed, a surface wind stress causes a logarithmic velocity profile in the topmost layer of water. This fact was recorded by Shemdin (1972) and also by Francis (1953) who experimentally examined the vertical velocity profile in steady circulation caused by water jets on the surface of a laboratory flume to simulate stress caused by a wind.

Lathbury et. al. (1960) observed a near surface logarithmic velocity profile in their work on the hypolimnion of Lake Mendota.

Baines and Knapp (1965), Fitzgerald and Mansfield (1965) and Koutitas and O'Connor (1980) all examined the turbulent flow in a closed channel acted upon

by a surface wind stress. The vertical profiles for velocity which they recorded are compared in Figure 6.1.

Verification of the existences of bottom and surface logarithmic boundary layers certainly aids in formulating an expression for the eddy viscosity in these regions. However, to obtain a complete picture, requires obtaining the Reynolds stresses, accurate measurements of which are very difficult to obtain. Heathershaw and Simpson (1978) report that the sampling error in measuring the Reynolds stress can be as high as 40%.

Amongst early investigators concerned with the measurement of the eddy viscosity were Nomitsu and Matsuzaki (1936) who examined the vertical distribution of eddy viscosity in rivers. Neglecting convection and horizontal diffusion terms and considering river flow to be steady and one dimensional yields the following momentum equation:

$$\frac{1}{h^2}\frac{\partial}{\partial \eta}\left(N\frac{\partial u}{\partial \eta}\right) = -g\rho\frac{\partial \zeta}{\partial x}. \tag{6.1.4}$$

Using field measurements of the surface slope and the vertical velocity profile, Nomitsu and Matsuzaki (1936) integrated the above equation resulting in a formulation for N. In large rivers tens of metres deep they found that N did not vary greatly with depth but was rather uniform except in the bottom one to two metres. They also found that the shallower the river, the larger the coefficient of eddy viscosity. The overall shape of the profile was found to be concave upwards especially in the upper parts of the fluid column and N increased rapidly near the bottom to eighty to ninety percent of its surface value. In shallower rivers, only

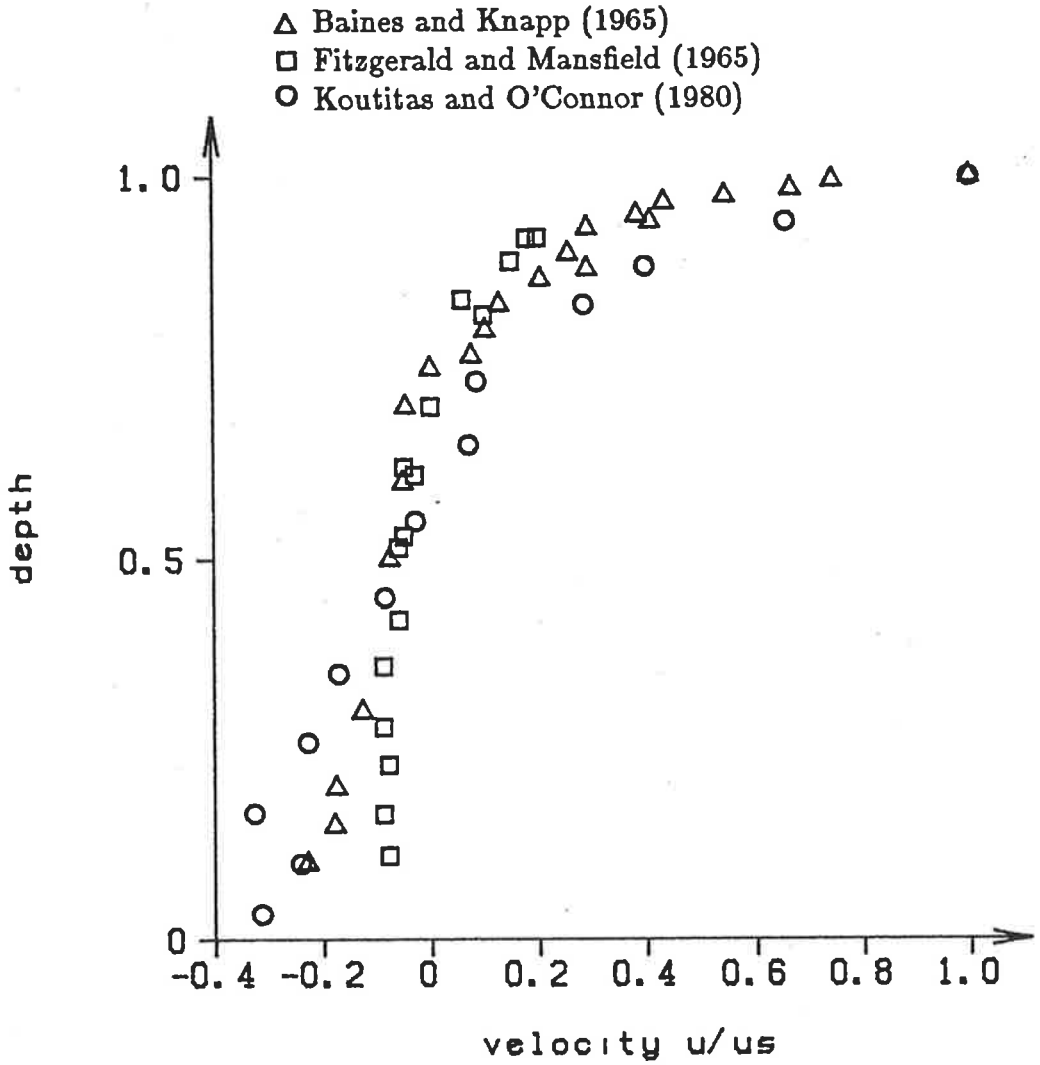

FIGURE 6.1: *Plots of the normalised wind driven velocity profile in a channel of uniform depth.*

a few metres deep, they observed that N seemed to vary with the square of the velocity except in the bottom layer of about one metre.

Bowden et. al. (1959) measured the Reynolds stresses as well as the vertical variation of velocity. From these measurements they concluded that N is greatest near mid-depths, with a maximum at $\eta = 0.375$. They also found that N attained its greatest value at times nearly three hours before and three hours after high water, when the current is greatest. No reliable estimates were available at times of high water when the currents and stress are small. They deduced that a good theoretical model for N which would describe the flow was one in which N increased linearly from $\eta = 0$ to a height $\eta = \alpha$ and then took the constant value

$$N = \kappa \alpha u_{*b} h \qquad \alpha \leq \eta \leq 1 \tag{6.1.5}$$

where κ is Von Karman's constant ($\kappa \approx 0.41$) and u_{*b} is the friction velocity at the bottom, that is, $u_{*b} = \sqrt{\tau_b/\rho}$ where τ_b is the bottm stress. They also found that the maximum value of N could be represented by

$$N_{\max} = 2.9\text{x}10^{-3}|U|h \tag{6.1.6}$$

where U is the depth integrated velocity.

Bowden and Hamilton (1975) suggest using the following expression for N in turbulent flow near a solid boundary where the velocity profile is logarithmic:

$$N = \kappa h u_{*b}(\eta + \eta_r) \tag{6.1.7}$$

where η_r is the roughness height.

For steady flow with no surface stress, Rossby and Montgomery (1935) deduced

$$N = \kappa h u_{*b} \eta (1 - \eta). \tag{6.1.8}$$

This parabolic form of N is zero at the bottom and top and reaches its maximum value at $\eta = 0.5$ with

$$N_{\max} = 0.25 \kappa h u_{*b}. \tag{6.1.9}$$

In a laboratory experiment, Jobson (1968) and Jobson and Sayre (1970) determined a parabolic distribution for the eddy viscosity similar to that described by Equation (6.1.8) in which u_{*b} is replaced by the shear velocity, u_*, of the fluid. This velocity was determined from the shear stress which was assumed to vary linearly from zero at the bottom to a value of $\gamma h S$ at the surface where γ is the weight of a unit volume of water and S is the energy gradient. Knight et. al. (1980), in their survey of the Great Ouse estuary, also plotted out the profile of N with depth. The measured values were much less than those predicted by Equation (6.1.8).

The eddy viscosity is also modified by the stability of the fluid. For example, Munk and Anderson (1948) introduced

$$N = N_0 (1 + 10 Ri)^{-1/2} \tag{6.1.10}$$

where N_0 is the eddy viscosity in conditions of neutral stability and Ri is the Richardson number defined by

$$Ri = -\frac{gh}{\rho} \frac{\partial \rho}{\partial \eta} \Big/ \left(\frac{\partial u}{\partial \eta} \right)^2. \tag{6.1.11}$$

The Delft Hydraulics Laboratory (1974) have investigated many different relationships for N in cases where a density gradient exists.

From the discussion so far it seems that an exact formulation for N is difficult to acquire. Certainly, assuming N to be independent of time is physically unrealistic. At the very least, N should be considered to vary with time according to the instantaneous values of $|u_{*b}|h$ or $|U|h$. The values of N determined in field investigations vary greatly. Indeed, Bowden and Fairbairn (1952) were unable to deduce the dependence of N on depth because of the large range of values obtained from different stations in the Irish Sea. They found values ranging from $10^{-3}\ m^2sec^{-1}$ to $10^{-2}\ m^2sec^{-1}$. Bowden et. al. (1959) estimate that the errors which occur in their values of N could be in error by as much as 50%.

When a wind is acting on the surface of the fluid, a formulation for N is still difficult to obtain from observation. Bowden (1964) relates N to wind speed, W, measured at a height of 15 m by

$$\rho N = W^2 \qquad \text{for } W > 6\ msec^{-1}. \tag{6.1.12}$$

Bengtsson (1973) experimentally examined the variations of the eddy viscosity with depth in a wind affected lake. The eddy viscosity was found to increase linearly with wind speed.

Koutitas and O'Connor(1980) also measured the eddy viscosity occurring in wind induced flow in a closed channel. Their resultant profile for N is shown in Figure 6.2

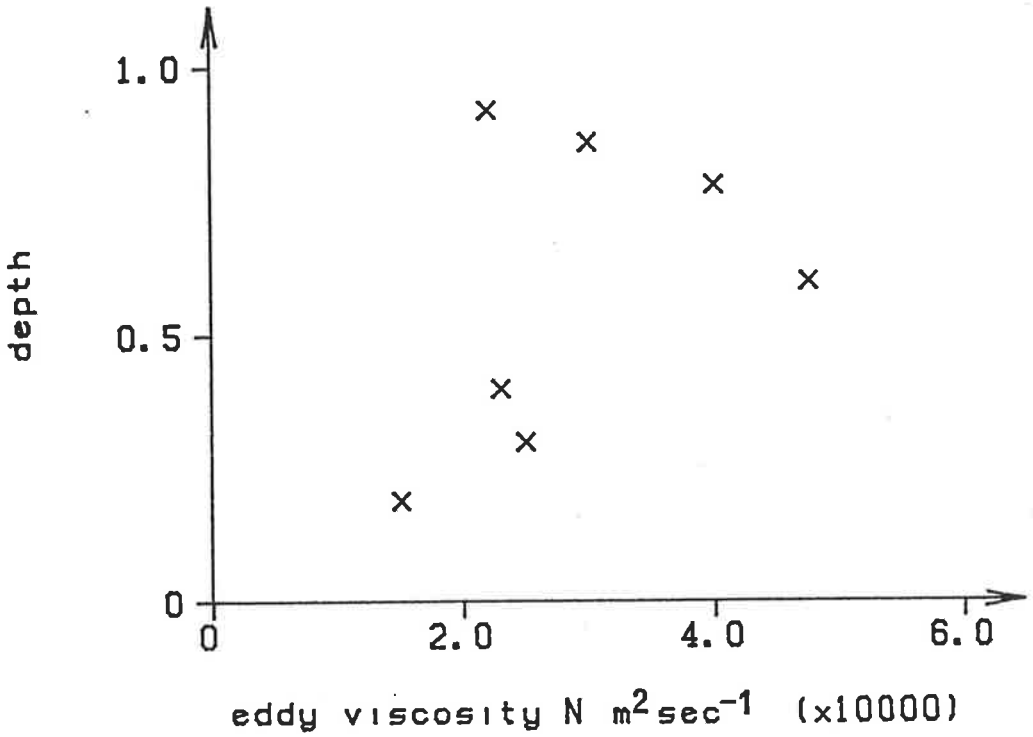

FIGURE 6.2: *Plots of the eddy viscosity profile in a channel of uniform depth as recorded by Koutitas and O'Connor (1980).*

Huang (1979) presents a list of values of N which have been experimentally deduced for both wind and tidal problems by different authors. He also gives forms of N which have been used in theoretical models. The experimentally determined values of N were found to vary considerably, from 0.1 $m^2 sec^{-1}$ to $4x10^{-3}$ $m^2 sec^{-1}$. Similarly, the expressions which have been used in theoretical models also vary greatly from a linear dependence on depth to a parabolic and even an exponential dependence.

§6.2 The Vertical Eddy Viscosity Used In Mathematical Models

The first workers examining the flow regime in wind forced motions occurring in shallow sea and estuaries assumed the eddy viscosity was an absolute constant (see, for example, Bowden (1953), Tarayev (1958(a)), Birchfield (1971), Heaps (1972) and Cooper and Pearce (1980)). Cooper and Pearce (1982) develop a three dimensional model for analysing the currents produced in seas during the passage of storms. They use Galerkin techniques in their model and it is capable of coping with any form of N which varies piecewise linearly with depth. However, they used a form of N invariant over depth when producing any results.

Reasonable results have been obtained when using a constant form of N as in the above models. However, a slip velocity condition at the bottom needed to be used to achieve this. A similar requirement was observed in models of tidal flow. Johns (1966) and Stolzenbach et. al. (1977) both obtained poor agreement with observed results when a constant N was used in conjunction with a no-slip

condition. However, Raney et. al. (1980) used a constant eddy viscosity with a no-slip bottom condition on velocity in a three dimensional storm surge model. Like the tidal model of Lee (1969), which employs the same assumptions, this model surprisingly produced good qualitative results but the model was not well validated.

Using the constant eddy viscosity model with a slip condition, Heaps (1972) also examined the sensitivity of the bottom current and the surface elavation to the value chosen for N (see Figure 6.3). Figure 6.4 shows the velocity profiles for both u and v obtained using different values of N and r, the linear friction coefficient. The profiles obtained are much more sensitive to changes in N than r. Clearly, from these two figures, the value of the eddy viscosity coefficient can significantly affect the results from an oceanographic model. The best value of N which should be used is usually obtained by "tuning" the model with observed results. If a constant value of N is not used then just as much care should be taken in obtaining a good approximation for the variation of N with depth.

In a later paper, Heaps (1982) developed a three layered numerical model to describe the motions of a stratified sea. This spectral model was applied to the Celtic Sea which has a mean depth of about 100 m. The bottom layer of the model was assumed to be of depth 60 m, the middle layer to be 15 m deep and the top layer was 25 m deep. Within each layer, the density was assumed to be constant but was different between layers. The vertical eddy viscosity was modelled similarly. In the bottom layer, the eddy viscosity was taken to be $N_1 =$

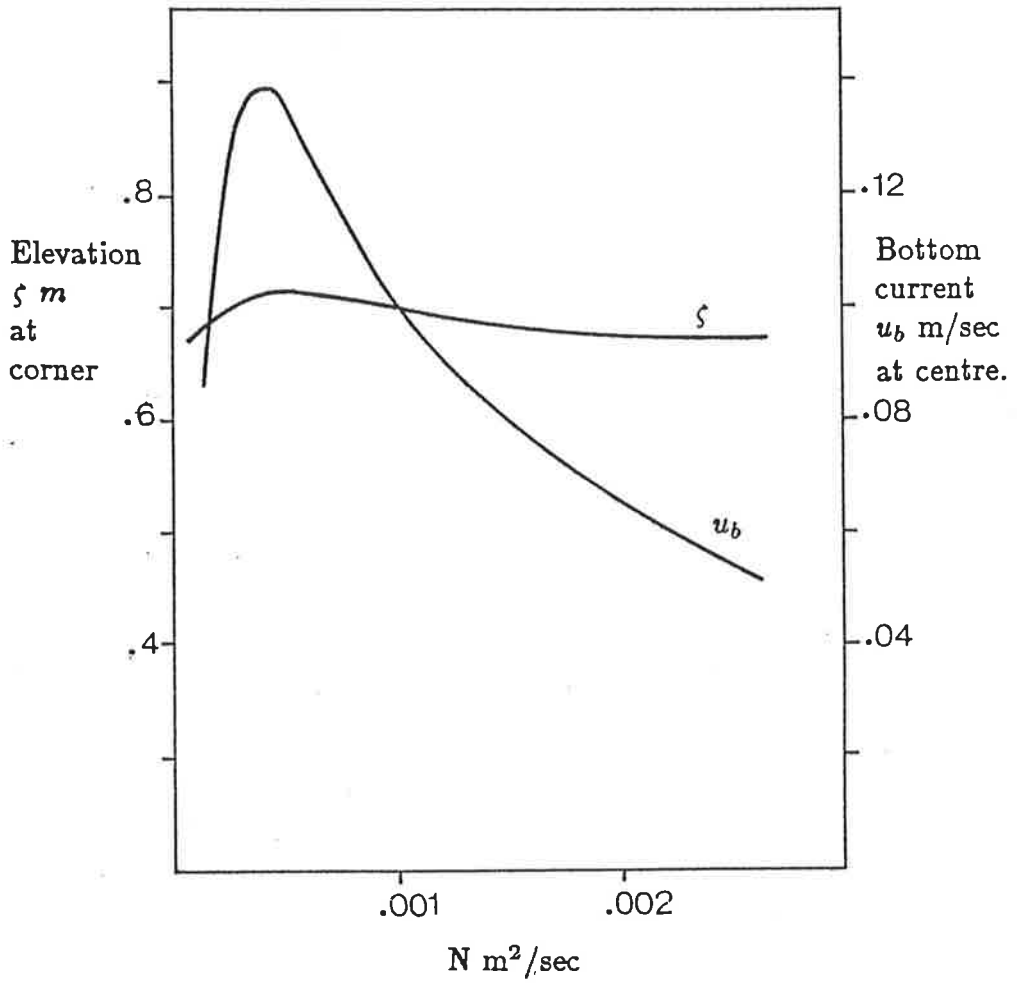

FIGURE 6.3: *Variation with vertical eddy viscosity coefficient, N, of*
(a) mean surface elevation, ς m at the corner of a rectangular basin of depth 65 m, length 800/17 km. and breadth 400/9 km. and
(b) bottom current speed u_b m/sec at a central position
in the equilibrium situation produced by a steady wind stress of 1.5 N/m².
After Heaps (1972)

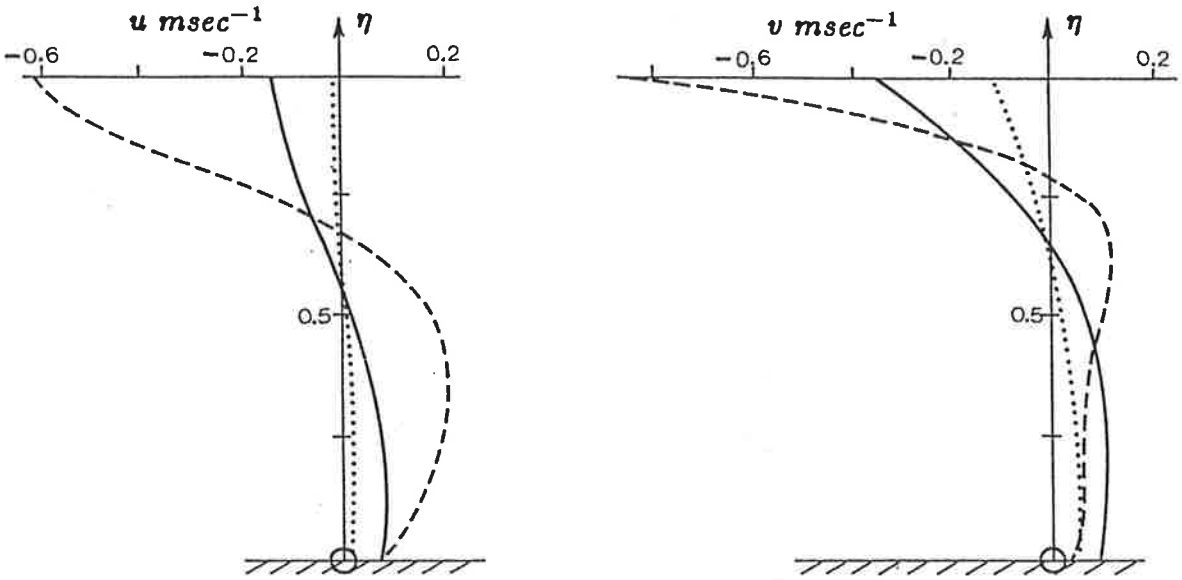

FIGURE 6.4(a): *Depth distribution of components of the horizontal current at the centre of a rectangular basin as described in Figure 6.3 after the establishment of a steady circulation produced by a longitudinal wind stress of 1.5 N/m^2. The results are computed for r = 0.002 m/sec and various values of the eddy viscosity coefficient, namely,*

$N = 0.013\ m^2/sec$ – – – – – – –

$N = 0.065\ m^2/sec$ ————————

$N = 0.260\ m^2/sec$ .....

After Heaps (1972)

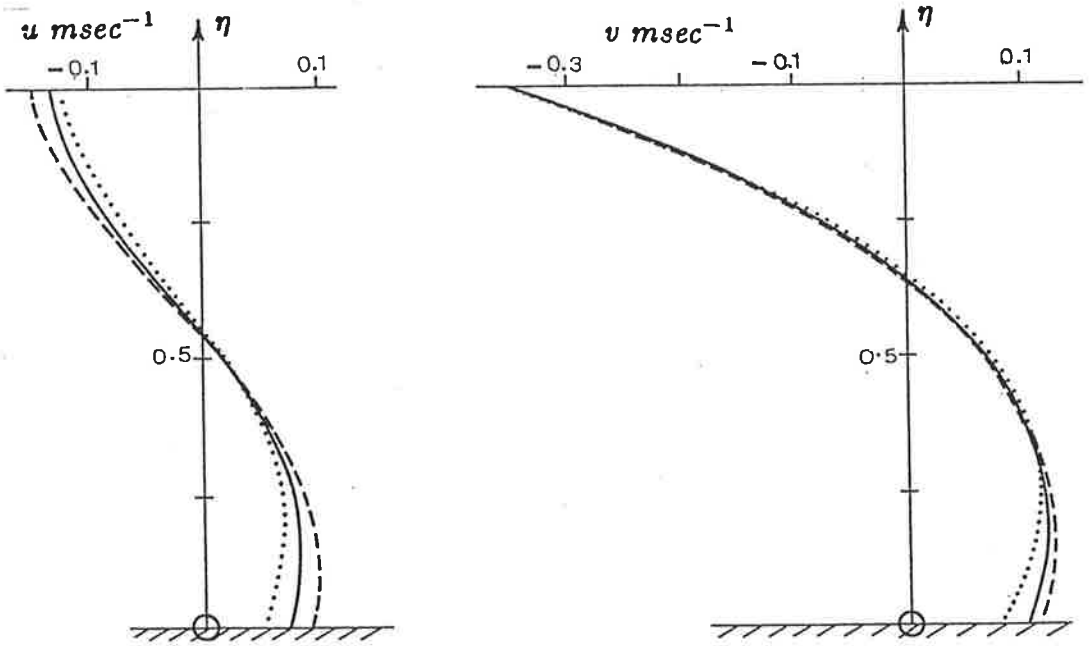

FIGURE 6.4(b): *As in Figure 6.4(a) except that N takes the constant value 0.065 m^2/sec and r takes various values, namely,*

r=0.001 m/sec – – – – – – –

r=0.002 m/sec ————————

r=0.004 m/sec .....

After Heaps (1972)

$10^{-2}\ m^2 sec^{-1}$, in the middle layer $N_2 = 10^{-3}\ m^2 sec^{-1}$ was used and in the top layer $N_3 = 3\text{x}10^{-2}\ m^2 sec^{-1}$. The value of N_3 is an estimate corresponding to a wind stress of 0.1 Nm^{-2}. The comparitively low value of N_2 was chosen to reflect a situation of vertical stability in the thermocline, while the value of N_1 was taken to be larger than N_2 since vertical stability in the bottom layer was comparitively weak. However N_1 was taken to be smaller than N_3 due to the separation of the bottom layer from the wind force upper layer by the middle layer.

Davies (1977) also used a constant eddy viscosity with a slip condition in his three dimensional model of a closed, rectangular rotating basin acted upon by a homogeneous wind. He used finite difference techniques in the horizontal combined with Galerkin techniques over depth. The effect of using different basis functions is examined in later papers (for example, see Davies (1980(a)) and Davies and Owen (1979)). Davies also proposed an eddy viscosity whose depth variation is shown in Figure 6.5. The effect of varying N_0, N_1 and N_2 on the vertical velocity profiles is also examined. Results from this work can be found in, for example, Davies (1980(b), 1982(a),(b),(c) and 1983).

In Davies (1981) a three dimensional ocean shelf model is developed. Both stratified and homogeneous seas are considered. In the latter case, a constant eddy viscosity was defined by

$$N = c|U|^2/\sigma \tag{6.2.2}$$

where $\sigma = 10^{-4} sec^{-1}$ and $c = 2\text{x}10^{-5}$ were considered appropriate values for an M_2 tide on a shelf. When the effect of a wind on a stratified sea was considered, an

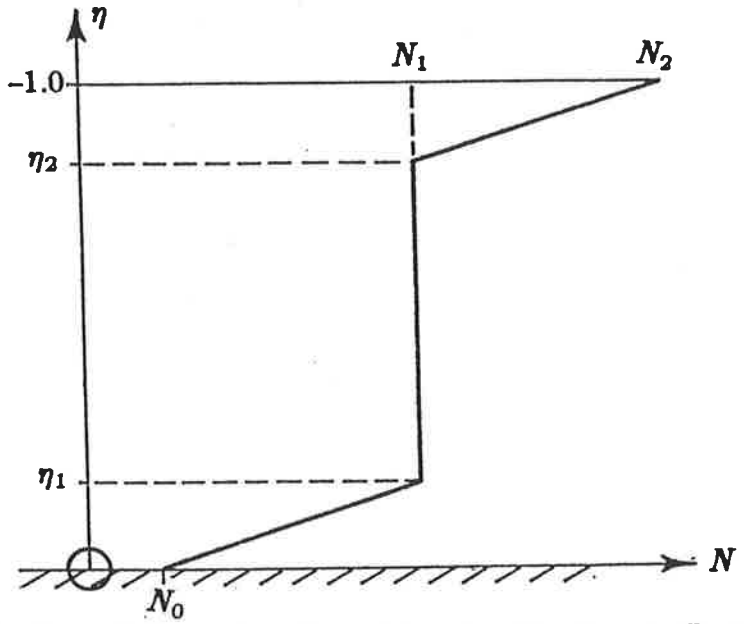

FIGURE 6.5: *Depth variation of vertical eddy viscosity used by Davies (1980(b), 1982(a), (b), and (c) and 1983).*

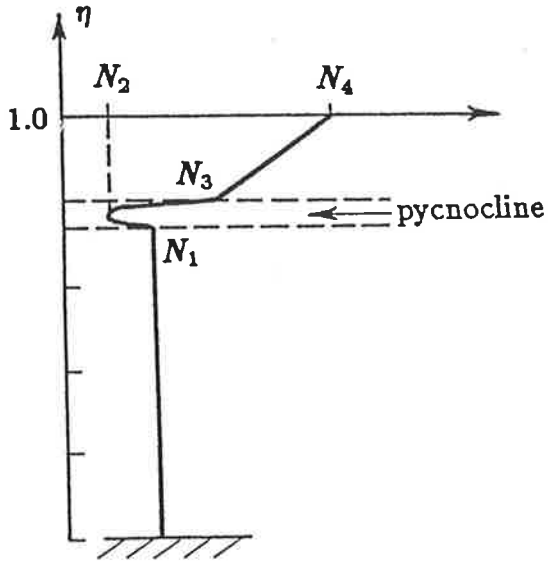

FIGURE 6.6: *Vertical variation of eddy viscosity for a stratified lake as proposed by Davies (1981).*

eddy viscosity formulation was used which did not vary with horizontal position or time and had the vertical distribution shown in Figure 6.6. The eddy viscosity was assumed to decrease linearly in the top 50 m of the water column with $N_4 = 5\text{x}10^{-2}\ m^2 sec^{-1}$ and $N_3 = 2\text{x}10^{-2}\ m^2 sec^{-1}$. This represents a surface layer in which the wind generated turbulence decreases linearly with depth. Below the surface layer, there is a layer of 10 m. thickness corresponding to the pycnocline. Within this layer, turbulence is suppressed and this reduction is modelled by a reduction in the value of the eddy viscosity to a value of $N_2 = 10^{-3}\ m^2 sec^{-2}$ in the centre of the pycnocline. Below this layer, turbulence was assumed to be of tidal origin and a constant value of $N_1 = 10^{-2}\ m^2 sec^{-1}$ was used throughout the remaining depth of water.

Pearce and Cooper (1981) also developed a numerical model similar to those of Heaps and Davies mentioned above. The form of eddy viscosity used was similar to that shown in Figure 6.5 except $N_1 = N_0$. The value at the surface was chosen to be $2.5\text{x}10^{-6}\ m^2 sec^{-1}$ and at depths below $\eta = 0.8$, an eddy viscosity given by $N_0 = u_{*s}h/12$ was prescribed. The form near the surface was originally proposed by Csanady (1978) while the latter formulation was previously used by Townsend (1976). This model gives good agreement with the experimental results of Baines and Knapp (1965) and Shemdin (1968).

There is an important feature of models such as that used by Pearce and Cooper (1981). An expression to determine the bottom stress is usually required. An equation such as (1.2.5(b)) or its linear equivalent is often used but Pearce and

Cooper (1981) used a linear stress law given by

$$\tau_b = C_b' \rho u_b. \tag{6.2.3}$$

The drag law coefficient, C_b' which depends on the flow must be prescribed. To fit the experimental data of Baines and Knapp (1965), a value of $C_b' = 5\text{x}10^{-5}\ msec^{-1}$ was used but to fit the data of Shemdin (1968), a value of $C_b' = 2\text{x}10^{-2}\ msec^{-1}$ was required. The fact that this parameter may take a value within such a large range makes the model difficult to apply to any real situation for which there are no experimental results available with which the numerical model may be calibrated.

Simons (1971) and Leendertse et. al. (1975(a),(b)) also used layered models. In both models, the fluid is divided into several layers within which the eddy viscosity is assumed constant.

Since a logarithmic velocity profile is expected near the surface, Johnson (1967) chose

$$N = \kappa_s h u_{*s}(1-\eta) \tag{6.2.4(a)}$$

near the surface and

$$N = \kappa h u_{*b} \eta \tag{6.2.4(b)}$$

near the bottom. The constants κ_s and κ are the "mixing constants" and so κ is Von Karman's constant for wall flow and κ_s is the analogous quantity for surface flow ($0.4 \leq \kappa_s \leq 1.0$). Johnson (1967) then postulates that the form of N for the entire flow is

$$N = \kappa u_{*b} h \eta (1-\eta)(1+\beta\eta) \tag{6.2.5}$$

for some constant β and for which it was assumed that

$$\kappa_s u_{*s}/\kappa u_{*b} = 1. \tag{6.2.6}$$

The results of a model using Equation (6.2.5) are compared with the experimental results of Fitzgerald and Mansfield (1965) in Figure 6.7. Good agreement for the vertical form of the horizontal veclocity profile was achieved near the surface and bottom, but the agreement in the central regions is not good. The formulation described by Equation (6.2.4) with $\kappa_s = \kappa$ was also used by Madsen (1977) in a model of wind driven ocean flows. In the middle regions of the flow N was assumed constant. Thus, the profile is similar to that shown in Figure 6.5 with $N_0 = N_2 = 0$. The slopes of the lines at the top and bottom are determined by Equation (6.2.4). For very shallow water Madsen (1977) proposed $\eta_1 = \eta_2$.

A more complicated form for N was proposed by Dyke (1977) in his model of the surface layer of an ocean acted upon by a steady wind stress. His formulation was

$$N = N_0 \left(1 - \alpha h(\eta - 1)\right)^2 \tag{6.2.7}$$

for some constant α.

M^{c}Phee (1979) in contrast chose

$$N = u_{*s}\kappa h(1 - \eta) \exp\left(cfh(\eta - 1)/u_{*s}\right) \tag{6.2.8}$$

in his model of the effect of pack ice moving over the surface of a deep ocean. This expression for N implies that the eddy viscosity reaches its maximum value

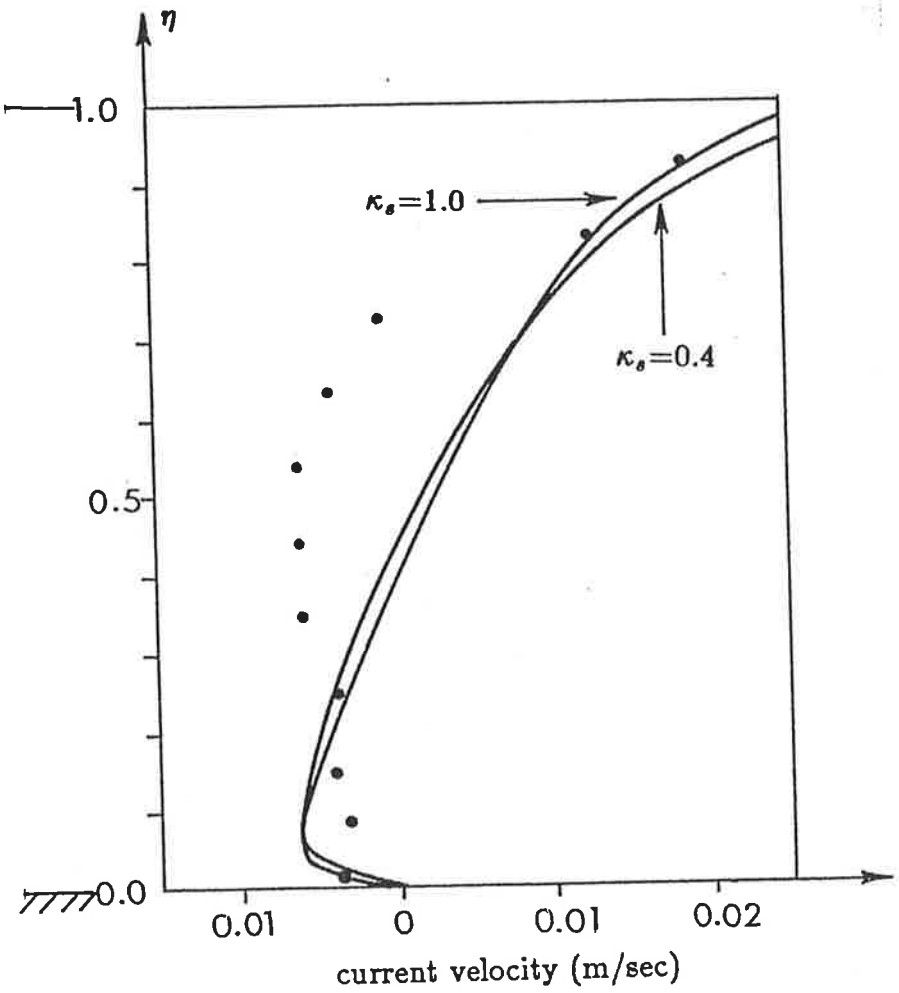

FIGURE 6.7: *Comparison of experimental data (•) obtained by Fitzgerald and Mansfield (1965) with theoretical velocity profiles computed by Johnson (1967) for two values* κ_s.

just below the surface and decreases below that. The parameter f in the above equation is the Coriolis parameter whilst c was given by a function involving u_{*s}, N, f, h and η.

Thomas (1975) in his study of shallow basins acted upon by a steady wind, used a linear variation of N as given by Equation 6.2.4(a)). A no-slip condition on velocity was used at the bottom. An iterative scheme was developed so that the analytic formulation for u was forced to be asymptotic to a logarithmic profile at the bottom. Good results were obtained but only with great computational effort and complexity. These computational difficulties caused Witten and Thomas (1976) to abandon this method of solution in favour of more conventional methods. Stolzenbach et. al. (1977) found that analytic results obtained using Equation (6.2.4(b)) and the equations describing wind driven flow in an infinite channel and a channel of finite length were in poor agreement with laboratory results.

Tarayev (1958(b)) used a vertical eddy viscosity coefficient with only a linear dependence on η, namely,

$$N = \gamma\eta \tag{6.2.9}$$

for some constant γ, in his model of an oscillating wind over a shallow sea. He states that a deficiency in his model is the neglect of time dependence in his formulation of N and concludes that any a priori attempt to define such a dependence would be extremely difficult unless it is defined to depend on u_{*b} or u, as in several of the previously discussed models.

Analytic solutions describing the near bed velocity profile in a tidal channel in which an oscillating boundary condition is imposed on the velocity at the open of the channel, are presented in Lavelle and Mofjeld (1983). A time dependent eddy viscosity coefficient whose vertical profile varied as shown in Figure 6.5 (with $N_1 = N_2$) was used. The actual formulation used was

$$N = \begin{cases} \kappa|u_b|h\eta & \eta_r \leq \eta \leq \eta_1 \\ \kappa|u_b|h\eta_1 & \eta > \eta_1 \end{cases} \qquad (6.2.10(a))$$

in which η_r is the roughness height and u_b is a function of time and is a modified bottom friction velocity defined by

$$u_b = \left[u_{*b}^2 + \epsilon^2 u_{*b}^2(t + T/4)\right]^{1/2}, \qquad (6.2.10(b))$$

where T is the period of the oscillation of the velocity at the open end and ϵ is a constant given the value of 0.2. The height, η_1, at which N becomes a constant was determined by the intensity of the flow. An alternative form of N for which numerical solutions were obtained was also used by Lavelle and Mofjeld (1983). It was

$$N = \kappa|u_b|\eta h \exp(-\eta h/\eta_1) \qquad (6.2.11)$$

which describes an eddy viscosity increasing linearly above the bottom to reach a maximum at η_1 and then decreases in value.

Ottesen-Hansen (1975) has carried out a numerical study of the effects of a wind stress acting on the surface of a deep stratified lake. Only the upper layer of the lake was considered and in this layer N was assumed to be a constant over

nearly the whole depth. At the bottom and surface of the upper layer, the eddy viscosity was assumed to decay logarithmically to zero. Using this formulation, the entrainment velocity of the upper layer was successfully modelled.

The form of vertical eddy viscosity used by Nihoul (1977) and Nihoul et. al. (1980) in their three dimensional model of wind affected continental seas was

$$N(x,y,z,t) = F(x,y,t)\lambda(\eta)(h+\varsigma)^2 \tag{6.2.12}$$

where F and λ are some functions. A parabolic form of λ was used and it was given by

$$\lambda(\eta) = \eta(1-\eta/2) \tag{6.2.13}$$

The function F was determined from the bottom stress, the depth averaged velocity components, the surface stress and surface slopes.

Both Engelund (1978) and Koutitas (1978) also used parabolic formulations for the eddy viscosity in studies concerned with wind driven flows. The former proposed

$$N = \kappa u_{*_s} h\eta(\eta-1) \tag{6.2.14}$$

while Koutitas (1978) used

$$N = N_0\eta(\eta-1) \tag{6.2.15}$$

for some constant N_0. Both of these formulations were found to provide reasonable results when compared with the laboratory experiments of Stolzenbach et. al. (1977).

Liggett (1970) proposed the formula

$$N = N_0 + (N_1 - N_0)\eta^n \tag{6.2.16}$$

in his studies of lake circulation. In this equation the parameters N_0, N_1 and n are all constants and Liggett used $n = 0.5$ in all test runs.

From the above review of the forms of eddy viscosity which have been used in models of wind driven flows, it is apparent that many varied formulations have been used by different workers. The above review is concerned mainly with wind driven flows although most of the formulations presented could also be used in tidal flow models. Likewise, some formulations which are used in tidal flow problems could also be used in wind driven flow problems. Some further formulations which have been used in tidal flow models may be found in Kagan (1979), Swift et. al. (1979), Johns (1966, 1968, 1969, 1970), Johns and Dyke (1971), Ianiello (1977), Tee (1979), M^{c}Gregor (1972), Jordan and Baker (1980), Noye et. al. (1981), Bowden (1964), Kajiura (1964), Ricco (1982), Blumberg (1975) and Owen (1980).

§6.3 Turbulent Energy Closure Schemes

As has been shown, the Boussinesq approximation is a popularly applied concept. Unfortunately, the exact form of N is difficult to establish. A wide range of formulations have been measured or proposed for use in various oceanographic models. Indeed, the comment of Shanahan and Harleman (1982) that "the vertical eddy viscosity will be a problematic parameter for the circulation model" is

frustratingly accurate. In recent years, however, work has been carried out which enables the form of the eddy viscosity to be calculated in addition to the other flow properties. This is a reasonable approach because N is not a property of the fluid but rather of the flow itself and so is difficult to quantify without knowledge of the flow.

There are two types of turbulent models commonly employed in models of wind forced or tidal flows. These models are referred to as one-equation and two-equation models. Both use a transport equation for the kinetic energy of the turbulent motion (per unit mass). For high Reynolds' number this equation is, for non buoyant flows,

$$\frac{\partial k}{\partial t} + u_i \frac{\partial k}{\partial x_i} = \frac{\partial}{\partial x_i} \overline{\left[u_i' \left(\frac{u_j' u_j'}{2} + \frac{P}{\rho} \right) \right]} - \overline{u_i' u_j'} \frac{\partial u_i}{\partial x_j} - \nu \overline{\frac{\partial u_i'}{\partial x_j} \frac{\partial u_i'}{\partial x_j}} \qquad (6.3.1)$$

The exact form of the k equation given above is of no use as presented because new unknown correlations involving u_i' terms appear. To obtain a closed set some extra assumptions are made. Firstly, the diffusion flux is assumed to be proportional to the gradient of k. That is,

$$\overline{u_i' \left(\frac{u_j' u_j'}{2} + \frac{P}{\rho} \right)} = \frac{N}{\sigma_k} \frac{\partial k}{\partial x_i} \qquad (6.3.2)$$

for some constant σ_k. This is a common assumption and is used in the derivation of the usual transport equation for a scalar quantity. The last term on the right hand side of Equation (6.3.1) is usually denoted by a scalar quantity, ϵ. Expressions enabling ϵ to be obtained are given later in this section. Substituting these assumptions and Equation (1.3.1) into Equation (6.3.1) yields

$$\frac{\partial k}{\partial t} + u_i \frac{\partial k}{\partial x_i} = \frac{\partial}{\partial x_i} \left(\frac{N}{\sigma_k} \frac{\partial k}{\partial x_i} \right) + N \left(\frac{\partial u_i}{\partial x_j} + \frac{\partial u_j}{\partial x_i} \right) \frac{\partial u_i}{\partial x_j} - \epsilon. \qquad (6.3.3)$$

Using assumptions such as those made in deriving the momentum equations (for example, neglecting horizontal gradients) simplifies Equation (6.3.3) to the usual form of the k equation used in oceanographic models, namely,

$$\frac{\partial k}{\partial t}+u\frac{\partial k}{\partial x}+v\frac{\partial k}{\partial y}+\omega\frac{\partial k}{\partial \eta}=\frac{N}{\hbar^2}\left[\left(\frac{\partial u}{\partial \eta}\right)^2+\left(\frac{\partial v}{\partial \eta}\right)^2\right]+\frac{1}{\hbar^2}\frac{\partial}{\partial \eta}\left(\frac{N}{\sigma_k}\frac{\partial k}{\partial \eta}\right)-\epsilon. \quad (6.3.4)$$

A value of $\sigma_k = 1$ is commonly used.

In one equation models, the dissipation of turbulent energy, ϵ, and the eddy viscosity N are related to a length scale, l. The Kolmogorov-Prandtl law is used to define N by

$$N = c'^{1/4} l k^{1/2} \quad (6.3.5)$$

with $c' \approx 0.08$. The dissipation is usually modelled by

$$\epsilon = c'^{3/4} k^{3/2} l^{-1}. \quad (6.3.6)$$

It remains now only to specify l so that a value for N may be obtained. However, a formulation for l is difficult to establish. Johns (1977 and 1978) and Vager and Kagan (1969(a),(b) and 1971) suggest using Von Karman's expression for l, namely,

$$l = -\frac{\kappa h k^{1/2} l^{-1}}{\partial\left(k^{1/2} l^{-1}\right)/\partial \eta} \quad (6.3.7)$$

which is solved subject to $l = \kappa h \eta_r$ at $\eta = 0$.

The appropriate boundary conditions for Equation (6.3.4) are somewhat contentious. In many turbulent models the boundary conditions are not applied at

the bottom but empirical laws are applied at a small distance away from the wall. The Reynolds stresses are assumed constant within this distance which leads to a logarithmic velocity profile as mentioned previously. Also in this layer the production and dissipation of k are assumed to be in equilibrium and this leads to the condition

$$k = u_{*b}^2/\sqrt{c} \qquad \text{at } \eta = \eta_1, \tag{6.3.8}$$

where η_1 defines the bottom boundary in which the Reynolds stresses are constant. However, many workers using equations of this type in oceanographic modelling of the type being discussed here have used boundary conditions at the bottom, $\eta = 0$. Because of this, and also to be consistent with the formulation of the momentum equations for which a boundary condition at $\eta = 0$ is employed, a condition for k at $\eta = 0$ is given here. Because of the no-slip condition for velocity at $\eta = 0$ the fluctuating velocities u_i' are also equal to zero at $\eta = 0$. Thus,

$$k = 0 \qquad \text{at } \eta = 0. \tag{6.3.9}$$

At the surface, the boundary condition is more difficult to quantify. If there is no surface stress, then, as for other scalar quantities, the surface is considered to be a symmetry line. Thus,

$$\frac{\partial k}{\partial \eta} = 0 \qquad \text{at } \eta = 1 \tag{6.3.10}$$

is the condition when there is no surface stress. If a surface stress does exist then the top boundary condition is difficult to determine. There is little experimental evidence to provide assistance for a correct formulation. A reasonable approximation would be to consider the stress imparted at the surface by a wind to behave

like the stress imparted by a solid boundary. That is, the surface is considered to behave like a wall. Thus a condition analogous to Equation (6.3.8) could be used, namely,

$$k = \frac{u_{*s}^2}{\sqrt{c}} \qquad \text{at } \eta = 1. \tag{6.3.11}$$

The effect, if any, of using Equation (6.3.10) or (6.3.11) will be examined in relation to wind driven flows, in the next chapter.

Johns (1978) used a one equation model to study oscillating tidal flow in a channel of variable width and depth. Vager and Kagan (1969(a)) applied the method to examine the flow in the bottom turbulent boundary layer in a homogeneous deep sea. In a later paper, Vager and Kagan (1969(b)) studied the tidal flow in a shallow sea. The model was extended further in Vager and Kagan (1971) to account for a stratified boundary layer in a tidal flow. In all cases, N was found to vary considerably over a tidal cycle.

Instead of using Equation (6.3.6) to determine ϵ, a transport equation similar to Equation (6.3.4) may be developed for ϵ. Using assumptions similar to those used in deriving Equation (6.3.4), the following equation is obtained

$$\begin{aligned} &\frac{\partial \epsilon}{\partial t} + u\frac{\partial \epsilon}{\partial x} + v\frac{\partial \epsilon}{\partial y} + \omega\frac{\partial \epsilon}{\partial \eta} \\ &\qquad = \frac{c_1 \epsilon N}{k\hbar^2}\left[\left(\frac{\partial u}{\partial \eta}\right)^2 + \left(\frac{\partial v}{\partial \eta}\right)^2\right] + \frac{1}{\hbar^2}\frac{\partial}{\partial \eta}\left(\frac{N}{\sigma_\epsilon}\frac{\partial \epsilon}{\partial \eta}\right) - \frac{c_2 \epsilon^2}{k} \end{aligned} \tag{6.3.12}$$

where $c_1 = 1.44$ and $c_2 = 1.92$. In this two equation model the eddy viscosity is defined by

$$N = \frac{ck^2}{\epsilon} \tag{6.3.13}$$

with $c = 0.09$.

Using similar assumptions to those made in deriving Equation (6.3.8), a wall condition for ϵ may be obtained. It is

$$\epsilon = \frac{u_{*b}^3}{\kappa \eta_1} \qquad \text{at } \eta = \eta_1. \tag{6.3.14}$$

In most numerical models, the value of η_1 required in Equations (6.3.8) and (6.3.14) is taken to be the distance the first grid point is above the wall. The depth of the viscous sublayer η_1, can, however be related to a non-dimensional depth, η^+, by

$$\eta_1 = \frac{\eta^+ \nu}{u_{*b}} \tag{6.3.15}$$

where $30 \leq \eta^+ \leq 100$ (see Rastogi and Rodi (1974)) and the numerical grid is chosen so the Equation (6.3.15) is valid.

However, as was the case for the k equation, a boundary condition applicable at the bottom is required. Launder and Spalding (1974) report that measurements indicate that the turbulence energy dissipation is constant in the immediate vicinity of a wall. This suggests using

$$\frac{\partial \epsilon}{\partial \eta} = 0 \qquad \text{at } \eta = 0. \tag{6.3.16}$$

This was the boundary condition used by Lam and Bremhorst (1978) in a low Reynolds number $k - \epsilon$ model. However, Jones and Launder (1972) reported difficulty in this approach. Instead, they chose to add an extra term to the k

equation which is exactly equal to the dissipation rate at the wall and then use $\epsilon = 0$ at the wall. Jones and Launder (1972) and Launder and Spalding (1974) calculate that the dissipation at the wall is equal to $2\nu(\partial k^{1/2}/\partial x_j)^2$. For flows considered here we have consistently neglected viscous effects and so a good approximation at the boundary must be

$$\epsilon = 0 \qquad \text{at } \eta = 0, \tag{6.3.17}$$

with the k equation remaining as shown in Equation (6.3.4). This is the condition used in this work. The effects, if any, of using either Equation (6.3.17) or Equation (6.3.16) will be examined in the next chapter.

If there is no surface stress, then a symmetry condition applies for ϵ. Thus,

$$\frac{\partial \epsilon}{\partial \eta} = 0 \qquad \text{at } \eta = 1. \tag{6.3.18}$$

A condition analogous to Equation (6.3.14) will be used at the surface when there is an applied wind stress. Combining Equations (6.3.14) and (6.3.15) yields

$$\epsilon = \frac{u_{*s}^4}{\kappa \nu \eta^+} \qquad \text{at } \eta = 1. \tag{6.3.19}$$

The effect of using Equation (6.3.18) and (6.3.19) when there exists a wind stress will be examined later.

Such two equation models have been used by Blumberg and Mellor (1978) in their numerical model of coastal seas. Svensson (1979) extended the above turbulent equations to accomodate rotating flows. His model was found to compare favourably with laboratory experiments of channel flow and wind induced channel

flow. The turbulent equations are examined in detail by Mellor and Yamada (1974). Several turbulent models are presented and all compare favourably with one another. Marchuk et. al. (1977) used a two equation model to study the temperature profile occurring in the upper ocean.

A major drawback of turbulent energy closure schemes is that the amount of computational effort required to solve hydrodynamic problems increases appreciably. In an effort to overcome this problem, Smith (1982) formulated an expression for N like

$$N = M(x, y, t)F(\eta) \tag{6.3.20}$$

where M is a function determined using the depth integrated turbulent kinetic energy and the dissipation of such energy. Using the depth integrated turbulence equations greatly reduces the computational effort. The vertical profile of eddy viscosity was determined by $F(\eta)$ and two forms were proposed, namely,

$$F(\eta) = (1-\eta)^{1/2}\mathrm{erf}(4\eta) \tag{6.3.21(a)}$$

and

$$F(\eta) = 2\alpha\eta\exp(-\alpha\eta) \tag{6.3.21(b)}$$

where α was determined to have a value of 3.2. Results from this model compared favourably with results from a two equation turbulent model.

The two equation model will be used in the next chapter together with analytic solutions involving various formulations for N to model wind induced flow in a channel. Results will be compared with laboratory experiments.

CHAPTER 7

WIND DRIVEN FLOW IN A CHANNEL

7.1 The Equations For Wind Driven Flow In a Channel

The previous chapter presented many different formulations for the eddy viscosity profile which have been used in the study of both wind forced and tidally induced flows. Some of the more commonly used profiles will be used in this chapter to develop analytic solutions to solve for the set-up and for the horizontal velocity which occurs when a wind is blown over a long, narrow channel. The vertical profiles of velocity and the set-up will be compared with results from laboratory experiments. Finally, the performance of a numerical model which calculates the eddy viscosity as part of the solution procedure will be examined. The vertical profiles of N for which analytic solutions are developed are displayed in Figure 7.1.

The problem which is to be modelled is essentially two dimensional; it has variation in the x and z directions. The linear equations which are to be solved analytically are, therefore,

$$\frac{\partial u}{\partial t} = -g\frac{\partial \zeta}{\partial x} + \frac{\partial}{\partial x}\left(N\frac{\partial u}{\partial z}\right) \qquad (7.1.1(a))$$

$$\frac{\partial}{\partial x}\int_{-H}^{0} u\,dz = -\frac{\partial \zeta}{\partial t} \qquad (7.1.1(b))$$

$$u = 0 \qquad \text{at } x = 0, L \qquad (7.1.1(c))$$

$$u = 0 \qquad \text{at } z = -H \qquad (7.1.1(d))$$

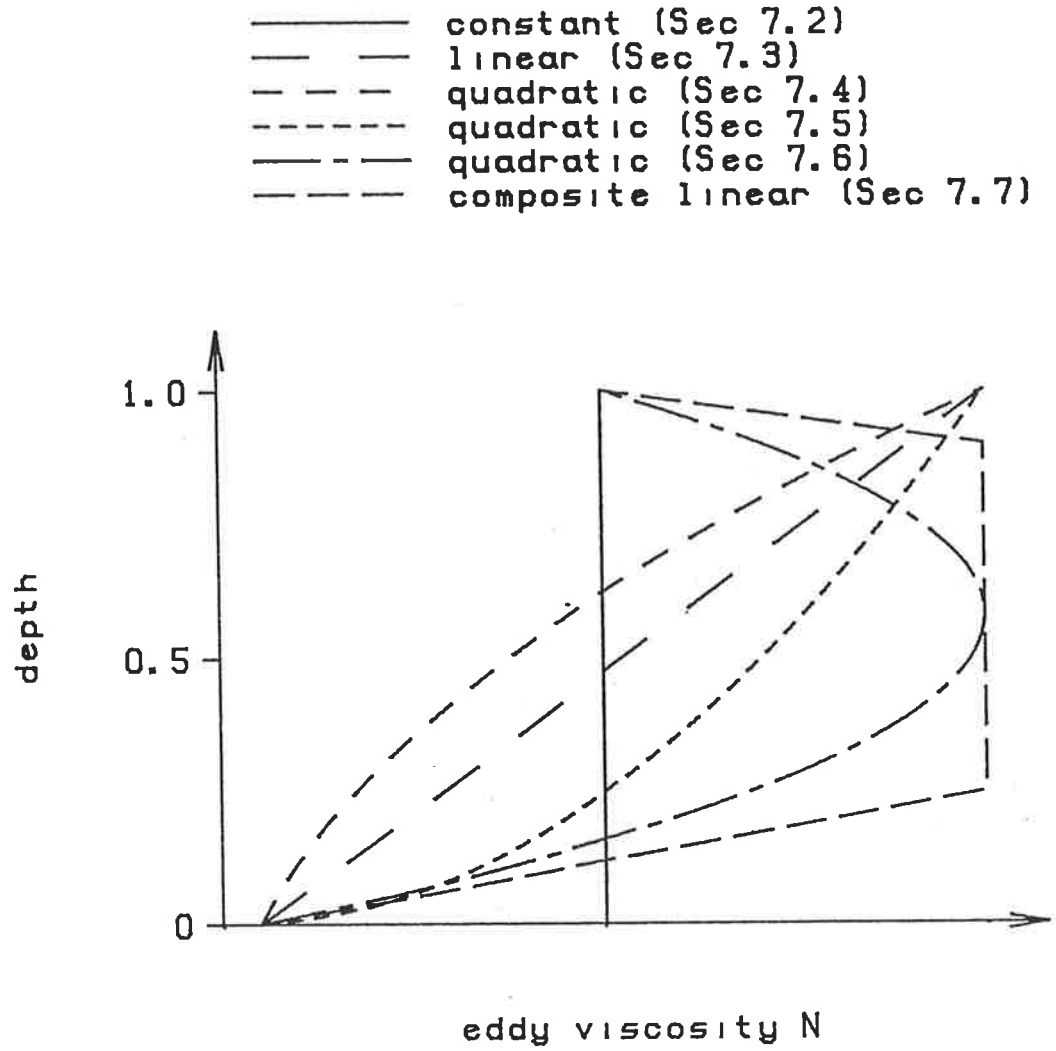

FIGURE 7.1: *Profiles of eddy viscosity considered in Chapter 7.*

and

$$\rho N \frac{\partial u}{\partial z} = \tau_s \qquad \text{at } z = 0 \qquad (7.1.1(e))$$

where H is the constant depth of the channel, N is the vertical eddy viscosity, u is the horizontal velocity of the fluid and ς is the elevation of the surface of the water above the mean water depth. The undisturbed surface water level is denoted by $z = 0$. For the purpose of developing analytic solutions it will be assumed that N varies only with depth and is constant with respect to time and horizontal position. The density ρ is assumed to be constant. The wind stress at the surface is denoted by τ_s.

Boundary condition (7.1.1(c)) implies that the velocity and thus, using Equations (7.1.1(b) and (c)), the surface elevation and wind stress may be described by

$$u(x,z,t) = \sum_{p=1}^{\infty} U_p(z,t)\sin(K_p x), \qquad (7.1.2(a)$$

$$\varsigma(x,t) = \sum_{p=1}^{\infty} \varsigma_p(t)\cos(K_p x), \qquad (7.1.2(b)$$

$$\tau_s(x,t) = \sum_{p=1}^{\infty} \tau_p(t)\sin(K_p x), \qquad (7.1.2(c)$$

in which

$$K_p = \frac{p\pi}{L} \text{ for integer } p. \qquad (7.1.3)$$

The wind stress is assumed to be homogeneous in space varying sinusoidally with time with amplitude τ_0; that is,

$$\tau_s = \tau_0 e^{\iota\sigma t}, \qquad (7.1.4)$$

which may also be written as

$$\tau_s = \tau_0 e^{\iota\sigma t} \frac{4}{L} \sum_{n=1}^{\infty} \frac{\sin(K_{2n-1}x)}{K_{2n-1}} \tag{7.1.5}$$

where K_{2n-1} is defined in (7.1.3). Therefore, we write

$$\tau_p(t) = T_p e^{\iota\sigma t} \tag{7.1.6}$$

where

$$T_p = \begin{cases} \frac{4\tau_0}{K_p L} & \text{for } p = 2n-1 \qquad n = 1, 2, \ldots \\ 0 & \text{for } p = 2n \qquad n = 1, 2, \ldots \end{cases} \tag{7.1.7}$$

and look for solutions for U_p and ζ_p of the form

$$U_p(z,t) = u_p(z) e^{\iota\sigma t} \tag{7.1.8(a)}$$

$$\zeta_p(t) = Z_p e^{\iota\sigma t} \tag{7.1.8(b)}$$

for odd integers.

Using the above formulations for u and ζ together with the depth transformation described by

$$\eta = \frac{z+H}{H} \tag{7.1.9}$$

results in the system of equations

$$\frac{d}{d\eta}\left[N(\eta)\frac{du_p(\eta)}{d\eta}\right] - H^2 \iota\sigma u_p(\eta) = -gK_p Z_p H^2, \tag{7.1.10(a)}$$

$$HK_p \int_0^1 u_p(\eta)d\eta = -\iota\sigma Z_p, \tag{7.1.10(b)}$$

$$u_p(\eta) = 0, \qquad \eta = 0 \tag{7.1.10(c)}$$

$$\frac{\rho N}{H}\frac{du_p(\eta)}{d\eta} = T_p, \qquad \eta = 1. \tag{7.1.10(c)}$$

This set of equations is now solved for various forms of $N(\eta)$.

§7.2 N CONSTANT, VIZ. $N(\eta) = N_0$

The solution to this problem is available from Walsh(1974) and it is

$$\varsigma(x,t) = \frac{4b\tau_0}{L\rho g}\sum_{n=1}^{\infty}\frac{\cos K_{2n-1}x}{K_{2n-1}^2}\left[\sinh bH - R_{2n-1}\cosh bH\right]e^{\iota\sigma t}, \quad (7.2.1(a))$$

$$u(x,\eta,t) = \frac{4\tau_0}{L\rho N_0 b}\sum_{n=1}^{\infty}\frac{\sin K_{2n-1}x}{K_{2n-1}}\Big\{\sinh(bH(\eta-1)) + \sinh bH + R_{2n-1}[\cosh(bH(\eta-1)) - \cosh bH]\Big\}e^{\iota\sigma t} \quad (7.2.1(b)$$

where

$$R_p = \frac{\sinh bH[N_0 b^5 + \epsilon_p K_p bH] + \epsilon_p K_p[1-\cosh bH]}{\cosh bH[N_0 b^5 + \epsilon_p K_p bH] - \epsilon_p K_p \sinh bH},$$

$$b^2 = \frac{\iota\sigma}{N_0},$$

and

$$\epsilon_p = \frac{gK_p}{N_0}.$$

The equilibrium response due to a steady uniform wind is found by letting $\sigma \to 0$ in Equation (7.2.1) to give

$$\varsigma(x) = \frac{3\tau_0}{2\rho g H}\left(x - \frac{L}{2}\right), \quad (7.2.2(a))$$

$$u(x,z) = \frac{H\tau_0}{2\rho N_0}\eta\left(\frac{3\eta}{2} - 1\right). \quad (7.2.2(b))$$

§7.3 N LINEAR, VIZ. $N(\eta) = N_0 + (N_1 - N_0)\eta,\ N_1 \neq N_0$

A linear formulation (see Figure 7.1) for $N(\eta)$, namely,

$$N(\eta) = N_0 + (N_1 - N_0)\eta, \qquad N_1 \neq N_0 \quad (7.3.1)$$

for some constant values of N_0 and N_1, is substituted into Equations (7.1.10). The substitution,

$$\xi(\eta) = \{(N_0 + (N_1 - N_0)\eta\}^{1/2}, \tag{7.3.2}$$

transforms Equations (7.1.10(a)) into the following

$$\frac{d^2 u_p}{d\xi} + \frac{1}{\xi}\frac{du_p}{d\xi} + \lambda_1^2 u_p = \frac{gK_p Z_p \lambda_1^2}{\iota\sigma}, \tag{7.3.3}$$

where

$$\lambda_1^2 = \frac{-4H^2\iota\sigma}{(N_1 - N_0)^2}.$$

The solution to this equation is (see Abramowitz and Stegun(1972))

$$u_b(\xi) = A_{1p}J_0(\lambda_1\xi) + B_{1p}Y_0(\lambda_1\xi) + \frac{gK_pZ_p}{\iota\sigma} \tag{7.3.4}$$

where J_0 and Y_0 are the Bessel functions of zero order and A_{1p} and B_{1p} are arbitrary unknown constants.

The boundary conditions (7.1.10(c) and (d)) imply

$$\xi\frac{du_p}{d\xi} = \frac{2T_pH}{\rho(N_1 - N_0)} \qquad \text{at } \xi = \sqrt{N_1} \tag{7.3.5(a)}$$

and

$$u_p(\xi) = 0 \qquad \text{at } \xi = \sqrt{N_0}. \tag{7.3.5(b)}$$

The remaining equation to be satisfied, namely, Equation (7.1.10(b)) becomes

$$\int_{\sqrt{N_0}}^{\sqrt{N_1}} \xi u_p(\xi)d\xi = -\frac{\iota\sigma Z_p(N_1 - N_0)}{2}. \tag{7.3.5(c)}$$

For $N_0 \neq 0$, Equation (7.3.4) may be substituted into Equation (7.3.5(b)) to yield an expression for Z_p. This expression together with Equations (7.3.4) and (7.3.5(c)) enables the unknown A_{1p} to be expressed in terms of B_{1p}. Finally, Equation (7.3.5(a)) is used to solve for B_{1p}. This process yields the solutions

$$u_p(\xi) = B_{1p}\Big\{-R_{1p}\Big(J_0(\lambda_1\xi) - J_0(\lambda_1\sqrt{N_0})\Big) + \Big(Y_0(\lambda_1\xi) - Y_0(\lambda_1\sqrt{N_0})\Big)\Big\}, \tag{7.3.6(a)}$$

$$Z_p = -B_{1p}\frac{\iota\sigma}{gK_p}\Big\{-R_{1p}J_0(\lambda_1\sqrt{N_0}) + Y_0(\lambda_1\sqrt{N_0})\Big\} \tag{7.3.6(b)}$$

with

$$R_{1p} = \Bigg[\Big(Y_1(\lambda_1\sqrt{N_1}) - \frac{\lambda_1\sqrt{N_1}}{2}Y_0(\lambda_1\sqrt{N_0})\Big)\sqrt{N_1} - \Big(Y_1(\lambda_1\sqrt{N_0}) - \frac{\lambda_1\sqrt{N_0}}{2}Y_0(\lambda_1\sqrt{N_0})\Big)\sqrt{N_0} + \frac{\sigma^2\lambda_1(N_1 - N_0)Y_0(\lambda_1\sqrt{N_0})}{2gK_p^2H}\Bigg] \Bigg/ \Bigg[\Big(J_1(\lambda_1\sqrt{N_1}) - \frac{\lambda_1\sqrt{N_1}}{2}J_0(\lambda_1\sqrt{N_0})\Big)\sqrt{N_1} - \Big(J_1(\lambda_1\sqrt{N_0}) - \frac{\lambda_1\sqrt{N_0}}{2}J_0(\lambda_1\sqrt{N_0})\Big)\sqrt{N_0} + \frac{\sigma^2\lambda_1(N_1 - N_0)J_0(\lambda_1\sqrt{N_0})}{2gK_p^2H}\Bigg] \tag{7.3.6(c)}$$

and

$$B_{1p} = \frac{2T_pH}{\rho\lambda_1(N_1 - N_0)\sqrt{N_1}\left(R_{1p}J_1(\lambda_1\sqrt{N_1}) - Y_1(\lambda_1\sqrt{N_1})\right)} \tag{7.3.6(d)}$$

where T_p is defined by Equation (7.1.7).

The solutions for $u(x,\eta,t)$ and $\varsigma(x,t)$ are then immediately available from the above system of equations using Equations (7.1.2) together with (7.3.2). For completeness, they are presented below:

$$u(x,\eta,t) = e^{\iota\sigma t}\sum_{n=1}^{\infty} B_{12n-1}\sin(K_{2n-1}x)\Big\{-R_{12n-1}\left[J_0(\lambda_1\xi(\eta)) - J_0(\lambda_1\sqrt{N_0})\right] + Y_0(\lambda_1\xi(\eta)) - Y_0(\lambda_1\sqrt{N_0})\Big\} \qquad (7.3.7(a))$$

and

$$\varsigma(x,t) = -\frac{\iota\sigma}{g}e^{\iota\sigma t}\sum_{n=1}^{\infty} B_{12n-1}\frac{\cos(K_{2n-1}x)}{K_{2n-1}}\Big\{-R_{12n-1}J_1(\lambda_1\sqrt{N_0}) + Y_0(\lambda_1\sqrt{N_0})\Big\} \qquad (7.3.7(b))$$

where $\xi(\eta)$ is defined in equation (7.3.2) and the constants R_{12n-1} and B_{12n-1} are defined by Equations (7.3.6(c) and (d)) respectively. Note that the above solution holds only for $N_0 \neq 0$.

The equilibrium solutions for u and ς are obtained from the above analysis by letting $\sigma \to 0$. For the case $N_0 \neq 0$, the solutions for u and ς are:

$$u(x,\eta) = B_1'\tau_0\left\{1 - \frac{\xi^2}{N_0} - R_1'\left(\log\xi - \frac{\xi^2\log\sqrt{N_0}}{N_0}\right)\right\} \qquad (7.3.8(a))$$

and

$$\varsigma(x) = -\frac{\tau_0(N_1 - N_0)^2}{\rho g H^2 N_0}\left(1 - R_1'\log\sqrt{N_0}\right)(x - L/2), \qquad (7.3.8(b))$$

where

$$R_1' = \left[N_1\left(1 - \frac{N_1}{2N_0}\right) - \frac{N_0}{2}\right] \Big/ \left[N_1\left(\log\sqrt{N_1} - \frac{N_1\log\sqrt{N_0}}{2N_0} - \frac{1}{2}\right) - N_0\left(\log\sqrt{N_0} - \frac{\log\sqrt{N_0}}{2} - \frac{1}{2}\right)\right] \qquad (7.3.9(a))$$

and

$$B_1' = -\frac{2H}{\rho(N_1 - N_0)\left(R_1'(1 - \frac{2N_1\log\sqrt{N_0}}{N_0} + \frac{2N_1}{N_0}\right)}. \qquad (7.3.9(b))$$

§7.4 N QUADRATIC, VIZ. $N = (\sqrt{N_0} + (\sqrt{N_1} - \sqrt{N_0})\eta)^2$, $N_1 \neq N_0$

In this section, solutions are obtained for the eddy viscosity function given by (see also Figure 7.1)

$$N(\eta) = \left\{\sqrt{N_0} + (\sqrt{N_1} - \sqrt{N_0})\eta\right\}^2, \qquad N_1 \neq N_0. \tag{7.4.1}$$

The substitution

$$\xi(\eta) = \sqrt{N_0} + (\sqrt{N_1} - \sqrt{N_0})\eta \tag{7.4.2}$$

is made in Equations (7.1.10) which then become

$$\xi^2 \frac{d^2 u_p}{d\xi^2} + 2\xi \frac{du_p}{d\xi} - \lambda_2 u_p = -\frac{gK_p Z_p}{\iota\sigma}\lambda_2, \tag{7.4.3(a)}$$

$$\int_{\sqrt{N_0}}^{\sqrt{N_1}} u_p(\xi)d\xi = \frac{\iota\sigma Z_p(\sqrt{N_1} - \sqrt{N_0})}{HK_p}, \tag{7.4.3(b)}$$

$$u_p = 0 \qquad \text{at } \xi = \sqrt{N_0}, \tag{7.4.3(c)}$$

$$\xi^2 \frac{d^2 u_p}{d\xi^2} = \frac{T_p H}{\rho(\sqrt{N_1} - \sqrt{N_0})} \qquad \text{at } \xi = \sqrt{N_1}, \tag{7.4.3(d)}$$

where

$$\lambda_2 = \frac{\iota\sigma H^2}{\rho(\sqrt{N_1} - \sqrt{N_0})}. \tag{7.4.4}$$

The general solution to Equation (7.4.3(a)) is

$$u_p = A_{2p}\xi^{r_1} + B_{2p}\xi^{r_2} + \frac{gK_p Z_p}{\iota\sigma}, \tag{7.4.5}$$

where

$$r_1, r_2 = \left(-1 \pm \sqrt{1 + 4\lambda_2}\right) \Big/ 2 \tag{7.4.6}$$

and A_{2p} and B_{2p} are arbitrary unknown coefficients.

Following a similar procedure to that used in the previous section yields the following solutions for u_p and Z_p for the case $N_0 \neq 0$:

$$u_p = B_{2p}\left\{\xi^{r_2} - N_0^{r_2/2} - R_{2p}\left(\xi^{r_1} - N_0^{r_1/2}\right)\right\}, \qquad (7.4.7(a))$$

$$Z_p = -B_{2p}\frac{\iota\sigma}{gK_p}\left\{N_0^{r_2/2} - R_{2p}N_0^{r_1/2}\right\} \qquad (7.4.7(b))$$

where

$$B_{2p} = \frac{T_p H}{\rho N_1(\sqrt{N_1} - \sqrt{N_0})\left(-R_{2p}r_1 N_1^{(r_1-1)/2} + r_2 N_1^{(r_2-1)/2}\right)} \qquad (7.4.8(a))$$

and

$$R_{2p} = \left[\sqrt{N_1}\left(\frac{N_1^{r_2/2}}{r_2+1} - N_0^{r_2/2}\right) + N_0^{r_2/2}\left(\frac{r_2}{r_2+1}\sqrt{N_0} + \frac{\sigma^2}{gHK_P^2}(\sqrt{N_1} - \sqrt{N_0})\right)\right]$$
$$\Big/ \left[\sqrt{N_1}\left(\frac{N_1^{r_1/2}}{r_1+1} - N_0^{r_1/2}\right) + N_0^{r_1/2}\left(\frac{r_1}{r_1+1}\sqrt{N_0} + \frac{\sigma^2}{gHK_P^2}(\sqrt{N_1} - \sqrt{N_0})\right)\right] \qquad (7.4.8(b))$$

with T_p defined by Equation (7.1.7).

The exact formulation for $u(x,\eta,t)$ and $\varsigma(x,t)$ is derived from Equations (7.4.7) with the aid of Equations (7.1.2) and (7.4.2). This procedure was outlined in the previous section. However, because these resultant equations are so strongly related to the expressions for u_p and Z_p and are readily available from these expressions, they will not be presented explicitly in this section or in the following sections.

The following solutions are the equilibrium solutions for u and ς. Once again, these solutions are only valid for $N_0 \neq 0$. With the parameters, R_2' and B_2', defined

as

$$R_2' = \left[\sqrt{N_1}\left(1 - \frac{\log\sqrt{N_1} - 1}{\log\sqrt{N_0}}\right) - \sqrt{N_0}\left(1 - \frac{\log\sqrt{N_0} - 1}{\log\sqrt{N_0}}\right)\right] \Big/ \left[\frac{\sqrt{N_1}\left(\log\sqrt{N_1} - 1\right)}{\sqrt{N_0}\log\sqrt{N_0}} - \log\sqrt{N_1} - \frac{\left(\log\sqrt{N_0} - 1\right)}{\log\sqrt{N_0}} + \log\sqrt{N_0}\right] \quad (7.4.9(a))$$

and

$$B_2' = \frac{\sqrt{N_0}H\log\sqrt{N_0}}{\rho(\sqrt{N_1} - \sqrt{N_0})\left(-R_2'(\sqrt{N_0}\log\sqrt{N_0} + \sqrt{N_1}) - \sqrt{N_0}\sqrt{N_1}\right)}, \quad (7.4.9(b))$$

then the equilibrium solutions for u and ζ are

$$u(x,t) = B_2'\tau_0\left\{1 - \frac{\log\xi}{\log\sqrt{N_0}} - R_2'\left(\frac{\log\xi}{\sqrt{N_0}\log\sqrt{N_0}} - \frac{1}{\xi}\right)\right\} \quad (7.4.10(a))$$

and

$$\zeta(x) = -\frac{B_2'\tau_0(1 + R_2'/\sqrt{N_0})(\sqrt{N_1} - \sqrt{N_0})^2(x - L/2)}{gH^2\log\sqrt{N_0}}. \quad (7.4.10(b))$$

§7.5 N QUADRATIC, VIZ. $N = (N_0^2 + (N_1^2 - N_0^2)\eta)^{1/2}$, $N_1 \neq N_0$

The solution to the problem for an alternative quadratic eddy viscosity (see Figure 7.1) defined by

$$N(\eta) = \left(N_0^2 + (N_1^2 - N_0^2)\eta\right)^{1/2}, \; N_1 \neq N_0 \quad (7.5.1)$$

is developed in this section. Again, a coordinate transformation is made to facilitate the process of finding a solution. For this case

$$\xi(\eta) = \left\{N_0^2 + (N_1^2 - N_0^2)\eta\right\}^{1/2} \quad (7.5.2)$$

is chosen. This transforms Equation (7.1.10(a)) to

$$\frac{1}{\xi}\frac{d^2u_p}{d\xi^2} - \lambda_3^2 u_p = -\frac{gK_pZ_p}{\iota\sigma}\lambda_3^2 \tag{7.5.3}$$

where

$$\lambda_3^2 = -\frac{4H^2\iota\sigma}{(N_1^2 - N_0^2)^2}.$$

The solution to this equation is available from Abramowitz and Stegun (1972) and is

$$u_p = \xi^{1/2}\left\{A_{3p}H_{1/3}^{(1)}\left(\frac{2\lambda_3\xi^{3/2}}{3}\right) + B_{3p}H_{1/3}^{(2)}\left(\frac{2\lambda_3\xi^{3/2}}{3}\right)\right\} + \frac{gK_pZ_p}{\iota\sigma}, \tag{7.5.4}$$

where $H_{1/3}^{(1)}(z)$ and $H_{1/3}^{(2)}(z)$ are the Hankel functions of the first and second kind of order 1/3. The above solution could also be written in terms of Airy functions. However, doing so further complicates the expressions for A_{3p} and B_{3p} due to Equation (7.1.10(b)) which necessitates a calculation of the form $\int xAi(x)dx$. It is easier to work with an expression for u_p as defined above and then, to obtain numerical results, convert the results into expressions involving Airy functions.

Boundary condition (7.1.10(c)) may be used as before to derive an expression for Z_p. This results in

$$Z_p = -\frac{\iota\sigma}{gK_p}\left\{\sqrt{N_0}A_{3p}H_{1/3}^{(1)}\left(\frac{2\lambda_3N_0^{3/2}}{3}\right) + \sqrt{N_0}B_{3p}H_{1/3}^{(2)}\left(\frac{2\lambda_3N_0^{3/2}}{3}\right)\right\}. \tag{7.5.5}$$

Substituting the above equation into Equation (7.5.4) yields an expression for u_p which contains the unknowns A_{3p} and B_{3p}. Expressions for these unknowns are

obtained using Equations (7.1.10(b) and (d)). This process results in the following equations:

$$u_p = B_{3p}\left\{-R_{3p}\left(\xi^{1/2}H^{(1)}_{1/3}\left(\frac{2\lambda_3\xi^{3/2}}{3}\right) - \sqrt{N_0}H^{(1)}_{1/3}\left(\frac{2\lambda_3 N_0^{3/2}}{3}\right)\right)\right.$$
$$\left. + \xi^{1/2}H^{(2)}_{1/3}\left(\frac{2\lambda_3\xi^{3/2}}{3}\right) - \sqrt{N_0}H^{(2)}_{1/3}\left(\frac{2\lambda_3 N_0^{3/2}}{3}\right)\right\} \quad (7.5.6(a))$$

and

$$Z_p = -B_{3p}\frac{\iota\sigma}{gK_p}\left\{-R_{3p}\sqrt{N_0}H^{(1)}_{1/3}\left(\frac{2\lambda_3 N_0^{3/2}}{3}\right) + \sqrt{N_0}H^{(2)}_{1/3}\left(\frac{2\lambda_3 N_0^{3/2}}{3}\right)\right\} \quad (7.5.6(b))$$

where

$$R_{3p} = \left[\frac{N_0}{\lambda_3}H^{(2)}_{-2/3}\left(\frac{2\lambda_3 N_0^{3/2}}{3}\right) - \frac{\sqrt{N_0}N_1^2}{2}H^{(2)}_{1/3}\left(\frac{2\lambda_3 N_0^{3/2}}{3}\right)\right.$$
$$\left. - \frac{N_1}{\lambda_3}H^{(2)}_{-2/3}\left(\frac{2\lambda_3 N_1^{3/2}}{3}\right) + \frac{\sqrt{N_0}}{2}H^{(2)}_{1/3}\left(\frac{2\lambda_3 N_0^{3/2}}{3}\right)\left(N_0^2 + \frac{\sigma^2(N_1^2 - N_0^2)}{gK_p^2 H}\right)\right]$$
$$\Big/ \left[\frac{N_0}{\lambda_3}H^{(1)}_{-2/3}\left(\frac{2\lambda_3 N_0^{3/2}}{3}\right) - \frac{\sqrt{N_0}N_1^2}{2}H^{(1)}_{1/3}\left(\frac{2\lambda_3 N_0^{3/2}}{3}\right) - \frac{N_1}{\lambda_3}H^{(1)}_{-2/3}\left(\frac{2\lambda_3 N_1^{3/2}}{3}\right)\right.$$
$$\left. + \frac{\sqrt{N_0}}{2}H^{(1)}_{1/3}\left(\frac{2\lambda_3 N_0^{3/2}}{3}\right)\left(N_0^2 + \frac{\sigma^2(N_1^2 - N_0^2)}{gK_p^2 H}\right)\right] \quad (7.5.7(a))$$

and

$$B_{3p} = \frac{2HT_p}{\lambda_3\rho N_1(N_1^2 - N_0^2)\left(-R_{3p}H^{(1)}_{-2/3}\left(\frac{2\lambda_3 N_1^{3/2}}{3}\right) + H^{(2)}_{-2/3}\left(\frac{2\lambda_3 N_1^{3/2}}{3}\right)\right)}. \quad (7.5.7(b))$$

For the purposes of computing the above expressions, it is convenient to now use Airy functions and the following relationships:

$$\xi^{1/2}H^{(1)}_{1/3}\left(\frac{2\lambda_3\xi^{3/2}}{3}\right) = \frac{\sqrt{3}e^{-\frac{\pi\iota}{6}}}{\lambda^{1/3}}\left[A_i\left(-\lambda^{2/3}\xi\right) - \iota B_i\left(-\lambda^{2/3}\xi\right)\right]$$

$$= A_+(\xi), \tag{7.5.8(a)}$$

$$\xi H^{(1)}_{-2/3}\left(\frac{2\lambda_3\xi^{3/2}}{3}\right) = \frac{\sqrt{3}e^{\frac{5\pi\iota}{6}}}{\lambda^{2/3}}\left[A_i'\left(-\lambda^{2/3}\xi\right) - \iota B_i'\left(-\lambda^{2/3}\xi\right)\right]$$

$$= B_+(\xi), \tag{7.5.8(b)}$$

$$\xi^{2/3} H^{(2)}_{1/3}\left(\frac{2\lambda_3\xi^{3/2}}{3}\right) = \frac{\sqrt{3}e^{\frac{\pi\iota}{6}}}{\lambda^{1/3}}\left[A_i\left(-\lambda^{2/3}\xi\right) + \iota B_i\left(-\lambda^{2/3}\xi\right)\right]$$

$$= A_-(\xi) \tag{7.5.8(c)}$$

and

$$\xi H^{(2)}_{-2/3}\left(\frac{2\lambda_3\xi^{3/2}}{3}\right) = \frac{\sqrt{3}e^{-\frac{5\pi\iota}{6}}}{\lambda^{2/3}}\left[A_i'\left(-\lambda^{2/3}\xi\right) + \iota B_i'\left(-\lambda^{2/3}\xi\right)\right]$$

$$= B_-(\xi), \tag{7.5.8(d)}$$

where A_i and B_i are the Airy functions (see Abramowitz and Stegun (1972)) and A_i' and B_i' denote the derivatives of these functions.

Hence, Equations (7.5.6) and (7.5.7) may be written as

$$u_p = B_{3p}\left\{-R_{3p}\left(A_+(\xi) - A_+(N_0)\right) + A_-(\xi) - A_-(N_0)\right\}, \tag{7.5.9(a)}$$

$$Z_p = -B_{3p}\frac{\iota\sigma}{gK_p}\left\{-R_{3p}A_+(N_0) + A_-(N_0)\right\} \tag{7.5.9(b)}$$

in which

$$R_{3p} = \left[\frac{B_-(N_0) - B_-(N_1)}{\lambda_3} + \frac{A_-(N_0)}{2}(N_0^2 - N_1^2)\left(1 - \frac{\sigma^2}{gK_p^2H}\right)\right] \Bigg/ \left[\frac{B_+(N_0) - B_+(N_1)}{\lambda_3} + \frac{A_+(N_0)}{2}(N_0^2 - N_1^2)\left(1 - \frac{\sigma^2}{gK_p^2H}\right)\right] \tag{7.5.9(c)}$$

and

$$B_{3p} = \frac{2HT_p}{\lambda_3\rho(N_1^2 - N_0^2)\left(-R_pB_+(N_1) + B_-(N_1)\right)}. \tag{7.5.9(d)}$$

The Airy functions are calculated using

$$A_i(z) = c_1 f(z) - c_2 g(z), \tag{7.5.10(a)}$$

$$B_i(z) = \sqrt{3}\,[c_1 f(z) + c_2 g(z)] \qquad (7.5.10(b))$$

where

$$f(z) = \sum_{k=0}^{\infty} 3^k \left(\frac{1}{3}\right)_k \frac{z^{3k}}{(3k)!}, \qquad (7.5.11(a))$$

$$g(z) = \sum_{k=0}^{\infty} 3^k \left(\frac{2}{3}\right)_k \frac{z^{3k+1}}{(3k+1)!} \qquad (7.5.11(b))$$

with

$$(\alpha + 1/3)_0 = 1$$

and

$$3^k(\alpha + 1/3)_k = (3\alpha + 1)(3\alpha + 4)\ldots(3\alpha + 3k - 2)$$

for arbitrary α. The derivatives of the Airy functions are easily obtained from Equations (7.5.10) and (7.5.11).

The equilibrium solutions are once again obtained from the above result by letting $\sigma \to 0$. The solutions for u and ς are as follows:

$$u(x,t) = \frac{2H\tau_0}{\rho(N_1^2 - N_0^2)(1 + 3R_3' N_1^2)} \left\{-R_3'(N_0^3 - \xi^3) + \xi - N_0\right\}, \qquad (7.5.12(a))$$

$$\varsigma(x) = \frac{3R_3'\tau_0(x - L/2)}{\rho g H(1 + 3R_3' N_1^2)}, \qquad (7.5.12(b))$$

in which

$$R_3' = \frac{N_1^2(N_1/3 - N_0/2) + N_0^3/6}{N_1^2(N_0^3/2 - N_1^3/5) - 3N_0^5/10}. \qquad (7.5.13)$$

§7.6 N QUADRATIC, VIZ. $N = N_s\eta^2 + N_t\eta + N_0$

In this section, the system of Equations (7.1.10) are solved for the general quadratic form given by

$$N(\eta) = N_s\eta^2 + N_t\eta + N_0, \tag{7.6.1}$$

where

$$N_s = (N_0 - N_m)\left(1 + \frac{N_m - N_1}{N_m - N_0} + 2\sqrt{\frac{N_m - N_1}{N_m - N_0}}\right) \tag{7.6.2(a)}$$

and

$$N_t = 2(N_m - N_0)\left(1 + \sqrt{\frac{N_m - N_1}{N_m - N_0}}\right) \tag{7.6.2(b)}$$

which ensure that the value of N at the surface is N_1 and at the bottom is N_0.

The formulation for $N(\eta)$ given above may be written in the form

$$N(\eta) = N_s(\eta + \alpha)(\eta + \beta) \tag{7.6.3}$$

where

$$\alpha, \beta = \frac{N_t \pm \sqrt{N_t^2 - 4N_sN_0}}{2N_s}. \tag{7.6.4}$$

The above expression for N together with the depth transformation

$$\xi(\eta) = (\eta + \beta)/(\beta - \alpha) \tag{7.6.5}$$

are substituted into Equation (7.1.10). This yields the following system of equations:

$$\xi(\xi - 1)\frac{d^2u_p}{d\xi^2} + (2\xi - 1)\frac{du_p}{d\xi} + \lambda_4 u_p = -\frac{gK_pZ_pH^2}{N_s}, \tag{7.6.6(a)}$$

$$\int_{\xi_b}^{\xi_s} u_p d\xi = -\frac{\iota\sigma Z_p}{(\beta-\alpha)HK_p}, \qquad (7.6.6(b))$$

$$u_p(\xi) = 0 \qquad \text{at } \xi = \xi_b, \qquad (7.6.6(c))$$

$$\xi(\xi-1)\frac{du_p}{d\xi} = \frac{HT_p}{\rho N_s(\beta-\alpha)} \qquad \text{at } \xi = \xi_s, \quad (7.6.6(d))$$

where,

$$\lambda_4 = -\iota\sigma H^2/N_s, \qquad (7.6.7(a))$$

$$\xi_b = \frac{\beta}{\beta-\alpha} \qquad (7.6.7(b))$$

and

$$\xi_s = \frac{\beta+1}{\beta-\alpha}. \qquad (7.6.7(c))$$

The general solution to the homogeneous form of Equation (7.6.6(a)) is

$$u_p = A_{4p}F(a,b;1;\xi) + B_{4p}\Big\{F(a,b;1;\xi)\log\xi + \sum_{n=1}^{\infty}\frac{(a)_n(b)_n\xi^n}{(n!)^2}[\psi(a+n)-\psi(a)+\psi(b+n)-\psi(b)-2\psi(n+1)+2\psi(1)]\Big\} \qquad (7.6.8)$$

for unknown coefficients A_{4p} and B_{4p}, and where

$$a+b=1, \qquad ab=\lambda_4. \qquad (7.6.9(a))$$

The function $\psi(z)$ in Equation (7.6.8) is defined by

$$\psi(z) = \Gamma'(z)/\Gamma(z), \qquad (7.6.9(b))$$

which implies

$$\psi(z+1) = \psi(z) + 1/z \text{ with } \psi(1) = -\gamma, \qquad (7.6.9(c))$$

and the function $(z)_n$ is defined by

$$(z)_n = z(z+1)\dots(z+n-1)$$

$$= \Gamma(z+n)/\Gamma(z). \qquad (7.6.9(d))$$

In the above equations

$\Gamma(z)$ is the Gamma function,

$\Gamma'(z)$ denotes the derivative of the Gamma function,

γ is Euler's constant ($\gamma = 0.5772156649\dots$) and

$F(a,b;1;\xi)$ is the hypergeometric function.

The hypergeometric function (see Abramowitz and Stegun (1972)) may be simplified using the definition

$$F(a,b;1;\xi) = \frac{\Gamma(1)}{\Gamma(a)\Gamma(b)} \sum_{n=0}^{\infty} \frac{\Gamma(a+n)\Gamma(b+n)}{\Gamma(1+n)} \frac{\xi^n}{n!} \qquad (7.6.10)$$

which yields

$$F(a,b;1;\xi) = F(\xi) = 1 + \sum_{n=1}^{\infty} \prod_{j=0}^{n-1} (\lambda_4 + j + j^2) \frac{\xi^n}{(n!)^2}. \qquad (7.6.11)$$

The term in Equation (7.6.8) which involves the summation may also be simplified giving

$$\sum_{n=1}^{\infty} \frac{(a)_n (b)_n \xi^n}{(n!)^2} [\psi(a+n) - \psi(a) + \psi(b+n) - \psi(b) - 2\psi(n+1) + 2\psi(1)]$$

$$= \sum_{n=1}^{\infty} a_n \xi^n, \qquad (7.6.12)$$

where

$$a_n = \frac{n - 2\lambda_4}{n^3} b_{n-1} + \frac{\lambda_4 + n(n-1)}{n^2} a_{n-1} \qquad (7.6.13(a))$$

and

$$b_n = \frac{\lambda_4 + n(n-1)}{n^2} b_{n-1}, \qquad (7.6.13(b))$$

with $b_0 = 1$ and $a_0 = 0$.

The general solution to Equation (7.6.6(a)) may therefore be written as

$$u_p = A_{4p} F(\xi) + B_{4p} \left\{ F(\xi) \log \xi + \sum_{n=1}^{\infty} a_n \xi^n \right\} + \frac{g K_p Z_p}{\iota \sigma} \qquad (7.6.14)$$

where F is defined in (7.6.11) and a_n is defined in (7.6.13).

Using procedures similar to those used in the previous sections, Equations (7.6.6(b), (c) and (d)) may now be used in conjunction with Equation (7.6.14) to give the following solutions for u_p and Z_p:

$$u_p = B_{4p} \Big\{ -R_{4p} \left(F(\xi) - F(\xi_b) \right) + F(\xi) \log(\xi) - F(\xi_b) \log(\xi_b) + \sum_{n=1}^{\infty} a_n (\xi^n - \xi_b^n) \Big\}, \qquad (7.6.15(a))$$

$$Z_p = -B_{4p} \frac{\iota \sigma}{g K_p} \left\{ -R_{4p} F(\xi_b) + F(\xi_b) \log(\xi_b) + \sum_{n=1}^{\infty} a_n \xi_b^n \right\}, \qquad (7.6.15(b))$$

in which

$$R_{4p} = \Bigg[f_2(\xi_s) - \xi_s F(\xi_b) \log(\xi_b) + \sum_{n=1}^{\infty} \frac{a_n}{n+1} \left(\xi_s^{n+1} - \xi_b^{n+1} \right) - \xi_s \sum_{n=1}^{\infty} a_n \xi_b^n + \xi_b \sum_{n=1}^{\infty} \xi_b^n - f_2(\xi_b) + \xi_b F(\xi_b) \log(\xi_b) + \frac{\sigma^2}{g H K_p^2 (\beta - \alpha)} \left(F(\xi_b) \log(\xi_b) + \sum_{n=1}^{\infty} a_n \xi_b^n \right) \Bigg] \Bigg/ \left[F_1(\xi_s) - F_1(\xi_b) + F(\xi_b) \xi_b - F(\xi_b) \xi_s + \frac{\sigma^2 F(\xi_b)}{g H K_p^2 (\beta - \alpha)} \right] \qquad (7.6.16(a))$$

and

$$B_{4p} = T_p H \Big/ \Big[\rho N_s(\beta-\alpha)\xi_s(\xi_s-1)(-R_{4p}F'(\xi_s) + F'(\xi_s)\log(\xi_s) + F(\xi_s)/\xi_s + \sum_{n=1}^{\infty} a_n n \xi_s^{n-1})\Big], \qquad (7.6.16(b))$$

with the functions F', F_1 and f_2 defined by

$$F_1(\xi) = \xi + \sum_{n=1}^{\infty}\prod_{j=0}^{n-1}\frac{(\lambda_4 + j + j^2)\xi^{n+1}}{(n+1)(n!)^2}, \qquad (7.6.16(c))$$

$$f_2(\xi) = \xi\log\xi - \xi + \sum_{n=1}^{\infty}\prod_{j=0}^{n-1}\frac{(\lambda_4 + j + j^2)\xi^{n+1}}{(n+1)(n!)^2}\left(\log\xi - \frac{1}{n+1}\right) \qquad (7.6.16(d))$$

and

$$F'(\xi) = \frac{dF(\xi)}{d\xi}. \qquad 7.6.16(e))$$

The above solutions for u_p and Z_p are valid only for $\xi_s, \xi_b \neq 0$.

The equilibrium solutions for this form of eddy viscosity are

$$u(x,\eta) = B_4'\tau_0\left\{\frac{\log|\xi-1|}{\log|\xi_b-1|} + 1 - R_4'\left(\frac{\log|\xi-1|}{\log|\xi_b-1|}\log\frac{|\xi_b-1|}{|\xi_b|} + \log\frac{|\xi-1|}{|\xi|}\right)\right\} \qquad (7.6.17(a))$$

and

$$\zeta(x) = -B_4'\frac{N_s}{gH^2\log|\xi_b-1|}\left\{1 - R_4'\log\frac{|\xi_b-1|}{|\xi_b|}\right\}\left(x - \frac{L}{2}\right) \qquad (7.6.17(b))$$

where

$$R_4' = \Big[-(\xi_s-1)(\log|\xi_s-1|-1)/\log|\xi-1| + \xi_s - \xi_b + (\xi_b-1)(\log|\xi_b-1|-1)/\log|\xi_b-1|\Big] \Big/ \Big[(\xi_s-1)\left\{\frac{(1-\log|\xi_s-1|)}{\log|\xi_b-1|}\log\frac{|\xi_b-1|}{|\xi_b|} + \log|\xi_s-1| - 1\right\} - \xi_s(\log\xi_s - 1) - (\xi_b-1)\left\{\frac{(1-\log|\xi_b-1|)}{\log|\xi_b-1|}\log\frac{|\xi_b-1|}{|\xi_b|} + \log|\xi_b-1| - 1\right\} + \xi_b(\log\xi_b - 1)\Big] \qquad (7.6.18(a))$$

and

$$B_4' = H \Big/ \left[\rho N_s(\beta-\alpha)\xi_s\left(-\frac{1}{\log|\xi_b-1|} - R_4'\left(\frac{1}{\xi_s} - \frac{\log(|\xi_b-1|/|\xi_b|)}{\log|\xi_b-1|}\right)\right)\right]. \tag{7.6.18(b)}$$

§7.7 N Composite Linear

In this section a solution to Equations (7.1.10) is found for an eddy viscosity profile made up of three distinct linear sections. Near the bottom, N is assumed to increase linearly with height above the bottom to a value of N_1 at $\eta = \eta_1$ which is assumed to be the value of the eddy viscosity in the mid-depths, that is, $N = N_1$ for $\eta_1 \leq \eta \leq \eta_2$. Near the surface where $\eta \geq \eta_2$, N is assumed once again to vary linearly from a value of N_1 to a value of N_2 at the surface $\eta = 1$. Hence, the eddy viscosity is defined by

$$N(\eta) = \begin{cases} N_0 + \frac{N_1-N_0}{\eta_1}\eta & 0 \leq \eta \leq \eta_1 \\ N_1 & \eta_1 \leq \eta \leq \eta_2 \\ N_2 + \frac{N_2-N_1}{\eta_2-1} + \frac{N_1-N_2}{\eta_2-1}\eta & \eta_2 \leq \eta \leq 1 \end{cases} \tag{7.7.1}$$

and this form is also displayed in Figure 7.1.

The solutions for u_p and Z_p in each depth section are available from the previous sections. From Equation (7.3.4) we have that the solution for the velocity in the bottom section, $0 \leq \eta \leq \eta_1$, which is denoted by u_{1p} is

$$u_{1p} = A_{1p}J_0\left(\frac{\lambda_5\xi_1}{B_1}\right) + B_{1p}Y_0\left(\frac{\lambda_5\xi_1}{B_1}\right) + \frac{gK_pZ_p}{\iota\sigma} \tag{7.7.2}$$

where

$$\xi_1 = (N_0 + B_1\eta)^{1/2}, \tag{7.7.3(a)}$$

$$\lambda_5^2 = -4H^2\iota\sigma \tag{7.7.3(b)}$$

and

$$B_1 = \frac{N_1 - N_0}{\eta_1}. \tag{7.7.3(c)}$$

Similarly, the solution in the upper section, $\eta_2 \leq \eta \leq 1$, is denoted by u_{3p} and is

$$u_{3p} = A_{3p}J_0\left(\frac{\lambda_5\xi_3}{b_3}\right) + B_{3p}Y_0\left(\frac{\lambda_5\xi_3}{b_3}\right) + \frac{gK_pZ_p}{\iota\sigma} \tag{7.7.4}$$

where

$$\xi_3 = \{(N_2 + B_3(\eta - 1)\}^{1/2} \tag{7.7.5(a)}$$

and

$$B_3 = \frac{N_1 - N_2}{\eta_2 - 1}. \tag{7.7.5(b)}$$

The general solution for the central region, $\eta_1 \leq \eta \leq \eta_2$, is

$$u_{2p} = A_{2p}\cos\left(\frac{\lambda_5\eta}{2\sqrt{N_1}}\right) + B_{2p}\sin\left(\frac{\lambda_5\eta}{2\sqrt{N_1}}\right) + \frac{gK_pZ_p}{\iota\sigma}. \tag{7.7.6}$$

The boundary conditions which apply to the expressions for u_{1p}, u_{2p} and u_{3p} are:

$$u_{1p} = 0 \qquad \text{at } \eta = 0, \tag{7.7.7(a)}$$

$$u_{1p} = u_{2p} \qquad \text{at } \eta = \eta_1, \tag{7.7.7(b)}$$

$$\frac{du_{1p}}{d\eta} = \frac{du_{2p}}{d\eta} \qquad \text{at } \eta = \eta_1, \tag{7.7.7(c)}$$

$$u_{2p} = u_{3p} \qquad \text{at } \eta = \eta_2, \tag{7.7.7(d)}$$

$$\frac{du_{2p}}{d\eta} = \frac{du_{3p}}{d\eta} \qquad \text{at } \eta = \eta_3, \tag{7.7.7(e)}$$

$$\frac{\rho N}{H}\frac{du_{3p}}{d\eta} = T_p \qquad \text{at } \eta = 1, \tag{7.7.7(f)}$$

and

$$HK_p\left\{\int_0^{\eta_1} u_{1p} + \int_{\eta_1}^{\eta_2} u_{2p} + \int_{\eta_2}^{1} u_{3p}\right\} = -\iota\sigma Z_p. \qquad (7.7.7(g))$$

The above conditions yield seven equations enabling the seven unknowns A_{1p}, A_{2p}, A_{3p}, B_{1p}, B_{2p}, B_{3p} and Z_p to be found. For $N_0 \neq 0$ and $N_2 \neq 0$, the following set of equations may then be developed.

The last boundary condition, (7.7.7(g)) implies

$$\begin{aligned} Z_p\left(1 - \frac{gHK_p^2}{\sigma^2}\right) = -\frac{2HK_p}{\iota\sigma\lambda_5}\Bigg\{ & A_{1p}\left(\sqrt{N_1}J_1\left(\frac{\lambda_5\sqrt{N_1}}{B_1}\right) - \sqrt{N_0}J_1\left(\frac{\lambda_5\sqrt{N_0}}{B_1}\right)\right) \\ & + B_{1p}\left(\sqrt{N_1}Y_1\left(\frac{\lambda_5\sqrt{N_1}}{B_1}\right) - \sqrt{N_0}Y_1\left(\frac{\lambda_5\sqrt{N_0}}{B_1}\right)\right) \\ & + A_{3p}\left(\sqrt{N_2}J_1\left(\frac{\lambda_5\sqrt{N_2}}{B_3}\right) - \sqrt{N_1}J_1\left(\frac{\lambda_5\sqrt{N_1}}{B_3}\right)\right) \\ & + B_{3p}\left(\sqrt{N_2}Y_1\left(\frac{\lambda_5\sqrt{N_2}}{B_3}\right) - \sqrt{N_1}Y_1\left(\frac{\lambda_5\sqrt{N_1}}{B_3}\right)\right) \\ & + A_{2p}\left(\sqrt{N_1}\sin\left(\frac{\lambda_5\eta_2}{2\sqrt{N_1}}\right) - \sqrt{N_1}\sin\left(\frac{\lambda_5\eta_1}{2\sqrt{N_1}}\right)\right) \\ & + B_{2p}\left(\sqrt{N_1}\cos\left(\frac{\lambda_5\eta_1}{2\sqrt{N_1}}\right) - \sqrt{N_1}\cos\left(\frac{\lambda_5\eta_2}{2\sqrt{N_1}}\right)\right)\Bigg\}. \qquad (7.7.8(a)) \end{aligned}$$

The remaining boundary conditions (7.7.7(a)-(f)) yield, in turn,

$$A_{1p}J_0\left(\frac{\lambda_5\sqrt{N_0}}{B_1}\right) + B_{1p}Y_0\left(\frac{\lambda_5\sqrt{N_0}}{B_1}\right) + \frac{gK_pZ_p}{\iota\sigma} = 0, \qquad (7.7.8(b))$$

$$\begin{aligned} & A_{1p}J_0\left(\frac{\lambda_5\sqrt{N_1}}{B_1}\right) + B_{1p}Y_0\left(\frac{\lambda_5\sqrt{N_1}}{B_1}\right) \\ & \quad - A_{2p}\cos\left(\frac{\lambda_5\eta_1}{2\sqrt{N_1}}\right) - B_{2p}\sin\left(\frac{\lambda_5\eta_1}{2\sqrt{N_1}}\right) = 0, \qquad (7.7.8(c)) \\ & - A_{1p}J_1\left(\frac{\lambda_5\sqrt{N_1}}{B_1}\right) - B_{1p}Y_1\left(\frac{\lambda_5\sqrt{N_1}}{B_1}\right) \\ & \quad + A_{2p}\sin\left(\frac{\lambda_5\eta_1}{2\sqrt{N_1}}\right) - B_{2p}\cos\left(\frac{\lambda_5\eta_1}{2\sqrt{N_1}}\right) = 0, \qquad (7.7.8(d)) \end{aligned}$$

$$A_{3p}J_0\left(\frac{\lambda_5\sqrt{N_1}}{B_3}\right)+B_{3p}Y_0\left(\frac{\lambda_5\sqrt{N_1}}{B_3}\right)$$
$$-A_{2p}\cos\left(\frac{\lambda_5\eta_2}{2\sqrt{N_1}}\right)-B_{2p}\sin\left(\frac{\lambda_5\eta_2}{2\sqrt{N_1}}\right)=0, \qquad (7.7.8(e))$$

$$-A_{3p}J_1\left(\frac{\lambda_5\sqrt{N_1}}{B_3}\right)-B_{3p}Y_1\left(\frac{\lambda_5\sqrt{N_1}}{B_3}\right)$$
$$+A_{2p}\sin\left(\frac{\lambda_5\eta_2}{2\sqrt{N_1}}\right)-B_{2p}\cos\left(\frac{\lambda_5\eta_2}{2\sqrt{N_1}}\right)=0, \qquad (7.7.8(f))$$

$$A_{3p}J_1\left(\frac{\lambda_5\sqrt{N_2}}{B_3}\right)+B_{3p}Y_1\left(\frac{\lambda_5\sqrt{N_2}}{B_3}\right)=-\frac{2T_pH}{\rho\lambda\sqrt{N_2}}. \qquad (7.7.8(g))$$

The above equations may now be solved to obtain solutions for the velocity in each section and also for the elevation.

The equilibrium case may also be developed. The following solution applies for the special cases of $N_0 \neq 0$ and $N_2 \neq 0$.

The equations which describe the velocity and elevation for the equilibrium case are given by Equations (7.1.10) with $\sigma = 0$. After substituting the eddy viscosity given by Equation (7.7.1) into this new set of equations, the following general solutions are obtained for the velocity:

$$u_{1p}=-\frac{gH^2K_pZ_p}{B_1^2}\xi_1^2+A_{1p}\log\xi_1+B_{1p}, \qquad (7.7.9(a))$$

$$u_{2p}=\frac{gH^2K_pZ_p}{2N_1}\eta^2+A_{2p}\eta+B_{2p}, \qquad (7.7.9(b))$$

$$u_{3p}=-\frac{gH^2K_pZ_p}{B_3^2}\xi_3^2+A_{3p}\log\xi_3+B_{3p}, \qquad (7.7.9(c))$$

where, as before, u_{1p} is the solution for the velocity in the bottom region, $\eta \leq \eta_1$, u_{3p} is the solution in the top region, $\eta \geq \eta_2$, and u_{2p} describes the velocity in the central region in which the eddy viscosity is a constant.The variables, ξ_1, ξ_3, B_1

and B_3 are given in Equations (7.7.3) and (7.7.5) and A_{1p}, A_{2p}, A_{3p}, B_{1p}, B_{2p} and B_{3p} denote arbitrary constants.

The above expressions for velocity are subject to the boundary conditions (7.7.7(a)-(f)) as well the condition (7.7.7(g)) in which the right hand side is replaced by zero.

The last of these conditions implies

$$
\begin{aligned}
&- Z_p \frac{gH^2 K_p}{2} \left\{ \frac{N_1^2 - N_0^2}{B_1^3} + \frac{N_2^2 - N_1^2}{B_3^3} + \frac{\eta_2^3 - \eta_1^3}{3N_1} \right\} \\
&+ A_{1p} \frac{1}{B_1} \left\{ N_1 \log \sqrt{N_1} - \frac{N_1}{2} - N_0 \log \sqrt{N_0} + \frac{N_0}{2} \right\} + B_{1p} \frac{N_1 - N_0}{B_1} \\
&+ A_{2p} \left\{ \frac{\eta_2^2 - \eta_1^2}{2} \right\} + B_{2p} \{\eta_2 - \eta_1\} + B_{3p} \frac{N_2 - N_1}{B_3} \\
&+ A_{3p} \frac{1}{B_3} \left\{ N_2 \log \sqrt{N_2} - \frac{N_2}{2} - N_1 \log \sqrt{N_1} + \frac{N_1}{2} \right\} = 0. \qquad (7.7.10(a))
\end{aligned}
$$

The other six boundary conditions imply

$$
\begin{aligned}
-\frac{gH^2 K_p N_0}{B_1^2} Z_p + A_{1p} \log \sqrt{N_0} + B_{1p} &= 0, (7.7.10(b)) \\
-gH^2 K_p \left(\frac{N_1}{B_1^2} - \frac{\eta_1^2}{2N_1} \right) Z_p + A_{1p} \log \sqrt{N_1} + B_{1p} - A_{2p}\eta_1 - B_{2p} &= 0, (7.7.10(c)) \\
-gH^2 K_p \left(\frac{1}{B_1} - \frac{\eta_1}{N_1} \right) Z_p + A_{1p} \frac{B_1}{2N_1} - A_{2p} &= 0, (7.7.10(d)) \\
-gH^2 K_p \left(\frac{N_1}{B_3^2} - \frac{\eta_2^2}{2N_1} \right) Z_p - A_{2p}\eta_2 - B_{2p} + A_{3p} \log \sqrt{N_1} + B_{3p} &= 0, (7.7.10(e)) \\
-gH^2 K_p \left(\frac{1}{B_3} - \frac{\eta_2}{N_1} \right) Z_p - A_{2p} + A_{3p} \frac{B_3}{2N_1} &= 0, (7.7.10(f)) \\
-\frac{2gH^2 K_p}{B_3^2} Z_p + \frac{A_{3p}}{N_2} = \frac{2T_p H}{\rho N_2}. \qquad (7.7.10(g))
\end{aligned}
$$

The above set of equations may be written in matrix form as

$$
A_p \mathbf{x_p} = T_p \mathbf{b} \qquad (7.7.11)
$$

where

$$\mathbf{x_p} = (Z_p\ A_{1p}\ B_{1p}\ A_{2p}\ B_{2p}\ A_{3p}\ B_{3p}\ )^T\ ,$$

$$\mathbf{b} = \left(0\,0\,0\,0\,0\,0\,\frac{2H}{\rho N_2}\right)^T$$

and the matrix A_p is available from the system of equations given by Equation (7.7.10).

A solution for the vector $\mathbf{x_p}$ could be obtained from the above matrix equation and then using Equations (7.7.9) and (7.1.2), solutions for the equilibrium velocity $u(x,t)$ and the displacement $\varsigma(x)$ could be derived. However, as in the equilibrium solutions given in the previous sections, the above solution may be simplified to an expression which does not involve a summation over infinity.

Note that the elements in the first column of matrix A_p all contain the factor $-gH^2K_p$. Hence, we may write

$$A_p = MC_p, \tag{7.7.12}$$

where M is the matrix A_p except that the factor $-gH^2K_p$ has been removed from the first column and replaced by 1 so that M is now independent of the index p and C_p is a 7x7 diagonal matrix given by

$$C_p = \text{diag}\left(-gH^2K_p, 1, 1, 1, 1, 1, 1\right).$$

Hence, the solution for $\mathbf{x_p}$ may be expressed by

$$\mathbf{x_p} = T_p(MC_p)^{-1}\mathbf{b} \tag{7.7.13}$$

and if

$$\mathbf{p} = M^{-1}\mathbf{b}, \tag{7.7.14}$$

then

$$\mathbf{x_p} = \begin{bmatrix} Z_p \\ A_{1p} \\ B_{1p} \\ A_{2p} \\ B_{2p} \\ A_{3p} \\ B_{3p} \end{bmatrix} = T_p \begin{bmatrix} -\frac{p_1}{gH^2K_p} \\ p_2 \\ p_3 \\ p_4 \\ p_5 \\ p_6 \\ p_7 \end{bmatrix} \tag{7.7.15}$$

where $p_i, i = 1, \ldots, 7$ denote the elements of the vector $\mathbf{p}$. Using Equations (7.7.9) and (7.1.2) together with the above values for the unknowns gives the following equilibrium solutions:

$$u(x,\eta) = \begin{cases} \tau_0(p_1\xi_1^2/B_1^2 + p_2 \log \xi_1 + p_3) & 0 \le \eta \le \eta_1 \\ \tau_0(-p_1\eta^2/2N_1 + p_4\eta + p_5) & \eta_1 \le \eta \le \eta_2 \\ \tau_0(p_1\xi_3^2/B_3^2 + p_6 \log \xi_3 + p_7) & \eta_2 \le \eta \le 1 \end{cases} \tag{7.7.16}$$

Similarly, the solution for the equilibrium elevation $\varsigma(x)$ is

$$\varsigma(x) = \frac{\tau_0 p_1}{gH^2}(x - L/2). \tag{7.7.17}$$

§7.8 A Turbulent Energy Closure Scheme

The turbulent energy closure scheme in which the eddy viscosity is calculated as part of the solution procedure (see Chapter 6) will be used here to model the same problem for which analytic solutions have been obtained in the previous section of this chapter. In particular, the so-called $k - \epsilon$ equations will be used together with the usual equations of continuity and momentum to model the wind set up and the horizontal velocity which occurs when a wind is blowing over a long narrow channel filled with an incompressible fluid.

Because the physical problem is essentially two dimensional, equations involving only a horizontal and a vertical component of velocity will be used. Also,

because a numerical model is used to obtain solutions, the non-linear equations are used. The complete set of equations is available from the previous chapter and Chapter 1 and are:

$$\frac{\partial \zeta}{\partial t} + \frac{\partial U}{\partial x} = 0, \tag{7.8.1(a)}$$

$$\frac{\partial u}{\partial t} + u\frac{\partial u}{\partial x} + \omega\frac{\partial u}{\partial \eta} = -g\frac{\partial \zeta}{\partial x} + \frac{1}{\hbar^2}\frac{\partial}{\partial \eta}N\frac{\partial u}{\partial \eta}, \tag{7.8.1(b)))}$$

$$\omega = \frac{1}{\hbar}\left[\eta\frac{\partial}{\partial x}U - \frac{\partial}{\partial x}\hbar U(\eta)\right], \tag{7.8.1(c))}$$

$$\frac{\partial k}{\partial t} + u\frac{\partial k}{\partial x} + +\omega\frac{\partial k}{\partial \eta} = \frac{N}{\hbar^2}\left(\frac{\partial u}{\partial \eta}\right)^2 + \frac{1}{\hbar^2}\frac{\partial}{\partial \eta}\left(\frac{N}{\sigma_k}\frac{\partial k}{\partial \eta}\right) - \epsilon \tag{7.8.1(d))}$$

and

$$\frac{\partial \epsilon}{\partial t} + u\frac{\partial \epsilon}{\partial x} + \omega\frac{\partial \epsilon}{\partial \eta} = \frac{c_1 \epsilon N}{k\hbar^2}\left(\frac{\partial u}{\partial \eta}\right)^2 + \frac{1}{\hbar^2}\frac{\partial}{\partial \eta}\left(\frac{N}{\sigma_\epsilon}\frac{\partial \epsilon}{\partial \eta}\right) - \frac{c_2\epsilon^2}{k}. \tag{7.8.1(e))}$$

This set of equations is subject to to the boundary conditions

$$u = 0 \qquad \text{at } x = 0, L, \tag{7.8.2(a))}$$

$$u = \omega = k = \epsilon = 0 \qquad \text{at } \eta = 0, \tag{7.8.2(b))}$$

$$\omega = 0 \qquad \text{at } \eta = 1, \tag{7.8.2(c))}$$

$$k = \frac{u_{*s}^2}{\sqrt{c}} \qquad \text{at } \eta = 1, \tag{7.8.2(d))}$$

$$\epsilon = \frac{u_{*b}^3}{\kappa\eta_1} \qquad \text{at } \eta = 1 \tag{7.8.2(e))}$$

and

$$N\frac{\partial u}{\partial \eta} = \frac{\hbar\tau_0}{\rho}. \tag{7.8.2(f))}$$

Note that the explicit equation for the transformed vertical velocity, ω, given by Equation (7.8.1(c)) automatically satisfies the boundary conditions $\omega = 0$ at $\eta = 0$ and $\eta = 1$.

A finite difference scheme is used to solve the above mentioned set of partial differential equations and associated boundary conditions. A smoothly varying grid spacing, based on the kappa method (see Noye (1983), is used in the vertical direction since this permits more accurate differencing of velocities which change rapidly over depth; in particular this process occurs in the boundary layers near the sea floor and the sea surface. Constant grid spacings using a staggered grid system as shown in Figure 5.1 are used in the horizontal plane.

The horizontal grid elements consist of the two points X and $\rightarrow$ used in Chapter 5. At the $\rightarrow$-points, the horizontal component of velocity is calculated. All other variables are calculated at X points. The notation $u|^n_{i,k}$ is used to represent the approximation for $u(x,\eta,t)$ computed at the $\rightarrow$ point of the i^{th} element at the k^{th} depth level at time $n\Delta t$, where Δt is the constant time step. The $(k-1)^{th}$ and the k^{th} layers are separated by a distance $\Delta\eta_k$, that is,

$$\Delta\eta_k = \eta_k - \eta_{k-1} \qquad , k = 1, \ldots, ND \tag{7.8.3}$$

where η_k defines the height of the k^{th} layer above the bottom of the channel and there are $(ND+1)$ depth levels. The distance between each depth layer is given by the kappa method of Noye(1983) and so $\Delta\eta_k = \Delta\eta_{k-1}(1-\kappa\Delta\eta_{k-1})$ for some constant κ. The $k=1$ layer is at the bottom of the basin, that is, at $\eta = 0$, whilst the surface, $\eta = 1$, is defined by $k = ND$.

The governing equations are discretised in the form

$$\left.\frac{\partial\zeta}{\partial t}\right|^n_i + \left.\frac{\partial U}{\partial x}\right|^n_i = 0, \tag{7.8.4(a)}$$

$$\frac{\partial u}{\partial t}\Big|_{i,k}^{n} + u\frac{\partial u}{\partial x}\Big|_{i,k}^{n} + \omega\frac{\partial u}{\partial \eta}\Big|_{i,k}^{n} = -\frac{g}{2}\left(\frac{\partial \zeta}{\partial x}\Big|_{i}^{n+1} + \frac{\partial \zeta}{\partial x}\Big|_{i}^{n}\right) + \frac{1}{2\hbar^2}\left(\frac{\partial}{\partial \eta}N\frac{\partial u}{\partial \eta}\Big|_{i,k}^{n} + \frac{\partial}{\partial \eta}N\frac{\partial u}{\partial \eta}\Big|_{i,k}^{n+1}\right), \qquad (7.8.4(b))$$

$$\frac{\partial k}{\partial t}\Big|_{i,k}^{n} + u\frac{\partial k}{\partial x}\Big|_{i,k}^{n} + \omega\frac{\partial k}{\partial \eta}\Big|_{i,k}^{n} = \frac{N}{\hbar^2}\left(\frac{\partial u}{\partial \eta}\right)^2\Big|_{i,k}^{n} + \frac{1}{2\hbar^2}\left(\frac{\partial}{\partial \eta}\left(\frac{N}{\sigma_k}\frac{\partial k}{\partial \eta}\right)\Big|_{i,k}^{n} + \frac{\partial}{\partial \eta}\left(\frac{N}{\sigma_k}\frac{\partial k}{\partial \eta}\right)\Big|_{i,k}^{n+1}\right) - \frac{1}{2}\left(\epsilon|_{i,k}^{n} + \epsilon|_{i,k}^{n+1}\right) \qquad (7.8.4(c))$$

$$\frac{\partial \epsilon}{\partial t}\Big|_{i,k}^{n} + u\frac{\partial \epsilon}{\partial x}\Big|_{i,k}^{n} + \omega\frac{\partial \epsilon}{\partial \eta}\Big|_{i,k}^{n} = \frac{c_1 \epsilon N}{k\hbar^2}\left(\frac{\partial u}{\partial \eta}\right)^2\Big|_{i,k}^{n} + \frac{1}{2\hbar^2}\left(\frac{\partial}{\partial \eta}\left(\frac{N}{\sigma_\epsilon}\frac{\partial \epsilon}{\partial \eta}\right)\Big|_{i,k}^{n} + \frac{\partial}{\partial \eta}\left(\frac{N}{\sigma_\epsilon}\frac{\partial \epsilon}{\partial \eta}\right)\Big|_{i,k}^{n+1}\right) - c_2\frac{\epsilon}{k}\Big|_{i,k}^{n}\epsilon|_{i,k}^{n+1}, \qquad (7.8.4(d))$$

$$\omega|_{i,k}^{n} = \frac{1}{\hbar}\left[\eta\frac{\partial}{\partial x}U - \frac{\partial}{\partial x}\hbar U(\eta)\right]\Big|_{i,k}^{n} \qquad (7.8.4(e))$$

and

$$N|_{i,k}^{n} = c^2k^2|_{i,k}^{n}/\epsilon|_{i,k}^{n}. \qquad (7.8.4(f))$$

Equations (7.8.4(a)-(d)) are used together with values of ζ, u, k and ϵ at the n^{th} time level to calculate the value of these variables at the new time level $(n+1)$. Equation (7.8.4(a)) is calculated first, providing an approximation for $\zeta|_{i}^{n+1}$ using values for U calculated at time level n. This value of ζ is used in the time and space centred approximations for the momentum equations to provide an approximation for u at the new time level $(n+1)$. Once this value for u has been obtained, a more accurate approximation for ζ is calculated using an equation like (7.8.4(a)) except that this time an average of the velocity components at time n and $(n+1)$ is used when approximating the velocity term in this equation. The remaining equations (7.8.4(e) and (f)) are all explicit and use these values to calculate N and ω at

the new time level. Note that the dissipation, ϵ, which appears on the right hand side of the turbulent energy equation involves a term at the $(n+1)$ time level. It is therefore necessary that Equation (7.8.4(d)) be solved before (7.8.4(c)). Note also that the second order derivatives with respect to η which appear in Equations (7.8.4(a)-(d)) also involve terms at the $(n+1)$ time level. Time centering in this manner results in an implicit scheme which contributes to the overall stability of the method.

The discretisation of the individual terms in the governing equations is now discussed.

All the time derivatives are approximated by the forward time form

$$\left.\frac{\partial \zeta}{\partial t}\right|_{i,k}^{n} = \frac{1}{\Delta t}\left(\zeta_i^{n+1} - \zeta_i^n\right) + O\left\{\Delta t\right\}. \tag{7.8.9}$$

Centred differencing is used to model all the spatial derivatives. For example,

$$\left.\frac{\partial u}{\partial x}\right|_{i,k}^{n} = \frac{1}{4\Delta x}\left(u_{i,k}^n - u_{i-1,k}^n\right) + O\left\{(\Delta x)^2\right\}. \tag{7.8.10}$$

Because a variable grid spacing is used in the vertical, to keep the differencing second order accurate, the following formula must be used for derivatives with respect to η

$$\left.\frac{\partial u}{\partial \eta}\right|_{i,k}^{n} = \frac{1}{r_k \Delta\eta_k \Delta\eta_{k+1}}\left(\Delta\eta_k u_{i,k}^n - \Delta\eta_{k+1}(r_k - 1)u_{i,k-1}^n + r_k(r_k - 2)u_{i,k}^n\right) + O\left\{\Delta\eta_k \Delta\eta_{k+1}\right\} \tag{7.8.10}$$

where $r_k = \Delta\eta_{k+1}/\Delta\eta_k + 1$ (see Noye (1983)). The corresponding formula for the second order derivatives with respect to η is derived by first using Equation

(7.8.10) with u replaced by $N\partial u/\partial\eta$, for example, and the three depth levels are taken to be the k^{th}, the level halfway between the k^{th} and $(k-1)^{th}$, denoted $(k-1/2)$ and the level $(k+1/2)$ which is halfway between the k^{th} and $(k+1)^{th}$ levels. This yields an equation containing derivatives at levels $(k-1/2)$, $(k+1/2)$ and k. At the k^{th} level, Equation (7.8.10) is applied. Centred differences are used to represent the first order derivatives at the two levels $(k-1/2)$ and $(k+1/2)$. For example,

$$\left.\frac{\partial u}{\partial \eta}\right|^n_{i,k+1/2} = \frac{u^n_{i,k+1}-u^n_{i,k}}{\Delta\eta_{k+1}} + O\left\{(\Delta\eta_{k+1})^2\right\}. \tag{7.8.11}$$

This procedure yields the formula

$$\begin{aligned}
\left.\frac{\partial}{\partial\eta}\left(N\frac{\partial u}{\partial\eta}\right)\right|^n_{i,k} = {} & \frac{u^n_{i,k-1}}{r_k(\Delta\eta_k)^2}\Big[(r_k-1)(\bar{N}^n_{i,k-1}+\bar{N}^n_{i+1,k-1}) \\
& \qquad -(r_k-2)(N^n_{i,k}+N^n_{i+1,k}\Big] \\
& + \frac{u^n_{i,k}}{r_k(\Delta\eta_k)^2(\Delta\eta_{k+1})^2}\Big[-(\Delta\eta_k)^2(N^n_{i,k}+N^n_{i+1,k}) \\
& \qquad -(r_k-1)(\Delta\eta_{k+1})^2(\bar{N}^n_{i,k-1}+\bar{N}^n_{i+1,k-1}) \\
& \qquad +r_k(r_k-2)^2(\Delta\eta_k)^2(N^n_{i,k}+N^n_{i+1,k})\Big] \\
& + \frac{u^n_{i,k+1}}{r_k(\Delta\eta_{k+1})^2}\Big[(\bar{N}^n_{i,k}+\bar{N}^n_{i+1,k}) \\
& \qquad +(r_k-2)(N^n_{i,k}+N^n_{i+1,k})\Big]
\end{aligned} \tag{7.8.12}$$

where $\bar{N}n_{i,k} = (N^n_{i+1,k}+N^n_{i,k})/2$.

The integrals which appear in the equations are computed using the Trapezoidal rule. For example,

$$\begin{aligned}
U = \int_0^1 u d\eta \Big|^n_1 = \frac{1}{2}\Big[& \Delta\eta_1(u^n_{i,0}+u^n_{i,1}) + \Delta\eta_2(u^n_{i,1}+u^n_{i,2}) + \ldots \\
& \ldots + \Delta\eta_{ND}(u^n_{i,ND-1}+u^n_{i,ND})\Big]
\end{aligned} \tag{7.8.13}$$

if there are $(ND+1)$ depth levels of variable spacing.

All of the boundary conditions for which boundary values are known are easily handled. These values are used in the finite difference equations applied at neighbouring grid points.

Derivative conditions are somewhat more difficult to incorporate. When approximating the derivatives with respect to η at the boundaries, second order accurate differencing has been used. For example, at the surface, $\eta = 1$, the following scheme was used:

$$\left.\frac{\partial u}{\partial \eta}\right|_{i,ND}^{n} = \frac{1}{\Delta\eta_{ND}}\left(\frac{r_1+1}{r_1}u_{i,ND}^{n} + \frac{r_1}{r_1-1}u_{i,ND-1}^{n} + \frac{1}{r_1(r_1-1)}u_{i,ND-2}^{n}\right] \tag{7.8.14}$$

in which $r_1 = \Delta\eta_{ND-1}/\Delta\eta_{ND} + 1$. A similar method as was used to derive Equation (7.8.12) was then used to construct the surface double derivative approximation, giving,

$$\begin{aligned}\left.\frac{\partial}{\partial\eta}\left(N\frac{\partial u}{\partial\eta}\right)\right|_{i,ND}^{n} &= \frac{3\tau_0}{\Delta\eta_{ND}}\left(H_{i+1}^{n}+H_{i}^{n}\right)\\ &+ \frac{u_{i,ND}^{n}}{(\Delta\eta_{ND})^2}\left[-4(\bar{N}_{i+1,ND}^{n}+\bar{N}_{i,ND-1}^{n}) + \frac{\Delta\eta_{ND-1}N_{i,ND-1}^{n}}{\Delta\eta_{ND}+\Delta\eta_{ND-1}}\right]\\ &+ u_{i,ND-1}^{n}\left[-2(\bar{N}_{i+1,ND}^{n}+\bar{N}_{i,ND-1}^{n}) - \frac{(\Delta\eta_{ND-1}-\Delta\eta_{ND})N_{i,ND-1}^{n}}{\Delta\eta_{ND-1}}\right]\\ &+ u_{i,ND-2}^{n}\left[\frac{-N_{ND-1}^{n}}{(\Delta\eta_{ND}+\Delta\eta_{ND-1})\Delta\eta_{ND-1}}\right].\end{aligned} \tag{7.8.15}$$

If required, a similar expression may be used for derivative conditions at the bottom.

Modelling the equations as shown results in a tridiagonal system of linear algebraic equations which must be solved. For example, the value of $u_{i,k}^{n+1}$ for $k = 1, \ldots, ND$ may be found from a system like

$$A_{i,k}^{n+1} u_{i,k-1}^{n+1} + B_{i,k}^{n+1} u_{i,k}^{n+1} + C_{i,k}^{n+1} u_{i,k+1}^{n+1} = D_{i,k}^{n}, \qquad k = 1, \ldots, ND-1 \quad (7.8.16)$$

in which $A_{i,k}^{n+1}$, $B_{i,k}^{n+1}$, $C_{i,k}^{n+1}$ and $D_{i,k}^{n+1}$ are known and $u_{i,0}^{n+1} = 0$. Systems of this form may be solved by the very efficient Thomas Algorithm for tridiagonal systems of equations described by Noye (1983). Note that the formulation used for the derivatives in the vertical direction at the surface (and at the bottom, if required) need to specially incorporated into this system before the Thomas Algorithm can be applied. For instance, consider the system of equations (7.8.16). Using Equation (7.8.15) results in an expression connecting terms $u_{i,ND}^{n+1}$, $u_{i,ND-1}^{n+1}$ and $u_{i,ND-2}^{n+1}$. However, Equation (7.8.16) with $k = ND - 1$ also contains terms in $u_{i,ND}^{n+1}$, $u_{i,ND-1}^{n+1}$ and $u_{i,ND-2}^{n+1}$ which may be used to eliminate $u_{i,ND-2}^{n+1}$ from Equation (7.8.15) thus yielding an expression involving only terms in $u_{i,ND}^{n+1}$ and $u_{i,ND-1}^{n+1}$ in the set of equations obtained at the surface. This gives the additional equation

$$A_{i,k}^{n+1} u_{i,k-1}^{n+1} + B_{i,k}^{n+1} u_{i,k}^{n+1} = D_{i,k}^{n} \qquad \text{for } k = ND. \qquad (7.8.17)$$

The system formed by Equations (7.8.16) and (7.8.17) is now in the required form for solution by the Thomas Algorithm.

§7.9 RESULTS

The analytic and numerical solutions which are presented in the previous sections are now used to analyse the performance of the various formulations for the eddy viscosity. Firstly, the equilibrium cases are examined. Each solution is in turn discussed and then compared with each other. The analytic solutions are then compared with some laboratory experiments. The performance of the $k - \epsilon$ model is also analysed by comparison with these experiments. Finally, the unsteady oscillating solutions are discussed.

In Figure 7.2 velocity profiles are displayed which have been obtained using the equilibrium solution for the velocity in which the eddy viscosity has a constant value, N_0 (see Equation (7.2.2)). The profiles are normalized with respect to the velocity obtained using a reference eddy viscosity value of N. The effect of increasing the eddy viscosity relative to the base value of N is examined. The value of N is arbitrary. The same normalized profiles will result using any value of N. Note that if this model was being used to provide quantitative profiles for a given basin, the actual value of N which needs to be used would have to be obtained by comparing, say, the predicted set-up with a measured set-up.

From Figure 7.2, it is clear that the velocity profile which is obtained is very sensitive to the value of N_0. As N_0 is increased, the velocity is greatly reduced. Doubling the value of the constant eddy viscosity more then halves the velocity values.

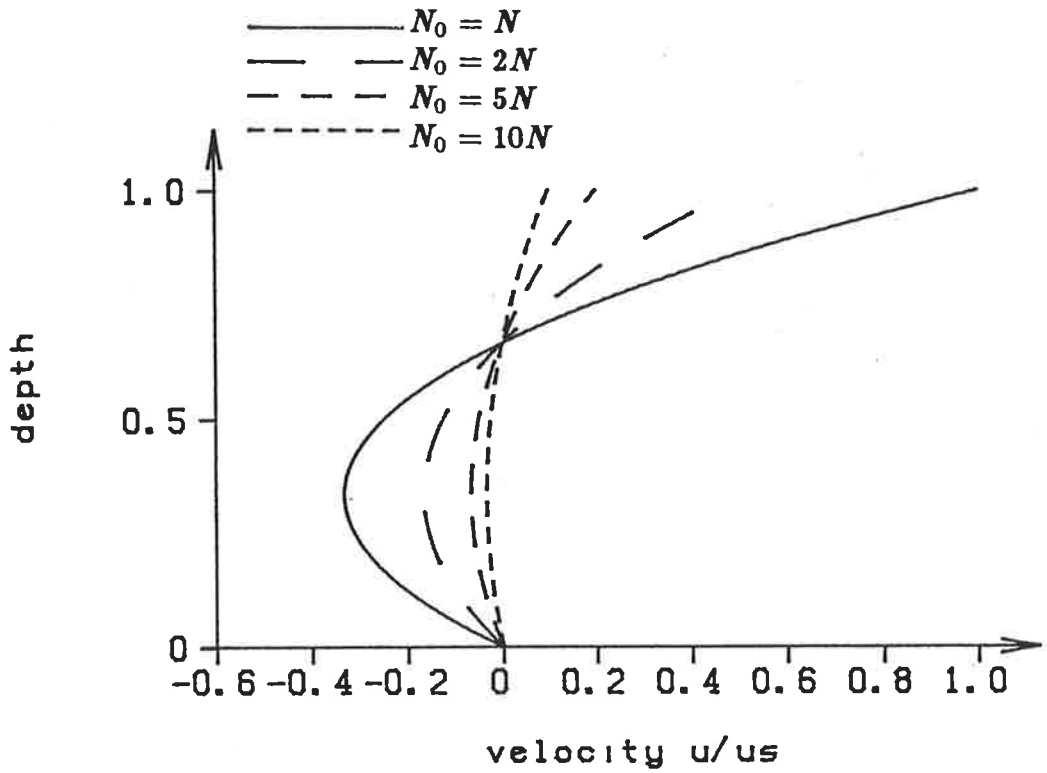

FIGURE 7.2: *Vertical profile of velocity obtained with various values of constant eddy viscosity (results are normalized with respect to the surface velocity obtained when the eddy viscosity, N_0, is equal to the constant value, N).*

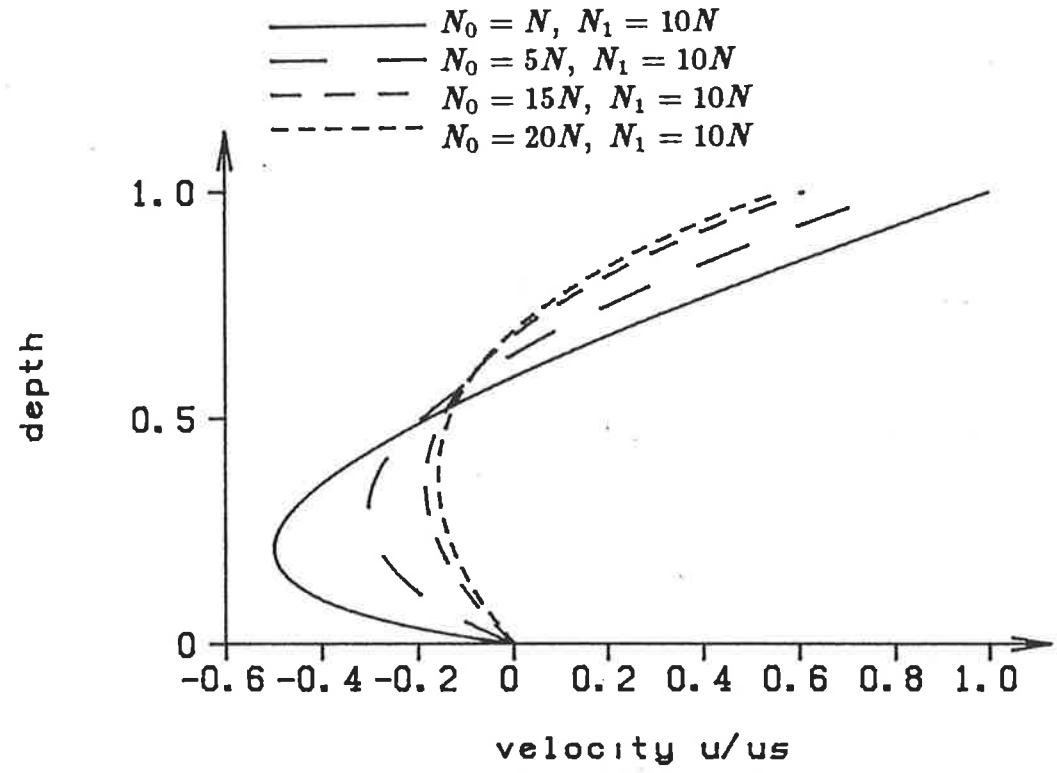

FIGURE 7.3: *Vertical profile of velocity obtained with a linear eddy viscosity for different values of N_0 and N_1 (results are normalized with respect to the surface velocity obtained with $N_0 = N$ and $N_1 = 10N$).*

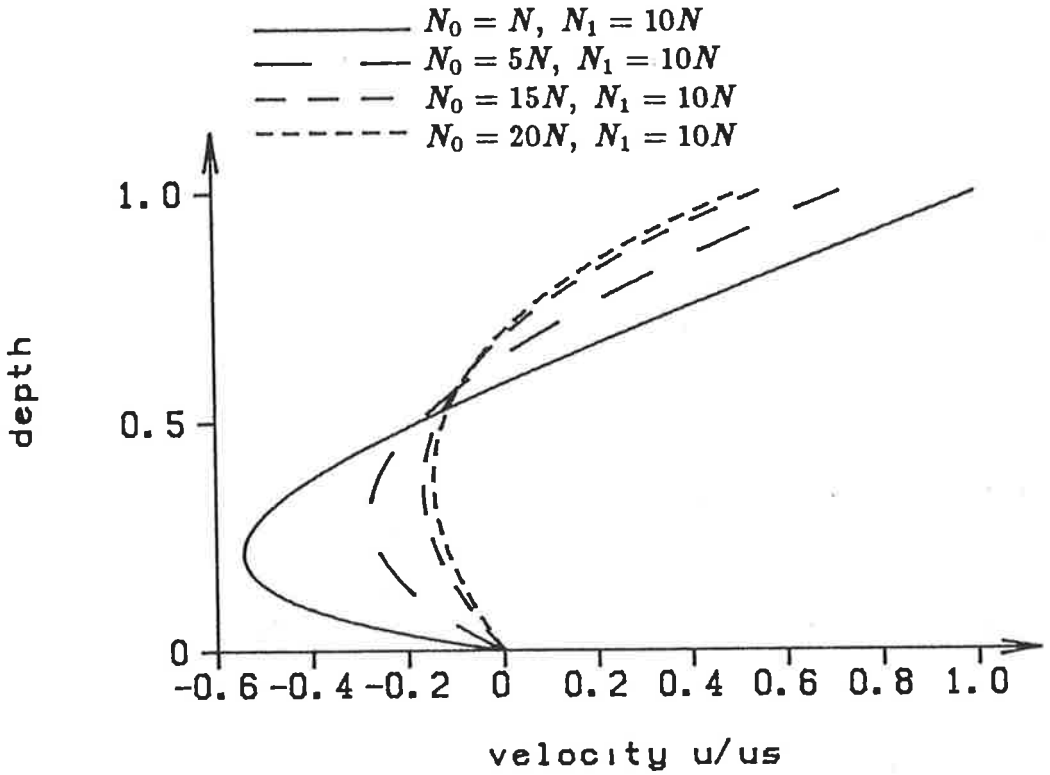

FIGURE 7.4: *Vertical profile of velocity obtained with the quadratic eddy viscosity defined in Section 7.4 for different values of N_0 and N_1 (results are normalized with respect to the surface velocity obtained with $N_0 = N$ and $N_1 = 10N$).*

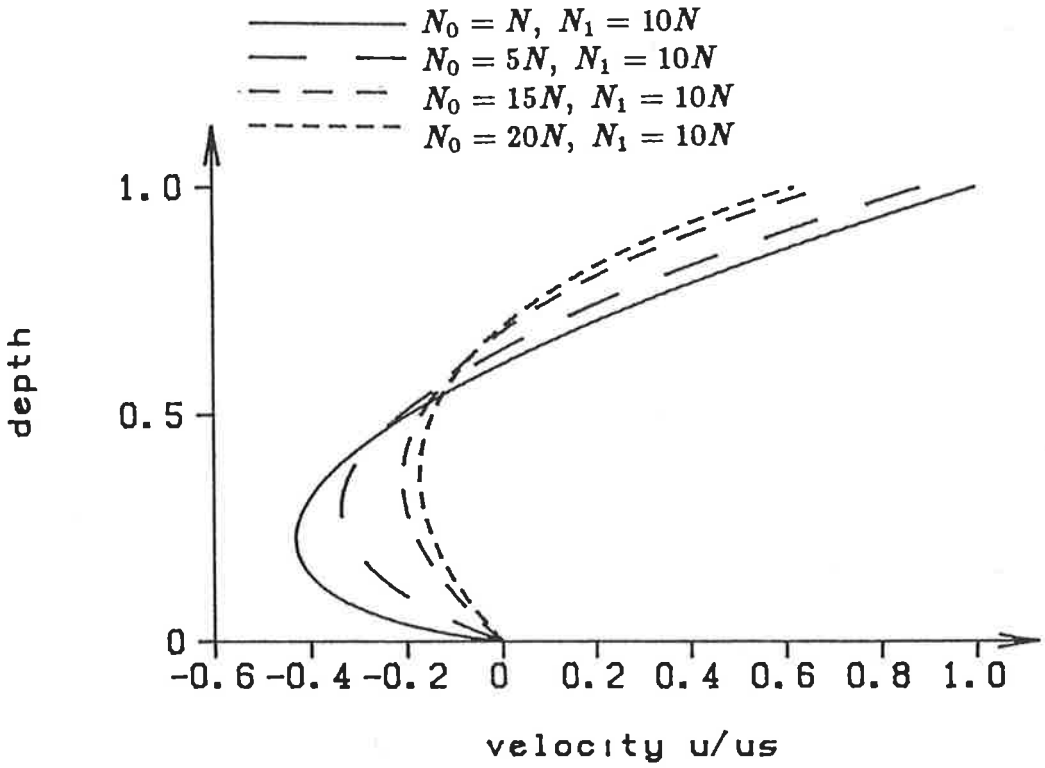

FIGURE 7.5: *Vertical profile of velocity obtained with the quadratic eddy viscosity defined in Section 7.5 for different values of N_0 and N_1 (results are normalized with respect to the surface velocity obtained with $N_0 = N$ and $N_1 = 10N$).*

In Figures 7.3, 7.4 and 7.5 similar results are displayed which have been obtained using the formulations for the eddy viscosity presented in Sections 7.3, 7.4 and 7.5. That is, results from the linear and the first two quadratic forms for N are displayed. Once again, the results have been normalized with respect to certain base values which in this case have been chosen to be $N_0 = N$ and $N_1 = 10N$. The profiles which are shown in these figures are very similar. In all cases, when the value of N_0, that is, the value of the eddy viscosity at the bottom, is greater than the value at the surface, N_1, the magnitude of velocity is considerably less than those obtained using values of $N_0 < N_1$. Also, when $N_0 > N_1$, the profiles are reasonably insensitive to changes in the relative values of N_0 and N_1. These profiles are all considerably different from the profiles obtained using the more conventional situation in which $N_1 > N_0$. For the two profiles shown in each figure for which $N_1 > N_0$, there is only a slight difference in the profiles between each figure. These profiles also show that for the three formulations of eddy viscosity considered in these figures, the profiles are less sensitive to changes in the value of the eddy viscosity than was the case for the constant eddy visosity. For example, decreasing the relative value between N_0 and N_1 from ten to two, decreased the velocity profile by only about 20% in the upper layers and 40% in the lower layers. It is also apparent that the second quadratic formulation (Figure 7.5) is less sensitive to changes in the relative values of N_0 and N_1 then is the case for the first quadratic formulation (Figure 7.4). There is also a clear difference in the profiles between these two figures although the basic shape is similar.

A substantial difference between the previous velocity profiles and the velocity profile obtained when using the quadratic formulation of Section 7.6 is evident in Figure 7.6. The profiles in this figure have all much the same value in the mid-depths. If the bottom and surface values of the eddy viscosity, N_0 and N_1, are kept constant and the value of the eddy viscosity in the mid-depths, N_m, is increased, the resultant profiles of velocity are substantially decreased. There is also a difference between the profiles as the relative values of N_0 and N_1 are changed and N_m is kept constant, although these differences are only slight.

Similar behaviour can be observed in the profiles displayed in Figure 7.7 which displays the results obtained using the composite formulation for the eddy viscosity (see Section 7.7). The results in Figure 7.7 are obtained using $\eta_1 = 0.25$ and $\eta_2 = 0.75$. Figure 7.8 displays profiles obtained for this particular eddy viscosity formulation for different values of the parameters η_1 and η_2. If η_2 is kept constant, and η_1 is changed, there is very little difference between the velocity profiles especially near the surface. If η_1 is kept constant and η_2 is changed, there is a larger difference between the velocity profiles at the surface but very little difference near the bottom.

The next series of figures examines the performance of the various analytic models when compared with the experimental results of Baines and Knapp (1965), Fitzgerald and Mansfield (1965) and Koutitas and O'Connor (1980). In all cases, the velocity profiles are normalized with respect to the surface velocity, u_s, obtained at $\eta = 1$.

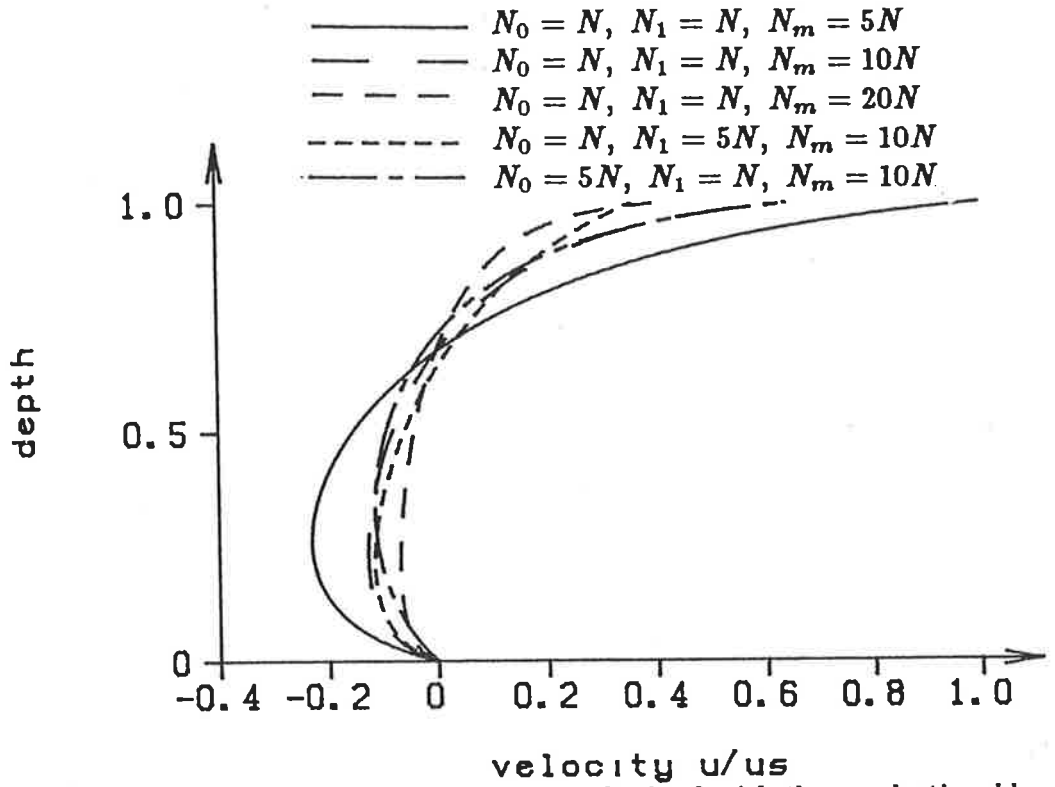

FIGURE 7.6: *Vertical profile of velocity obtained with the quadratic eddy viscosity defined in Section 7.6 for different values of N_0, N_1 and N_m (results are normalized with respect to the surface velocity obtained with $N_0 = N$, $N_1 = N$ and $N_m = 5N$).*

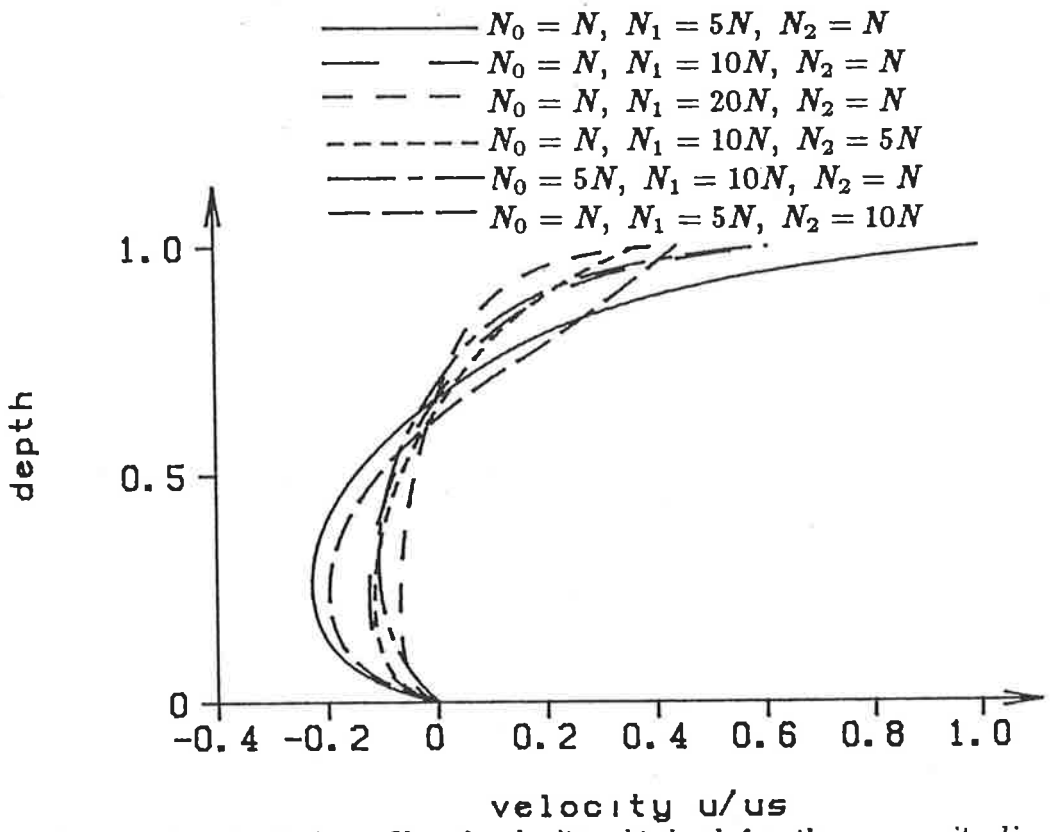

FIGURE 7.7: *Vertical profile of velocity obtained for the composite linear eddy viscosity defined in Section 7.7 for different values of N_0, N_1 and N_2 (results are normalized with respect to the surface velocity obtained with $N_0 = N$, $N_1 = 5N$ and $N_2 = N$). The parameters, η_1 and η_2 are given the values 0.25 and 0.75 respectively.*

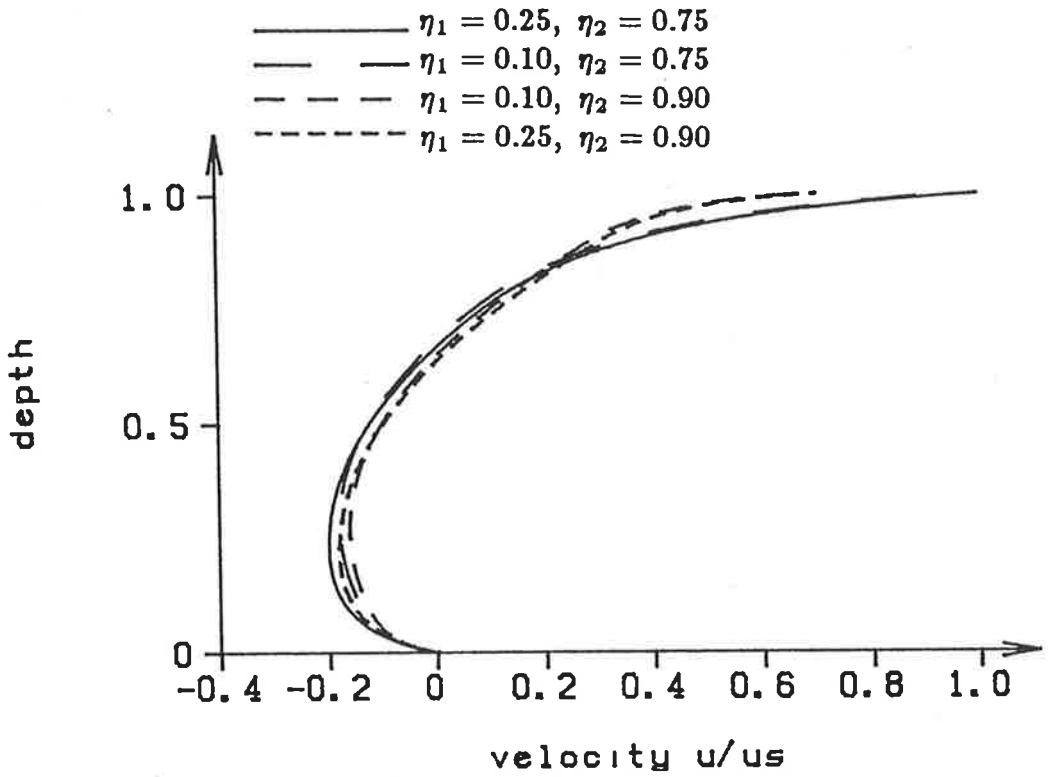

FIGURE 7.8: *Vertical profile of velocity obtained for the composite linear eddy viscosity for different values of η_1 and η_2 with $N_0 = N$, $N_1 = 10N$ and $N_2 = N$ (results are normalized with respect to the surface velocity obtained with $\eta_1 = 0.25$ and $\eta_2 = 0.75$).*

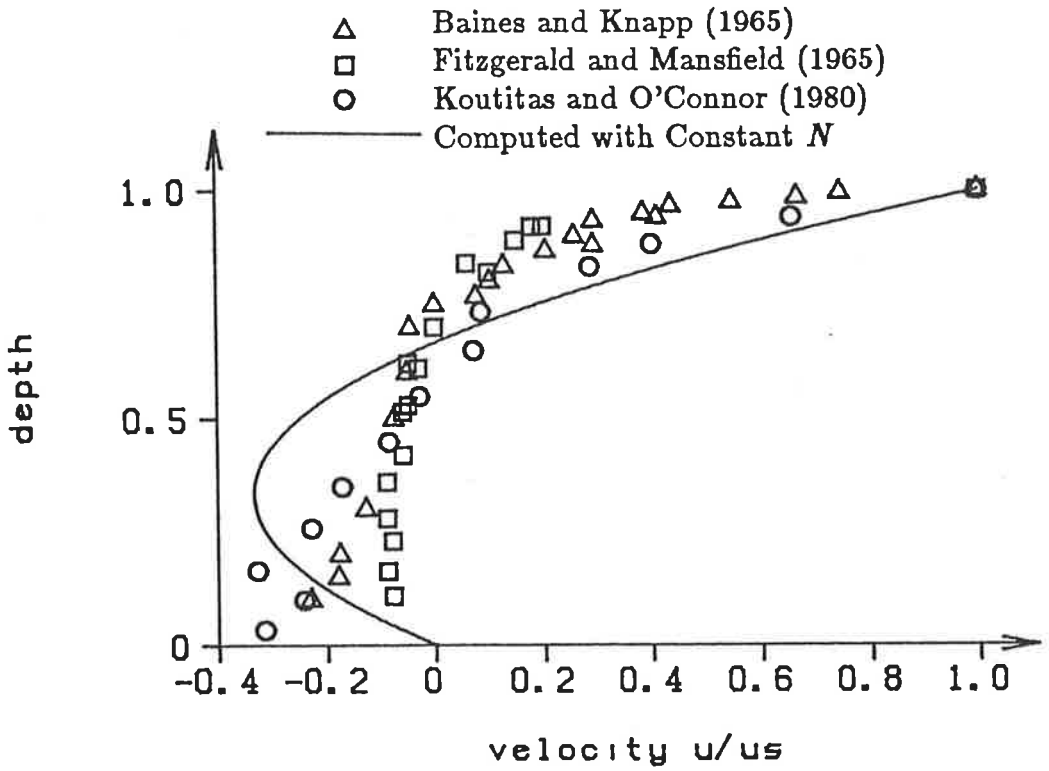

FIGURE 7.9: *Plots of the wind driven velocity profile in a channel of uniform depth as recorded from experiments compared with the analytic solution obtained with constant N.*

Figure 7.9 compares the velocity profile obtained using a constant eddy viscosity with the experimental profiles. Clearly,the analytic profile is not a very good approximation to the observed profiles.

Figures 7.10, 7.11 and 7.12 respectively compare the profiles obtained using the linear formulation for the eddy viscosity, and the two quadratic formulations presented in Sections 7.4 and 7.5. The relative values of N_0 and N_1 used in these figures were found to provide profiles which best fitted the observed results. As expected from the results in the previous figures, the profiles obtained using each of these three formulations for the eddy viscosity are very similar. In each of these three figures, for the case $N_1 = N_0/10$, the resultant velocity profiles agree reasonably well with the observed results near the surface layer. However, the agreement is not so good in the rest of the fluid column. The other profiles presented in these figures (when $N_1 = 1.5N_0$) provided about the best fit for the case $N_1 > N_0$. In this case, the agreement is not very good throughout the whole depth of the fluid.

The next two figures, namely Figures 7.13 and 7.14, provide profiles in much better agreement with the observed velocity profiles. For the quadratic formulation (Figure 7.13), reasonable agreement is achieved for all of the various values of N_0, N_1 and N_m which have been considered. Probably the best agreement is achieved for the formulation for which $N_1 = 10N_0$ and $N_m = 10^3 N_0$. This profile certainly provides good agreement with the observed profiles near the the surface and in the mid-depth regions. There is a considerable difference between the observed

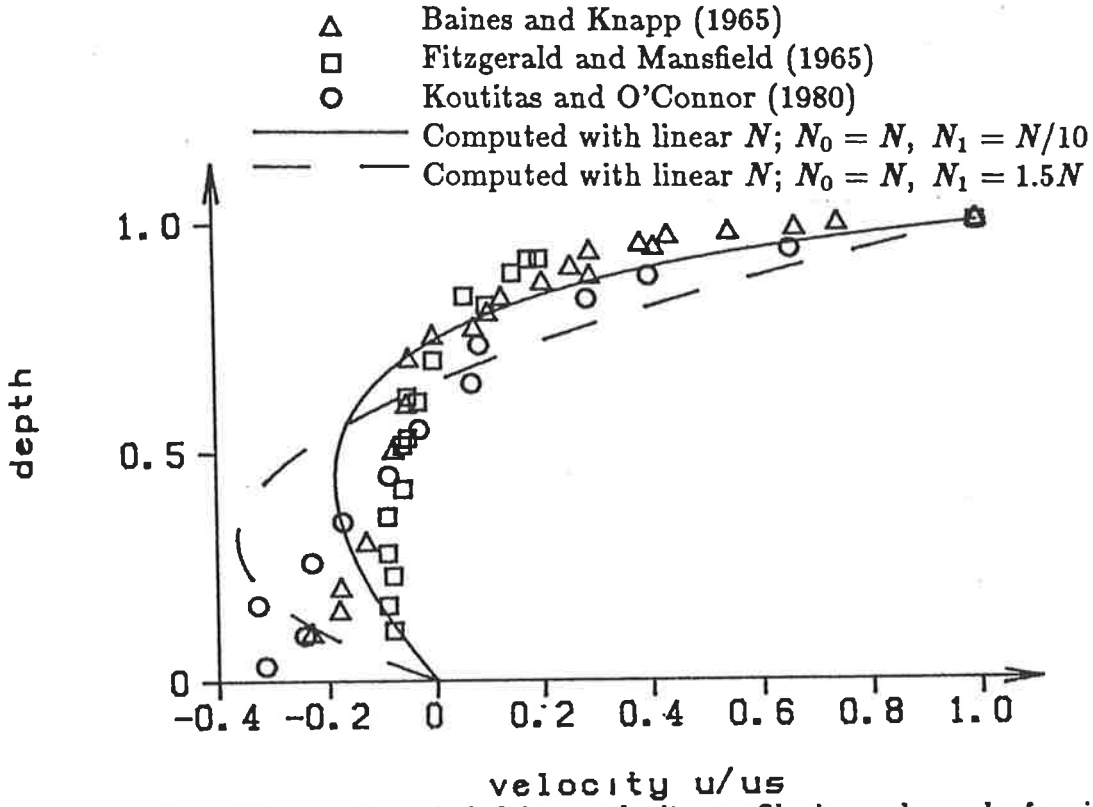

FIGURE 7.10: *Plots of the wind driven velocity profile in a channel of uniform depth as recorded from experiments compared with the analytic solution obtained with linear N.*

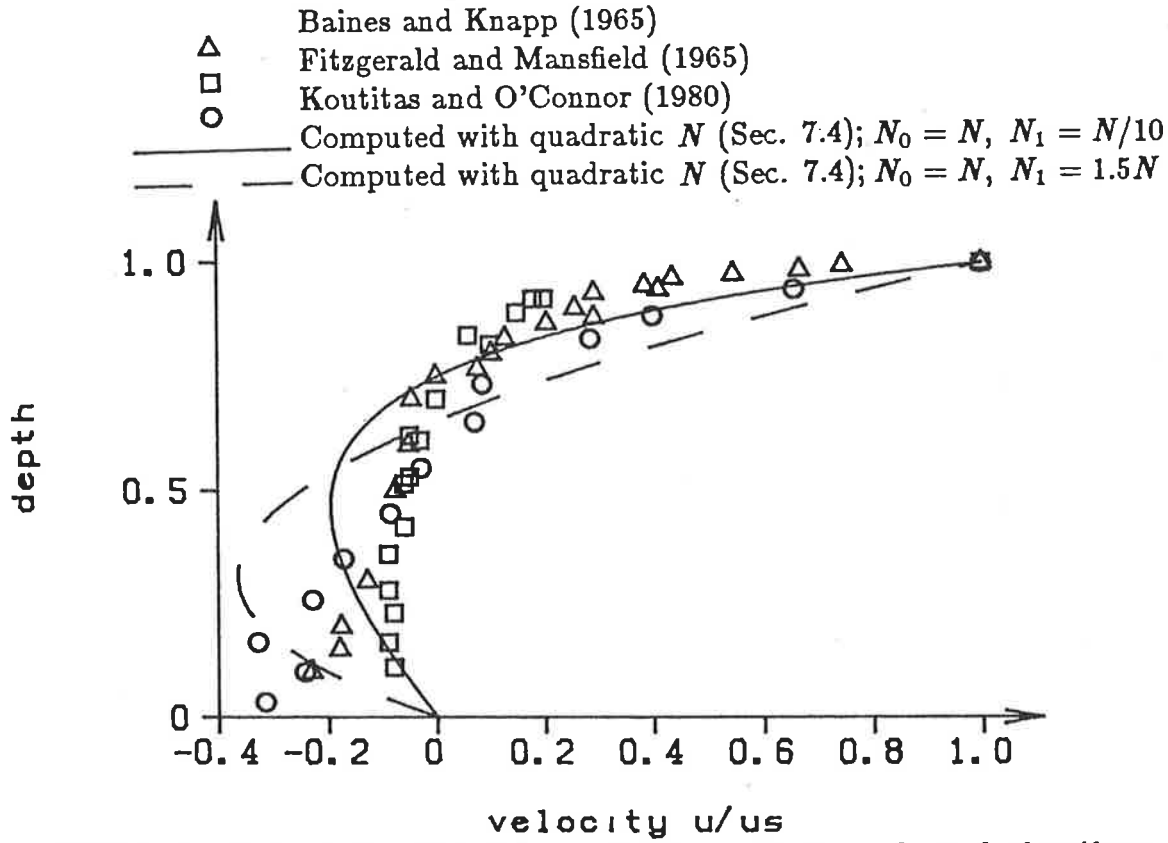

FIGURE 7.11: *Plots of the wind driven velocity profile in a channel of uniform depth as recorded from experiments compared with the analytic solution obtained with the quadratic N defined in Section 7.4.*

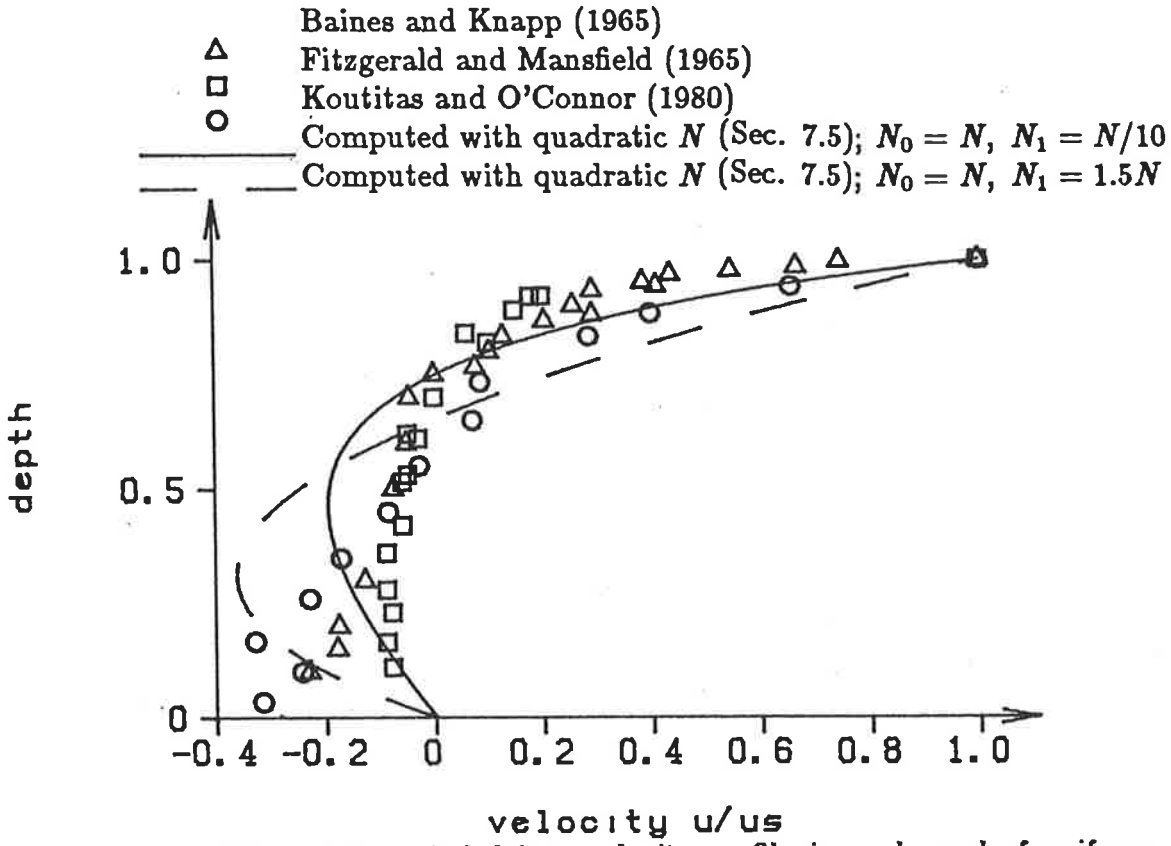

FIGURE 7.12: *Plots of the wind driven velocity profile in a channel of uniform depth as recorded from experiments compared with the analytic solution obtained with the quadratic N defined in Section 7.5.*

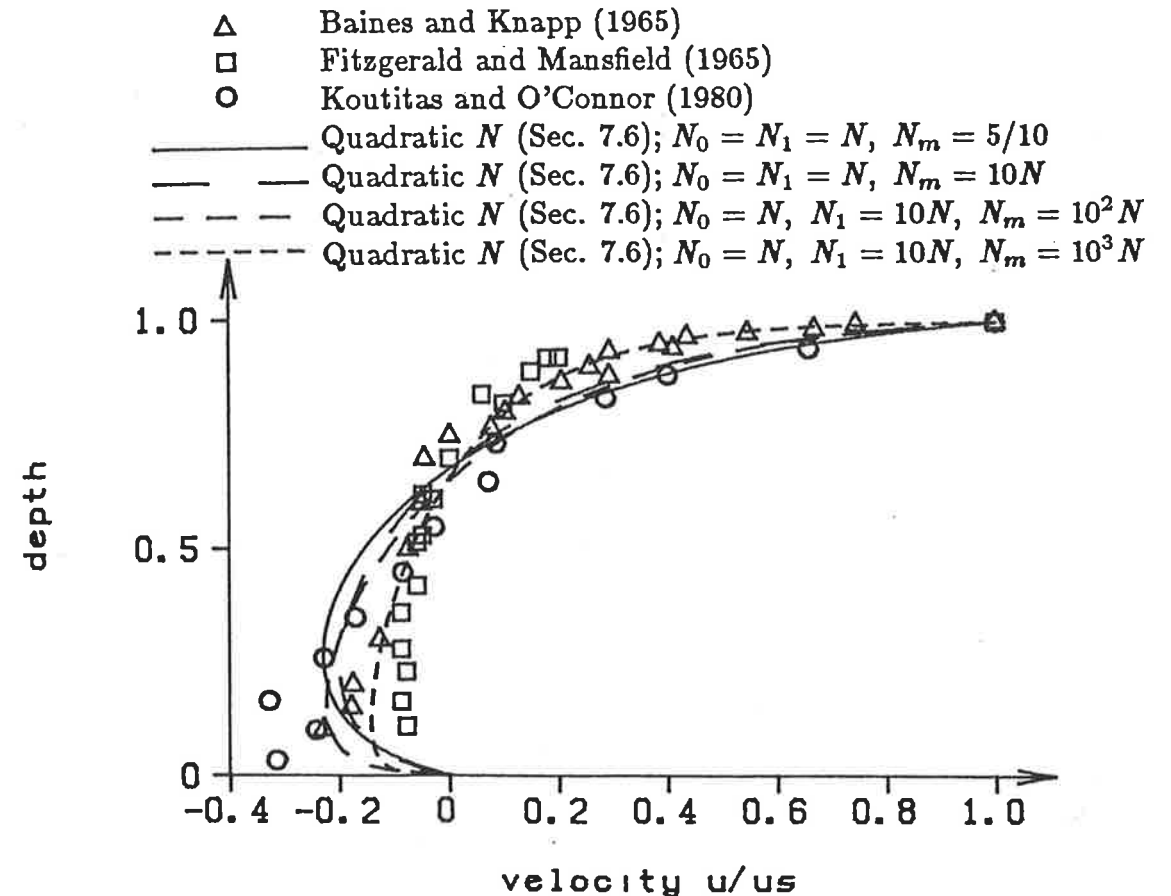

FIGURE 7.13: *Plots of the wind driven velocity profile in a channel of uniform depth as recorded from experiments compared with the analytic solution obtained with the quadratic N defined in Section 7.6.*

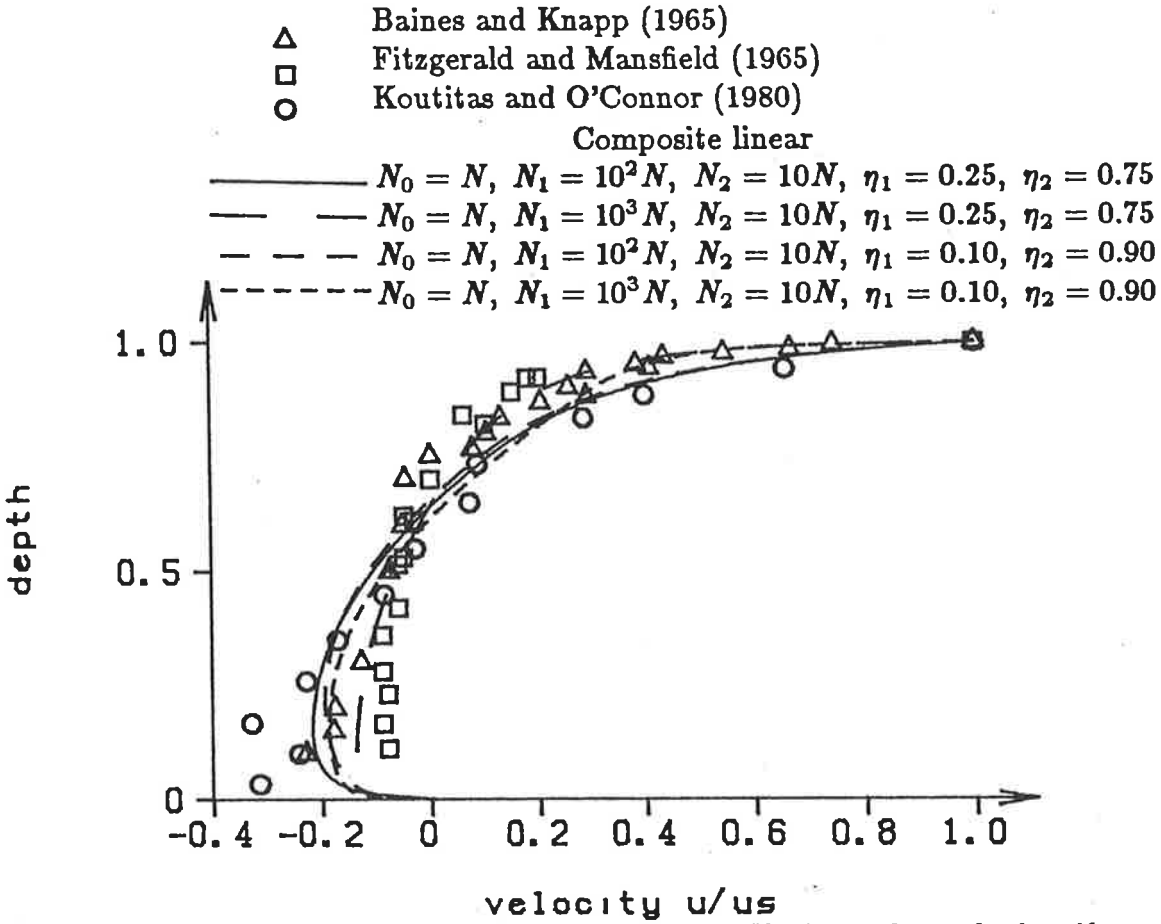

FIGURE 7.14: *Plots of the wind driven velocity profile in a channel of uniform depth as recorded from experiments compared with the analytic solution obtained with the composite linear formulation for N.*

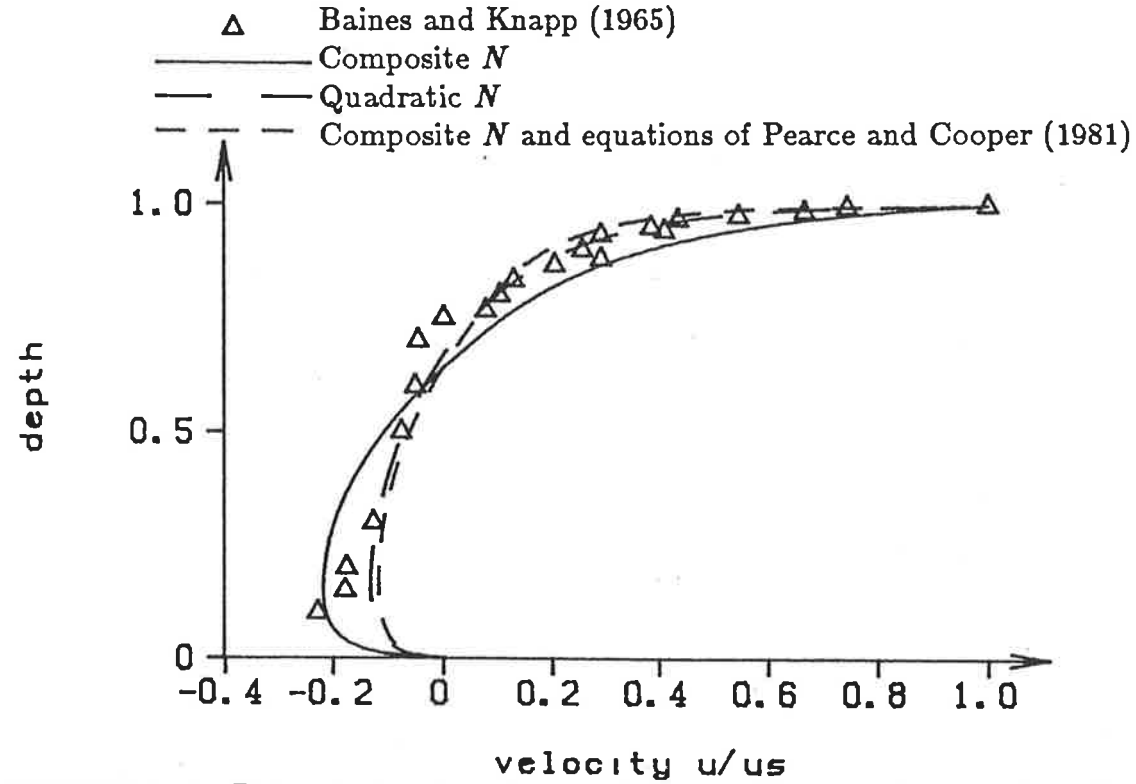

FIGURE 7.15: *Plots of the wind driven velocity profile in a channel of uniform depth as recorded by Baines and Knapp (1965) compared with results obtained using the third quadratic formulation (Sec. 7.6) , the composite linear form and the composite linear form suggested by Pearce and Cooper (1981).*

near the bottom but certainly the agreement between the observed profiles and the analytic solution is acceptable.

Similar profiles are displayed in Figure 7.14 which shows the results obtained using the composite formulation for the eddy viscosity. The best agreement is again achieved with $N_2 = 10N_0$ and $N_1 = 10^3 N_0$. For these parameters, two profiles are displayed; one with $\eta_1 = 0.25$ and $\eta_2 = 0.75$ and the other with $\eta_1 = 0.1$ and $\eta_2 = 0.9$. The best overall results are obtained with the first set of parameters. In fact, the profile obtained with these η values and the above mentioned relative values for N_0, N_1 and N_2, is very similar to the best profile obtained in the previous figure for the quadratic case.

Clearly, the last two analytic models provide the best agreement with experiment.

In Chapter 6, mention was made of a numerical model developed by Pearce and Cooper (1981). The formulation for the eddy viscosity proposed in this model is essentially the composite linear formulation with $N_1 = N_0$. A method for calculating the values of N_0 and N_2 was also described. The value of the eddy viscosity at the surface was taken to be $2.5\text{x}10^{-6}\ m^2 sec^{-1}$ and a value given by $u_{*s}h/12$ was used below $\eta = 0.8$. This special case of the composite formulation is used to produce the profile in Figure 7.15 where a comparison is made with the experiment of Baines and Knapp (1965). This formulation for the eddy viscosity provided good agreement with the observed results. Good agreement was also achieved by Pearce and Cooper (1981) but, however, they obtained their results

from a numerical model not an analytic model as is done here. For comparison, also plotted on this graph are the best curves mentioned above which were obtained using the three parameter quadratic formulation described in Section 7.6 and the composite formulation.

A final comparison between the various analytic solutions is made in Figure 7.16. The relative values of the parameters between the various formulations are kept consistent where the formulations are similar. Clearly, the profiles can be divided into three distinct groups; those with one parameter describing the eddy viscosity (the constant formulation), those using two parameters (the linear and first two quadratic formulations) and those using three parameters (the last quadratic and composite formulations). The difference between the two profiles in this last group is particularly small.

The next group of figures display some results obtained using the $k-\epsilon$ model. In Figure 7.17, the normalized velocity profile obtained using the $k-\epsilon$ model presented in Section 8 of this chapter is compared with the laboratory experiments. Clearly, the agreement is very good.

As was mentioned in Chapter 6, various boundary conditions for the $k-\epsilon$ equations have been used by authors in the past. The effect of using some of these alternative conditions is displayed in the next two figures.

The effect of using symmetry conditions at the surface, that is $\partial k/\partial \eta = \partial \epsilon/\partial \eta = 0$ at $\eta = 1$, is examined in Figure 7.18. The effect of using this boundary

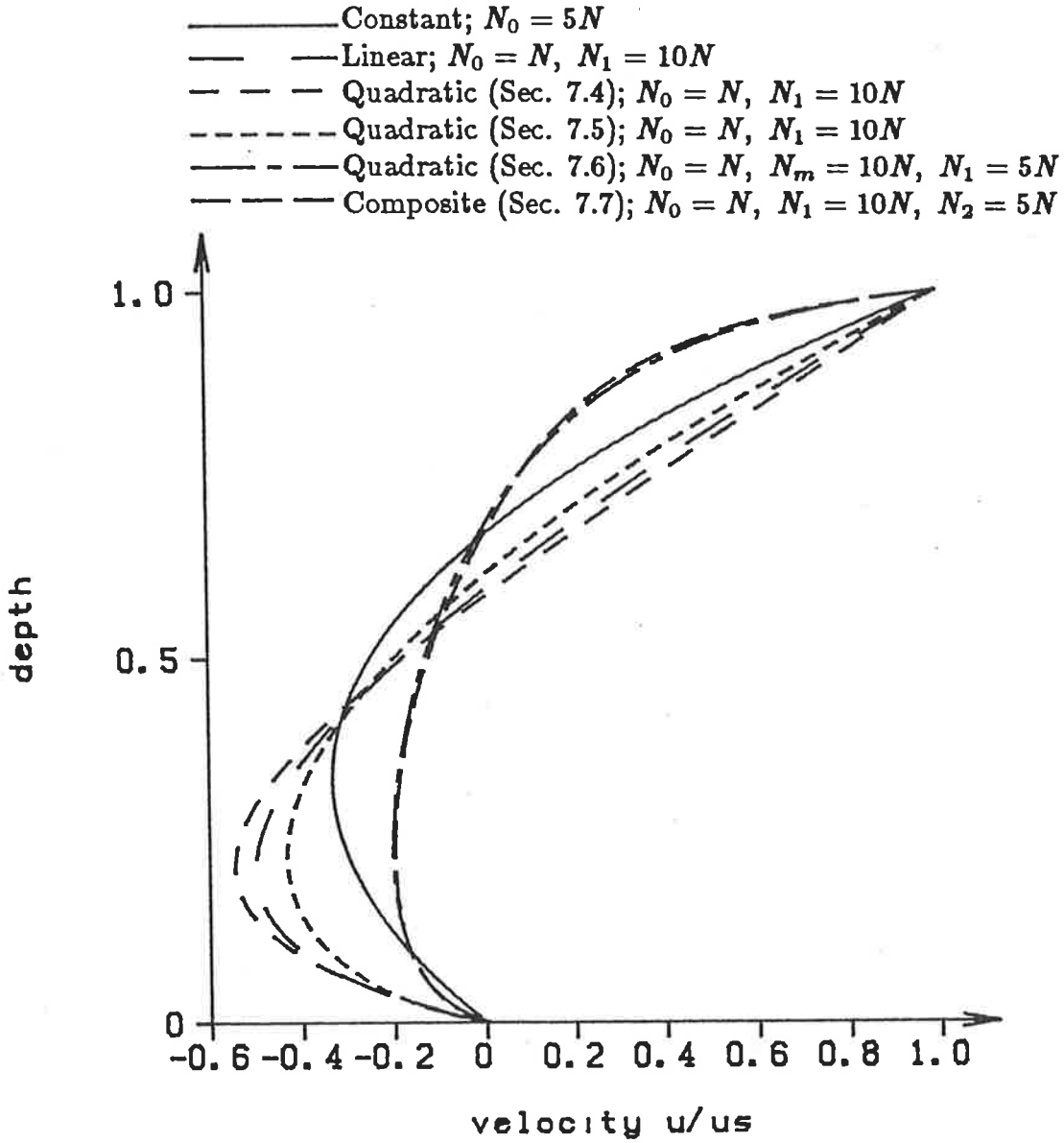

FIGURE 7.16: *Plots of the wind driven velocity profile in a channel of uniform depth obtained with various formulations of eddy viscosity (results are normalized with respect to the surface velocity).*

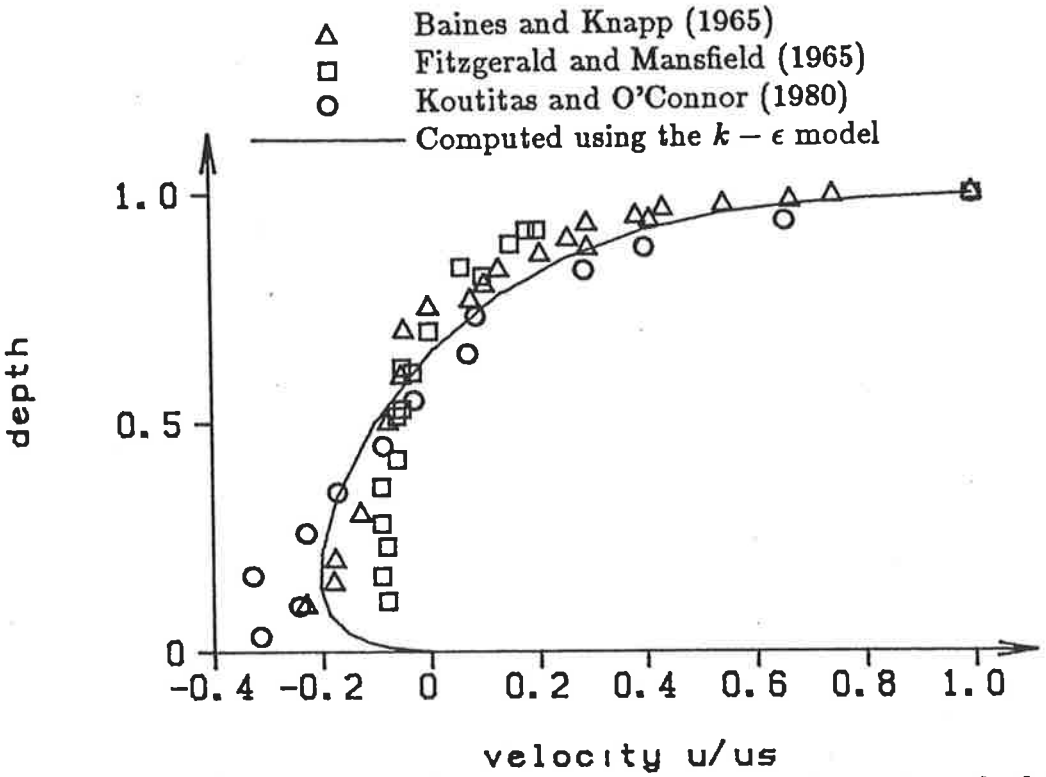

FIGURE 7.17: *Plots of the wind driven velocity profile in a channel of uniform depth as recorded from experiments compared with that predicted by the $k-\epsilon$ model.*

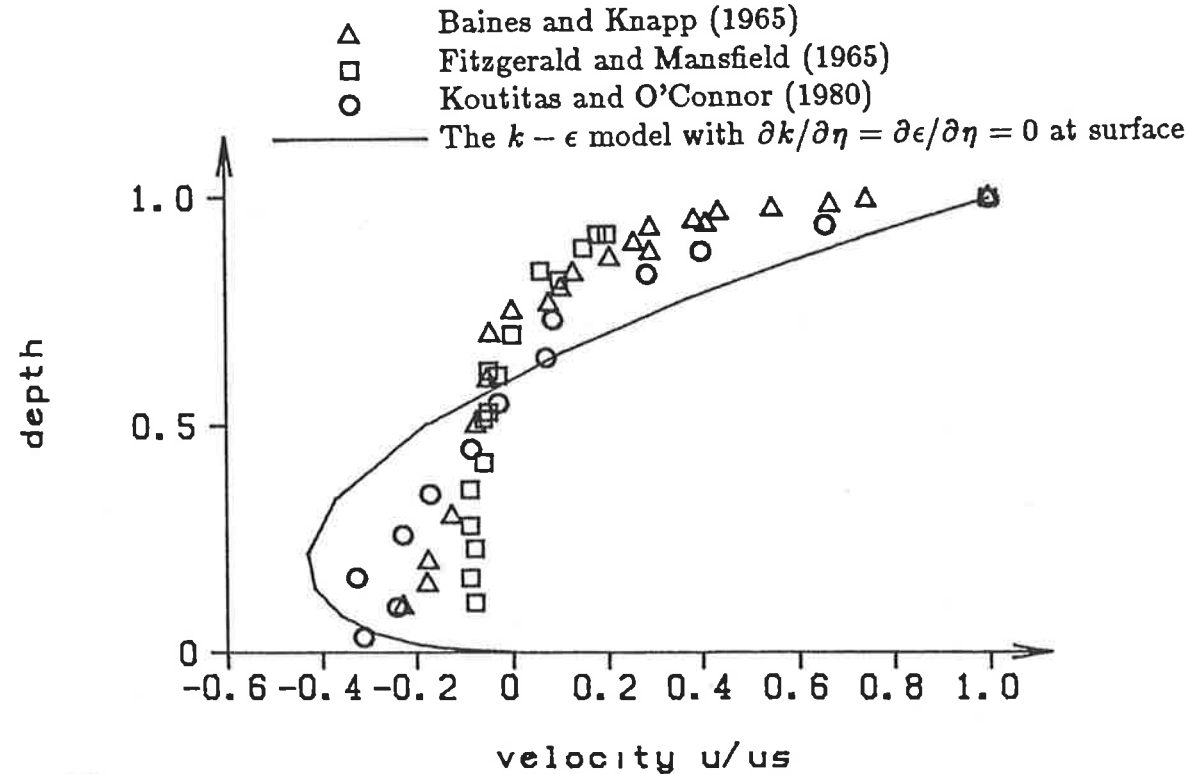

FIGURE 7.18: *Plots of the wind driven velocity profile in a channel of uniform depth as recorded from experiments compared with that predicted by the $k-\epsilon$ model.*

condition is dramatic and the result is unsatisfactory. Clearly, surface values for k and ϵ which are dependent on the surface stress need to be used as the surface boundary conditions. This is done using the wall conditions proposed in Chapter 6.

As was mentioned in Chapter 6, a derivative boundary condition for ϵ at the bottom has also been proposed. The effect of using $\partial\epsilon/\partial\eta = 0$ at $\eta = 0$ is shown in Figure 7.19. For comparison, the profile obtained using $\epsilon = 0$ at $\eta = 0$ is also displayed. There is very little difference between the two curves, with only a slight difference occurring near the bottom. The $\epsilon = 0$ condition used in the $k-\epsilon$ model proposed in this thesis is to be preferred because of the ease with which it can programmed.

The next three figures examine more closely the experiments of Koutitas and O'Connor (1981). In Figure 7.20, the velocity profile predicted by the $k-\epsilon$ model is compared with the observed values. In this figure, the actual raw values of velocity are displayed. This figure illustrates the value of the $k-\epsilon$ method. Not only is the normalized profile successfully predicted by this model, but also the actual data values are successfully predicted. In contrast, although the last quadratic and composite analytic solutions can successfully predict the shape of the velocity profile, in order to obtain the actual, raw velocity values from these models they must be "tuned" with the particular experiment in order to find the correct value of the base value, N, which must be used.

Comparisons between the observed and predicted values for the turbulent

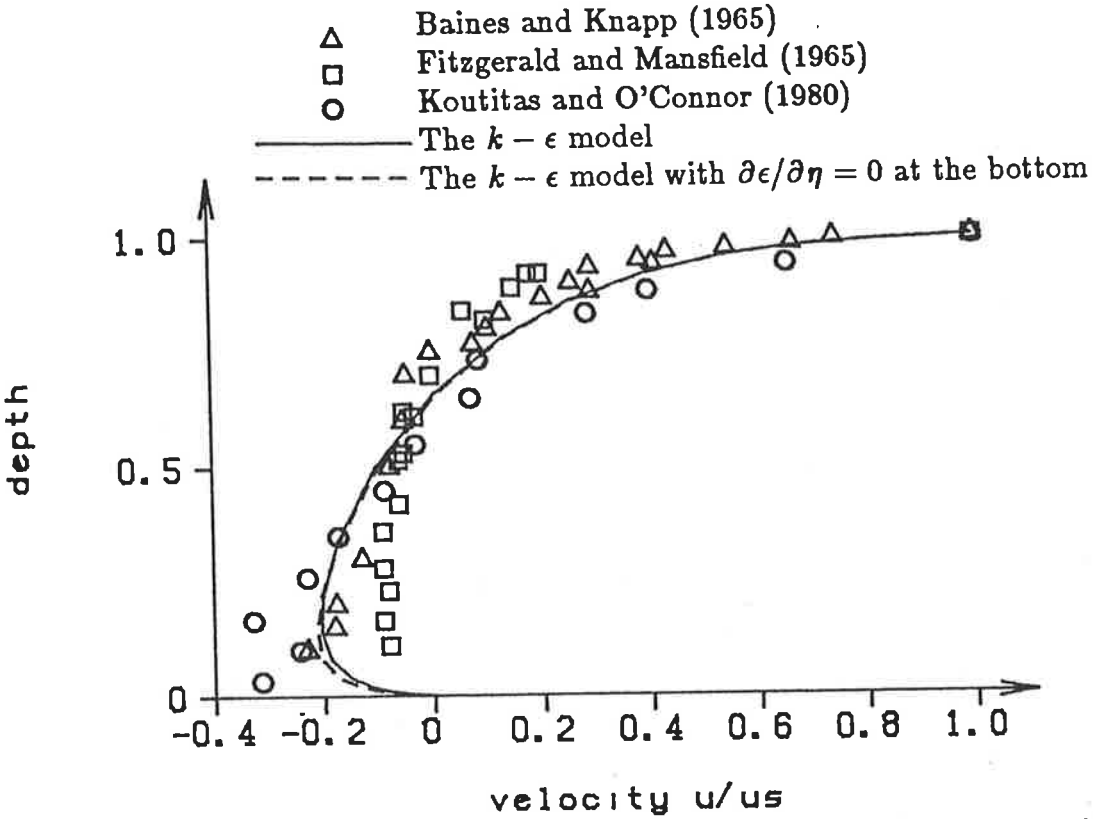

FIGURE 7.19: *Plots of the wind driven velocity profile in a channel of uniform depth as recorded from experiments compared with that predicted by the $k-\epsilon$ model.*

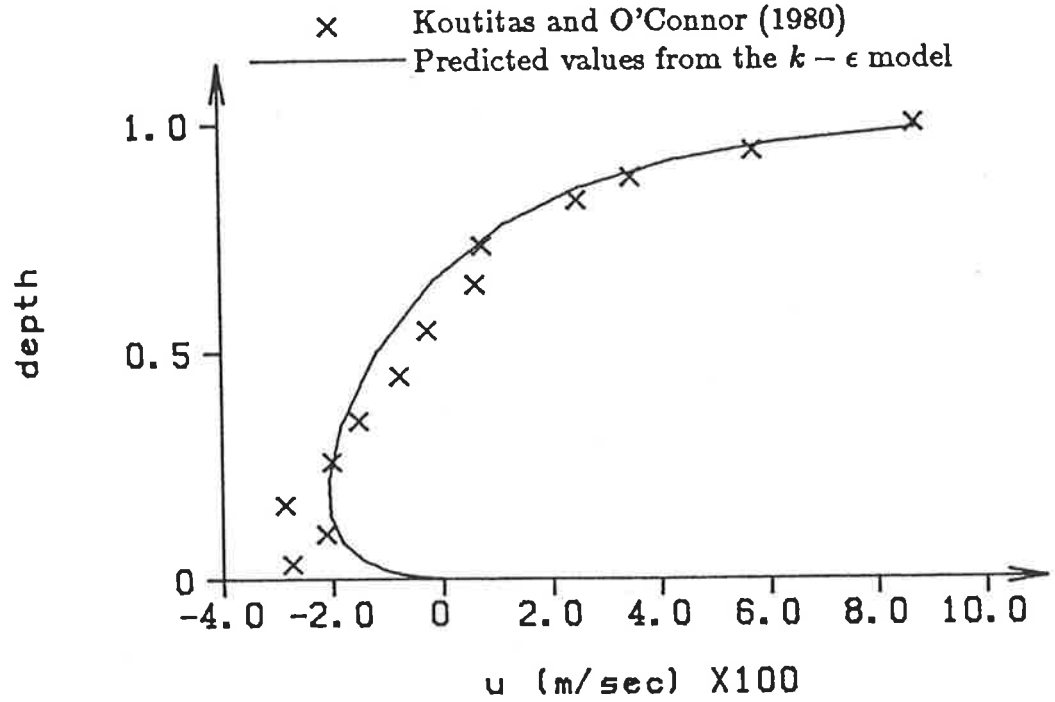

FIGURE 7.20: *Plots of the dimensional vertical velocity profile in a channel of uniform depth as recorded by Koutitas and O'Connor (1980) compared with that predicted by the $k-\epsilon$ model.*

kinetic energy and the eddy viscosity are made in Figures 7.21 and 7.22. The agreement in these two graphs between the observed and predicted values is not as good as previously obtained. However, it must be remembered that there is a great deal of difficulty in measuring these values in experiments as has been pointed out by several authors mentioned in Chapter 6.

The last series of figures deals with the unsteady solutions presented earlier in this chapter. A basin identical to that used by Baines and Knapp (1965) is modelled with an oscillating wind stress with a period, T, of ten minutes. Profiles of the velocity over depth obtained at times, $t = 0$, $T/8$, $T/4$ and $3T/8$ are displayed in the next figures.

Once again, the types of profiles obtained can be roughly divided into three groups depending on the number of parameters used to formulate the eddy viscosity. In Figures 7.23, 7.24, 7.25 and 7.26 the profiles obtained using the constant, linear and the first two quadratic formulations are displayed. There is not much difference between the profiles shown in these figures. Although there is a difference between the profiles obtained using a constant eddy viscosity and those obtained using a two parameter formulation for N, this difference is only relatively small.

The next figure, namely Figure 7.27, displays the profiles obtained using the three parameter quadratic formulation. This profile is similar to those shown in the previous figures except that the velocity increases much more rapidly near the bottom.

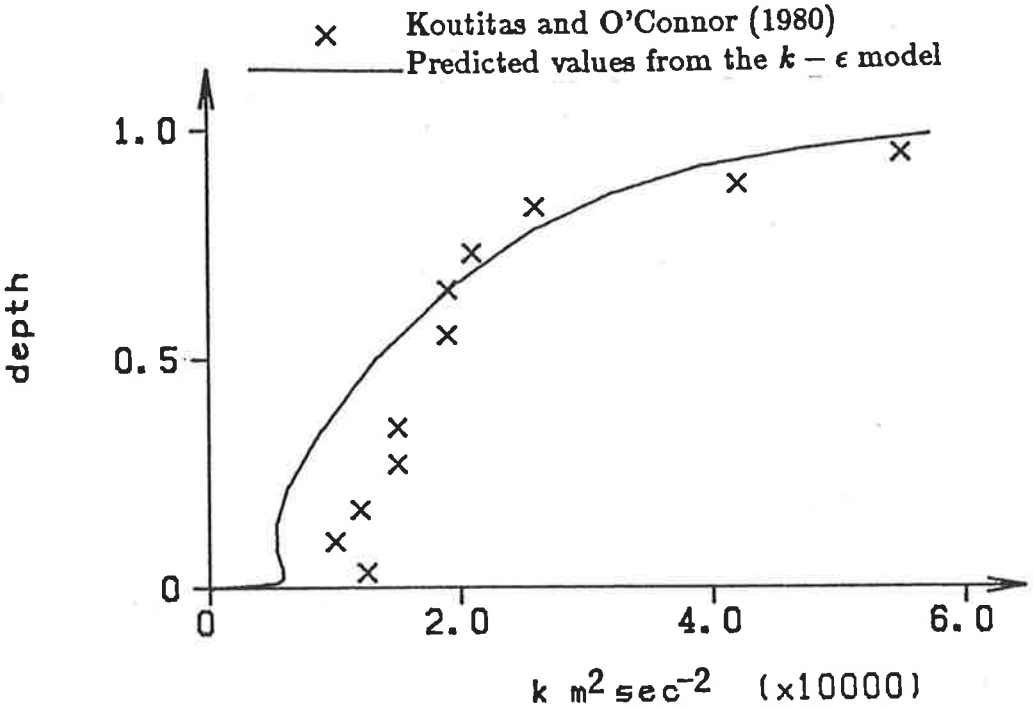

FIGURE 7.21: *Plots of the turbulent kinetic energy profile in a channel of uniform depth as recorded by Koutitas and O'Connor (1980) compared with that predicted by the $k-\epsilon$ model.*

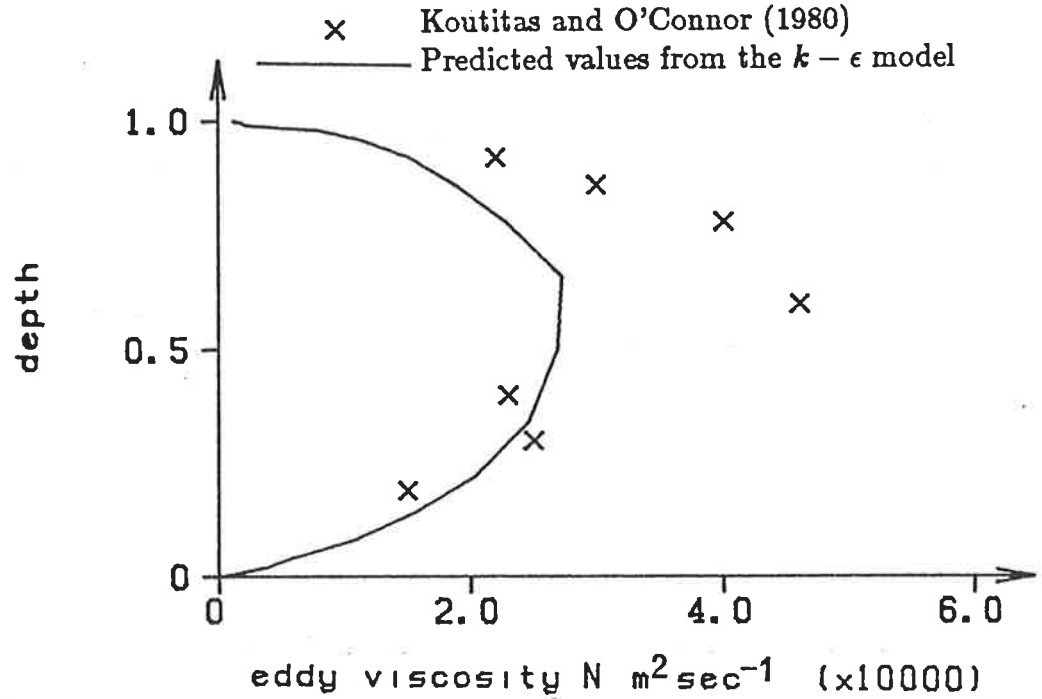

FIGURE 7.22: *Plots of the eddy viscosity profile in a channel of uniform depth as recorded by Koutitas and O'Connor (1980) compared with that predicted by the $k-\epsilon$ model.*

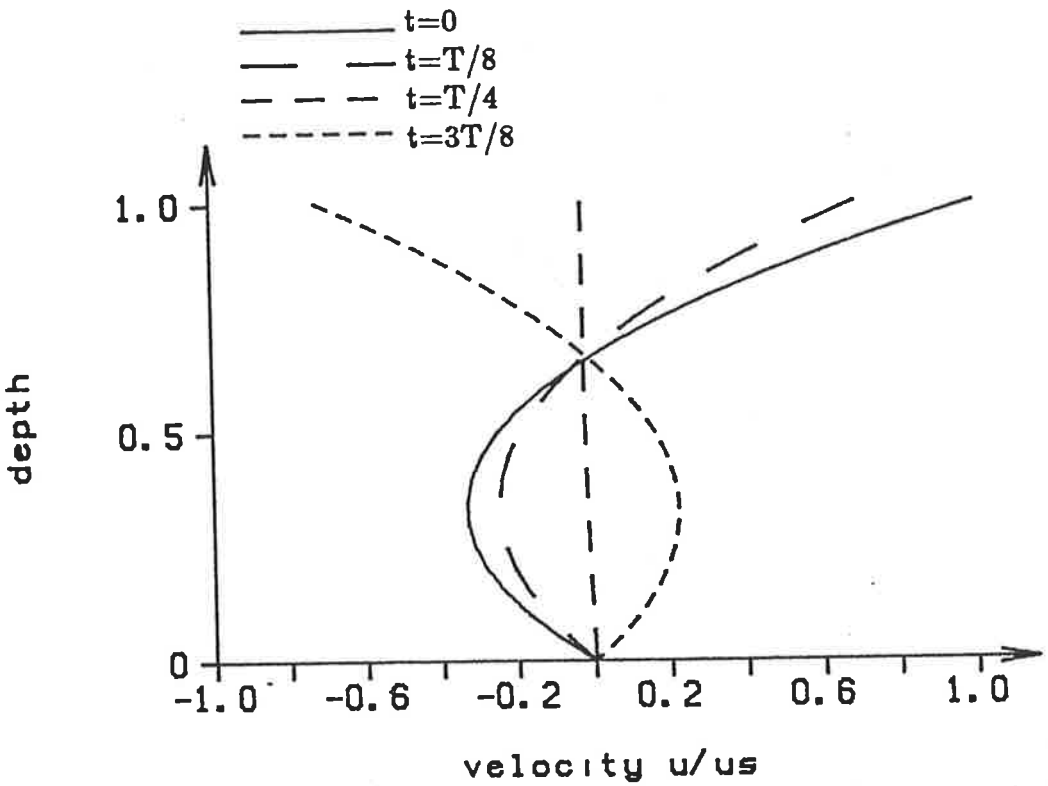

FIGURE 7.23: *Plots of the velocity profile caused by an oscillating wind of period T blowing over a channel of uniform depth (results are normalized with respect to the results at t=0). A constant N is used.*

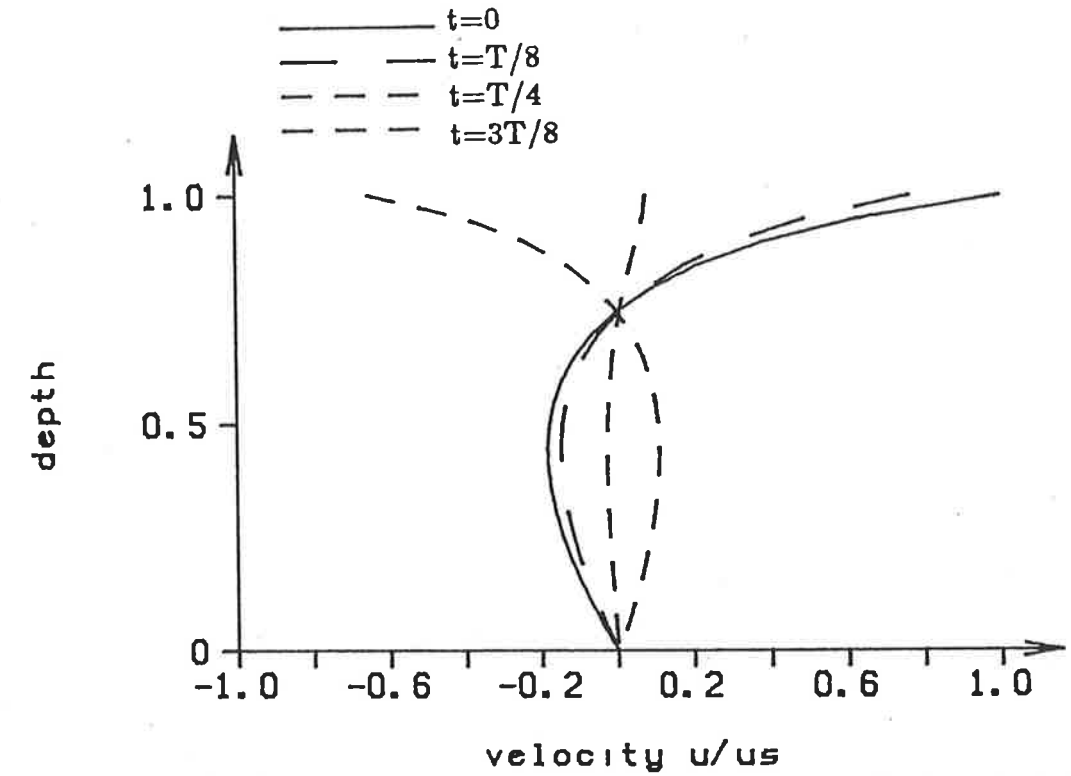

FIGURE 7.24: *Plots of the velocity profile caused by an oscillating wind of period T blowing over a channel of uniform depth (results are normalized with respect to the results at t=0). A linear N is used.*

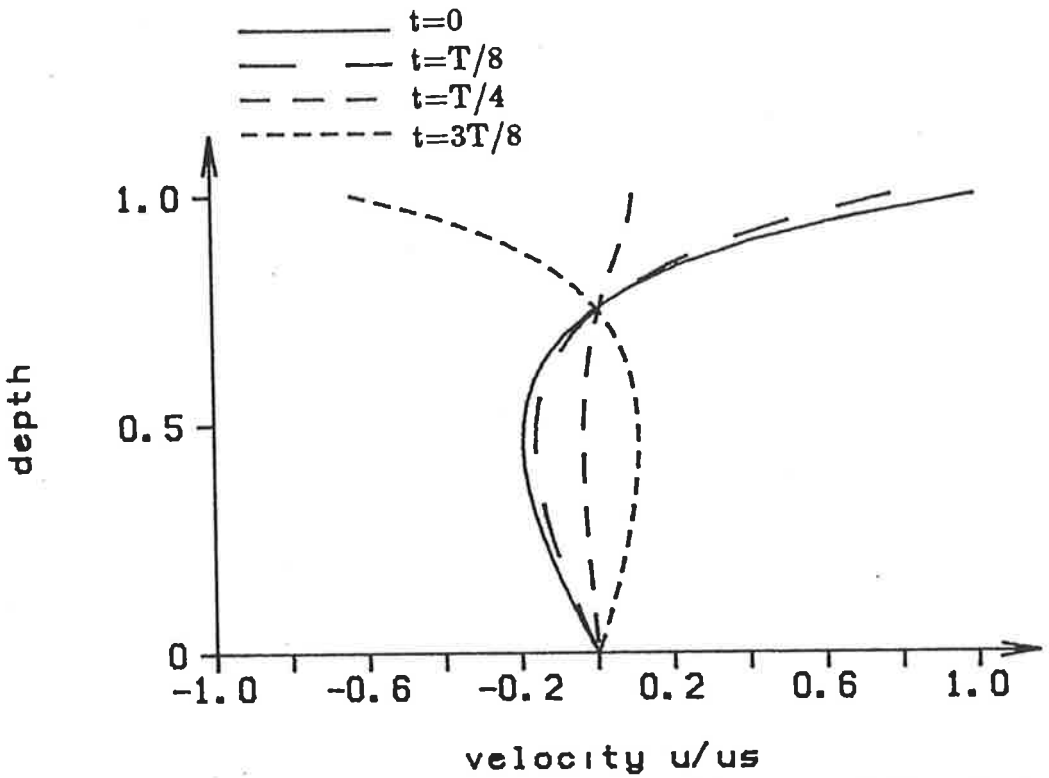

FIGURE 7.25: *Plots of the velocity profile caused by an oscillating wind of period T blowing over a channel of uniform depth (results are normalized with respect to the results at t=0). The quadratic N defined in Sec. 7.4 is used.*

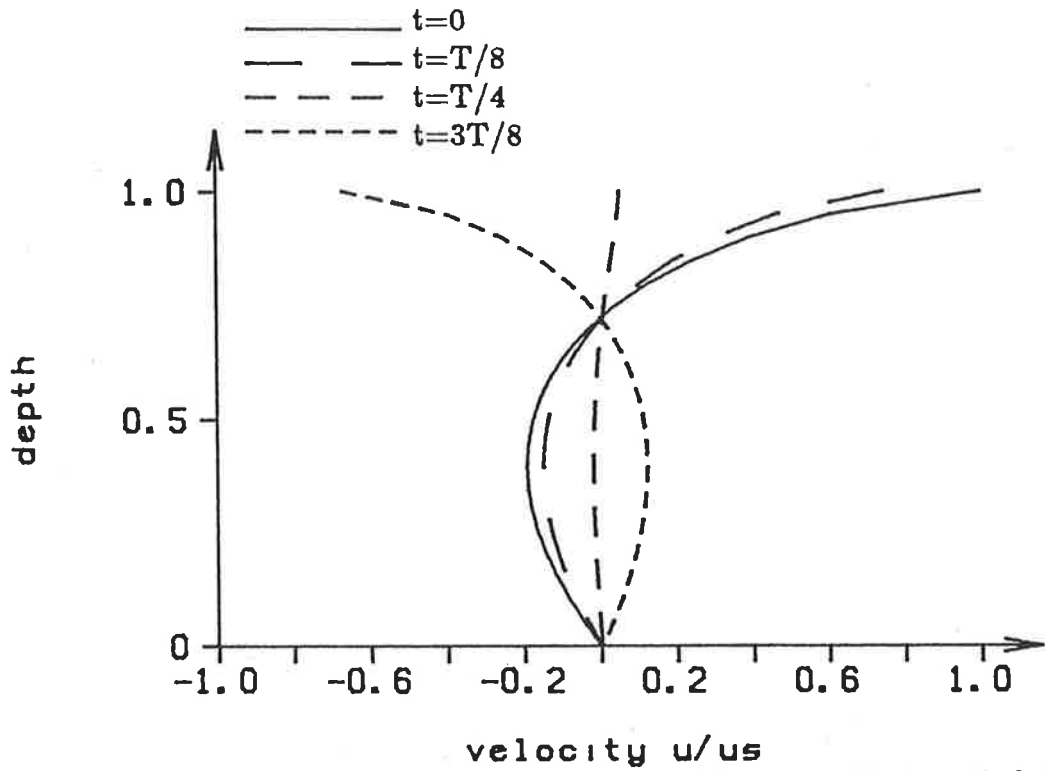

FIGURE 7.26: *Plots of the velocity profile caused by an oscillating wind of period T blowing over a channel of uniform depth (results are normalized with respect to the results at t=0). The quadratic N defined in Sec. 7.5 is used.*

Figure 7.28 displays the profiles obtained using the composite formulation. As in the previous figure, the velocity increases rapidly near the bottom. However, there is a major difference in the profiles in Figure 7.28 in that the magnitude of the velocity in the lower depths is much greater than is observed in Figure 7.27.

Figures 7.29 and 7.30 show the results obtained using the numerical $k - \epsilon$ model. Of all the analytic profiles presented so far, the profiles obtained using the three parameter quadratic formulation most closely resemble the profiles obtained by the $k - \epsilon$ model, shown in Figure 7.29.

The variation of eddy viscosity with time is displayed in Figure 7.30. Clearly, N is not constant with respect to time. Not only does the maximum value of the eddy viscosity change significantly with time, but also the position of this maximum varies with time.

The analytic solutions presented above for the oscillating wind case are derived from equations which do not include any convection terms. To examine the importance of these terms, a finite difference solution to the non linear equations described by Equations (7.8.1(a), (b) and (c)) was established, with N being defined by the three parameter quadratic formulation used earlier.

Results from this model are displayed in Figure 7.31. Clearly, there is a marked difference between the previous analytic solution in which convection terms were ignored (see Figure 7.27). In fact, the results displayed in Figure 7.31 are very similar to those presented in Figure 7.29 which were obtained using the $k - \epsilon$

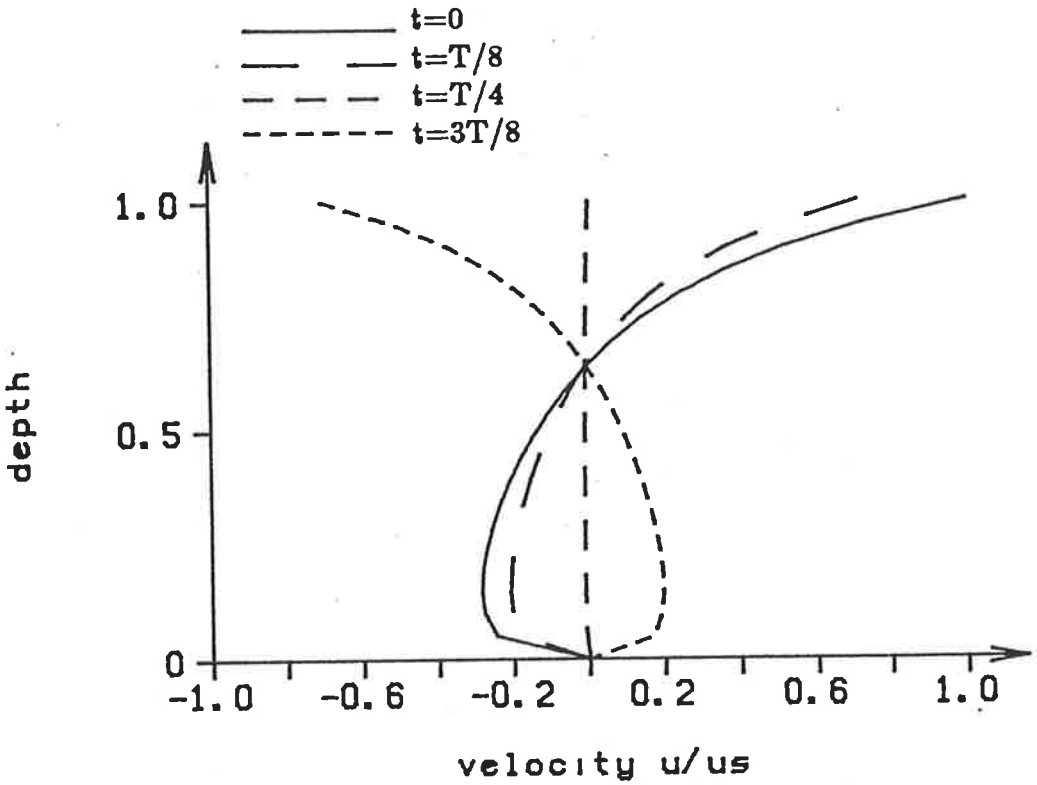

FIGURE 7.27: *Plots of the velocity profile caused by an oscillating wind of period T blowing over a channel of uniform depth (results are normalized with respect to the results at t=0). The quadratic N defined in Sec. 7.6 is used.*

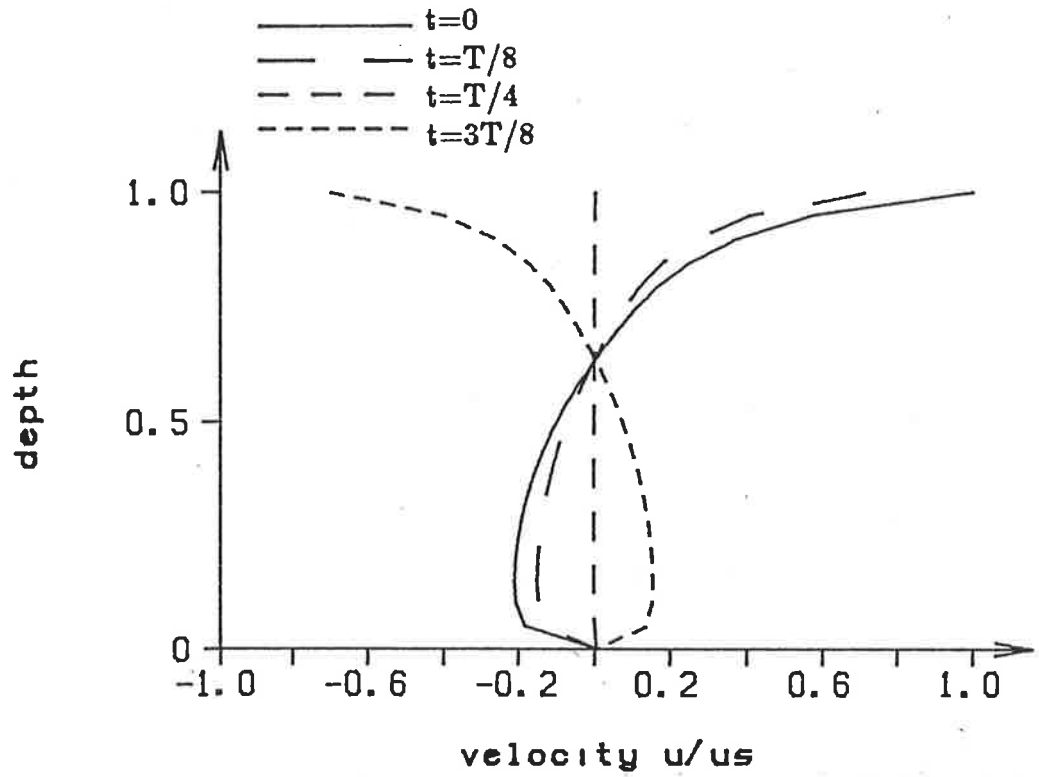

FIGURE 7.28: *Plots of the velocity profile caused by an oscillating wind of period T blowing over a channel of uniform depth (results are normalized with respect to the results at t=0). The composite linear N defined in Sec. 7.7 is used.*

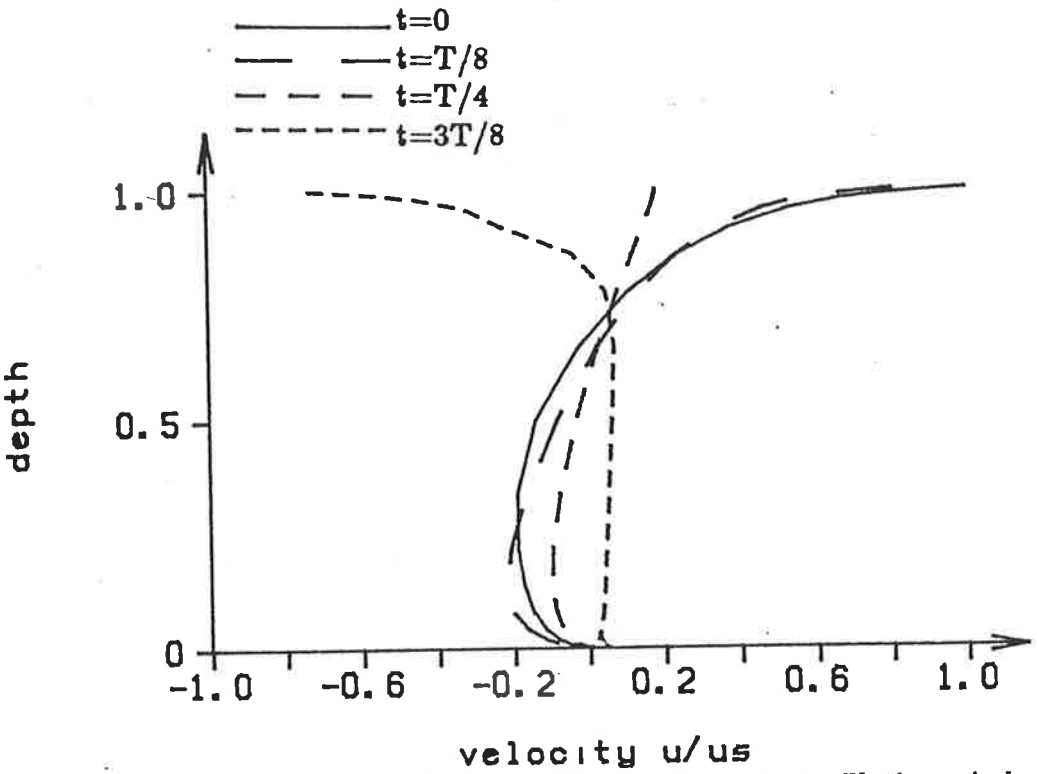

FIGURE 7.29: *Plots of the velocity profile caused by an oscillating wind of period T blowing over a channel of uniform depth (results are normalized with respect to the results at t=0). These results are obtained using the $k-\epsilon$ model.*

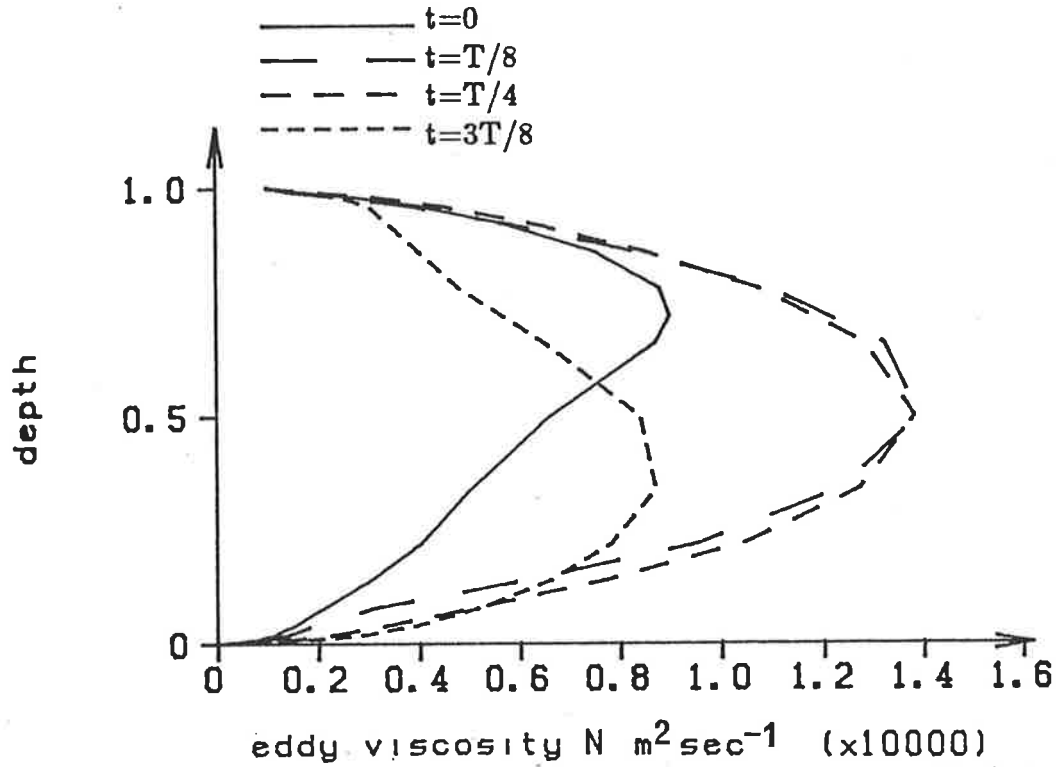

FIGURE 7.30: *Plots of the eddy viscosity profile caused by an oscillating wind of period T blowing over a channel of uniform depth (results are normalized with respect to the results at t=0). These results are obtained using the $k-\epsilon$ model.*

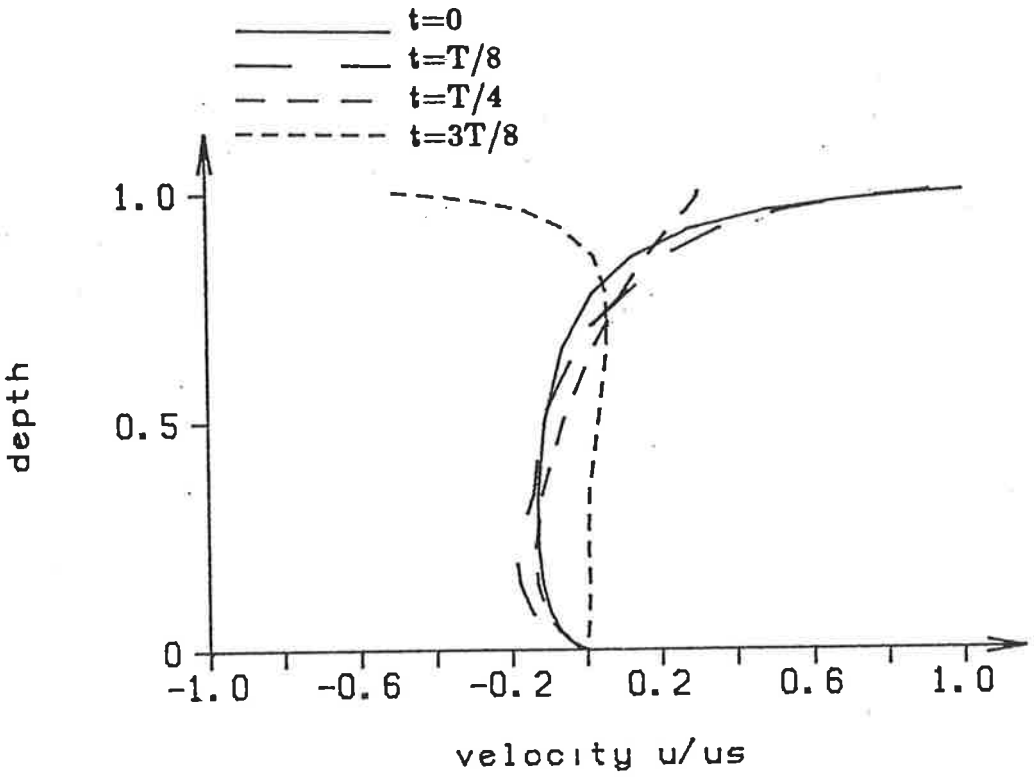

FIGURE 7.31: *Plots of the velocity profile caused by an oscillating wind of period T blowing over a channel of uniform depth (results are normalized with respect to the results at t=0). These results are obtained using the three parameter quadratic eddy viscosity formulation of Sec. 7.6*

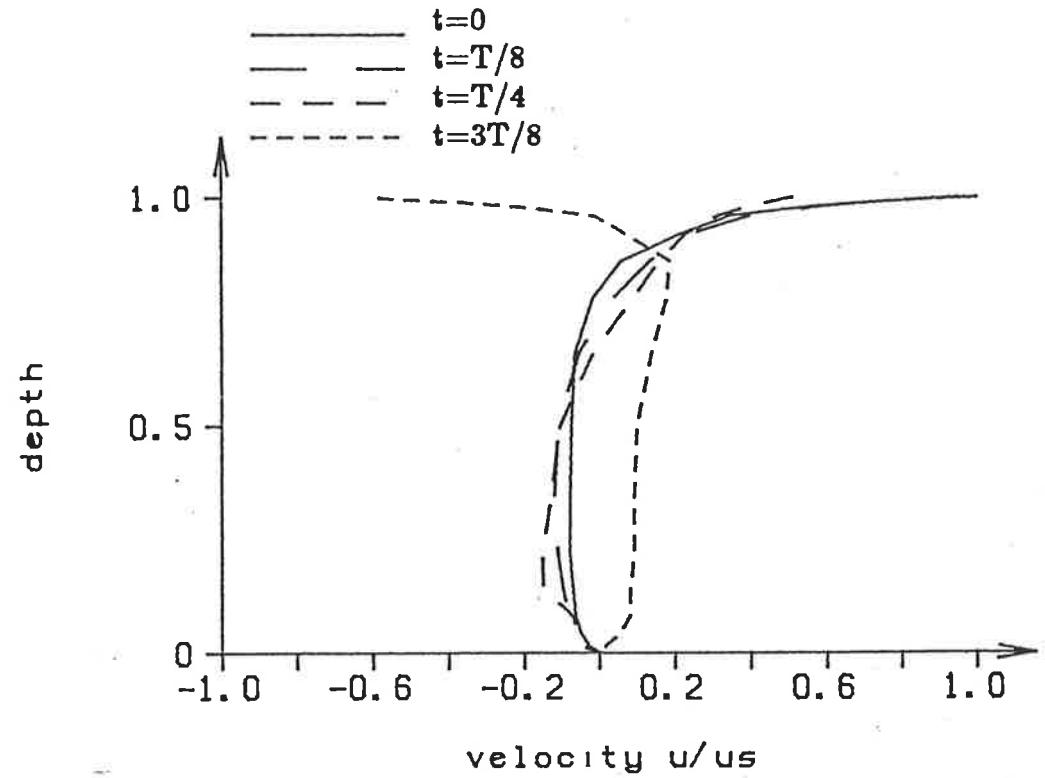

FIGURE 7.32: *Plots of the velocity profile caused by an oscillating wind of period T blowing over a channel of uniform depth (results are normalized with respect to the results at t=0). These results are obtained using the three parameter quadratic eddy viscosity formulation of Sec. 7.6 which is dependent on the magnitude of the surface stress.*

model. By adjusting the parameters in the eddy viscosity formulation, the profiles presented in Figure 7.31 could be altered somewhat. However, the parameters used in this figure are those which provided the best agreement for the equilibrium case.

The effect of using a time varying eddy viscosity was also examined. The same vertical profile of N as was used in the previous figure is again used here but the expression is multiplied by the factor τ_s thus forcing the eddy viscosity to vary with time. The results from this model, shown in Figure 7.32, do not differ appreciably from the results obtained using the time invariant eddy viscosity (see Figure 7.31) except at time $3T/8$ when a considerably larger velocity is predicted.

§7.10 CONCLUSION

In this chapter, analytic solutions for the equilibrium case of a wind blowing over the surface of a channel, have been presented. Good agreement with experimental observations was obtained provided an appropriate formulation for the eddy viscosity was used. The three parameter quadratic and the composite linear formulations provided the best agreement.

A disadvantage with these analytic solutions is that to provide quantitative results they must be "tuned" with observed data. For this reason, a turbulent energy closure scheme was discussed. A numerical solution to the non linear equations of mass, momentum, turbulent kinectic energy and dissipation of such energy was also presented. Such a numerical scheme can be easily expanded to cater for three dimensional flows. This $k-\epsilon$ model provided excellent quantitative

results. No "tuning" was necessary. It must be pointed out, however, that the analytic solutions using the above mentioned formulations of N provided profiles in close agreement with the $k-\epsilon$ profiles. Hence, provided that the necessary data is available so that the analytic models can be "tuned", then these solutions can be used successfully to provide quantitative results.

For the oscillating wind case, the agreement between the analytic solutions and the $k-\epsilon$ model was not as good as for the equilibrium case. This appears to be due mainly to neglecting the convection terms rather then being due to using a time invariant eddy viscosity. Once these convection terms were included, profiles very similar to these obtained using the $k-\epsilon$ model were achieved. This suggests that even for non steady flows, a time invariant eddy viscosity formulation can be successfully used provided that there is adequate data available for "tuning" and the correct formulation for N is used.

APPENDIX A

A SECOND ORDER METHOD FOR THE NEUMANN CONDITION WITH CURVED BOUNDARIES

§A.1 INTRODUCTION

When finite difference methods are used to solve a system of equations in a domain bounded by an arbitrary curve, problems arise in the discretisation of derivatives at grid points adjacent to the curved boundary. Care must be taken at these points if the finite difference approximations near the boundary are to be as accurate as those approximations used in the interior.

A common treatment of the boundary is to reshape it so that it is made up of straight lines which are parallel to the grid lines. Once the boundary has been treated in this way, any boundary conditions can be easily dealt with using existing methods (see, for example, Noye (1983)). However, this approach results in a contribution of the order of either the horizontal or vertical grid spacing in the discretisation error at grid points adjacent to the boundary.

Clearly, a method is required in which the shape of the boundary is not altered and which also provides finite difference approximations adjacent to the boundary which are as accurate as those used in the interior region. In general, second order schemes are used in the interior of the region so that a second order treatment for approximations to the derivatives at the grid points near the curved boundary is

required. Such a scheme is available for problems involving the Dirichlet condition in which the dependent variable is specified on the boundary. Noye (1983) presents such a solution using a Taylor Series approach. Fox (1944) proposed a scheme for the Neumann condition in which the normal derivative of the dependent variable is specified at the boundary. This scheme was, however, only first order accurate. Noye (1983) describes the basis for a second order solution using a Taylor Series approach but he did not give final expressions. In this work, second order finite difference approximations to the derivatives, $\partial/\partial x$, $\partial/\partial y$, $\partial^2/\partial x^2$, $\partial^2/\partial y^2$ and $\partial^2/\partial x \partial y$ will be obtained using the techniques suggested by Noye (1983).

§A.2 SOLUTION

In the following discussion, interior grid points are defined as those for which no neighbouring grid point in the direction of either coordinate axis lies outside the boundary. Grid points, interior to the curved boundary, but which have at least one neighbouring grid point in the direction of either coordinate axis lying outside the boundary are termed boundary points.

In Figure A.1, the point P is a boundary point whilst points labelled Q and T are interior points. The vectors labelled η_R, η_N and η_S give the direction of the normal derivative to the curve at the points R, N and S. If Z is the dependent variable, then the value of $\partial Z/\partial n$ is assumed to be known at the points R, N and S. The angles, γ, define the angle between the normal to the curve and the X axis. This angle is always measured in an anti-clockwise sense with the positive X

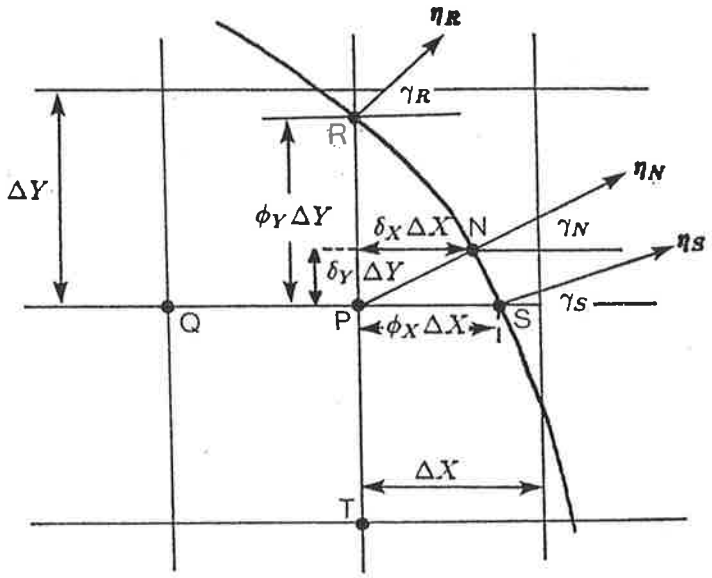

FIGURE A1: *Geometry of a boundary point, P, for which two of the neighbouring grid points are outside of the boundary.*

axis corresponding to $\gamma = 0$. The distance between grid points in the X direction is ΔX while ΔY gives the distance between vertical grid lines. The parameters ϕ_X, ϕ_Y, δ_X and δ_Y all have the property that $0 < \phi_X, \phi_Y, \delta_X, \delta_Y < 1$ and simply define the distances between the point P and the points R, N and S as shown on Figure A.1.

Finite diference expressions for the derivatives, $\partial Z/\partial X$, $\partial Z/\partial Y$, $\partial^2 Z/\partial X^2$, $\partial^2 Z/\partial Y^2$ and $\partial^2 Z/\partial X \partial Y$ at P may be obtained by constructing the Taylor Series expansions, centred at point P, of the variable Z at the points Q, T, R, N and S.

For example, consider the point R in Figure A.1. The Taylor Series expansion, centred at P, for the variable Z calculated at R is

$$Z_R = Z_P + \phi_Y \Delta Y \frac{\partial Z}{\partial Y}\bigg|_P + \frac{1}{2}(\phi_Y \delta Y)^2 \frac{\partial^2 Z}{\partial Y^2}\bigg|_P + \ldots \qquad (A1)$$

in which notation such as Z_P denotes the value of Z calculated at the point P. Replacing Z by $\partial Z/\partial X$ and then by $\partial Z/\partial Y$ yields the two equations

$$\frac{\partial Z}{\partial X}\bigg|_R = \frac{\partial Z}{\partial X}\bigg|_P + \phi_Y \Delta Y \frac{\partial^2 Z}{\partial Y \partial X}\bigg|_P + O\left\{(\phi_Y \Delta Y)^2\right\}, \qquad (A2(a))$$

$$\frac{\partial Z}{\partial Y}\bigg|_R = \frac{\partial Z}{\partial Y}\bigg|_P + \phi_Y \Delta Y \frac{\partial^2 Z}{\partial Y^2}\bigg|_P + O\left\{(\phi_Y \Delta Y)^2\right\}. \qquad (A2(b))$$

The normal derivative may be related to the derivatives in the X and Y directions by the relation

$$\frac{\partial Z}{\partial n} = \frac{\partial Z}{\partial X}\cos\gamma + \frac{\partial Z}{\partial Y}\sin\gamma, \qquad (A.3)$$

where the angle γ specifies the direction relative to the X axis of the normal to

the boundary. Equations (A.2) and (A.3) may be combined to yield

$$\left.\frac{\partial Z}{\partial n}\right|_R = \left(\left.\frac{\partial Z}{\partial X}\right|_P + \phi_Y \Delta Y \left.\frac{\partial^2 Z}{\partial X \partial Y}\right|_P\right) \cos\gamma_R + \left(\left.\frac{\partial Z}{\partial Y}\right|_P + \phi_Y \Delta Y \left.\frac{\partial^2 Z}{\partial Y^2}\right|_P\right) \sin\gamma_R + O\left\{(\phi_y \Delta Y)^2\right\} \qquad (A.4)$$

Two similar equations may be derived for the points N and S. Adding to these three equations the two Taylor Series expansions about P for Z_Q and Z_T gives a total of five equations containing the unknown derivatives $\partial Z/\partial X|_P$,$\partial Z/\partial Y|_P$, $\partial^2 Z/\partial X^2|_P$, $\partial^2 Z/\partial Y^2|_P$ and $\partial^2 Z/\partial X \partial Y^2|_P$. These five equations may be written in matrix form as shown below:

$$\begin{bmatrix} \Delta X & 0 & -(\Delta X)^2/2 & 0 & 0 \\ \cos\gamma_S & \sin\gamma_S & \phi_X \Delta X \cos\gamma_S & \phi_X \Delta X \sin\gamma_S & 0 \\ \cos\gamma_N & \sin\gamma_N & \delta_X \Delta X \cos\gamma_N & (\delta_Y \Delta Y \cos\gamma_N + \delta X \Delta X \sin\gamma_N) & \delta Y \Delta Y \sin\gamma_N \\ \cos\gamma_R & \sin\gamma_R & 0 & \phi_Y \Delta Y \cos\gamma_R & \phi_Y \Delta Y \sin\gamma_R \\ 0 & \Delta Y & 0 & 0 & -(\Delta Y)^2/2 \end{bmatrix} \begin{bmatrix} \left.\frac{\partial Z}{\partial X}\right|_P \\ \left.\frac{\partial Z}{\partial Y}\right|_P \\ \left.\frac{\partial^2 Z}{\partial X^2}\right|_P \\ \left.\frac{\partial^2 Z}{\partial X \partial Y}\right|_P \\ \left.\frac{\partial^2 Z}{\partial Y^2}\right|_P \end{bmatrix}$$

$$= \begin{bmatrix} Z_P - Z_Q \\ \left.\frac{\partial Z}{\partial n}\right|_S \\ \left.\frac{\partial Z}{\partial n}\right|_N \\ \left.\frac{\partial Z}{\partial n}\right|_R \\ Z_P - Z_T \end{bmatrix} + O\left\{(\Delta X)^2, \Delta X \Delta Y, (\Delta Y)^2\right\} \qquad (A.5)$$

With the aid of a symbolic manipulation program such as MACSYMA, the above matrix equation was solved to give second order accurate expressions for the unknown derivatives. Expressions for the required derivatives at the point P near a curved boundary as shown in Figure A.1 follow. For simplicity, it has been assumed that $\Delta X = \Delta Y = h$. The first order derivative with respect to X is

$$Z_X = \frac{\partial Z}{\partial X} = \frac{s_{X1} Z_T + s_{X2} Z_Q + s_{X3} Z_P + h s_{X5}}{h s_{X4}} + O\left\{h^2\right\} \qquad (A.6(a))$$

where

$$s_{X1} = 2\left\{F_3^{NSR}\left[\phi_Y(\phi_X - \delta_X) - \delta_Y\phi_X\right] + \delta_Y\phi_Y(F_2^{NSR} - F_2^{RSN})\right\}, \qquad (A.6(b))$$

$$\begin{aligned} s_{X2} = -2\big\{&\phi_X\phi_Y\left[2\delta_X(F_2^{RSN} - F_2^{NRS}) - 2\delta_Y F_1^{NSR} + F_1^{RSN}(2\delta_Y + 1)\right] \\ &+ \delta_X\left[\phi_X(F_2^{RSN} - F_2^{NRS}) - \phi_Y F_1^{NRS}\right] - \delta_Y\phi_X F_1^{NSR}\big\}, \end{aligned} \qquad (A.6(c))$$

$$\begin{aligned} s_{X3} = -2\big\{&\phi_X\phi_Y\left[F_3^{NSR} + 2\delta_X(F_2^{NRS} - F_2^{RSN}) + 2\delta_Y F_1^{NSR} - F_1^{RSN}(2\delta_Y + 1)\right] \\ &- F_3^{NSR}(\delta_X\phi_Y + \delta_Y\phi_X) - F_2^{RSN}(\delta_Y\phi_Y + \delta_X\phi_X) \\ &+ \phi_X(\delta_X F_2^{NRS} + \delta_Y F_1^{NSR}) + \phi_Y(\delta_Y F_2^{NSR} + \delta_X F_1^{NRS})\big\}, \end{aligned} \qquad (A.6(d))$$

$$\begin{aligned} s_{X4} = &2\phi_X\phi_Y\left[F_2^{RSN}(2\delta_X + 1) - 2\delta_X F_2^{NRS} - 2\delta_Y F_1^{NSR} + F_1^{RSN}(2\delta_Y + 1)\right] \\ &+ (2\delta_X + 1)(F_2^{RSN}\phi_X - F_1^{NRS}\phi_Y) + (2\delta_Y + 1)(F_1^{RSN}\phi_Y - F_2^{NSR}\phi_X) \\ &- 2\phi_Y(\delta_X F_2^{NRS} + \delta_Y F_1^{NSR}) - 2\phi_X(\delta_X F_2^{NRS} + \delta_Y F_1^{NSR}) \\ &+ \delta_X(F_2^{NSR} - F_2^{NRS}) + \delta_Y(F_1^{NRS} - F_1^{NSR}) \end{aligned} \qquad (A.6(e))$$

and

$$\begin{aligned} s_{X5} = &\left.\frac{\partial Z}{\partial n}\right|_N \left[\phi_X(2\phi_Y + 1)\sin\gamma_R - \phi_Y\cos\gamma_R\right]\sin\gamma_S \\ &+ \left.\frac{\partial Z}{\partial n}\right|_R \left[(-\phi_X(2\delta_Y + 1) + \delta_X)\sin\gamma_N + \delta_Y\cos\gamma_N\right]\sin\gamma_S \\ &+ \left.\frac{\partial Z}{\partial n}\right|_S \big\{-(\delta_X\sin\gamma_N + \delta_Y\cos\gamma_N)(1 + 2\phi_Y)\sin\gamma_R \\ &\qquad + \phi_Y(2\delta_Y + 1)\cos\gamma_R\sin\gamma_N\big\}. \end{aligned} \qquad (A.6(f))$$

The functions, F_i^{ABC} which appear in the above equations are defined by

$$F_1^{ABC} = \cos\gamma_A\cos\gamma_B\sin\gamma_C, \qquad (A.7(a))$$

$$F_2^{ABC} = \sin\gamma_A\sin\gamma_B\cos\gamma_C, \qquad (A.7(b))$$

$$F_3^{ABC} = \sin\gamma_A \sin\gamma_B \sin\gamma_C \qquad (A.7(c))$$

and

$$F_4^{ABC} = \cos\gamma_A \cos\gamma_B \cos\gamma_C. \qquad (A.7(d))$$

The solution for $\partial Z/\partial Y$, denoted by Z_Y, is

$$Z_Y = \frac{\partial Z}{\partial Y} = \frac{s_{Y1}Z_T + s_{Y2}Z_Q + s_{Y3}Z_P + hs_{Y5}}{hs_{Y4}} + O\{h^2\}, \qquad (A.8(a))$$

where

$$s_{Y1} = -2\{\phi_X\phi_Y\left[F_2^{RSN}(2\delta_X+1) - 2\delta_X F_2^{NRS} + 2\delta_Y(F_1^{RSN} - F_1^{NSR})\right]$$
$$- \phi_Y(\delta_X F_2^{NRS} + \delta_Y F_1^{NSR}) + \delta_Y(\phi_Y F_1^{RSN} - \phi_X F_2^{NSR})\}, \qquad (A.8(b))$$

$$s_{Y2} = 2\left\{F_3^{NSR}\left[\phi_Y(\phi_X - \delta_X) - \delta_Y\phi_X\right] + \phi_X\delta_X(F_1^{NRS} - F_1^{RSN})\right\}, \qquad (A.8(c))$$

$$s_{Y3} = 2\{\phi_X\phi_Y\left[F_2^{RSN}(2\delta_X+1) - 2\delta_X F_2^{NRS} + 2\delta_Y(F_1^{RSN} - F_1^{NSR}) - F_3^{NSR}\right]$$
$$- \phi_Y(\delta_X F_2^{NRS} + \delta_Y F_1^{NSR}) + F_1^{RSN}(\delta_Y\phi_Y + \delta_X\phi_X) + F_3^{NSR}(\delta_X\phi_Y + \delta_Y\phi_X)$$
$$- \phi_X(\delta_Y F_2^{NSR} + \delta_X F_1^{NRS})\}, \qquad (A.8(d))$$

$s_{Y4} = s_{X4}$, as defined in (A.6(e)),

and

$$s_{Y5} = \left.\frac{\partial Z}{\partial n}\right|_N \left[\phi_Y(2\phi_X+1)\cos\gamma_S - \phi_X\sin\gamma_S\right]\cos\gamma_R$$
$$+ \left.\frac{\partial Z}{\partial n}\right|_R \left\{(\phi_X(2\delta_X+1)\sin\gamma_S - \delta_Y(2\phi_X+1)\cos\gamma_S)\cos\gamma_N\right.$$
$$\left. + \delta_X(2\phi_X+1)\sin\gamma_N\cos\gamma_S\right\}$$
$$+ \left.\frac{\partial Z}{\partial n}\right|_S \left[(\delta_Y - \phi_Y(2\delta_X+1))\cos\gamma_N + \delta_X\sin\gamma_N\right]\cos\gamma_R. \qquad (A.8(e))$$

The second order derivative in the X direction is given by

$$Z_{XX} = \frac{\partial^2 Z}{\partial X^2} = \frac{s_{XX1} Z_T + s_{XX2} Z_Q + s_{XX3} Z_P + h s_{XX5}}{h^2 s_{XX4}} + O\{h^2\}, \quad (A.9(a))$$

where

$$s_{XX1} = 4\{F_3^{NSR}[\phi_Y(\phi_X - \delta_X) - \delta_Y \phi_X] + \delta_Y \phi_Y (F_2^{NSR} - F_2^{RSN})\}, \quad (A.9(b))$$

$$\begin{aligned} s_{XX2} = 2\{&\phi_Y(2\phi_X F_2^{RSN} - F_1^{NRS} - 2\delta_X F_2^{NRS} - 2\delta_Y F_1^{NSR}) \\ &+ (2\delta_Y + 1)(\phi_Y F_1^{RSN} - \phi_X F_2^{NSR}) + F_2^{RSN}\phi_X \\ &+ \delta_X(F_2^{NSR} - F_2^{NRS}) + \delta_Y(F_1^{NRS} - F_1^{NSR})\}, \end{aligned} \quad (A.9(c))$$

$$\begin{aligned} s_{XX3} = -2\{&2\phi_X\phi_Y(F_3^{NSR} + F_2^{RSN}) - 2\delta_X\phi_Y(F_3^{NSR} + F_2^{NRS}) \\ &+ 2\delta_Y\phi_Y(F_2^{NSR} - F_2^{RSN} - F_1^{NSR}) - F_1^{NRS}\phi_Y + \phi_Y F_1^{RSN}(2\delta_Y + 1) \\ &+ \phi_X(F_2^{RSN} - 2\delta_Y F_3^{NSR}) - \phi_X F_2^{NSR}(2\delta_Y + 1) + \delta_X(F_2^{NSR} - F_2^{NRS}) \\ &+ \delta_Y(F_1^{NRS} - F_1^{NSR})\}, \end{aligned} \quad (A.9(d))$$

$s_{XX4} = s_{X4}$ (see Equation (A.6(e))) and

$$\begin{aligned} s_{XX5} = 2\Bigg\{ &\left.\frac{\partial Z}{\partial n}\right|_N [\phi_Y(2\phi_X \sin\gamma_R - \cos\gamma_R) + \phi_X \sin\gamma_R]\sin\gamma_S \\ &+ \left.\frac{\partial Z}{\partial n}\right|_R [-\delta_Y(2\phi_X \sin\gamma_N - \cos\gamma_N) + (\delta_X - \phi_X)\sin\gamma_N]\sin\gamma_S \\ &+ \left.\frac{\partial Z}{\partial n}\right|_S [-(\delta_X(2\phi_Y + 1)\sin\gamma_N + \delta_Y(2\phi_Y + 1)\cos\gamma_N)\sin\gamma_R \\ &+ \phi_Y(2\delta_Y + 1)\sin\gamma_N \cos\gamma_R]\Bigg\}. \end{aligned} \quad (A.9(e))$$

The cross derivative, $\partial^2 Z/\partial X \partial Y$, is expressed by

$$Z_{XY} = \frac{\partial^2 Z}{\partial X \partial Y} = \frac{s_{XY1} Z_T + s_{XY2} Z_Q + s_{XY3} Z_P + h s_{XY5}}{h^2 s_{XY4}} + O\{h^2\}, \quad (A.10(a))$$

where

$$s_{XY1} = -2\{\phi_Y(F_2^{NRS}(2\phi_X+1) - (2\delta_X+1)F_2^{RSN}) - \delta_Y F_2^{NRS}(2\phi_X+1) + \delta_Y F_2^{NSR}\}, \quad (A.10(b))$$

$$s_{XY2} = -2\{2\phi_Y F_1^{NSR}(\phi_X - \delta_X) + \phi_X(F_1^{NSR} - F_1^{RSN}(2\delta_Y+1)) + \delta_X(F_1^{NRS} - F_1^{NSR})\}, \quad (A.10(c))$$

$$s_{XY3} = 2\{\phi_Y\left[F_2^{NRS}(2\phi_X+1) - F_2^{RSN}(2\delta_X+1) + 2F_1^{NSR}(\phi_X - \delta_X)\right] + \phi_X\left[-F_1^{RSN}(2\delta_Y+1) - 2\delta_Y F_2^{NRS} + F_1^{NSR}\right] + \delta_X(F_1^{NRS} - F_1^{NSR}) + \delta_Y(F_2^{NSR} - F_2^{NRS})\}, \quad (A.10(d))$$

$s_{XY4} = s_{X4}$ (see Equation (A.6(e))) and

$$\begin{aligned} s_{XY5} = &-\left.\frac{\partial Z}{\partial n}\right|_N [(1+2\phi_X(2\phi_Y+1)+2\phi_Y)\sin\gamma_R\cos\gamma_S - \cos\gamma_R\sin\gamma_S] \\ &-\left.\frac{\partial Z}{\partial n}\right|_R \{-(1+2\delta_Y+2\phi_X(2\delta_Y+1))\sin\gamma_N\cos\gamma_S \\ &\qquad + (2\delta_X+1)\cos\gamma_N\sin\gamma_S\} \\ &-\left.\frac{\partial Z}{\partial n}\right|_S \{-(1+2\delta_X+2\phi_Y(2\delta_X+1))\cos\gamma_N\sin\gamma_R \\ &\qquad + (2\delta_Y+1)\sin\gamma_N\cos\gamma_R\}. \end{aligned} \quad (A.10(e))$$

The second order derivative in the Y direction is defined by

$$Z_{YY} = \frac{\partial^2 Z}{\partial Y^2} = \frac{s_{YY1}Z_T + s_{YY2}Z_Q + s_{YY3}Z_P + hs_{YY5}}{h^2 s_{YY4}} + O\{h^2\}, \quad (A.11(a))$$

where

$$s_{YY1} = 2\{\phi_Y\left[2\phi_X F_1^{RSN} - F_1^{NRS}(2\delta_X+1) + F_1^{RSN}\right]$$

$$+\phi_X\left[F_2^{RSN}(2\delta_X+1)-F_2^{NSR}-2\delta_X F_2^{NRS}-2\delta_Y F_1^{NSR}\right]$$

$$+\delta_X(F_2^{NSR}-F_2^{NRS})+\delta_Y(F_1^{NRS}-F_1^{NSR})\Big\}, \qquad (A.11(b))$$

$$s_{YY2}=4\left\{F_4^{NRS}\left[\phi_Y(\phi_X-\delta_X)-\delta_Y\phi_X\right]+\delta_X\phi_X(F_1^{NRS}-F_1^{RSN})\right\}, \qquad (A.11(c))$$

$$s_{YY3}=-2\Big\{2\phi_X\phi_Y(F_1^{RSN}+F_4^{NRS})-\phi_Y F_1^{NRS}(1+2\delta_X)+F_1^{RSN}(\phi_Y-2\delta_X\phi_X)$$

$$+\phi_X\left[F_2^{RSN}(2\delta_X+1)-F_2^{NSR}+2\delta_X F_1^{NRS}-2\delta_X F_2^{NRS}-2\delta_Y F_1^{NSR}\right]$$

$$-2F_4^{NRS}(\delta_X\phi_Y+\delta_Y\phi_X)+\delta_X(F_2^{NSR}-F_2^{NRS})$$

$$+\delta_Y(F_1^{NRS}-F_1^{NSR})\Big\}, \qquad (A.11(d))$$

$s_{YY4}=s_{X4}$ as defined by Equation (A.6(e)) and

$$s_{YY5}=2\Bigg\{\left.\frac{\partial Z}{\partial n}\right|_N\left[\phi_Y(2\phi_X+1)\cos\gamma_S-\phi_X\sin\gamma_S\right]\cos\gamma_R$$

$$+\left.\frac{\partial Z}{\partial n}\right|_S\left[-\cos\gamma_N(\phi_Y(2\delta_X+1)-\delta_Y)+\delta_X\sin\gamma_N\right]\cos\gamma_R$$

$$+\left.\frac{\partial Z}{\partial n}\right|_R\Big[\phi_X((2\delta_X+1)\sin\gamma_S-2\delta_Y\cos\gamma_S)\cos\gamma_N$$

$$-(\delta_X(2\phi_X+1)\sin\gamma_N+\delta_Y\cos\gamma_N)\cos\gamma_S\Big]\Bigg\}. \qquad (A.11(e))$$

In any situation involving curved boundaries, the point P, which has two adjacent grid points exterior to the domain of interest as shown in Figure A.1, can be surrounded by the boundary in any of four different orientations as shown in Figure A.2. For each orientation, slightly different versions of the discretisations of the derivatives are obtained. Presented below is a systematic method of expressing the derivatives at P in terms of the solutions in Equations (A.6), (A.8), (A.9), (A.10) and (A.11).

The orientation defined by 11 in Figure A.2 is simply the case considered in deriving the above formulae. Hence, for this orientation, the expressions for the

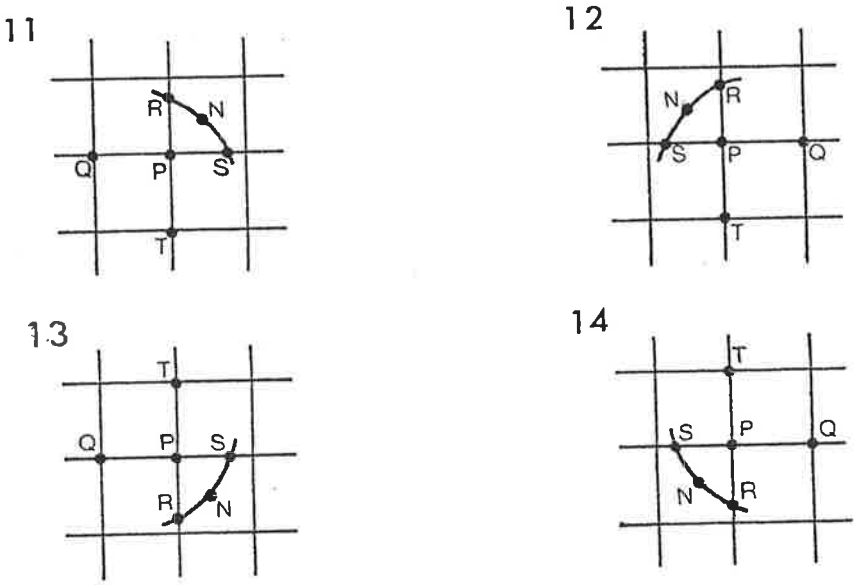

FIGURE A2: *The various orientations, denoted 11, 12, 13 and 14, which a boundary point, P, can be surrounded by a curved boundary such that two of the neighbouring grid points lie outside of the boundary.*

derivatives at the point P are

$$\frac{\partial Z}{\partial x} = Z_X, \qquad (A.12(a))$$

$$\frac{\partial Z}{\partial y} = Z_Y, \qquad (A.12(b))$$

$$\frac{\partial^2 Z}{\partial x^2} = Z_{XX}, \qquad (A.12(c))$$

$$\frac{\partial^2 Z}{\partial x \partial y} = Z_{XY}, \qquad (A.12(d))$$

and

$$\frac{\partial^2 Z}{\partial y^2} = Z_{YY}, \qquad (A.12(e))$$

where in the expressions for Z_X, Z_Y, Z_{XX}, Z_{XY} and Z_{YY} which are defined by Equations (A.6(a)), (A.8(a)), (A.9(a)), (A.10(a)) and (A.11(a)), the coordinate X has been replaced by x and Y has been replaced by y.

If the point, P, is the grid point labelled j, then using the notation described in Chapter 5, the points Q and T are defined by

$$Z_Q = Z_{j1}, \qquad (A.13(a))$$

and

$$Z_T = Z_{j-1}. \qquad (A.13(b))$$

The orientation 12 described in Figure A.2 is obtained from that shown in Figure A.1 by the coordinate transformation

$$x = -X, \qquad (A.14(a))$$

$$y = Y. \qquad (A.14(b))$$

This necessitates the following replacements which must be made to Equations (A.6), (A.8), (A.9), (A.10) and (A.11) in order to obtain the formulae. Firstly, the angles γ are replaced by $\pi - \gamma$, that is,

$$\gamma_S \leftarrow \pi - \gamma_S, \qquad (A.15(a))$$

$$\gamma_N \leftarrow \pi - \gamma_N, \qquad (A.15(b))$$

and

$$\gamma_R \leftarrow \pi - \gamma_R. \qquad (A.15(c))$$

The expressions for the derivatives at the point P for orientation 12 are then

$$\frac{\partial Z}{\partial x} = -Z_X, \qquad (A.16(a))$$

$$\frac{\partial Z}{\partial y} = Z_Y, \qquad (A.16(b))$$

$$\frac{\partial^2 Z}{\partial x^2} = Z_{XX}, \qquad (A.12(d))$$

$$\frac{\partial^2 Z}{\partial x \partial y} = -Z_{XY}, \qquad (A.16(d))$$

and

$$\frac{\partial^2 Z}{\partial y^2} = Z_{YY}, \qquad (A.16(e))$$

where X has been replaced by x and Y by y in the right hand sides of the above equations. In this orientation, the values at the points Z_Q and Z_T are defined by

$$Z_Q = Z_{j2}, \qquad (A.17(a))$$

and

$$Z_T = Z_{j-1}. \qquad (A.17(b))$$

It is important to note that the distances ϕ_X, δ_X etc. are always taken to be positive no matter what orientation is being considered.

Similarly, for the orientation 13 shown in Figure A.2, the coordinate transformation $x = X$ and $y = -Y$ applies and the following expressions hold;

$$\frac{\partial Z}{\partial x} = Z_X, \qquad (A.18(a))$$

$$\frac{\partial Z}{\partial y} = -Z_Y, \qquad (A.18(b))$$

$$\frac{\partial^2 Z}{\partial x^2} = Z_{XX}, \qquad (A.18(c))$$

$$\frac{\partial^2 Z}{\partial x \partial y} = -Z_{XY}, \qquad (A.18(d))$$

and

$$\frac{\partial^2 Z}{\partial y^2} = Z_{YY}, \qquad (A.18(e))$$

in which

$$\gamma_S \leftarrow 2\pi - \gamma_S, \qquad (A.19(a))$$

$$\gamma_N \leftarrow 2\pi - \gamma_N, \qquad (A.19(b))$$

$$\gamma_R \leftarrow 2\pi - \gamma_R \qquad (A.19(c))$$

$$Z_Q = Z_{j1}, \qquad (A.19(d))$$

and

$$Z_T = Z_{j+1}. \qquad (A.19(e))$$

For the orienation 14 in Figure A.2, the following expressions hold for the derivatives at P

$$\frac{\partial Z}{\partial x} = -Z_X, \qquad (A.20(a))$$

$$\frac{\partial Z}{\partial y} = -Z_Y, \qquad (A.20(b))$$

$$\frac{\partial^2 Z}{\partial x^2} = Z_{XX}, \qquad (A.20(c))$$

$$\frac{\partial^2 Z}{\partial x \partial y} = Z_{XY}, \qquad (A.20(d))$$

and

$$\frac{\partial^2 Z}{\partial y^2} = Z_{YY}, \qquad (A.20(e))$$

in which

$$\gamma_S \leftarrow \gamma_S - \pi, \qquad (A.21(a))$$

$$\gamma_N \leftarrow \gamma_N - \pi, \qquad (A.21(b))$$

$$\gamma_R \leftarrow \gamma_R - \pi, \qquad (A.21(c))$$

$$Z_Q = Z_{j2} \qquad (A.21(d))$$

and

$$Z_T = Z_{j+1}. \qquad (A.21(e))$$

A computer program using techniques described in Chapter 5 can readily identify which of the orientations are applicable. For each orientation, the formulae described above are calculated and Equations (A.6), (A.8), (A.9), (A.10) and (A.11) used to find the required derivatives at point P.

The above analysis is applicable only for a boundary point for which two of the four neighbouring grid points are interior points. If the radius of curvature of the boundary in the vicinity of a boundary point is not as great as that shown

in Figure A.1, then only one of the neighbouring grid points may be outside of the region. This is the case shown in Figure A.3. A new set of expressions for the required derivatives at boundary points such as P in Figure A.3 must now be derived.

The analysis is similar to that performed above for the situation presented in Figure A.1. Indeed, the only effect of this new boundary configuration is to change the fourth row of the square matrix and the fourth element in the right side vector of the matrix equation (A.5). The new fourth row is

$$\begin{bmatrix} 0 & -\Delta Y & 0 & 0 & -(\Delta Y)^2/2 \end{bmatrix} \qquad (A.22(a))$$

and the new fourth element is

$$Z_P - Z_R. \qquad (A.22(b))$$

The resultant matrix equation may be solved, yielding the following second order accurate expressions for the derivatives at the point P for the curved boundary shown in Figure A.3:

$$\bar{Z}_X = \frac{\partial Z}{\partial X} = \frac{q_{X1} Z_T + q_{X2} Z_Q + q_{X3} Z_R + q_{X4} Z_P + 2h q_{X6}}{2h q_{X5}} + O\left\{h^2\right\}, \quad (A.23(a))$$

where the overbar is used to distinguish between these formulae and those for the previous case. The coefficients q_{X1} etc. are given by the following formulae:

$$q_{X1} = -\left\{(\delta_X + \phi_X(2\delta_Y - 1))\sin\gamma_N + \delta_Y \cos\gamma_N\right\}\sin\gamma_S, \qquad (A.23(b))$$

$$q_{X2} = -4\phi_X \left\{\delta_X \cos\gamma_N \sin\gamma_S - (\delta_X \sin\gamma_N + \delta_Y \cos\gamma_N)\cos\gamma_S\right\}, \qquad (A.23(c))$$

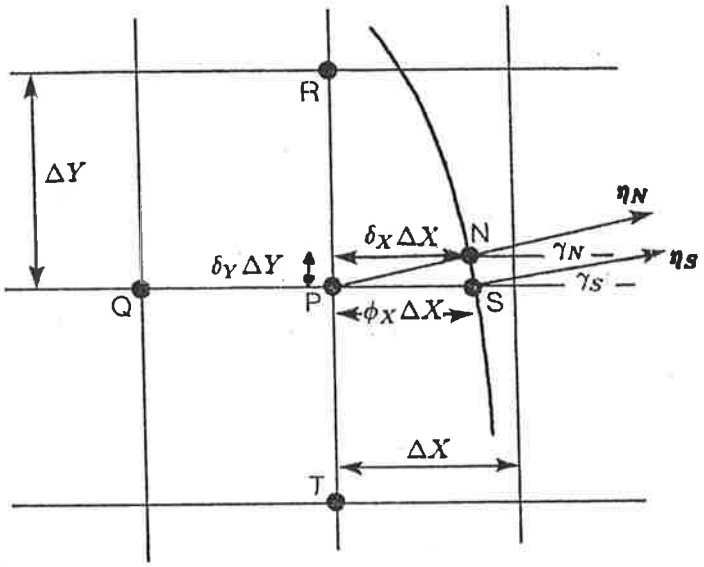

FIGURE A3: *Geometry of a boundary point, P, for which only one of the neighbouring grid points is outside of the boundary.*

$$q_{X3} = -\{(\phi_X(2\delta_Y + 1) - \delta_X)\sin\gamma_N - \delta_Y\cos\gamma_N\}\sin\gamma_S, \qquad (A.23(d))$$

$$q_{X4} = 4\phi_X\{(\delta_Y\sin\gamma_N + \delta_X\cos\gamma_N)\sin\gamma_S$$

$$-(\delta_X\sin\gamma_N + \delta_Y\cos\gamma_N)\cos\gamma_S\}, \qquad (A.23(e))$$

$$q_{X5} = \phi_X(2\delta_X + 1)\cos\gamma_N\sin\gamma_S$$

$$-(2\phi_X + 1)(\delta_X\sin\gamma_N + \delta_Y\cos\gamma_N)\cos\gamma_S, \qquad (A.23(f))$$

and

$$q_{X6} = \left.\frac{\partial Z}{\partial n}\right|_N \phi_X\sin\gamma_S - \left.\frac{\partial Z}{\partial n}\right|_S (\delta_X\sin\gamma_N + \delta_Y\cos\gamma_N). \qquad (A.23(g))$$

The solution for $\partial^2 Z/\partial X^2$ at the point P is

$$\bar{Z}_{XX} = \frac{\partial^2 Z}{\partial X^2} = \frac{q_{XX1}Z_T + q_{XX2}Z_Q + q_{XX3}Z_R + q_{XX4}Z_P + hq_{XX6}}{h^2 q_{XX5}} + O\{h^2\}, \qquad (A.24(a))$$

where

$$q_{XX1} = -\{(\phi_X(2\delta_Y - 1) + \delta_X)\sin\gamma_N + \delta_Y\cos\gamma_N\}\sin\gamma_S, \qquad (A.24(b))$$

$$q_{XX2} = 2\{(\phi_X\sin\gamma_S - \delta_Y\cos\gamma_S)\cos\gamma_N - \delta_X\sin\gamma_N\cos\gamma_S\}, \qquad (A.24(c))$$

$$q_{XX3} = -\{(\phi_X(2\delta_Y + 1) - \delta_X)\sin\gamma_N - \delta_Y\cos\gamma_N\}\sin\gamma_S, \qquad (A.24(d))$$

$$q_{XX4} = 2\{\phi_X(2\delta_Y\sin\gamma_N - \cos\gamma_N)\sin\gamma_S$$

$$+(\delta_X\sin\gamma_N + \delta_Y\cos\gamma_N)\cos\gamma_S\}, \qquad (A.24(e))$$

$q_{XX5} = q_{X5}$ is defined in (A.23(f)) and

$$q_{XX6} = 2\left\{\left.\frac{\partial Z}{\partial n}\right|_N \phi_X\sin\gamma_S - \left.\frac{\partial Z}{\partial n}\right|_S (\delta_X\sin\gamma_N - \delta_Y\cos\gamma_N)\right\}. \qquad (A.24(f))$$

The cross derivative $\partial^2 Z/\partial X \partial Y$ is given by

$$\bar{Z}_{XY} = \frac{\partial^2 Z}{\partial X \partial Y} = \frac{q_{XY1} Z_T + q_{XY2} Z_Q + q_{XY3} Z_r + q_{XY4} Z_p + 2h q_{XY6}}{2h^2 q_{XY5}} + O\{h^2\}, \quad (A.25(a))$$

where

$$q_{XY1} = (2\delta_Y - 1)(2\phi_X + 1)\sin\gamma_N \cos\gamma_S + (2\delta_X + 1)\cos\gamma_N \sin\gamma_S, \quad (A.25(b))$$

$$q_{XY2} = 4(\delta_X - \phi_X)\cos\gamma_N \cos\gamma_S, \quad (A.25(c))$$

$$q_{XY3} = (2\delta_Y + 1)(2\phi_X + 1)\sin\gamma_N \cos\gamma_S - (2\delta_X + 1)\cos\gamma_N \sin\gamma_S, \quad (A.25(d))$$

$$q_{XY4} = -4\{\delta_Y(2\phi_X + 1)\sin\gamma_N + (\delta_X - \phi_X)\cos\gamma_N\}\cos\gamma_S \quad (A.25(e))$$

$q_{XY5} = q_{X5}$ (see Equation (A.23(f))) and

$$q_{XY6} = \left.\frac{\partial Z}{\partial n}\right|_S (2\delta_X + 1)\cos\gamma_S - \left.\frac{\partial Z}{\partial n}\right|_N (2\phi_X + 1)\cos\gamma_N. \quad (A.25(f))$$

The two remaining derivatives, which are dependent only on the Y direction, are easily handled since the two grid points above and below point P both lie inside the boundary. Hence, existing second order formulae may be used for these derivatives at point P. That is,

$$\bar{Z}_Y = \frac{\partial Z}{\partial Y} = \frac{Z_R - Z_T}{2h} + O\{h^2\} \quad (A.26)$$

and

$$\bar{Z}_{YY} = \frac{\partial^2 Z}{\partial X \partial Y} = \frac{Z_R + Z_T - 2Z_P}{h^2} + O\{h^2\}. \quad (A.27)$$

As before, the boundary point P in Figure A.3 may be surrounded by a curved boundary in any of four orientations which are shown in the Figure A.4.

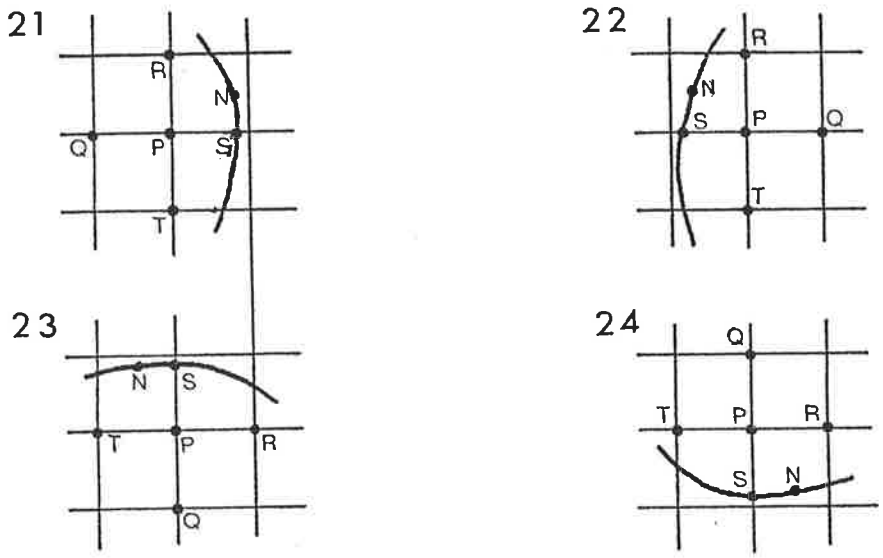

FIGURE A4: *The various orientations, denoted 21, 22, 23 and 24, which a boundary point, P, can be surrounded by a curved boundary such that only one of the neighbouring grid points lie outside of the boundary.*

For the orientation labelled 21 in Figure A.4 the expressions for the derivatives at P are immediately available from the preceeding analysis. In fact,

$$\frac{\partial Z}{\partial x} = \bar{Z}_X, \qquad (A.28(a))$$

$$\frac{\partial Z}{\partial y} = \bar{Z}_Y, \qquad (A.28(b))$$

$$\frac{\partial^2 Z}{\partial x^2} = \bar{Z}_{XX}, \qquad (A.28(c))$$

$$\frac{\partial^2 Z}{\partial x \partial y} = \bar{Z}_{XY}, \qquad (A.28(d))$$

$$\frac{\partial^2 Z}{\partial y^2} = \bar{Z}_{YY}, \qquad (A.28(e))$$

where the expressions on the right hand sides may be obtained from Equations (A.23(a)), (A.24(a)), (A.25(a)), (A.26(a)) and (A.27(a)). For this particular orientation, the values Z_Q, Z_R and Z_T are defined by

$$Z_Q = Z_{j1}, \qquad (A.29(a))$$

$$Z_R = Z_{j+1} \qquad (A.29(b))$$

and

$$Z_T = Z_{j-1}. \qquad (A.29(c))$$

For the orientation 22 in Figure A.4, the following formulae hold:

$$\frac{\partial Z}{\partial x} = -\bar{Z}_X, \qquad (A.30(a))$$

$$\frac{\partial Z}{\partial y} = \bar{Z}_Y, \qquad (A.30(b))$$

$$\frac{\partial^2 Z}{\partial x^2} = \bar{Z}_{XX}, \qquad (A.30(c))$$

$$\frac{\partial^2 Z}{\partial x \partial y} = -\bar{Z}_{XY}, \qquad (A.30(d))$$

$$\frac{\partial^2 Z}{\partial y^2} = \bar{Z}_{YY}, \qquad (A.30(e))$$

in which

$$\gamma_S \leftarrow \pi - \gamma_S, \qquad (A.31(a))$$

$$\gamma_N \leftarrow \pi - \gamma_N, \qquad (A.31(b))$$

$$Z_Q = Z_{j2}, \qquad (A.31(a))$$

$$Z_R = Z_{j+1} \qquad (A.31(b))$$

and

$$Z_T = Z_{j-1}. \qquad (A.31(c))$$

As before, the symbol $\leftarrow$ indicates that the angles γ_S and γ_N which appear in the formula for Z_X, Z_Y, Z_{XY} etc. are to be replaced by the angles $\pi - \gamma_S$ and $\pi - \gamma_N$ respectively.

A coordinate transformation of $y = X$ and $x = Y$ applied to the situation in Figure A.3 yields the orientation labelled 23 in Figure A4. The resultant formulae for the derivatives are, therefore,

$$\frac{\partial Z}{\partial x} = \bar{Z}_Y, \qquad (A.32(a))$$

$$\frac{\partial Z}{\partial y} = \bar{Z}_X, \qquad (A.32(b))$$

$$\frac{\partial^2 Z}{\partial x^2} = \bar{Z}_{YY}, \qquad (A.32(c))$$

$$\frac{\partial^2 Z}{\partial x \partial y} = \bar{Z}_{XY}, \qquad (A.32(d))$$

$$\frac{\partial^2 Z}{\partial y^2} = \bar{Z}_{XX}, \qquad (A.32(e))$$

in which

$$\gamma_S \leftarrow \pi/2 - \gamma_S, \qquad (A.33(a))$$

$$\gamma_N \leftarrow \pi/2 - \gamma_N, \qquad (A.33(b))$$

$$Z_Q = Z_{j-1}, \qquad (A.33(c))$$

$$Z_R = Z_{j2} \qquad (A.33(d))$$

$$Z_T = Z_{j1} \qquad (A.33(e))$$

$$\delta_X \leftarrow \delta_Y \qquad (A.33(f))$$

and

$$\delta_Y \leftarrow \delta_X. \qquad (A.33(g))$$

The final orientation to be considered is that which is labelled 24 in Figure A.4. For this case, the derivatives at the point P are given by

$$\frac{\partial Z}{\partial x} = \bar{Z}_Y, \qquad (A.34(a))$$

$$\frac{\partial Z}{\partial y} = -\bar{Z}_X, \qquad (A.34(b))$$

$$\frac{\partial^2 Z}{\partial x^2} = \bar{Z}_{YY}, \qquad (A.34(c))$$

$$\frac{\partial^2 Z}{\partial x \partial y} = -\bar{Z}_{XY}, \qquad (A.34(d))$$

$$\frac{\partial^2 Z}{\partial y^2} = \bar{Z}_{XX}, \qquad (A.34(e))$$

in which

$$\gamma_S \leftarrow \gamma_S - 3\pi/2, \qquad (A.35(a))$$

$$\gamma_N \leftarrow \gamma_N - 3\pi/2, \qquad (A.35(b))$$

$$Z_Q = Z_{j+1}, \qquad (A.35(c))$$

$$Z_R = Z_{j2}, \qquad (A.35(d))$$

$$Z_T = Z_{j-1}, \qquad (A.35(e))$$

$$\delta_X \leftarrow \delta_Y \qquad (A.35(f))$$

and

$$\delta_Y \leftarrow \delta_X. \qquad (A.35(g))$$

There remains one final case to consider for the point P which has been discussed above. In Figure A.3, the point N is displayed lying on the boundary between the points S and R. It is just as likely that a suitable N may be found which lies between the point S and T. If this is the case, the analysis is identical to that presented above except that in the formulae for $\bar{Z}_X$, $\bar{Z}_Y$, etc., the following replacement is made

$$\delta_Y \leftarrow -\delta_Y \qquad (A.36)$$

That is, for this positioning of N, whenever a δ_Y appears in the formulae for the derivatives, it is replaced by $-\delta_Y$.

§A.3 Conclusion

Presented in this work are finite difference formulae which may be used to approximate the derivatives $\partial Z/\partial x$, $\partial Z/\partial y$, $\partial^2 Z/\partial x^2$, $\partial^2 Z/\partial x \partial y$ and $\partial^2 Z/\partial y^2$ at a point which is next to a curved boundary along which a normal gradient boundary condition is imposed. These approximations are second order accurate. A systematic method which can be readily incorporated into a computer program has also been given to account for the several various ways in which the curved

boundary may surround a given boundary point. Using techniques described in Chapter 5, a program may be written which identifies the type of boundary point (that is, whether there are one or two neighbouring grid points outside of the boundary) and then calculates the type of orientation (as shown in Figures A.2 and A.4). Once these factors have been determined, the required modifications can be made to the general expressions for Z_X, $\bar{Z}_X$, Z_Y, $\bar{Z}_Y$, etc.

Although the coefficients s_{X1}, q_{X1} etc. which appear in the finite difference approximations are complicated, theymay be used in finite difference scheme with only a small increase in computer time. In most problems nearly all the grid points are interior points and so the formulae above only need to be applied to a small number of boundary points. Also, all the coefficients need only to be calculated once for each boundary point and this further prevents any major increase in computing time.

BIBLIOGRAPHY

ABRAMOWITZ, M. and STEGUN, I. A., (1970), Eds., *Handbook Of Mathematical Functions,* Dover, New York.

BAINES, W. D. and KNAPP, D. J., (1965), *Wind Driven Water Currents,* Proc. ASCE, J. Hyd. Div., **91(2)**, pp. 205-221.

BALTZER, R. A. and LAI, C., (1968), *Computer Simulation Of Unsteady Flows In Waterways,* Proc. ASCE, J. Hyd. Div., **94**, pp. 1083-1115.

BANAUGH, R. P. and GOLDSMITH, W., (1963), *Diffraction Of Steady Acoustic Waves By Surfaces Of Arbitrary Shape,* J. Acoust. Soc. Amer., **35(10)**, pp. 1590-1601.

BENGTSSON, L., (1973), *Conclusions About Turbulent Exchange Coefficients From Model Studies,* Hydrology of Lakes, Proc. of Helsinki Symp., July 1973, IAHS-AISH, Publ. No. 109.

BIRCHFIELD, G.E., (1971), *Wind Driven Currents In A Large Lake Or Sea,* Argonne National Laboratory, ANL/ES-6 Waste Heat Disposal, 17pp.

BLUMBERG, A. F., (1975), *A Numerical Investigation Into The Dynamics Of Estuarine Circulation,* Chesapeake Bay Inst., John Hopkins Uni., Tech. Rep. 91.

BLUMBERG, A. F. and MELLOR, G. L., (1978), *A Coastal Ocean Numerical Model,* Proc. Int. Symp. on Mathematical Modelling of Estuarine Physics, Ed. J. Sundermann and K.-P. Holz, pp. 203-219.

BOWDEN, K. F., (1953), *Note On Wind Drift In A Channel In The Presence Of Tidal Currents,* Proc. Roy. Soc. Lond., **A219**, pp. 426-446.

BOWDEN, K. F., (1964), *Turbulence,* Oceanogr. Mar. Biol. Ann. Rev., **2**, pp. 11-30.

BOWDEN, K. F. and FAIRBAIRN, L. A., (1952), *A Determination Of The Frictional Forces In A Tidal Current,* Proc. Roy. Soc. Lond., **A214**, pp. 371-392.

BOWDEN, K. F. and HAMILTON, P., (1975), *Some Experiments With A Numerical Model Of Circulation And Mixing In A Tidal Estuary,* Estuarine and Coastal Mar. Sci., **3**, pp. 281-301.

BOWDEN, K. F., FAIRBAIRN, L. A. and HUGHES, P., (1959), *The Distribution Of Shearing Stresses In A Tidal Current,* Geophysical J., Roy. Astr. Soc., **2**, pp. 288-305.

COOPER, C. K. and PEARCE, B. R., (1980), *On The Forcing Mechanisms Affecting The Bottom Shear Stress In Coastal Waters,* J. Phys. Oceanogr., **10**, pp. 1870-1876.

COOPER, C. K. and PEARCE, B. R., (1982), *Numerical Simulations Of Hurricane Generated Currents,* J. Phys. Oceanogr., **12**, pp. 1071-1091.

CSANADY, G. T., (1978), *Turbulent Interface Layer,* J. Geophys. Res., **83(5)**, pp. 2329-2342.

DAVIES, A. M., (1977), *The Numerical Solution Of The Three-Dimensional Hydrodynamic Equations, Using A β-Spline Representation Of The Vertical Current Profile,* Bottom Turbulence, Proc. of the 8^{th} Liege Colloq. on Ocean Hydrdynamics, Ed. J. C. J. Nihoul, Elsevier Oceonography Series, **19**, pp. 27-48.

DAVIES, A. M., (1980(a)), *On Formulating A Three-Dimensional Hydrodynamic Sea Model With An Arbitrary Variation Of Vertical Eddy Viscosity,* Comp. Meth. in App. Mech. and Eng., **22**, pp. 53-68.

DAVIES, A. M., (1980(b)), *Application Of The Galerkin Method To The Formulation Of A Three-Dimensional Non-Linear Hydrdynamic Numerical Sea Model,* App. Math. Modelling, **4**, pp. 245-256.

DAVIES, A. M., (1981), *Three Dimensional Hydrodynamic Numeric Models,* in The Norwegian Coastal Current, Eds. R. Saetre and M. Mork.

DAVIES, A. M., (1982(a)), *Meteorologically Induced Circulation On TheNorth-West European Continental Shelf: From A Three-Dimensional Numerical Model,* Oceanologica Acta, **5(3)**, pp. 269-280.

DAVIES, A. M., (1982(b)), *On Computing The Three Dimensional Flow In A Stratified Sea Using The Galerkin Method,* App. Math. Modelling, **6(5)**, pp. 347-362.

DAVIES, A. M., (1982(c)), *Formulating A Three Dimensional Hydrodynamic Sea Model Using A Mixed Galerkin-Finite Difference Method,* in Proc. of the 4^{th} Int. Conf. on Finite Elements in Water Resources, Ed. K. P. Holz, Berlin Springer-Verlag, pp. 5.27-5.41.

DAVIES, A. M. (1983), *Formulation Of Linear Three Dimensional Hydrodynamic Sea Model Using a Galerkin Eigenfunction Method,* Int. J. for Num. Meths. in Fluids, **3(1)**, pp. 33-60.

DAVIES, A. M. AND OWEN, A., (1979), *Three Dimensional Numerical Sea Model Using The Galerkin Method With A Polynomial Basis Set,* App. Math. Modelling, **3**, pp. 421-428.

DELFT HYDRAULICS LABORATORY, (1974), *Momentum And Mass Transfer In Stratified Flow,* Laboratory Report R880.

DUNCAN W. J., THOM, A. S. and YOUNG, A. D., (1978), *Mechanics Of Fluids,* 2^{nd} ed., Edward Arnold Publ., 725 pp.

DYER, K. R., (1970), *Current Velocity Profiles In A Tidal Channel,* Geophys. J., Roy. Astr. Soc., **22**, pp. 153-161.

DYKE, P. P. G., (1977), *A Simple Ocean Surface Layer Model,* Rivista Italiana Di Geofisica E Scienze Affini, **4(1-2)**, pp. 31-34.

ENGELUND, F., (1973), *Steady Wind Set-Up In Prismatic Lakes,* Inst. Hydrodyn. and Hydraulic. Engrg., Tech. Univ. Denmark, Progr. Rep. 28, pp. 31-38.

ENGELUND, F., (1978), *Effect of Lateral Wind On Uniform Channel Flow,* Inst. of Hydrodynamic and Hydraulic Engineering, Tech. Uni. Denmark, Progr. Rep. **45**, pp. 33-36.

FITZGERALD, L. M. and MANSFIELD, W. W., (1965), *The Response Of Closed Channels To Wind Stresses,* Aust. J. Phys., **18**, pp. 219-226.

FLATHER, R. A., (1979), *Recent Results From A Storm Surge Prediction Scheme For The North Sea,* in Marine Forecasting, Ed. J. C. J. Nihoul, Elsevier, pp. 385-409.

FOX, L., (1944), *Numerical Solution Of Ordinary And Partial Differential Equations,* Addison-Wesley Publ. Co. Inc., Reading, Mass.

FRANCIS, J. R. D., (1953), *A Note On The Velocity Distribution And Bottom Stress In A Wind-Driven Water Current System,* J. Mar. Res., **12(1)**, pp. 93-98.

GRACE, S. F., (1929), *Internal Friction In Certain Tidal Currents,* Proc. Roy. Soc. Lond., **A124**, pp. 150-163.

HARVEY, J. G. and VINCENT, C. E., (1977), *Observations Of Shear In Near Bed Currents In The Southern North Sea,* Estuarine and Coastal Mar. Sc., **5**, pp. 715-731.

HEAPS, N. S., (1972), *On The Numerical Solution Of The Three Dimensional Hydrodynamical Equations For Tides And Storm Surges,* Memoires Societe Royale des Sciences de Liege, **6** serie, tome II, pp. 143-180.

HEAPS, N. S., (1982), *Development Of A Three-Layered Spectral Model For The Motion Of A Stratified Sea,* in Coastal and Shelf Dynamical Oceanography, Elsevier Oceanographic Series, Ed. B. Johns.

HEATHERSHAW, A., (1979), *The Turbulent Structure Of The Bottom Boundary Layer In A Tidal Current,* Geophys. J., Roy. Astr. Soc., **58**, pp. 395-430.

HEATHERSHAW, A. AND SIMPSON, J. H., (1978), *The Sampling Variability Of The Reynolds Stress And It's Relation To Boundary Shear Stress And Drag Coefficient Measurements,* Estuarine and Coastal Mar. Sc., **6**, pp. 263-274.

HELLSTROM, B., (1941), *Wind Effects On Lakes And Rivers,* Handlinger, Ingen. Ventensk., Akad., Stockh., No. 158.

HUANG, N. E., (1979), *On Surface Drift Currents In The Ocean,* J. Fluid Mech., **91**, pp. 191-208.

HWANG, L. and TUCK, E. O., (1970), *On The Oscillations Of Harbours Of Arbitrary Shape,* J. Fluid Mech., **42(3)**, pp. 447-464.

IANELLO, J. P., (1977), *Tidally Induced Residual Currents In Estuaries Of Constant Breadth And Depth,* J. Mar. Res., **35**, pp. 755-786.

JOBSON, H. E., (1968), *Vertical Mass Transfer In Open Channel Flow,* U. S. Geological Survey, open file report.

JOBSON, H. E.and SAYRE, W. W., (1970), *Vertical Transfer In Open Channel Flow,* Proc. ASCE, J. Hyd. Div., **96(3)**, pp. 703-724.

JOHNS, B., (1966), *On The Vertical Structure Of Tidal Flow In River Estuaries,* Geophys. J., Roy. Astr. Soc., **12**, pp. 103-110.

JOHNS, B., (1968), *The Damping Of Gravity Waves In Shallow Water Energy By Dissipation In A Turbulent Boundary Layer,* Tellus, **20(2)**, pp. 330-337.

JOHNS, B., (1969), *On The Representation Of The Reynolds Stress In A Tidal Estuary,* Geophys. J., Roy. Astr. Soc., **17**, pp. 39-44.

JOHNS, B., (1970), *On The Determination Of The Tidal Structure And Residual Current System In A Narrow Channel,* Geophys. J., Roy. Astr. Soc., **20**, pp. 159-175.

JOHNS, B., (1977), *Residual Flow And Boundary Shear Stress In The Turbulent Bottom Layer Beneath Waves,* J. Phys. Oceanogr., **8**, pp. 1042-1049.

JOHNS, B., (1978), *The Modelling Of Tidal Flow In A Channel Using A Turbulence Energy Closure Scheme,* J. Phys. Oceanogr., **8**, pp. 1042-1049.

JOHNS, B. and DYKE, P., (1971), *On The Determination Of The Structure Of An Off-Shore Tidal Stream,* Geophys. J., Roy. Astr. Soc., **23**, pp. 287-297.

JOHNSON, C. H. J., (1967), *On Wind Induced Flows In Closed Channels,* Aust. J. Phys., **20**, pp. 1-10.

JONES, W. P. and LAUNDER, B. E., (1972), *The Prediction Of Laminarization With A Two Equation Model Of Turbulence,* Int. J. Heat Mass Transfer, **15**, pp. 301-314.

JORDAN, T. F.and BAKER, J. R., (1980), *Vertical Structure Of Time Dependent Flow Dominated By Friction In A Well-Mixed Fluid,* J. Phys. Oceanogr., **10**, pp. 1091-1103.

KAGAN, B. A., (1979), *Sea-Bed Friction In One-Dimensional Tidal Current,* Izv. Atmos. and Oceanic Phys., **7(11)**, pp. 1190-1200.

KAJIURA, K., (1964), *On The Bottom Friction In An Oscillatory Current,* Bull. of the Earthquake Res. Inst., **42**, pp. 147-174.

KEULEGAN, G. H., (1951), *Wind Tides In Small Closed Channels,* J. Res. Nat. Bur. Stand., **46**, pp. 358-381.

KNIGHT, D. W., RODGER, J. G., SHIANO, K., WATERS, C. B. and WEST, J. R., (1980), *The Measurement Of Vertical Turbulent Exchange In Tidal Flows,* Sec. Int. Sympos. on Stratified Flows, Norwegian Inst. Tech., pp. 362-366.

KOUTITAS, C. G., (1978), *Numerical Solution Of The Complete Equations For Nearly Horizontal Flows,* Advances in Water Resources, **1(4)**, pp. 213-217.

KOUTITAS, C. G. and O'CONNOR, B., (1980), *Modelling Three Dimensional Wind Induced Flows,* Proc. ASCE, J. Hyd. Div., **106(11)**, pp. 1843-1865.

KUIPERS, J. and VREUGDENHIL, C. B., (1973), *Calculations Of Two Dimensional Horizontal Flow,* Delft Hydraulics Laboratory Report on Basic Research, S163.

LAM, C. K. G. and BREMHORST, K., (1978), *Modified Form Of The $k-\epsilon$ Model For Predicting Wall Turbulence,* Univ. Queensland, Dept. Mech. Engr., Res. Rept. 3/78.

LATHBURY, A., BRYSON, R. and LETTAU, B., (1960), *Some Observations Of Currents In The Hypolimnion Of Lake Mendota,* Limnology and Oceanogr., **5**, pp. 409-413.

LAUNDER, B. E. and SPALDING, D. B., (1974), *Numerical Calculation Of Turbulent Flow,* Comp. Meth. in Appl. Mech. and Engr., **3**, pp. 269-287.

LAVELLE, J. W. and MOFJELD, H. O., (1983), *Effects Of Time Varying Viscosity On Oscillatory Turbulent Channel Flow,* J. Geophys. Res., **88**, pp. 7607-7616.

LEE, J-J, (1969), *Wave Induced Oscillations In Harbours Of Arbitrary Shape,* W. M. Keck Lab. of Hyd. and Water Resources, Cal. Inst. Tech., Rep. KH-R-20.

LEE, J-J, (1971), *Wave Induced Oscillations In Harbours Of Arbitrary Geometry,* J. Fluid Mech., **45(2)**, pp. 375-394.

LEENDERTSE, J. J. and LIU, S., (1975(a)), *A Three-Dimensional Model For Estuaries And Coastal Seas: Vol. 2, Aspects Of Computation,* Rand Corporation, R-1764-OWRT, 123pp.

LEENDERTSE, J. J. and LIU, S., (1975(b)), *Modelling Of Three-Dimensional Flows In Estuaries,* Proc. of 2^{nd} Annual Sym. of Waterways, Harbours and Coastal Engineering Div., ASCE, on Modelling Techniques, San Francisco, California, **1**, pp. 625-642.

LIGGETT, J. A., (1970), *Cell Method For Computing Lake Circulation,* Proc. ASCE, J. Hyd. Div., **96(3)**, pp. 725-743.

MACSYMA, *A Symbolic Manipulation Program,* Developed at MIT Lab. Comp. Sci., trademark of Symbolics, Inc. of Cambridge, Mass.

MADSEN, O. S., (1977), *A Realistic Model Of The Wind Induced Ekman Boundary Layer,* J. Phys. Oceanogr., **7(2)**, pp. 248-255.

MARCHUK, G. I., KOCHERGIN, V. P., KLIMOK, V. Z. and SUKHORUKOV, V. S., (1977), *On The Dynamics Of The Ocean Surface Mixed Layer,* J. Phys. Oceanogr., **7**, pp. 865-875.

M^{c}GREGOR, R. C., (1972), *The Influence Of Eddy Viscosity On The Vertical Distribution Of Velocity In The Tidal Estuary,* Geophys. J., Roy. Astr. Soc., **29**, pp. 103-108.

M^{c}PHEE, M. G., (1979), *The Effect Of The Oceanic Boundary Layer On The Mean Drift Of Pack Ice: Application Of A Simple Model,* J. Phys. Oceanogr., **9**, pp. 388-400.

MELLOR, G. I. and YAMADA, T., (1974), *A Hierarchy Of Turbulence Closure Models For Planetry Boundary Layers,* J. Atmos. Sci., **31**, pp. 1791-1806.

MUNK, W. H. and ANDERSON, E. K., (1948), *Notes On The Theory Of Thermocline,* J. Mar. Res., **1**, pp. 41-67.

NIHOUL, J. C. J., (1977), *Three Dimensional Model Of Tides And Storm Surges In A Shallow Well-Mixed Continental Sea,* Dynamics of Atmos. and Oceans, **2**, pp. 29-47.

NIHOUL, J. C. J., RUNFOLA, Y. AND ROISIN, B., (1980), *Shear Effect Dispersion In A Shallow Tidal Sea,* in Marine Turbulence, Elsevier Oceanography Series, **28**, pp.345-362.

NOMITSU, T. and MATSUZAKI, T., (1936), *On The Vertical Distribution Of Eddy Viscosity In Rivers,* Jap. J. of Astr. and Geophys., **13(3)**, pp. 183-193.

NOYE, J., (1983), *Finite Difference Techniques For Partial Differential Equations,* in Computational Techniques for Differential Equations, Ed. J. Noye, North Holland Publ. Co., pp. 95-354.

NOYE, J. and FLATHER, R. A., (1985), *Hydrodynamical-Numerical Modelling Of Tides And Storm Surges,* to be published as an A. G. U. monograph.

NOYE, J., MAY, R. L. and TEUBNER, M. D., (1981), *Three-Dimensional Numerical Model Of Tides In Spencer Gulf,* Ocean Management, **6**, pp. 137-147.

OTTESEN-HANSEN, N. E., (1975), *Effect Of Wind Stress On Stratified Deep Lake,* ASCE, J. Hyd. Div., **101(8)**, pp. 1037-1052.

OWEN, A., (1980), *A Three-Dimensional Model Of The Bristol Channel,* J. Phys. Oceanogr., **10**, pp. 1290-1302.

PEARCE, B. R. and COOPER, C. K., (1981), *Numerical Circulation Model For Wind Induced Flow,* ASCE, J. Hyd. Div., **107(3)**, pp. 285-302.

POWELL, J. H., (1925), *On The Variation Of The Velocity In Tidal Streams With Depth,* Monthly Notices of Roy. Astr. Soc., pp. 270-280.

RANEY, D.C., DURHAM, D. L. and BUTLER, H. L., (1980), *Application Of A Three Dimensional Storm Surge Model,* in Hydrodynamics of Lakes, Eds. W. H. Graf and C. H. Mortimer, pp. 77-86.

RASTOGI, A. K. and RODI, W., (1974), *Predictions Of Heat And Mass Transfer In Open Channels,* Proc. ASCE, J. Hyd. Div., **104(3)**, pp. 399-419.

REID, R. O. and BODINE, B. R., (1968), *Numerical Model For Storm Surges In Galveston Bay,* Proc., ASCE, J. Wat., Harb. and Coast. Div., **94**, pp. 33-57.

REID, R. O., VASTANO, A. C., WHITAKER, R. E. and WANSTRATH, J. J., (1977), *Experiments In Storm Surge Simulation,* in The Sea, Eds. E. D. Goldberg et. al., **6**, Wiley, New York, pp. 145-168.

RICCO, R. D., (1982), *A Numerical Model Of The Vertical Circulation Of Tidal Strait And It's Application To The Messina Strait,* Il Nuovo Cimento, **5C(1)**, pp. 21-45

ROACHE, P. J., (1974), *Computational Fluid Dynamics,* Hermosa Publ., Alberquerque, 446 pp.

ROSSBY, C. B. and MONTGOMERY, R. B., (1935), *The Layer Of Frictional Influence In Wind And Ocean Currents,* Papers in Physical Oceanography, Meteorology, **3(3)**, pp. 1-101.

SHANAHAN, P. and HARLEMAN, D. R. F., (1982), *Linked Hydrodynamic Biogeochemical Models Of Water Quality In Shallow Seas,* R. M. Parsons Lab., MIT, Rep. 268.

SHEMDIN, O. H., (1972), *Wind Generated Current And Phase Speed Of Wind Waves,* J. Phys. Oceanogr., **2**, pp. 411-419.

SIMONS, T. J., (1971), *Development Of Numerical Models Of Lake Ontario,* Proc. 14^{th} Conf. Great Lakes Res., pp. 654-669.

SMITH, T. J., (1982), *On The Representation Of Reynolds Stress In Estuaries And Shallow Coastal Seas,* J. Phys. Oceanogr., **12**, pp. 914-921.

SOULSBY, R. L. and DYER, K. R., (1981), *The Form Of The Near-Bed Velocity Profile In A Tidally Accelerating Flow,* J. Geophys. Res., **86(9)**, pp. 8067-8074.

STERNBERG, R. W., (1968), *Friction Factors In Tidal Channels With Differing Bed Roughness,* Mar. Geol., **6**, pp. 243-260.

STEVENS, M. and NOYE, J., (1984), *An Improved Three-Dimensional Tidal Model For A Shallow Gulf,* in Computational Techniques and Applications: CTAC 83, Eds. J. Noye and C. Fletcher, North Holland, pp. 375-393.

STOLZENBACH, K. D., MADSEN, D. S., ADAMS, E. E., POLLACK, A. M. and COOPER C. K., (1977), *A Review And Evaluation Of Basic Techniques For Predicting The Behaviour Of Surface Oil Slicks,* R. M. Parsons Lab., MIT, Tech. Rep. No. 222.

SVENSSON, U., (1979), *The Structure Of the Turbulent Ekman Layer,* Tellus, **31**, pp. 340-350.

SWIFT, M.R., REICHARD, R. and CELIKKOL, B., (1979), *Stress And Tidal Current In A Well-Mixed Estuary,* ASCE, J. Hyd. Div., **105(7)**, pp. 785-799.

TARAYEV, B. A., (1958(A)), *Drift Currents Produced In A Shallow Sea By A Wind Variable In Time,* Izv. Geophys. Ser., pp. 605-612.

TARAYEV, B. A., (1958(B)), *Stationary Wind Set Up And Circulation In A Shallow Rectangular Basin,* Izv. Geophys. Ser., pp. 1139-1144.

TEE, K-T, (1979), *The Structure Of Three-Dimensional Tide Generating Currents, Part 1: Oscillating Currents,* J. Phys. Oceanogr., **9**, pp. 930-944

THOMAS, J. H., (1975), *A Theory Of Steady Wind-Driven Currents In Shallow Water With Variable Eddy Viscosity,* J. Phys. Oceanogr., **5**, pp. 136-142.

TOWNSEND, A. A., (1976), *The Structure Of The Turbulent Shear Flow,* Cambridge University Press.

VAGER, B. G. and KAGAN, B. A., (1969(a)), *The Dynamics Of The Turbulent Boundary Layer In A Tidal Current,* Izv. Atmos. and Oceanic Physics, **5(2)**, pp. 168-179.

VAGER, B. G. and KAGAN, B. A., (1969(b)), *The Determination Of The Turbulence Characteristics And Velocity Distribution Of A Tidal Flow In A Deep Ocean,* Izv. Atmos. and Oceanic Physics, **5(8)**, pp. 836-845.

VAGER, B. G. and KAGAN, B. A., (1971), *Vertical Structure And Turbulence In A Stratified Boundary Layer Of A Tidal Flow,* Izv. Atmos. and Oceanic Physics, **7(7)**, pp. 766-777.

VAN VEEN, J., (1938), *Water Movements In The Straits Of Dover,* J. du Conseil int. pour L'Exploration de la Mer, **13**, pp. 7-36.

WALSH, P. J., (1974), *Long Wave Wind Effects On Closed Lakes, With Special Application To The Murray Mouth Lakes, South Australia,* Ph. D. Thesis, Uni. of Adelaide.

WALSH, P. J. and NOYE, J., (1973), *Long Wave Wind Effects On The Lakes Of The Murray Mouth,* Proc. 2^{nd} Sth. Aust. Reg. Conf. on Phys. Oceanogr., pp. 187-215.

WELANDER, P., (1961), *Numerical Prediction Of Storm Surges,* Ad. in Geophys., **8**, pp. 336-342.

WILSON, B. W., (1960), *Note On The Surface Wind Stress Over Water At High Tide And Low Wind Speeds,* J. Geophys. Res., **65(3)**, pp. 3377-3382.

WITTEN, A. J. and THOMAS, J. H., (1976), *Steady Wind-Driven Currents In A Large Lake With Depth Dependent Eddy Viscosity,* J. Phys. Oceanogr., **6**, pp. 85-92.

WOLF, J., (1979), *Estimation Of Shearing Stresses In A Tidal Current With Application To The Irish Sea,* Marine Turbulence, Ed. J. C. J. Nihoul, Elsevier Oceanography Series, **28**, pp. 319-344.

WU, J., (1982), *Wind Stress Coefficients Over Sea Surface From Breeze To Hurricane,* J. Geophys. Res., **87**, pp. 9704-9706.

WURTELE, M. G., PEAGLE, J., and SIELECKI, A., (1971), *The Use Of Open Boundary Conditions With The Storm Surge Equations,* Monthly Weather Review, **99**, pp. 537-544.